NON-NEWTONIAN OPEN-CHANNEL FLOW: EFFECT OF SHAPE ON LAMINAR AND TRANSITIONAL FLOW

By

SYDWELL LUVO VANYAZA

BTech (Chemical Engineering) (Cape Technikon)

Thesis submitted in fulfillment of the requirements
for the degree of
Magister Technologiae

In the Department of Chemical Engineering
Cape Technikon

Supervisor: Dr R. Haldenwang

July 2004

ABSTRACT

When designing the open channels to transport the homogenous non-Newtonian slurries, the effect of channel shape is one of the parameters that should be checked and very little research has been conducted to address this matter. Open channels are commonly applied in the mining industry where mine tailings have to be transported to the disposal dams at high concentrations to save water consumption. This thesis addresses the effect of the cross-sectional shape of the channel with emphasis on laminar and transitional flow of non-Newtonian fluids.

The literature review on the flow of Newtonian and non-Newtonian fluids has been presented. The most relevant one to this topic is the work done by Straub *et al* (1958) for Newtonian fluids and the analytical work presented by Kozicki and Tiu (1967) for non-Newtonian fluids. Authors like Coussot (1994) and Haldenwang (2003) referred to their work but did not comprehensively verified it experimentally.

Three flume shapes were designed to investigate this problem namely, rectangular, semi circular, and trapezoidal flume shape. The test rig consisted of a 10 m long by 300mm wide tilting flume that can be partitioned into two sections to form a 150 mm wide channel. All three flume shapes were tested in both the 150 mm and 300 mm wide flumes. This flume is linked to the in-line tube viscometer with three tube diameters namely, 13 mm; 28 mm; and 80 mm. The experimental investigation covered a wide range of flow rates (0.1-45l/s), and flume slopes (1-5 degrees). The fluids tested were kaolin suspension (5.4 – 9% v/v), CMC solution (1 – 4% m/m), and bentonite suspension (4.6 and 6.2% m/m).

The models found in the literature were evaluated with the large database compiled from the test results to predict the laminar and transitional flow of these fluids with the aim of checking the effect of the cross-sectional shape of these channels selected in these flow regimes.

For all the flume shapes and non-Newtonian fluids selected in this thesis, it was found that in predicting the laminar flow, the effect of shape is adequately accounted for by the use of hydraulic radius. In predicting the transitional flow, it was found that the effect of shape does not have to be included.

DECLARATION

I, Sydwell Luvo Vanyaza hereby declare that this thesis represent my own unaided work and has not been submitted for a degree at another university or technikon. Further more it represents my own opinions and not necessarily those of the Cape Technikon.

_____

Sydwell Luvo Vanyaza

July 2004

DEDICATION

To my mother, who has always been a source of encouragement and beacon of light to me.

To my present and future family.

ACKNOWLEDGEMENTS

NOMENCLATURE

Symbol	Description	Unit
A	cross-sectional area	m^2
a	geometric coefficient of channel shape	
B	breath of the channel	m
b	geometric coefficient of channel shape	
C	concentration, constant	
C_v	solids concentration by volume	
C_w	solids concentration by mass	
D	internal pipe diameter	m
d	depth of the rectangular channel	m
E	sum of the mean error square	
f	Fanning friction factor	
f_L	Fanning friction factor for 'aminar flow	
Fr	Froude number	
g	gravitational acceleration	m/s^2
H_B	Herschel-Bulkley number	
He	Hedstrom number	
h	flow depth in the channel	m
h_f	frictional head	m
K	consistency index	$Pa.s^n$
K	open channel shape	
k_s	hydraulic roughness	m
L	distance between pressure tappings	m
M	mass	kg
M_w	mass of water	kg
m	inverse of the flow behaviour index	
N	number of data points	
NAF	normalised adherence function	
n	flow behaviour index	
n'	apparent flow behavior index	
P_w	wetted perimeter	m
P_L	plasticity number	
p	pressure	Pa
Δp	change in pressure	Pa
Q	volumetric flow rate	m^3/s
Re	Reynolds number	
Re_c	Critical Reynolds number	
$Re_{(K\&T)}$	Kozicki and Tiu's Reynolds number	
Re_2	Haldenwang's Reynolds number	
$Re_{2(BP)}$	Haldenwang's Reynolds number for Bingham fluids	
$Re_{2(PP)}$	Haldenwang's Reynolds number for power law fluids	

$Re_{2(YPP)}$	Haldenwang's Reynolds number for Herschel-Bulkley fluids	
R_h	hydraulic radius	m
S	energy gradient	
S	relative density	
t	time	s
V	average velocity	m/s
V_{turb}	turbulent velocity developed by Haldenwang m/s	
v	part of transition equation proposed by Coussot	
w	base of the trapezoidal channel	m
w	half width of rectangular channel	m
α	angle of inclination	radians
Δ	increment	
$\dot{\gamma}$	true shear rate	1/s
μ	dynamic viscosity	Pa.s
μ_{app}	apparent viscosity	Pa.s
ρ	density	kg/m^3
λ	half width to depth ratio of channel	
λ	Darcy-Weisbach friction factor	
ρ_m	slurry density	kg/m^3
ρ_w	density of water	kg/m^3
τ	shear stress	Pa
τ_0	wall shear stress	Pa
τ_y	yield stress	Pa
θ	angle of flume above the horizontal	degrees
v	kinematic viscosity	m^2/s
φ	Kozicki and Tiu's shape factor function	
ω	Angular velocity	rad/s

GLOSSARY

Open channel: Conduit for transporting fluids with a free surface open to atmosphere. It can be found natural or man-made.

Flume: Artificial open channel carrying fluids, slurries or tailings. The word is mainly used in laboratories.

Launder: Term often used in the mining industry referring to an open channel.

Rheology: The science of deformation and flow of matter.

Newtonian fluid: Any fluid that has a direct proportionality between shear stress and shear rate.

Non-Newtonian fluid: Any fluid that does not have a direct proportionality between shear stress and shear rate.

Laminar flow: The flow is laminar when the fluid elements flow in an orderly stream fashion without intermixing with the neighbouring fluid.

Turbulent flow: The flow is turbulent when the fluid elements flow randomly thus mixing with the neighbouring fluid.

Transition region: This is the region between the laminar and the turbulent flow.

Reynolds number: The ratio between the inertial and viscous forces.

Froude number: The ratio between the inertial and gravity forces.

LIST OF FIGURES

LIST OF TABLES

CHAPTER 1

CHAPTER 1

INTRODUCTION

1.1 BACKGROUND

The flow of water in open channels has been extensively researched in the past, and a substantial volume of literature has been accumulated. However, this cannot be said about the flow of homogenous non-Newtonian slurries in open channels. This field has received very little attention in the past by authors like Kozicki and Tiu (1967), Hao and Zhenghai (1982), and Cossot (1994). Recently Haldenwang (2003) did an extensive study on the flow of non-Newtonian fluids in rectangular open channels.

Of all the researchers in the field of open channel flow, only Straub *et al.* (1958) for Newtonian fluids and Kozicki and Tiu (1967) for non-Newtonian fluids presented some work about the effect of the cross-sectional shape of the channel. Kozicki and Tiu (1967) presented their analytical work without verifying it experimentally. Coussot (1994) and Haldenwang (2003) referred to Kozicki and Tiu's work without specifically addressing the issue of the shape effect.

The significance of this work is in the mining industries, where dense slurries have to be transported around the plants into the tailings dams (Sanders, Schaan, Gillies, McKibben, Sun and Shook, 2002). Another application of open channels is in the sewage plants that transport large volumes of sludge. South Africa experiences a problem of water shortage; therefore large industries such as mining industries are forced to operate at high concentrations to reduce water consumption. Open channels, because of their cheap cost can replace expensive pipelines in transporting slurries especially over short distances. In the past these open channels were often designed without properly researched design guidelines, therefore this study will help with a better understanding of the effect of the cross-sectional shape when designing these open channels.

Slurries flowing in open channels can be classified into three categories (Wilson, 1991). The first category is the homogenous slurries where particles are relatively small and are kept in suspension by a carrier fluid that is normally water. If no flow occurs, these particles will eventually settle at least partially. They are classified as homogenous non-Newtonian slurries and can be characterised rheologically.

There are also settling slurries that have larger particles. These are called rapid settling slurries. The third category is the mixed regime slurry, which is a mixture of the slow settling and rapid settling slurries (Wilson, 1991).

In this thesis only homogenous non-Newtonian slurries will be considered. The flow of these slurries is studied in rectangular, semi-circular, and trapezoidal channels to investigate the effect of shape on laminar and transitional flow.

1.2 STATEMENT OF THE RESEARCH PROBLEM

The effect of the cross-sectional shape of the flume in laminar and transition flow of non-Newtonian fluids is not yet well understood and no experimental work is reported in the literature. Design guidelines that take into consideration the effect of shape on flume design need to be compiled.

1.2.1 Laminar flow

To predict the laminar flow of open channels it is important to include the effect of the cross-sectional shape of the channel (Kozicki & Tiu, 1967). Some authors have suggested treating the laminar flow of open channels similarly to that of closed pipes (Abulnaga, 1997 and Haldenwang et al., 2002). There are some models in literature that predict the laminar flow of non-Newtonian fluids in open channels, but few of them have included

the effect of shape in this flow regime. Some of these models have not yet been validated experimentally.

1.2.2 Transitional flow

No models have been developed to specifically predict the transition of non-Newtonian fluids in open channels until Haldenwang (2003) developed a model that predicts this flow regime, however his model was only for the flow in a rectangular channel and does not include the effect of channel shape.

1.3 OBJECTIVE

The primary objective of this thesis is to evaluate if there is a need to include the effect of shape of the channel when designing the open channels. This will be possible by:

- Evaluating comprehensively the analytical work presented by Kozicki and Tiu (1967) on the effect of cross-sectional shape of the channel.

- Evaluating the models available in literature to predict the laminar and transitional flow.

- Evaluating the model presented by Haldenwang (2003) to predict the transition that includes the Froude number effect.

1.4 RESEARCH METHODOLOGY

In order to reach these objectives, the following research methodology will be followed. Viscous fluids to be tested will cover a wide range of viscous characteristics and will include materials that can be characterised using the following rheological models namely: power law, Bingham, and Herschel-Bulkley models.

1.4.1 Literature review

The literature reviews previous studies on Newtonian and non-Newtonian fluids as well as the rheological characterisation of the fluids.

Open-channel flow (as well as pipe flow) fundamentals are reviewed because some of the open channel flow models are derived from the pipe flow models. The non-Newtonian Reynolds number models are also presented and will be evaluated in Chapter 4.

1.4.2 Experimental procedure

The test rig was built and commissioned at the Cape Technikon Flow Process Research Centre to conduct all the test works. The rig consists of a 300mm wide by 10m long tilting flume that can be partitioned into two sections to form a 150mm-wide flume. In both flumes, three flume shapes were fitted, namely: rectangular, semi-circular and trapezoidal shapes. The flume is linked to an in-line tube viscometer with three diameter tube lines, namely: 13mm, 28mm, and 80mm lines. The tube viscometer enables one to test the rheology of the slurries and characterise them with the rheological models mentioned previously. Three slurries that exhibit three non-Newtonian fluid characteristics were tested over a wide range of laminar and turbulent flow rates in all the three flume shapes chosen over a range of slopes varying from 1-5 degrees.

1.4.3 Analysis of results and discussion

The database compiled from the experimental work is evaluated with the models presented in literature to predict the laminar and transition of non-Newtonian fluids. The results are then discussed with the emphasis on the effect of the cross-sectional shape of the flume.

1.4.4 Conclusions and recommendations

The conclusions are drawn from the results found in Chapter 4 and recommendations are listed for future work in non-Newtonian open channel flow.

1.5 DELINEATION

The following topics fall outside the scope of this thesis:

- The effect of shape on turbulent flow.

- The effect of surface roughness in open channel flow of non-Newtonian fluids.

- The velocity profiles of non-Newtonian fluid flow in smooth and rough surfaced channels.

- Time-dependent fluids.

1.6 SUMMARY

The background, the objectives and an overview of this thesis have been presented in this chapter.

CHAPTER 2

CHAPTER 2

LITERATURE REVIEW AND THEORY

2.1 INTRODUCTION

In this chapter the literature review and theory of Newtonian and non-Newtonian fluids is presented. As mentioned previously, the flow of non-Newtonian fluids in open channels has received very little attention in previous studies; the paucity of literature available about it is presented in this chapter.

As some of the models and theories of open-channel flow are derived from the pipe flow models, such relevant models of pipe flow are reviewed for both Newtonian and non-Newtonian fluids.

The classifications of the flow regimes are also discussed since they describe the nature of flow in both closed pipes and open channels.

The flow of non-Newtonian fluids is complex because, unlike Newtonian fluids it involves many parameters, therefore it is important to describe the rheology and rheological models of non-Newtonian fluids. The rheological model that is presented is the Herschel-Bulkley model, because it satisfies yield pseudoplastic, Bingham plastic and power-law fluids sometimes known as pseudoplastic fluid. In its simplest form it reverts to the Newtonian model.

The relevant non-Newtonian Reynolds number models for open channel flow are presented and they will be evaluated in Chapter 4.

2.2 FLOW REGIMES

For any fluid flowing through an open channel or a pipe conduit, there are two distinct types of flow that may be observed, namely laminar and turbulent flow. These types of flow are explained in the following section.

2.2.1 Laminar flow

In laminar flow the fluid elements flow in an orderly streamline fashion without any macroscopic intermixing with the neighbouring fluid (Bragg & Holland, 1995). This region occurs at low flow rates, high viscosities, or small diameters. Here the viscous forces are dominating. For Newtonian fluids this flow regime obeys Newton's law of viscosity, which says that the shear stress is proportional to the velocity gradient as follows (Bragg & Holland, 1995):

$$\tau = \mu\left(-\frac{du}{dy}\right) \qquad\qquad (2.1)$$

The proportionality constant (μ) is known as the coefficient of dynamic viscosity of the fluid.

2.2.2 Turbulent flow

In turbulent flow the fluid elements flow randomly thus mixing with the neighbouring fluid (Bragg & Holland, 1995). This causes properties such as pressure and the velocity to fluctuate at each location of the conduit (Bragg & Holland, 1995).

2.2.3 Laminar-turbulent transition

This is a region where the states are mixed, i.e., some of the fluid particles have laminar flow behaviour and some have turbulent flow behaviour. This is an unstable region and is called the transition zone.

2.2.4 Reynolds number

Osborne Reynolds was the first to study these flow regimes in 1883 and made measurements with different Newtonian fluids in pipes of various diameters (Bragg & Holland, 1995). He showed that the transition from laminar to turbulent flow occurs at a critical value of the quantity $\rho Vd/\mu$, which is known today as the Reynolds number. By definition it is a ratio of inertial forces to the viscous forces and is defined as follows:

$$Re = \frac{\rho VD}{\mu} \tag{2.2}$$

Under normal circumstances the laminar-turbulent transition occurs at a Reynolds number of about 2100 for Newtonian fluids flowing in pipes. For values less than 2100 the flow is said to be laminar, and for values more than 2100 the flow is said to be turbulent.

For open-channel flow, the diameter (D) in the Reynolds number equation becomes four times the hydraulic radius ($4R_h$), where R_h is the ratio of the channel area to the wetted perimeter (Chow, 1959). In open channel flow Chow (1959) observed that the transition occurs between a Reynolds number of 2000 and 4000.

2.3 FLUID BEHAVIOUR

Any fluid can behave either as a Newtonian or non-Newtonian fluid. In this section the fluids that are single-phase liquids and homogenous mixtures will be described.

2.3.1 Newtonian fluid behaviour

If a small sample of fluid can be sandwiched between two parallel plates that are at a distance dy apart and the force F is applied to the other upper plate as shown in Figure 2-1, the fluid is deformed until the internal forces balance the applied force (Bragg & Holland, 1995). The fluid will be subjected to a shearing deformation and the force applied will be a shear force. This shear force divided by the sheared area gives a shear stress. For the fluid to sustain a shear stress it should be continuously deformed, i.e., it should flow (Bragg & Holland, 1995). The rate of change of deformation is called the shear rate. The fluid is Newtonian if the shear stress has a linear relationship with a shear rate. This relationship obeys Newton's law of viscosity, which is:

$$\tau = \mu\left(-\frac{du}{dy}\right)$$

(2.1)
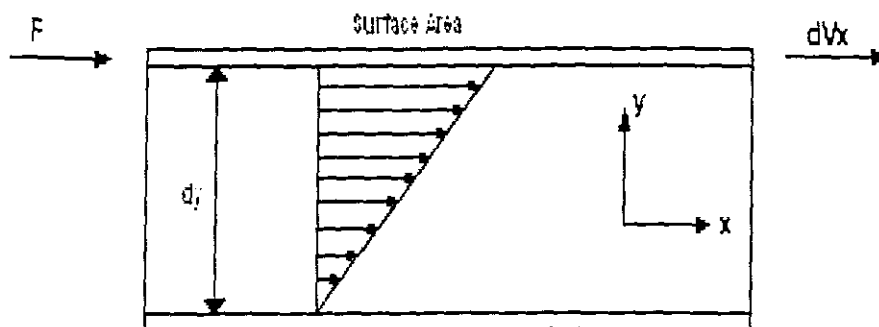
Figure 2-1. Schematic diagram of one directional shearing flow (Chhabra & Richardson, 1999)

A plot of shear stress versus shear rate will give a straight line passing through the origin. This plot is called a rheogram as shown in Figure 2-2, and the slope of it is called viscosity.

2.3.2 Non-Newtonian fluid behaviour

The fluid becomes non-Newtonian if the relationship between a shear stress and a shear rate is not linear or does not start from the origin. There are a number of relationships that characterise the non-Newtonian fluid behaviour, some of them are time-dependent and some are time-independent.

Figure 2-2 depicts some of these relationships (Chhabra & Richardson, 1999). The flow behaviour depicted in this figure is only for time-independent fluid, meaning that the fluid behaviour does not change with time.

Shear Rate
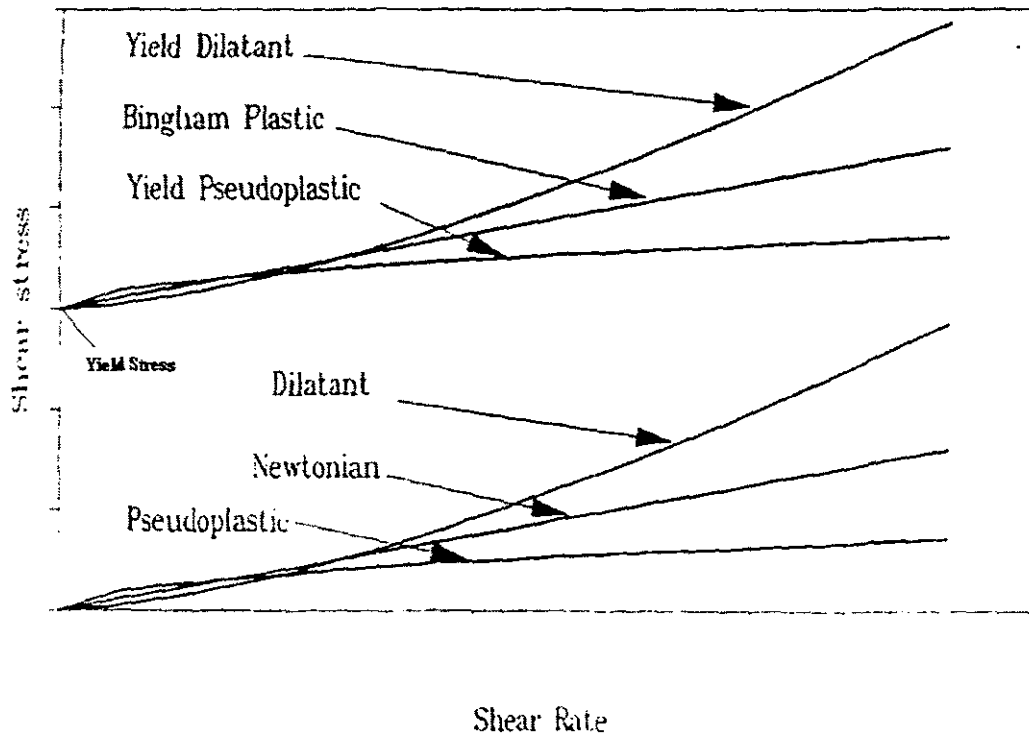
Figure 2-2. Rheological models

2.3.3 Non-Newtonian models (Chhabra & Richardson, 1999)

The models used to classify the slurries used in this study are: power-law or pseudoplastics, Bingham plastic, yield pseudoplastic or Herschel-Bulkley fluids models. These models are rheological models, therefore it is important to first define rheology. Rheology is the science of flow and deformation of matter.

2.3.3.1 Power-law model

These fluids are characterised by an apparent viscosity which decreases with an increase in shear rate (Chhabra & Richardson, 1999). The equation for this behaviour is as follows:

$$\tau = K\dot{\gamma}^{n} \tag{2.3}$$

The two parameters K and n are empirical curve fitting parameters, K is a fluid consistency index and n is a flow behaviour index.

If n< 1 the fluid exhibits shear thinning behaviour.
If n> 1 the fluid exhibits shear thickening behaviour.

The equation forms a curve that starts at the origin.

2.3.3.2 Bingham plastic model

The Bingham plastic model can be described as follows:

$$\tau = \tau_y + K\dot{\gamma} \tag{2.4}$$

The equation is linear and the y-intercept is the yield stress. This equation is the simplest to characterise a fluid with a yield stress (Chhabra & Richardson, 1999).

2.3.3.3 Herschel-Bulkley model

If a yield stress fluid exhibits a non-linear relationship, then the Herschel-Bulkley model can be used. The equation is as follows:

$$\tau = \tau_y + K\dot{\gamma}^n \tag{2.5}$$

This is mathematically more complex than the other models but it adequately describes kaolin suspensions (Slatter, 1994).

This model can easily accommodate other models described previously.

For example: If τ_y =0, the equation reverts to the power-law model.

If n =1, the equation reverts to the Bingham plastic model.

If n=1 and τ_y =0, the equation reverts to the Newtonian fluid equation.

2.3.4 Rheometry for non-Newtonian models

The rheological characterisation of non-Newtonian fluids is far from being easy (Chhabra & Richardson, 1999). The problem is that when one tries to measure the shear rate, it should be constant throughout the measuring system employed. When using the rotary viscometer, the shearing gap of the cone and the plate and bob and cup systems are generally small enough to overcome this, but when suspensions are tested, the particles of suspensions often prohibit the use of narrow gaps (Chhabra & Richardson, 1999).

Rheometry or viscometry deals with the establishment of a relationship between shear stress and shear rate. This is required to establish the rheological parameters such as τ_y, K, and n, which are used in relevant rheological models for the specific fluid.

2.3.4.1 Tube viscometry

Although there are advantages in using rotational viscometers, certain authors prefer tube viscometers for non-Newtonian slurries (Slatter, 1994). Lower shear rates can be obtained when using rotational viscometers; tube viscometers, on the other hand, have the advantage of having a similar geometry to that of a pipeline.

The tube viscometer consists of a fluid flowing in laminar steady flow at constant temperature and with a pressure drop between its ends (Chhabra & Richardson, 1999).

The relationship between the wall shear stress, τ_o, the volumetric flow rate, Q, and the shear stress is as follows:

$$\frac{8V}{D} = \frac{4Q}{\pi R^3} = \frac{4}{\tau_o^3} \int_0^{\tau_o} \tau^2 f(\tau) d\tau \tag{2.6}$$

with $\tau_o = \frac{R}{2}\left(-\frac{\Delta p}{L}\right)$, where $-\frac{\Delta p}{L}$ is the magnitude of the pressure drop per unit length of the tube.

And the shear stress at any radius r is: $- \tau = \frac{r}{2}\left(-\frac{\Delta p}{L}\right)$ \tag{2.7}

A graph of $Q/\pi R^3$ vs. τ_o gives a unique line for given materials for all values of R and ($-\Delta p/L$) (Chhabra & Richardson, 1999).

The problem with the tube viscometry is that 8V/D is not a true shear rate but the wall shear rate for Newtonian fluids, therefore this pseudo shear rate (8V/D) has to be corrected to obtain the true shear rate.

For the flow curves of unknown form, Equation 2.6 yields, after some mathematical manipulation, the following equation:

$$\left(-\frac{du}{dr}\right)_o = \frac{8V}{D}\left(\frac{3}{4} + \frac{1}{4}\frac{d\log(8V/D)}{d\log\tau_o}\right) \tag{2.8}$$

Various forms of this equation are used, a common form being the Rabinowitsch-Mooney equation, which is as follows:

$$\dot{\gamma}_o = \left(-\frac{du}{dr}\right)_o = \frac{8V}{D}\left(\frac{3n'+1}{4n'}\right) \qquad (2.9)$$

Where:

$$n' = \frac{d\log(\tau_o)}{d\log(8V/D)} \qquad (2.10)$$

On the logarithmic plot of τ_o versus $8V/D$, for the laminar flow region, n' is the slope of the tangent line of the graph.

The Rabinowitsch-Mooney correction factor for the pipe data can be summarised as follows (Chhabra & Slatter, 2001):

- From the tube viscometer measurement of V and Δp calculate $\tau_o = \dfrac{D\Delta p}{4L}$ and

  $\dfrac{8V}{D}$

- Plot $\tau_o = \dfrac{D\Delta p}{4L}$ versus $\dfrac{8V}{D}$ on logarithmic co-ordinates for different tube diameters that should coincide in the laminar region.

- Fit a mathematical function to the laminar flow data and obtain the first derivative of the equation. This will describe the slope of the equation (n').

- Calculate the value of $\dot{\gamma}_o$ using Rabinowitsch-Mooney factor in Equation 2.9

- Plot τ_o versus $\dot{\gamma}_o$ on arithmetic or logarithmic co-ordinates as required.

- Any non-Newtonian model can now be fitted to describe the curve most adequately. This could be Herschel-Bulkley (yield pseudoplastic), Bingham plastic or power law (pseudoplastic) model.

- From these models, rheological parameters such as τ_y, K, and n can be obtained.

2.3.4.2 The Slatter approach to rheological classification of tube viscometer data

The following approach was developed by Lazarus and Slatter (1988).

$$\frac{32Q}{\pi D^3} = \frac{8V}{D} = \frac{4n}{K^{\frac{1}{n}}\tau_o^3}(\tau_o - \tau_y)^{\frac{1+n}{n}}\left(\frac{(\tau_o - \tau_y)^2}{1+3n} + \frac{2\tau_y(\tau_o - \tau_y)}{1+2n} + \frac{\tau_y^2}{1+n}\right) \qquad (2.11)$$

When using this equation, one has to guess and optimise the rheological parameters such as τ_y, K, and n in calculating the value of 8V/D. This calculated value is then compared with the measured value of 8V/D by using the following method:

Equation 2.11 can be used to rheologically classify a fluid. The method is as follows:

- Plot the laminar flow data of $\tau_o = \dfrac{D\Delta p}{4L}$ versus $\dfrac{8V}{D}$ of N data points obtained from a tube viscometer for different tube diameters. The data points of all the tube diameters should coincide in the laminar region.

- Calculate the theoretical values $\dfrac{8V}{D}$ of the N data points using Equation 2.11 while assuming the values of τ_y, K, and n.

- These values for τ_y, K, and n must be optimised by minimising the sum of the mean error square of the N data points.

$$E = \sum_{i=1}^{N} \left(\frac{\left(\frac{8V}{D}\right)_{i\,obs} - \left(\frac{8V}{D}\right)_{i\,calc}}{\left(\frac{8V}{D}\right)_{i\,obs}} \right)^2$$ (2.12)

For a Herschel Bulkley fluid τ_y, K, and n will be optimised, for a Bingham fluid n will be 1 and the other parameters optimised, for a power law τ_y will be zero and other parameters optimised.

2.3.4.3 Errors in tube viscometry

- Wall slip

Wall slip occurs when the layers of particles near the wall are more dilute than the bulk flow (Heywood & Richardson, 1978). As a result the viscosity near the wall will be reduced and apparent slip will occur. Chhabra & Richardson (1999) warn that serious errors could occur when wall slip is not accounted for.

To account for the wall slip, more than one diameter tube should be used. Their laminar flow data should coincide if there is no wall slip. If they do not coincide then the slip velocity must be calculated for each tube and deducted from the measured mean velocity (Heywood & Richardson, 1978).

- Entrance and exit losses

It is important that the entrance and exit losses in the tubes that are used are minimised. This is possible by making sure that the flow is fully developed before differential pressure readings are taken. Slatter (1994) used 50 pipe diameters unobstructed flow before and after the test sections.

2.4 OPEN-CHANNEL FLOW

2.4.1 Newtonian open-channel flow

The flow of water in a conduit may be either open channel flow or pipe flow. These two kinds of flow are similar in many ways but differ in one important respect, which is in open channel flow there is a free surface (Chow, 1959).

Despite the similarities between these two kinds of flow, it is much more difficult to solve problems of flow in open channels than in pressure pipes (Chow, 1959). Flow conditions in open channels are complicated by the fact that the position of the free surface is likely to change with respect of time and space and also by the fact that the depth of flow, the discharge and the slopes of the channel bottom and of the free surface are interdependent (Chow, 1959). The following table shows the difference between the pipe flow and the open-channel flow (Chanson, 1999).

Table 2-1. Difference between pipe flow and open-channel flow

	PipePipe flow	Open-channel flow
Flow driven	Pressure	Gravity (i.e. potential energy).
Flow cross-section	Known (fixed by pipe geometry).	Unknown in advance because the flow depth is unknown before hand.
Characteristic flow geometry	Velocity deduced from the continuity equation.	Flow depth and velocity deduced by simultaneously solving the continuity and the momentum equation.
Specific boundary conditions		Atmospheric pressure at the flow free surface.

Lau (1979) stated that there are three factors affecting the flow in the flume namely: the roughness of the flume material, hydraulic radius, and the hydraulic gradient of the flume.

2.4.2 Advantages and disadvantages of an open-channel flow (Lau, 1979)

The most attractive advantages of the flumes are their low capital cost and that they require negligible routine maintenance. Other advantages are:

- They are flexible not only in installation but also in the kinds of material that can be transported.

- They require minimal or zero power.

- They are safe to be used.

The disadvantages are that the gradient of the flume must be in favour of the transported load and that there must be a plentiful supply of water.

2.4.3 Types of flow in open channels

Open-channel flow can be classified into many types and described in various ways as follows (Chow, 1959):

Steady and unsteady flow: - Open-channel flow is said to be steady if the depth of flow does not change with time. The flow is unsteady if the depth changes with time.

Uniform and varied flow: - Open-channel flow is said to be uniform if the depth of flow is the same at every section of the channel. The flow is varied if the depth of flow changes along the length of the channel.

In most open channel problems it is necessary to study the flow behaviour only under steady and uniform conditions (Chow, 1959).

2.4.4 The relationship between Reynolds number and friction factor

The laminar, transition, and turbulent flow of open channel can be differentiated from one another by expressing them on a diagram that shows the relationship between Reynolds number and friction factor (Chanson, 1999). This diagram is known as the "Moody diagram" after Moody (1944), and was developed for the flow in pipes as shown in Figure 2-3.
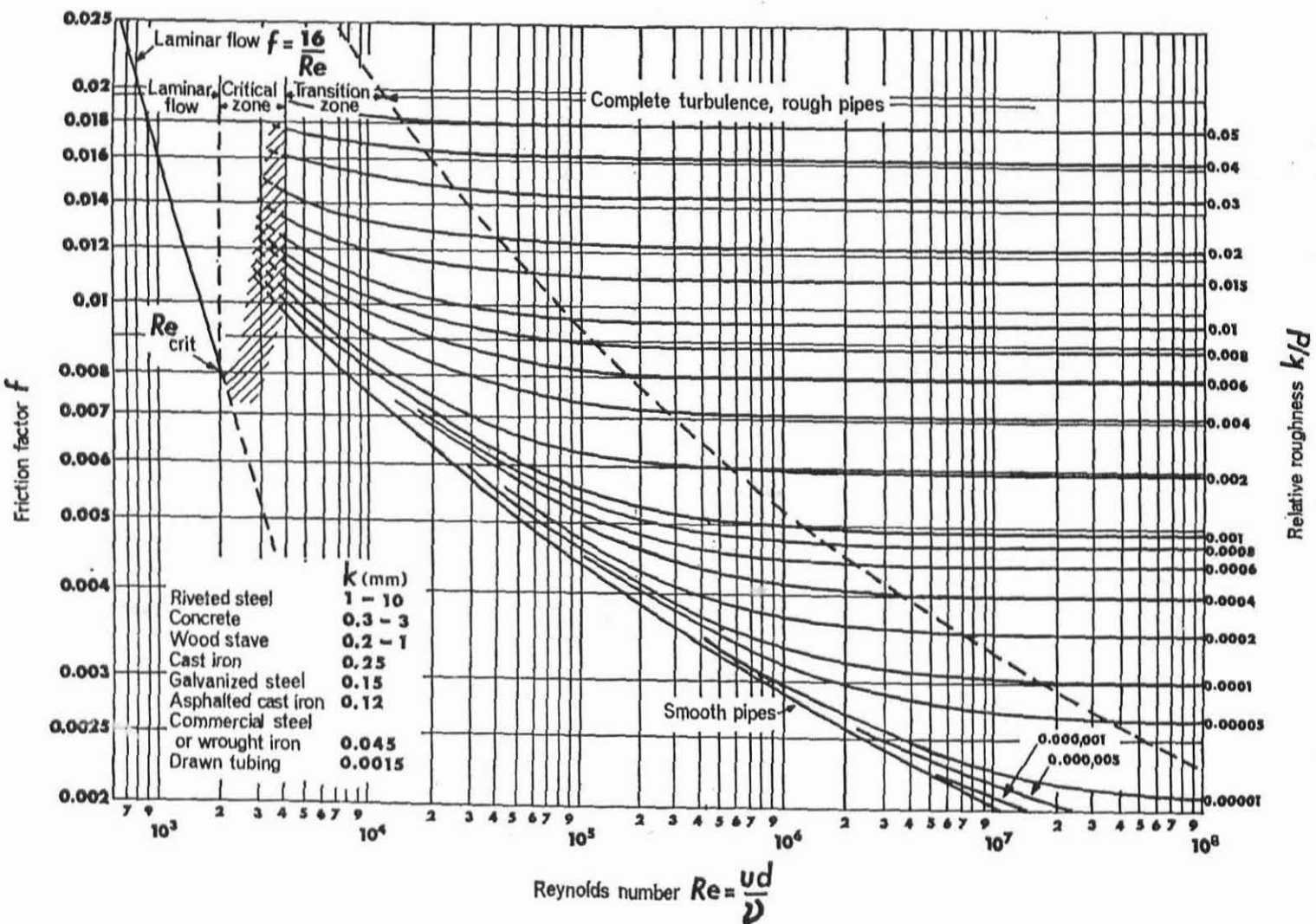
Figure 2-3. Moody diagram (Chanson, 1999)

Laminar flow $f = \dfrac{16}{Re}$

Laminar flow | Critical zone | Transition zone | Complete turbulence, rough pipes

Re_{crit}

Friction factor f

	k (mm)
Riveted steel	1 – 10
Concrete	0.3 – 3
Wood stave	0.2 – 1
Cast iron	0.25
Galvanized steel	0.15
Asphalted cast iron	0.12
Commercial steel or wrought iron	0.045
Drawn tubing	0.0015

Smooth pipes

0.000,001
0.000,005

Reynolds number $Re = \dfrac{ud}{\nu}$

Relative roughness p/k

The Reynolds number is the ratio of inertial forces to the viscous forces and is calculated as follows for the pipe flow:

$$Re = \frac{\rho VD}{\mu} \qquad (2.2)$$

For open-channel flow D is replaced by hydraulic radius (R_h), which is defined as the ratio of the cross-sectional area of the flume to the wetted perimeter of the flume (Chow, 1959 and Chanson, 1999).

$$R_h = \frac{A}{P_w} \qquad (2.13)$$

From Equation 2.2, d becomes: $D = 4R_h$ \qquad (2.14)

Then the Reynolds number for Newtonian open-channel flow becomes:

$$Re = \frac{4\rho VR_h}{\mu} \qquad (2.15)$$

The friction factor in the Moody diagram can be calculated using the Darcy-Weisbach formula for pipes, which is as follows (Chow, 1959):

$$h_f = \lambda \frac{L}{D} \frac{V^2}{2g} \qquad (2.16)$$

For open-channel flow this becomes:

$$h_f = \lambda \frac{L}{4R_h} \frac{V^2}{2g} \qquad (2.17)$$

The energy gradient is expressed as:

$$S = \frac{h_f}{L} \tag{2.18}$$

Then Equation 2.16 can be written in terms of the Darcy-Weibasch friction factor as:

$$\lambda = \frac{8SR_h g}{V^2} \tag{2.19}$$

The Darcy friction factor is four times the Fanning friction factor, therefore the above equation can be written in terms of the Fanning friction factor as:

$$f = \frac{2SR_h g}{V^2} \tag{2.20}$$

For the laminar flow the data can be defined by the following general equation (Chow, 1959):

$$f = \frac{16}{Re} \tag{2.21}$$

For the smooth wall turbulent flow, the friction factor can be calculated by the Blasius equation as follows (Chanson, 1999):

$$f = \frac{0.079}{Re^{0.25}} \tag{2.22}$$

2.4.4.1 Colebrook-White equation

The friction factor can also be estimated from the Colebrook-White equation for pipes as follows (Featherstone & Nalluri, 1995):

$$\frac{1}{\sqrt{f}} = -2\log\left(\frac{k_s}{3.71D} + \frac{2.51}{Re\sqrt{f}}\right) \tag{2.23}$$

This can be modified for open channels to become (Chanson, 1999):

$$\frac{1}{\sqrt{f}} = -2\log\left(\frac{k_s}{14.84R_h} + \frac{2.51}{Re\sqrt{f}}\right) \tag{2.24}$$

2.4.5 The flow of fluid down an inclined plane

The following derivation is for smooth open channel flow for a wide channel (Chhabra & Slatter, 2001)

By writing the momentum equation over a small control volume,
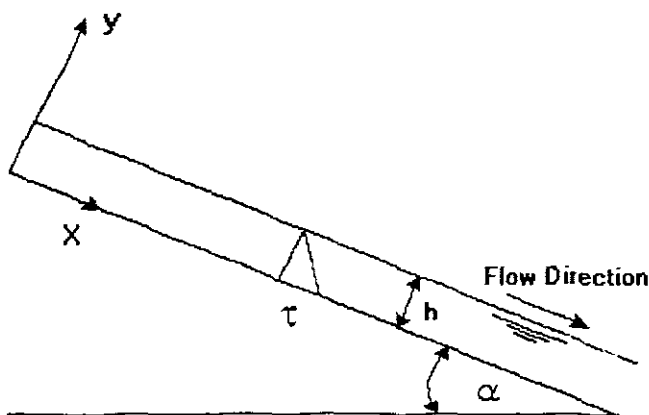
Figure 2-4. Flow down an inclined plane

$$\tau_{yx} = \rho g(h - y)\sin\alpha \qquad (2.25)$$

Since τ is in the direction of flow, Equation 2.1 can be written as:

$$\tau_{yx} = \mu \frac{dU_x}{dy} \qquad (2.26)$$

$$\therefore \frac{dU_x}{dy} = \left(\frac{\rho g \sin\alpha}{\mu}\right)(h - y) \qquad (2.27)$$

Integrate with respect to y gives:

$$U_x = \frac{\rho g \sin\alpha}{\mu}\left(hy - \frac{y^2}{2}\right) + C \qquad (2.28)$$

Where C is evaluated by applying the boundary condition at $y = 0$, $U_x = 0$, therefore $C = 0$

$$\therefore U_x = \frac{\rho g \sin\alpha}{\mu}\left(hy - \frac{y^2}{2}\right) \qquad (2.29)$$

The volumetric flow rate per unit width is:

$$\frac{Q}{B} = \int_0^h U_x dy = \frac{\rho g \sin\alpha}{\mu}\int_0^h\left(hy - \frac{y^2}{2}\right)dy \qquad (2.30)$$

$$= \frac{\rho g \sin\alpha}{\mu}\left(\frac{hy^2}{2} - \frac{y^3}{6}\right)_0^h = \frac{\rho g \sin\alpha}{\mu}\left(\frac{h^3}{2} - \frac{h^3}{6}\right) = \frac{\rho g \sin\alpha}{3\mu}h^3 \qquad (2.31)$$

The average velocity is the ratio of volumetric flow rate to the area of the channel as:

$$V = \frac{Q}{A} \qquad (2.32)$$

The wall shear stress can be calculated as follows (Haldenwang, 2003):

$$\tau_o = \rho\, gR_h \sin\alpha \qquad (2.33)$$

2.4.6 Open channel shapes and their formulae

The most commonly found open channel shapes are summarised in Table 2-2 below (Chanson, 1999).

Table 2-2. Open channel shapes and their characteristics

Channel shape	Flow depth h	Free-surface width, B	Cross-section Area A	Wetted perimeter, P	Hydraulic radius, R_h
Rectangular	h	B	Bh	B+2h	$\dfrac{Bh}{B+2h}$
Semi-circular, diameter D	$\dfrac{D}{4}\left(1-\cos\dfrac{\alpha}{2}\right)$	$D\sin\dfrac{\alpha}{2}$	$\dfrac{D^2}{8}(\alpha-\sin\alpha)$	$\alpha\dfrac{D}{2}$	$\dfrac{1}{4}D\left(1-\dfrac{\sin\alpha}{\alpha}\right)$
Trapezoidal, base width w	h	$w+2h\cot\alpha$	$(B+2h\cot\alpha)h$	$w+\dfrac{2h}{\sin\alpha}$	$\dfrac{w+2h\cot\alpha}{w+\dfrac{2h}{\sin\alpha}}$

2.4.7 Effect of gravity

The effect of gravity upon the state of flow is represented by the ratio of inertial forces to gravity forces (Chow, 1959). The Froude number gives this ratio after an English hydrodynamist Froude (1810-1879) (Chanson, 1999). The Froude number is expressed as follows:

$$Fr = \frac{V}{\sqrt{gd}} \tag{2-34}$$

where d is the hydraulic depth defined as the cross-sectional area of water normal to the direction of flow divided by the width of the free surface (Chow, 1959). For the rectangular channel this is equal to the depth of the flow (Chow, 1959 and Chanson, 1999).

For other channel shapes the Froude number is usually defined as:

$$Fr = \frac{V}{\sqrt{g\frac{A}{B}}} \tag{2-35}$$

where A is the cross-sectional area and B is the free surface width (Chanson, 1999).

If the Froude number is equal to unity, the flow is said to be in a critical state (Chow, 1959). This is an unstable region and should be avoided.
If the Froude number is less than unity, the flow is said to be sub-critical or tranquil. Here the gravity forces are dominating (Chow, 1959).

If the Froude number is greater than unity, then the flow is said to be supercritical. Here the inertial forces play a greater role in the state of flow and the velocity is high.

2.4.8 Effect of shape

The effect of shape on Newtonian open channel flow was first researched by Straub *et al.* (1958) where they studied open channel flow at low Reynolds numbers. They argue that the channel shape is important in laminar flow, but its entire effect may be determined theoretically. They defined friction factor for laminar flow as:

$$f = \frac{K}{Re} \tag{2.36}$$

They stated the value of K depends on the channel shape and were able to produce different values of K for different flume shapes. The relationship they proposed for K is as follows:

$$K = \frac{24}{\left(1 + \frac{h}{0.5B}\right)^2} \frac{1}{\left(1 - \frac{192}{\pi^5}\frac{h}{0.5B}\sum_{n=0}^{\infty}\frac{1}{(2n+1)^5}\tanh\left(\left(\frac{2n+1}{2}\right)\left(\frac{\pi 0.5B}{h}\right)\right)\right)} \tag{2.37}$$

For the rectangular channel shape, they found K to be between 15/Re and 20/Re. For the semi-circular channel shape, they found K as 64/Re, and for the trapezoidal channel shape, they found K to be 60/Re.

2.4.9 Laminar-turbulent transition of Newtonian open-channel flow

Just like in pipes, the laminar-turbulent transition in open channels does not occur at one point but over a range of Reynolds numbers. Straub *et al.* (1958) established that transition in open channels occurs at slightly higher Reynolds numbers than in closed pipes, depending exactly on the effect of channel shape. They found that the transition value ranges from 2000 to more than 3000.

Chanson (1999) published the Moody diagram for open-channel flow that has the transition zone ranging between the Reynolds number 2000 and 4000.

2.5 NON-NEWTONIAN OPEN-CHANNEL FLOW

There has been very little work done on non-Newtonian open-channel flow. This section presents the literature available on the flow of non-Newtonian fluids in open channels with the emphasis on laminar and the transitional flow.

2.5.1 Laminar flow

Some work has been presented on laminar flow of non-Newtonian fluids in open channels by Kozicki and Tiu (1967), Hao and Zhenghai (1982), Coussot (1994 and 1997), Abulnaga (1997), and Haldenwang (2002 and 2003).

Kozicki and Tiu (1967) presented some work that incorporates the effect of shape of the channel, but they did not verify their work experimentally. Coussot (1994) and Haldenwang (2003) referred to their work but could not comprehensively verify their work experimentally.

The work done by these researchers mentioned above is discussed as follows:

2.5.1.1 Work done by Kozicki and Tiu

Kozicki and Tiu (1967) presented analytical work on the effect of cross-sectional shape in laminar flow of non-Newtonian fluids in open channels.

2.5.1.1.1 Effect of shape

Effect of the cross-sectional shape of the channel was first defined by Straub *et al.* (1958) for Newtonian fluids in their open channel flow investigation. Kozicki and Tiu (1967) extended their work to non-Newtonian open channel flow.

Kozicki and Tiu (1967) proposed a general method for predicting the flow rate and the maximum velocity in the isothermal steady, uniform, and laminar flow of any incompressible, time-independent non-Newtonian fluids in straight open channels of arbitrary cross-section. They said this method requires knowledge of two geometric coefficients (a and b) and a function of a shear stress used to characterise the behaviour of the fluid model.

They evaluated the geometric coefficients for rectangular, semi-elliptical, triangular and semi-circular channel shapes. For the semi-circular channel shape they extended the geometric constants of a closed circular pipe to open channel. They found the numerical values of these geometric coefficients to be 0.25 and 0.75 for a and b respectively. These values are valid only for flow depth/diameter (h/B) ratios of up to 0.55 (Sestak, 1974). For the rectangular channel shape they evaluated these geometric coefficients as follows:

$$a = 0.5 \left(\frac{\lambda}{1+\lambda} \right)^{2} \left[1 - \frac{32}{\pi^{3}} \sum_{0}^{\infty} \left(\frac{(-1)^{n}}{(2n+1)^{3}} \right) \left(\frac{1}{\cosh \frac{(2n+1)}{2} \pi \lambda} \right) \right]^{-1} \qquad (2.38)$$

With:

$$\lambda = \frac{B}{h} \qquad (2.39)$$

and

$$b = a(3\varphi - 1) \qquad (2.40)$$

With:

$$\varphi = \frac{\left[1 - \frac{32}{\pi^3}\sum_0^\infty\left(\frac{(-1)^n}{(2n+1)^3}\right)\left(\frac{1}{\cosh\left(\frac{(2n+1)}{2}\pi\lambda\right)}\right)\right]}{\left(1 - \frac{192}{\pi^5}\frac{1}{\lambda}\sum_0^\infty\left(\frac{1}{(2n+1)^5}\right)\tanh\left(\frac{(2n+1)}{2}\pi\lambda\right)\right)} \qquad (2.41)$$

It can be seen that the geometric coefficients of the rectangular channel shape are mathematically complex.

Kozicki and Tiu (1967) used these geometric coefficients they evaluated to derive Reynolds numbers for different non-Newtonian fluid models such as the power law, Bingham, Ellis, meter, and Reiner-Rivlin models. In this thesis, two of these Reynolds number models will be tested, namely, the power law and Bingham models because they can be used for testing CMC solution and bentonite suspension.

2.5.1.1.2 Kozicki and Tiu's Reynolds number for power law fluids

They derived the following Reynolds number for power law fluids which incorporates the geometric shape factors (a and b) as follows:

$$Re = \frac{\rho V^{(2-n)} R_h^n}{2^{n-3} K \left(\dfrac{a + bn}{n} \right)^n}$$ (2.42)

The shape factors (a and b) account for the variation in aspect ratio as the depth increases.

2.5.1.1.3 Kozicki and Tiu's Reynolds number for the Bingham fluids

For the Bingham fluids they derived the following Reynolds number, which also incorporates the shape factors.

$$Re = \frac{4R_h V \rho}{K} \left[\frac{1}{a+b} - \frac{1}{b} \left(\frac{\tau_y}{\tau_o} \right) + \frac{a}{b(a+b)} \left(\frac{\tau_y}{\tau_o} \right)^{\left(1 + \frac{b}{a}\right)} \right]$$ (2.43)

With wall shear stress as:

$$\tau_o = \rho g R_h \sin \alpha$$ (2.44)

2.5.1.2 Work done by Hao and Zhenghai

Hao and Zhenghai (1982) studied the flow of yellow river in China. They mixed sediment particles of $d_{90} = 0.063$ mm, $d_{50} = 0.042$ mm, and $d_{10} = 0.01$ mm with water to form a mud or a slurry. They tested the rheological characteristic of the mud with a capillary viscometer and classified it as a Bingham fluid. They conducted the flume tests in a 43 m long concrete rectangular flume with only one slope and width.

They developed the Reynolds number model for the laminar flow, which is only valid for the Bingham fluids as follows:

$$Re = \frac{4R_h \rho V}{K + \left(\dfrac{\tau_y R_h}{2V} \right)}$$
(2.45)

They defined the friction factor as follows:

$$f = \frac{2gR_h \sin\alpha}{V^2}$$
(2.46)

2.5.1.3 Work done by Coussot

Coussot (1994) studied the steady laminar flow of concentrated mud suspension in open channels. He used kaolin suspension, which has a solid particle diameter of less than $40\mu m$. He characterised the clay suspension as a Herschel-Bulkley fluid and for various concentrations tested he fixed the value of n to 0.333.

From this he defined the Herschel-Bulkley number as follows:

$$H_b = \frac{\tau_y}{K} \left(\frac{h}{V} \right)^n$$

(2.47)

With this Herschel-Bulkley number he was able to propose the empirical expressions of the average wall shear stress for both rectangular and trapezoidal channel shapes as follows:

$$\tau_o = \tau_y \left(1 + a(H_B)^{(-0.9)} \right)$$
(2.48)

with "a" being the shape factor and differing for each channel shape.

For a rectangular channel shape he defined "a" as follows:

$$a = 1.93 - 0.43\left(\arctan\left(\left(\frac{10h}{B} \right)^{20} \right) \right) \qquad (2.49)$$

He found this to be valid only for (h/B) ratio less than one (h/B<1). He claimed that this equation could predict his experimental results to within an error range of 30%.

For the trapezoidal channel he defined the shape factor "a" as follows:

$$a = 1.93 - 0.6\left(\arctan\left(\left(\frac{0.4h}{B} \right)^{20} \right) \right) \qquad (2.50)$$

He claimed this to be valid for h/B<4 and could predict all his experimental results to within an error range of 35%.

Rewriting Equation 2.48 in terms of H_B yields the following equation:

$$H_B = \left(\frac{\frac{\tau_o}{\tau_y} - 1}{a} \right)^{-\frac{1}{0.9}} \qquad (2.51)$$

Coussot (1994) stated these empirical formulae are only valid for the Herschel-Bulkley fluids and that the value of n should be fixed to 0.333. With these restrictions these formulae can be used to compute the normal depth of any flow in the rectangular and trapezoidal channels. To do so one has to equate 2.47 to 2.51, with wall shear stress being:

$$\tau_o = \rho g R_h \sin\alpha \qquad (2.33)$$

2.5.1.4 Work done by Abulnaga

Abulnaga (1997) studied homogenous slurries that were the copper tailings from a Peruvian copper plant. He was asked to provide a design protocol for a tailings launder. He characterised the slurry as a Bingham fluid.

He argued for the flow of this Bingham slurry in a tailings launder, there are two numbers that need to be calculated and they are the Reynolds number and the plasticity number.

In the absence of well-defined models for the friction losses of Bingham slurries, Abulnaga (1997) proposed a methodology to modify some of the equations of full pipe flows to open channel flow by expressing the Reynolds number and Hedström number in terms of the hydraulic radius. He expressed the Reynolds number similar to that of Newtonian fluids as follows:

$$Re = \frac{4R_h V \rho}{K} \qquad (2.52)$$

and the plasticity number as follows:

$$P_L = \frac{\tau_o 4R_h}{KV} \qquad (2.53)$$

The Hedström number is the product of the plasticity and Reynolds number as follows:

$$He = \frac{16R_h^2 \rho \tau_o}{K^2} \qquad (2.54)$$

To calculate the friction factor he modified the Buckingham equation of laminar pipe flow to open channel flow as follows:

$$f_L = \frac{16}{Re}\left(1 + \frac{He}{6Re}\right)$$ (2.55)

He also suggested that the stability of the flow should be checked by avoiding the critical flows at Froude number range between $0.8 < Fr < 1.5$.

2.5.1.5 Work done by Haldenwang

Haldenwang *et al.* (2002) studied the laminar flow of non-Newtonian fluids in rectangular open channels. He studied different concentrations of CMC solutions, kaolin and bentonite suspensions. He characterised the CMC solution as a power law fluid, the kaolin suspension as a Herschel-Bulkley fluid and bentonite suspension as a Bingham fluid. He studied the flow of these non-Newtonian fluids in three different sizes of the rectangular flumes, which were 75 mm, 150 mm, and 300 mm wide. The 75 mm flume was 4.5 m long and the 150 mm and 300 mm flumes were 10 m long. He chose five different flume slopes, which were: 1, 2, 3, 4 and 5 degrees.

He modified the Slatter Reynolds number for non-Newtonian pipe flow to open channel flow by substituting the pipe diameter with hydraulic radius as follows:

$$Re_2 = \frac{8\rho V^2}{\tau_y + K\left(\frac{2V}{R_h}\right)^n}$$ (2.56)

This equation adequately predicted his experimental results for the Herschel-Bulkley fluids.

For power-law fluids the equation reduces to:

$$Re_2 = \frac{8\rho V^2}{K\left(\dfrac{2V}{R_h}\right)^n}$$ (2.57)

For the Bingham fluids the equation reduces to:

$$Re_2 = \frac{8\rho V^2}{\tau_y + K\left(\dfrac{2V}{R_h}\right)}$$ (2.58)

This Reynolds number adequately predicted the laminar flow of all the non-Newtonian fluids he chose for all his experimental results.

2.5.2 The laminar-turbulent transition

Very few researchers have studied the laminar–turbulent transition for non-Newtonian fluids in open channels. Some of them suggested that the laws of pipe flow could be applied to open channel flow (Wilson, 1991).

2.5.2.1 Work done by Hao and Zhengai

Hao and Zhenghai (1982) discovered by measuring the flow pulsations with a pressure micro-transducer that the pulsations in the transition region start in the lower regions of the flume and weaken towards the surface. In full turbulence the pulsations reach a maximum over the full depth of the flume.

They found that transition range occurs between Reynolds number 3000 and 5000 for different channel roughnesses and the friction factor ranges from 0.005 to 0.01.

2.5.2.2 Work done by Coussot

Coussot (1997) used the Hanks criteria to derive a formula that can predict the onset of turbulence of mudflow, which he characterised as a Herschel-Bulkley fluid. He did this for infinitely wide channels.

He suggests that the flow becomes turbulent when the depth of flow is larger than:

$$h = \frac{1}{\rho g \sin\alpha} \left[\tau_y + K \left(\frac{404(m+1)\rho(g\sin\alpha)^2}{Kv} \right)^{\left(\frac{1}{2m+1}\right)} \right]$$
(2.59)

with:

$$m = \frac{1}{n}$$
(2.60)

and

$$v = \left[\left(\frac{m}{2m+1} \right)^{\left(\frac{m}{m+1}\right)} - \left(\frac{m}{2m+1} \right)^{\left(\frac{2m+1}{m+1}\right)} \right]$$
(2.61)

2.5.2.3 Work done by Slatter and Wasp

Slatter and Wasp (2000) studied the flow of the laminar /turbulent transition in large pipes where they developed a simple criterion for practical design use, based on a generalised comparison of the most accurate theoretical approaches with each other. This criterion needs a prediction of the critical velocity or the transition velocity.

The critical velocity is determined by normalising the theoretical calculated laminar flow Reynolds number with the experimentally found Reynolds number. This method is called the normalised adherence function and is expressed as:

$$NAF = \frac{Re_{actual}}{Re_{calculated}}$$
(2.62)

The answer in this equation must be one. The transition occurs when the NAF value starts deviating from the value one. Therefore the critical velocity is determined by finding the corresponding velocity value in the experimental data. This critical velocity can be used to compare the accuracy of the theoretical approaches or models.

2.5.2.4 Work done by Haldenwang

Haldenwang (2003) developed a new model for predicting the onset of transition and the onset of turbulence for non-Newtonian open channel flow, and stated that the flow behaviour could be characterised by the Froude number and the Reynolds number.

He first used the Moody diagram to try to establish the relationship between the Reynolds number and the rheological parameters of the fluid tested, but because of the complex nature of many rheological parameters, it was impossible to determine the relationship that included all the parameters.

He then tried to establish one rheological parameter that could characterise the fluids tested, which was the apparent viscosity. This was done for shear rates of 50, 100, 200, and 500s^{-1}. At shear rate of 100s^{-1} the apparent viscosity was found to be similar for all the fluids tested.

He then plotted the Reynolds number against the Froude number to establish the relationship between the two, and discovered that the slope of the channel plays a role.

Therefore the relationship between these two numbers was plotted for 1 to 5 degrees on the same set of axes. On the resulting graph he found the linear relationship between all the slopes.

The linear relationship mentioned above was plotted against the apparent viscosity. From there a critical Reynolds number predicting the onset of transition was established using the Froude number. This Reynolds number was found to have a linear relationship with the Froude number for an apparent viscosity at $100s^{-1}$.

This critical Reynolds number Haldenwang (2003) developed is as follows:

$$Re_c = \frac{200}{\left(\mu_{app(100s^{-1})}\right)^{0.21}} Fr + \frac{71}{\left(\mu_{app(100s^{-1})}\right)^{0.75}} \tag{2.63}$$

To predict the onset of transition the following procedure is followed:

- Select the Reynolds number.

- Calculate f with laminar flow friction factor, which is: $f = 16/Re$.

- Guess the flow depth (h).

- Calculate the velocity V using Equation 2.20.

- Calculate Re_2 using Equation 2.56. This will differ from the selected Reynolds number.

- Optimise the flow depth until the two Reynolds numbers are the same.
- Calculate the Froude number equation using Equation 2.34.

- Calculate the Re transition using Equation 2.62.

- Optimise the flow depth until Re$_2$ is the same as Re$_c$ for onset of transition.

To predict the onset of turbulence, Haldenwang (2003) used the same procedure as for predicting the onset of transition with the only difference being that the linear relationship was at an apparent viscosity at 500s^{-1}. The new critical Reynolds number to predict the onset of turbulence is as follows:

$$Re_c = \frac{105}{\left(\mu_{app(500s^{-1})}\right)^{0.52}} Fr + \frac{108}{\left(\mu_{app(500s^{-1})}\right)^{0.65}}$$
(2.64)

To determine the onset of turbulence, the procedure is as follows:

- Complete the first seven steps used when predicting the onset of transition.

- Calculate the critical turbulent Reynolds number using Equation 2.63.

- Then optimise the depth until Re$_2$ is the same as Re$_c$ for the onset of turbulence.

2.5.2.4.1 Turbulent flow model

Haldenwang (2003) noted that before the onset of full turbulence can be established, the turbulent flow region must be established. He developed the velocity formula for turbulent flow as follows:

$$V = Re_* \left(2.5 \ln \frac{2R_h}{K} - 76.86 \mu_{app\,500} - 9.45 \right)$$
(2.65)

with $Re_* = \sqrt{gh\sin\alpha}$ (2.66)

The fanning friction factor is as follows:

$$f_{turb} = 0.66\left(\frac{2gh\sin\alpha}{V^2}\right)$$ (2.67)

The procedure is as follows:

- Select a depth slightly deeper than the depth obtained at the onset of transition.

- Calculate the hydraulic radius.

- Calculate the velocity Equation 2.64.

- From this velocity, the Reynolds number, Equation 2.56 and the friction factor, Equation 2.67, can be determined.

- Additional depths can be selected and the procedure can be repeated.

2.6 RESEARCH ISSUES IDENTIFIED

The main objective of this thesis is to evaluate if there is a need to include the effect of cross-sectional shape of the channel when predicting the laminar and transitional flow of non-Newtonian fluids in open channels. The models mentioned in tnis review will be used to establish this.

It has been shown that in non-Newtonian open-channel flow in general very little work has been conducted. Most of the previous researchers in non-Newtonian open-channel flow have restricted their research to one fluid, or one slope. or one channel shape.

Haldenwang (2003) did research on various fluids and slopes but did not investigate the effect of shape.

2.6.1 Laminar flow

Only Kozicki and Tiu (1967) and Coussot (1994) have presented some work that includes the effect of channel shape when predicting the laminar flow of non-Newtonian fluids. Kozicki and Tiu (1967) did not verify their analytical work experimentally; they used sets of pipe data. Coussot (1994) based his work on Herschel-Bulkley fluids over a certain range of slopes in rectangular and trapezoidal channels. The work of these researchers needs to be validated experimentally in the case of Kozicki and Tiu (1967) and extended to other channel slopes.

The work other researchers did in laminar flow of non-Newtonian fluids in open channels needs to be evaluated to see if there is a shape effect.

2.6.2 Transitional flow

Few researchers have addressed the transitional flow of non-Newtonian fluids in open channels. None of these researchers included the effect of channel shape, but their work will be evaluated to check if there is a need to include the effect of shape in predicting the transitional flow of non-Newtonian fluids in open channels.

2.7 CONCLUSION

There is sufficient evidence to prove that the field of non-Newtonian open-channel flow has not been extensively studied. This field needs an urgent attention because there is a growing importance of open-channel flow in the mining sector where high concentrations of slurries need to be transported especially over short distances.

This thesis will extend the research in this field by investigating the effect of cross-sectional shape of the channel on laminar and transitional flow. The models presented by the previous researchers will be evaluated with three non-Newtonian fluids that have the rheological characteristics of power law, Bingham, and Herschel-Bulkley fluids in three different channel shapes and over a wide range of slopes (1-5°).

CHAPTER 3

CHAPTER 3
EXPERIMENTAL WORK

3.1 INTRODUCTION

In this chapter the test apparatus used to gather all the data used to evaluate the models described in the literature is described as well as experimental procedures to gather such data.

All the apparatus was designed, built, and commissioned by Haldenwang (2003) at the Cape Technikon Flow Process Research Centre to establish the following:

- Accurate in-line rheological characterisation of all slurries used.

- Testing different slurries in three different flume shapes and half their sizes namely: 300mm rectangular, 300mm semi-circular, and 150mm trapezoidal shapes.

Three pipelines (13mm, 28mm and 80mm diameter) were connected to the test rig to establish the rheology of the slurry tested.

Materials tested for this study were: kaolin suspension (5.4%, 7.2%, and 9% concentration), bentonite suspension (4.6% and 6.2%), and Carboxymethyl cellulose solution (CMC) (1, 2, 3, 4% concentration).

3.2 APPARATUS

The apparatus used to gather the experimental data for this study are: in-line tube viscometers, and flumes of three different shapes and two sizes.
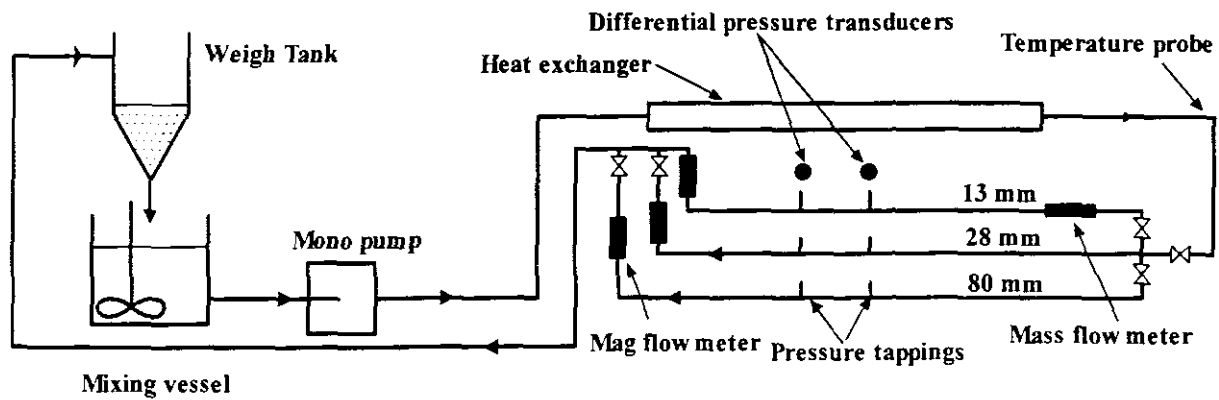
3.2.1 The tube viscometer rig

The tube viscometer rig consists of three PVC parallel tubes of 13mm, 28mm, and 80mm diameter respectively. These tubes are connected to the mixing tank, weigh tank, pumps and the flume with a series of pipelines and valves.

Each tube includes two pressure tappings that are a meter apart to measure the pressure difference along the tube during the test. These two pressure tappings are connected to two differential pressure transducers (DPTs) to measure the differential pressure in that tube.

Each tube also has an in-line magnetic flow meter to measure the flow rates of the flowing fluid. These tubes are fed by a 100mm, 30 bar progressive ca ity positive displacement pump with a variable speed drive. This pump pumps the slurry from the 2500 litres mixing tank with a three-blade impeller connected to an electrical mixer. This mixer should runs continuously during testing to avoid settling of solids. The 13mm tube line also has a mass flow meter, which can also measure the temperature and the density of the slurry being tested. All these flow meters are calibrated with a 500 litres weigh tank mounted over the mixing tank. The inlet to the weigh tank is suspended from the roof beam by means of the load cell. The load cell is used to weigh the load of the fluid diverted from the flow meters.

Along the series of pipelines connecting the mixing tank, pump, and the parallel tubes there is a heat exchanger used to cool the temperature of the slurry that is raised by viscous heating and friction along the pipeline. At the end of the heat exchanger there is a temperature probe used to measure the temperature of the slurry after it has been cooled.

All the outputs from the flow meters, DPTs temperature probe, and the load cell are connected to a data acquisition unit linked to the personal computer (PC). The schematic layout of the rig is depicted in Figure 3-1.

Figure 3-1 The layout of the tube viscometer rig (Haldenwang, 2003)

3.2.2 Pressure Tappings and DPTs

The pressure tappings that are in each of the three lines each has an isolation pod that prevents the solids from entering the DPTs when the differential pressure is measured. A waterline is fed to the pod to flush the system so that no air bubbles can disturb the differential pressure reading during testing. This waterline is also used to flush the DPTs to remove such air bubbles that might result inside the DPTs during testing. The layout of the pressure tapping and the pod are depicted in Figure 3-2.
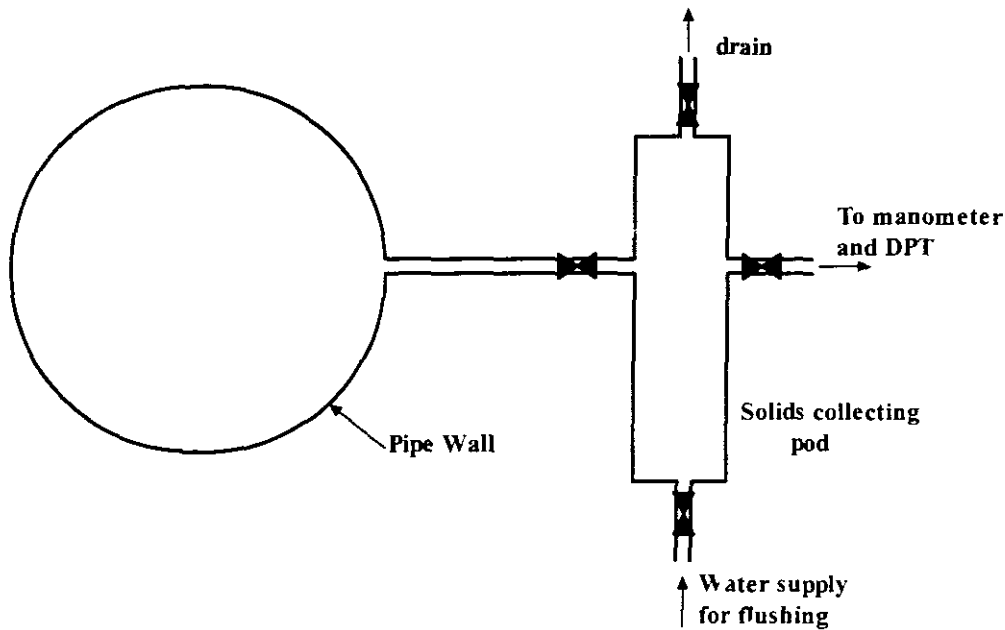
Figure 3-2. Detail of pressure tapping and pod (Haldenwang, 2003)

3.2.3 Weigh tank

The weigh tank, which is a 500 litres plastic container, is mounted over the mixing tank with one end swivelling on the brackets on top of the mixing tank and another end being supported from the roof beam. In the support there is a 500kg load cell connected to the data logger to measure the load of the fluid diverted to the flow meters. The tank is fed by the by-pass connected to the pipeline on the rig. At the bottom of the tank there is a valve that discharges the fluid at the bottom of the tank. The schematic layout of the weigh tank is depicted in Figure 3-3.
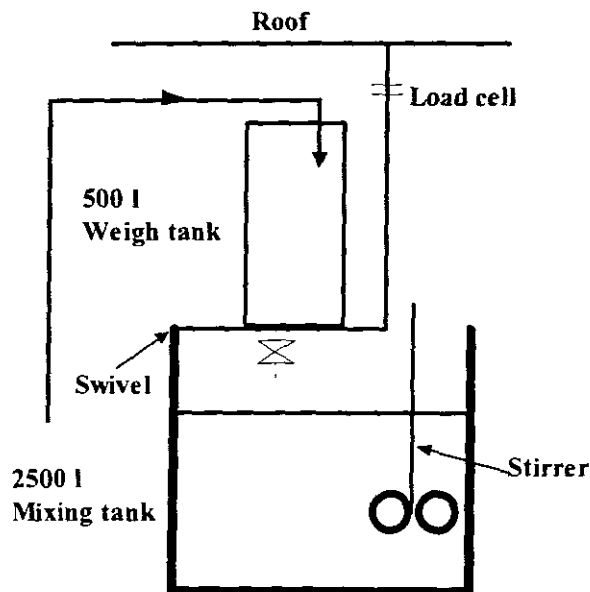
Figure 3-3. The layout of the weigh tank

3.2.4 Manometer and the pressure- tapping layout

The manometer is used to calibrate the two differential pressure transducers (DPT's) by setting up a range of air over water differential heads and comparing them with the DPT outputs. The schematic layout of the manometer board and pressure tapping is depicted in Figure 3-4.
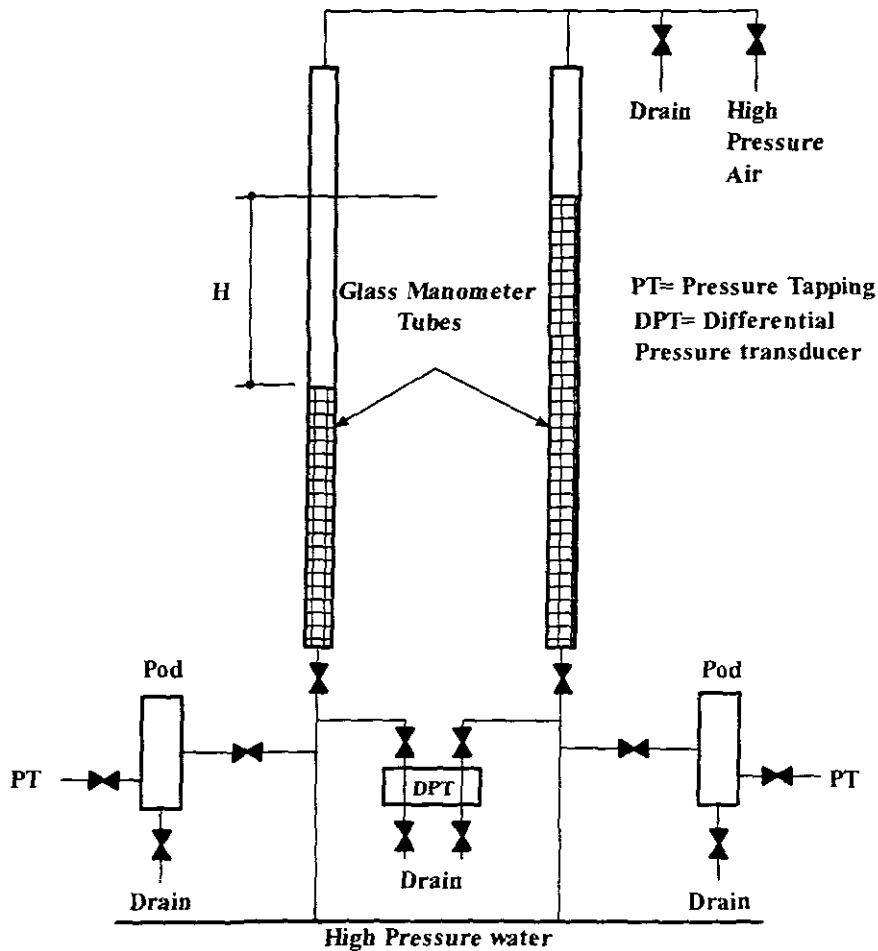
Figure 3-4. Layout of the Manometer Board and pressure tapping (Haldenwang, 2003)

3.2.5 The flume rig

The flume used in this study is 10m long with a width of 300mm and depth of 300mm. At the centre of the flume there is a partitioning section where the panels can be fitted to form half the flume size. The shape of this flume is rectangular and is made in a way that other flume shapes can be fitted on it. The flume shapes that are fitted are semi-circular and trapezoidal shapes and they can also be fitted when the partitioning panels are inserted to create a flume of 150mm size.

The slope of the flume can be changed using an electrical hydraulic ram fitted that can tilt the flume up to 5 degrees. The inlet tank to the flume has a capacity of 600l and is fitted with baffles to streamline the flow. The pipeline connected from the tube viscometer rig supplies this tank with fluid for flume tests. The schematic layout of the flume is depicted in Figure 3-5 and the flume shapes that were used are depicted in Figure 3-6. Detailed drawings are presented in Appendix B.

Figure 3-5. Layout of the 10m long tilting flume

The flume shapes that are used in this investigation are as follows:
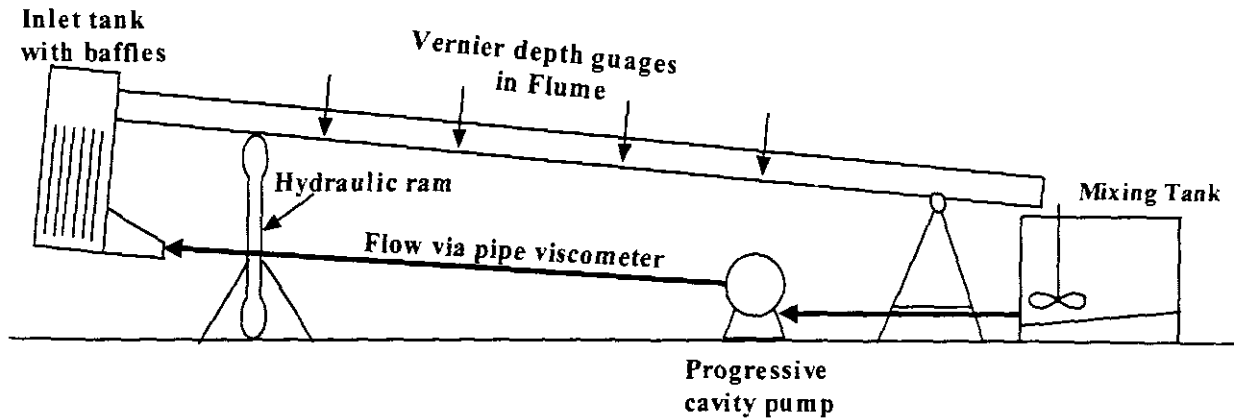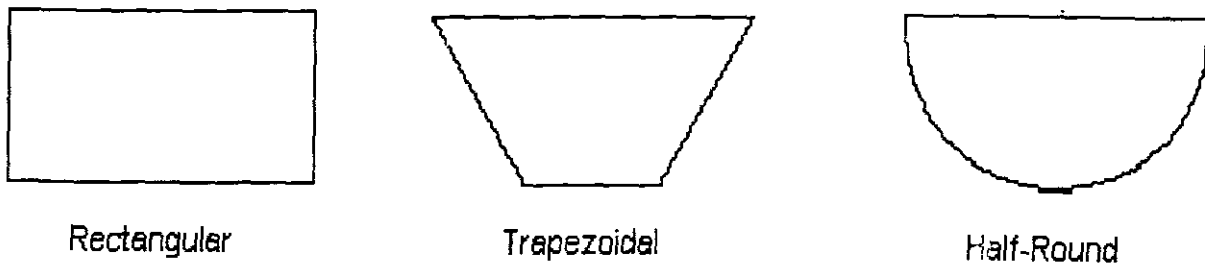

Figure 3-6. The flume shapes

3.2.6 The pumps

A 100mm, 30bar progressive cavity pump driven by a 17kW motor regulated by a variable speed drive, feeds the pipeline linking tube viscometer rig and the flume. This pump is able to deliver approximately 25l/s of water.

To minimise pump pulsations, a dampener unit was fitted at the delivery end of the pump. This dampener unit consists of two vertical clear pipes with steel end caps and steel nipples to let air into the system when required. These pipes should always have a clear section during testing to see the effectiveness of the dampener unit. If the pipes are full, the steel caps are opened to let the air into the system so that it drops the fluid level in the pipes. The clear section is protected by stainless steel wire mesh. The layout of the dampener unit is depicted in Figure 3-7 below.
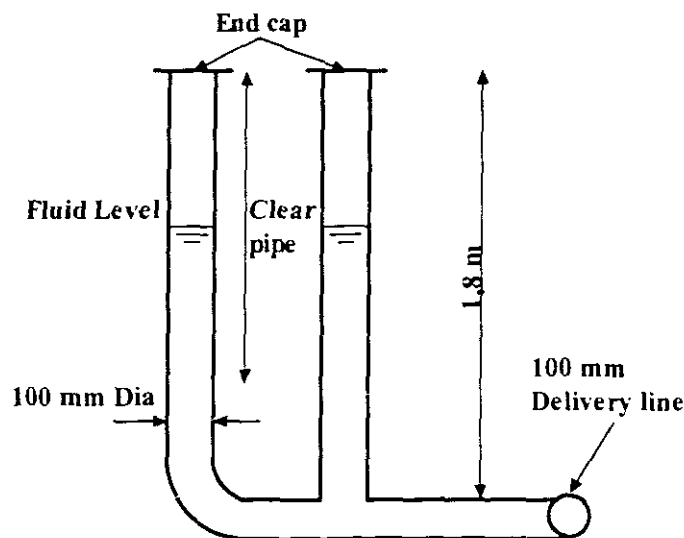
Figure 3-7. Pulsation Dampening Unit

The progressive cavity pump delivers flow rates of up to 25 l/s, which are not sufficient to obtain turbulence especially with highly viscous slurries. To obtain high flow rates a centrifugal pump was fitted to the system. To minimise the head losses caused by friction and fittings, the centrifugal pump was not fitted to the tube viscometer rig, but to the

flume via a pipeline section of 100mm pipe diameter. In this section a magnetic flow meter was also installed to read the flow rate in the 100mm pipe. The centrifugal pump can deliver flow rates of up to 45 l/s. The layout of the centrifugal pump linked to the flume is depicted in Figure 3-8.
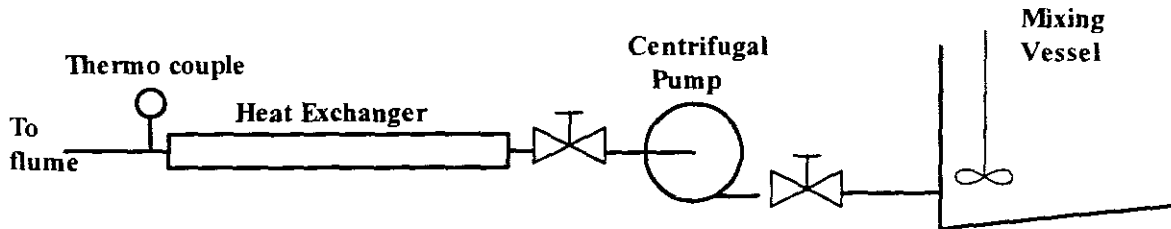
Figure 3-8. Layout of the centrifugal pump linked to the flume

3.3 CALIBRATION PROCEDURE

Most of the instruments used in the test work are electronically connected to the data logger, which is linked to the personal computer, which in turn reads the data electronically; therefore the measuring instruments need to be calibrated before they are used for test purposes. The outputs from the instruments are electrically interpreted in volts by the HP-Data-logger. The calibration procedure of these instruments is explained in the following section.

3.3.1 Load cell

The load cell that supports the weigh tank depicted in figure 3-3 is used to weigh the fluid diverted from the flow meters. To calibrate it, the water is weighed in a container using an electronic scale. The water is then poured in the weigh tank, and the container is weighed again to take the difference in masses. Once the difference in masses between the container with water and the empty container is taken, the voltage output is recorded. For every increase in load, the increase in voltage is recorded.

The recorded values of the increase in load are plotted against the recorded values of the corresponding voltage as shown in Figure 3-9. A linear regression of the plot will give the relationship between the load and the corresponding voltage. This is then entered in the program to be used to calculate the flow rate.
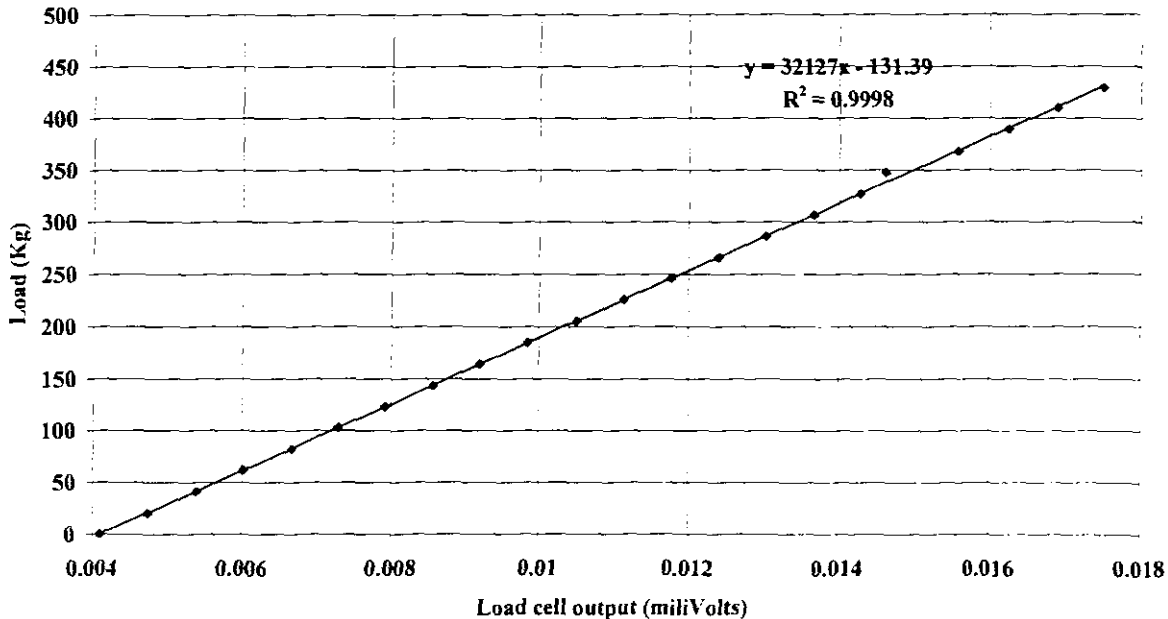
Figure 3-9. Load cell calibration (linear regression)

The linear regression over the range tested gives a correlation coefficient (R^2) value close to 1, showing the calibration of the load cell was good.

3.3.2 The flow meters

The materials tested vary in chemical composition and concentration, so each material is tested over the flow rates used by diverting the flow into the weigh tank. The flow meters that measure the flow rates are, according to the manufacturers, accurate for slurries. To confirm that each flow meter is calibrated with each slurry concentration that will be tested, the calibration procedure is as follows:

For each flow meter the flow rate range is divided into about 12 different flow rates over the whole range the flow meter can measure. Each flow rate is then weighed with time in the weigh tank. The data logger continuously samples the change in weight with time, and from these readings the average flow rate is calculated. The sampling period varies from 120s for low flow rates to 12s for the high flow rates. This is repeated for all the flow rates.

The flow rates versus voltages are then plotted and the straight-line regression gives the relationship between flow rate and volts as well as the error fit.

A typical test result for the 28 mm magnetic flow meter calibration is shown in Figure 3-10 below.
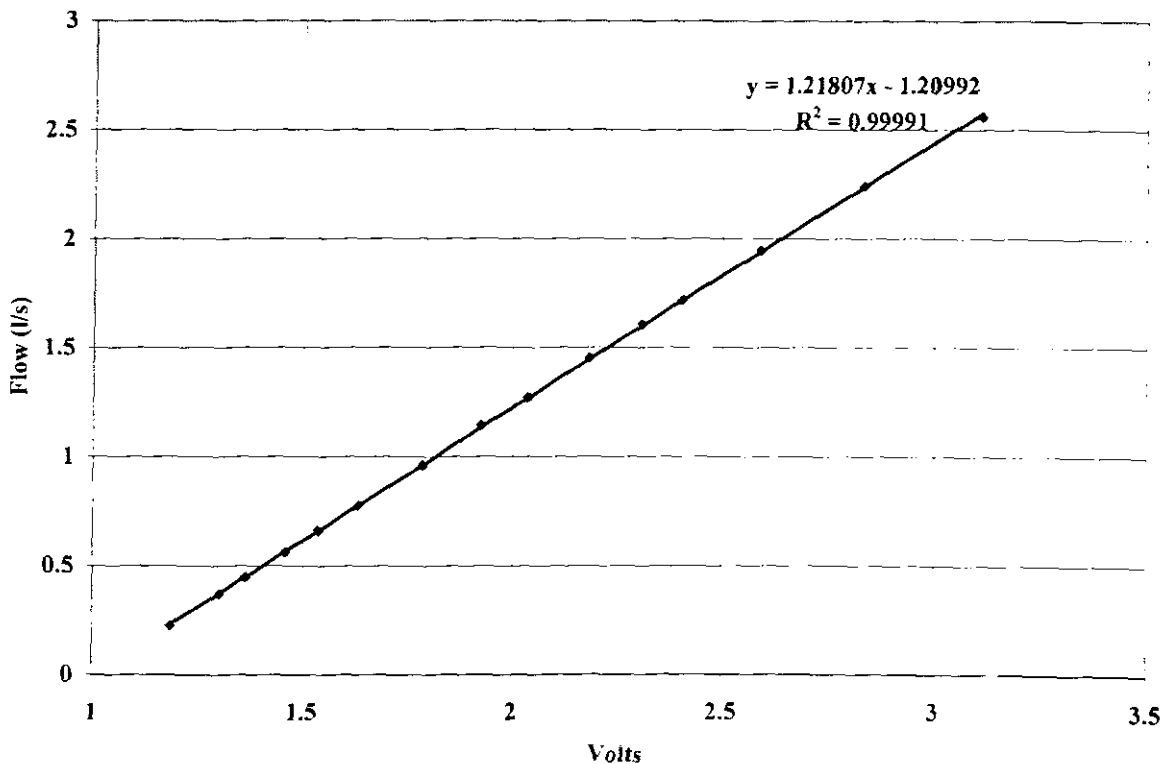
Figure 3-10. 28 mm magnetic flow meter calibration for 5.4% kaolin

The linear regression over the range tested gives a correlation coefficient value of almost 1, which shows a good calibration test.

3.3.3 Differential Pressure Transducers (DPTs)

The two DPTs, one with a range of 0-4kPa and the other 0-30kPa, were calibrated with water over air glass u-tube manometer. The procedure was as follows:

- The two ends of the DP cell are connected to the two legs of the manometer.

- The whole system is flushed to make sure that all the air is out of the system.

- The u-tube manometer is zeroed and then a differential pressure is set up. The difference between the two legs is then measured and the pressure head calculated.

$$\Delta p = \rho_{water} gH \quad (m) \tag{3.1}$$

- The voltage recorded by the DP cell is also recorded with the data-logger.

- The differential pressure is then increased and the same procedure is followed. Several points over the range of the DP cell are recorded.

- The differential pressures versus voltages are then plotted and the least square linear regression gives the relationship between differential pressure and volts as well as the error of the fit.

A typical test result for the high DP cell is shown in Figure 3-11.

The chart shows a linear plot with:
- Y-axis labeled "Differential Pressure" ranging from 0 to 2500
- X-axis labeled "Volts" ranging from 1 to 3.5
- Equation: y = 959.0998x - 943.0300
- R² = 0.9987
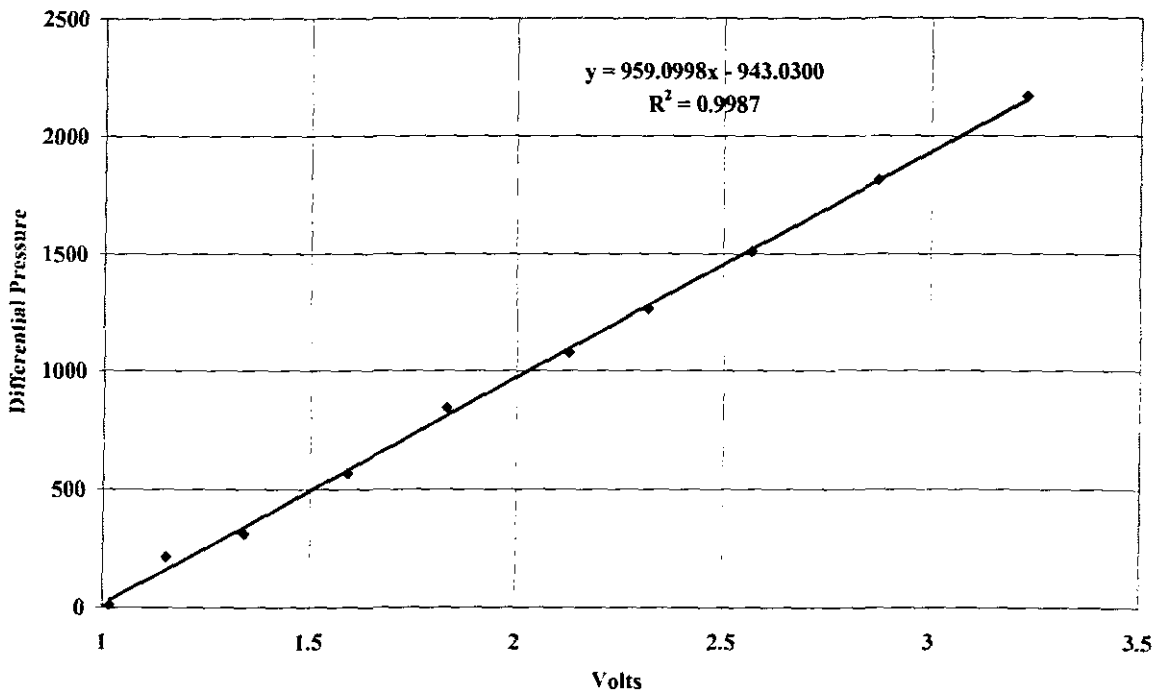
Figure 3-11. Low differential pressure transducer calibration

In Figure 3-11 the correlation coefficient (R^2) is almost 1, thus indicating the calibration of DPTs was good. According to the manufacturers the accuracy of the DPTs are within 0.1% of full scale. This means that for the high range DPT the differential pressure is +/- 30 Pa and for the low range DPT the differential pressure error is +/- 4 Pa.

3.3.4 Clear water test in pipe viscometer.

After the flow meters and the DPTs are calibrated, the water test is conducted in all three tubes of the tube viscometer rig. The aim of this test is to see if the calibratir n procedures were done correctly.

The Colebrook-White equation is used to calculate the friction factor (f), which is as follows:

$$\frac{1}{\sqrt{4f}} = -2\log\left(\frac{k}{3.7D} + \frac{2.51}{Re\sqrt{4f}}\right) \qquad (2.23)$$

By using the Darcy-Weibasch equation for a friction head as follows:

$$h_f = \frac{4fLV^2}{2gD} \qquad (3.2)$$

and $\quad \tau_o = \dfrac{D\Delta p}{4L} = \dfrac{D\rho gh_f}{4L} \qquad (3.3)$

By definition the relationship between the wall shear stress and the friction factor is as follows:

$$\tau_o = \frac{f\rho V^2}{2} \qquad (3.4)$$

The experimental procedure for the water test is as follows:

- The flow in each tube is measured and the average velocity is calculated.

- The differential pressure is measured over a distance L that is 1m for all three tubes.

- The average wall shear stress (τ_o) is calculated using Equation 3.3 which is:

$$\tau_o = \frac{D\Delta p}{4L}$$

- The wall shear stress is then plotted against average velocity V.

- The Colebrook –White equation is then used to calculate the theoretical value of f, which will then be used to calculate the wall shear stress.

- This is done by assuming a value for a pipe roughness (k), calculating the Reynolds number and optimising the Colebrook-White equation to obtain the friction factor (f).

- The friction factor is then used to calculate the theoretical value for wall shear stress using Equation 3.4.

- The theoretical and actual data are then plotted for all three pipes as shown in Figure 3-12 to Figure 3-14. If the pipe is not smooth, the k value is optimised to find the actual pipe roughness.
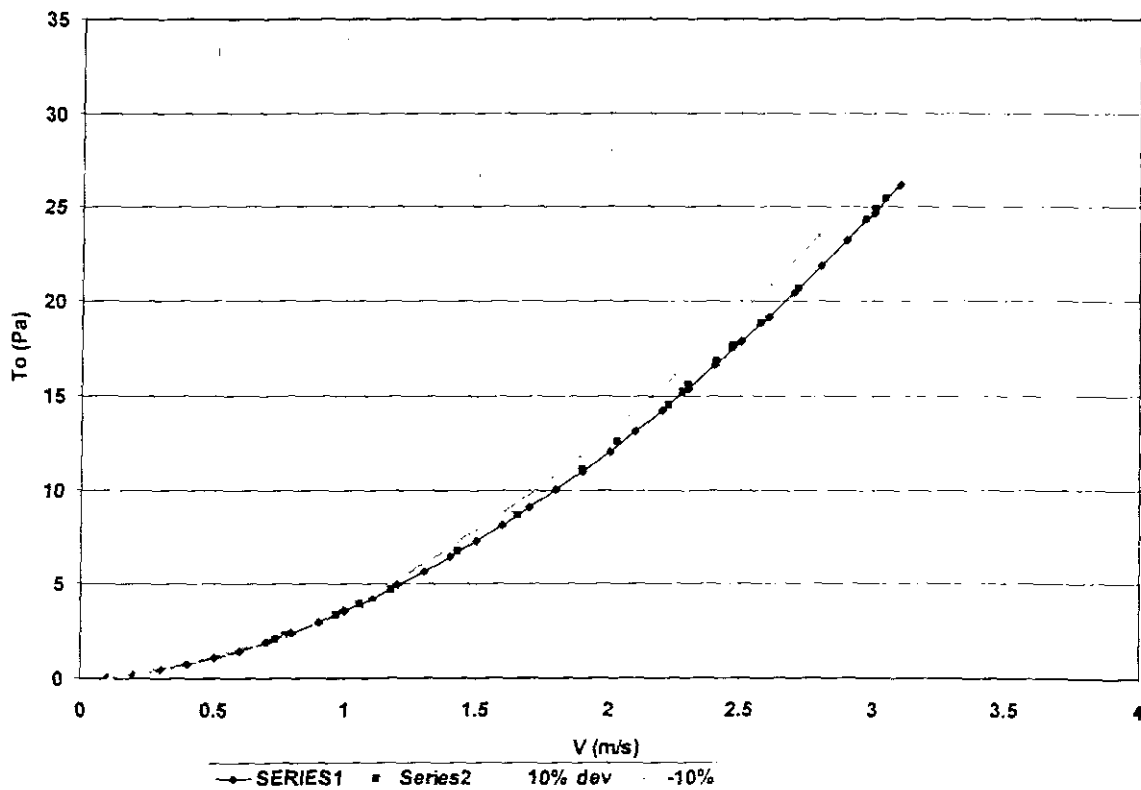

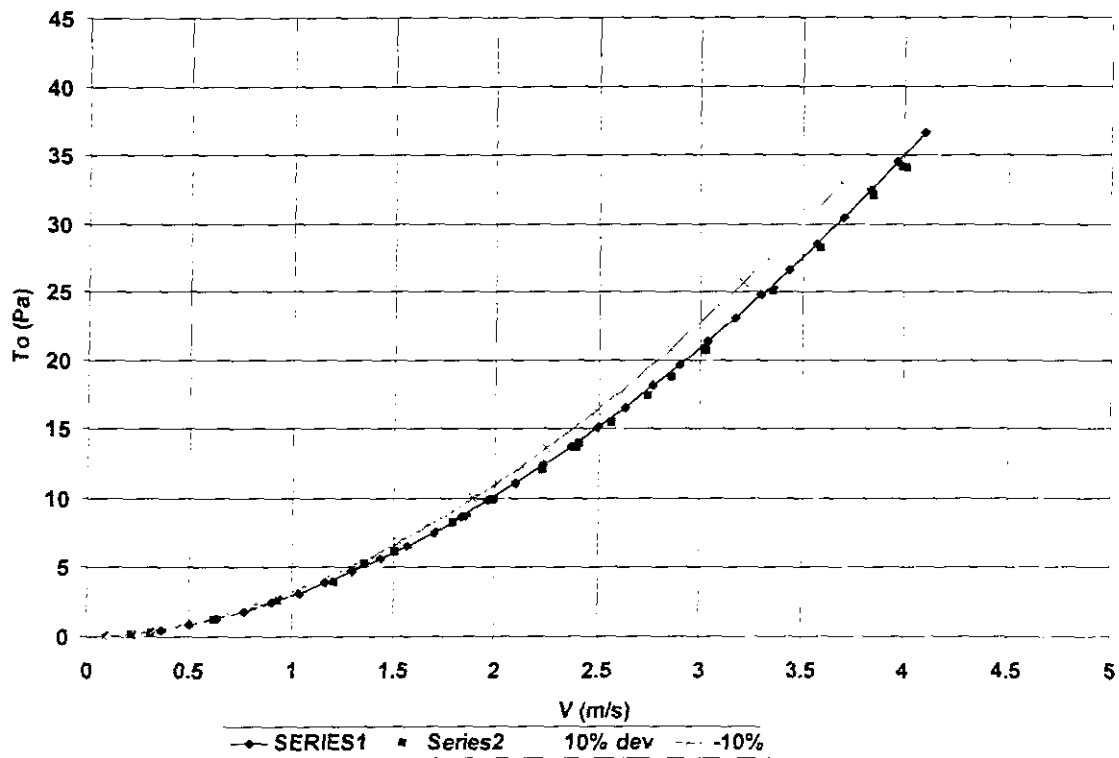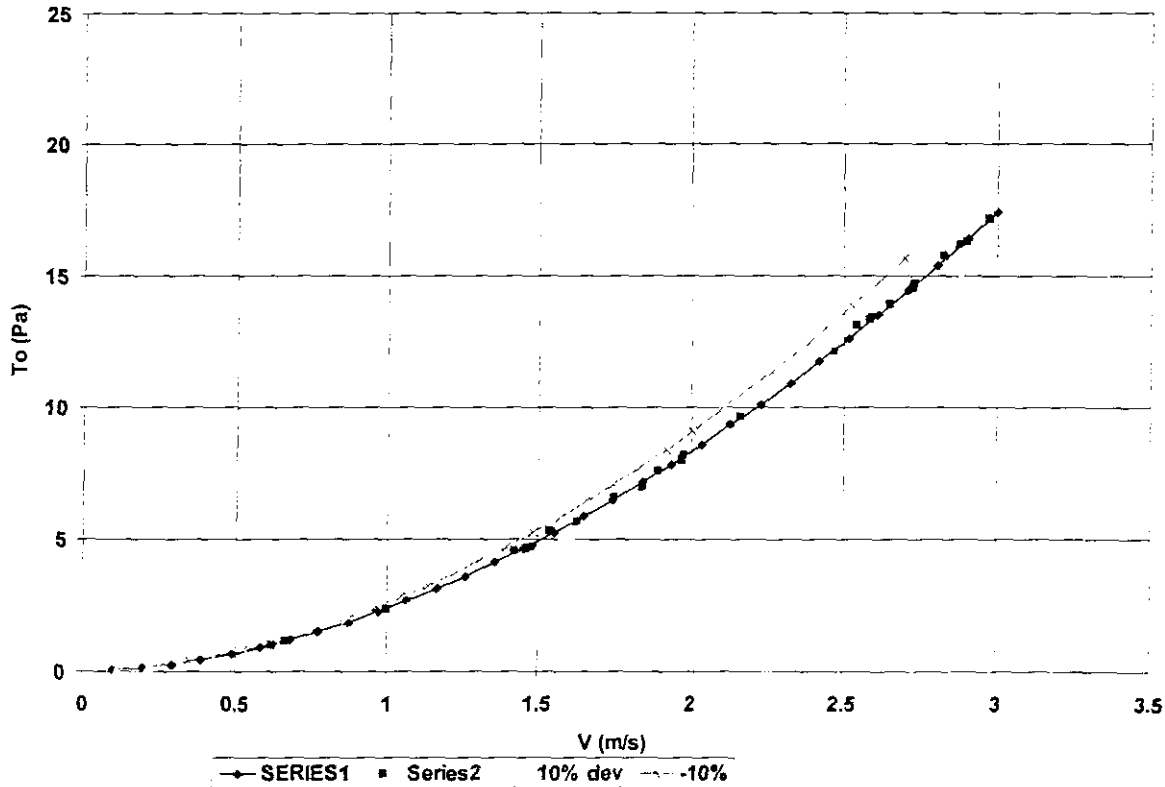**Figure 3-12. Clear water test in 13mm tube using the Colebrook-White equation**

Figure 3-13. Clear water test in 28mm tube using the Colebrook-White equation

Figure 3-14. Clear water test in 80mm tube using the Colebrook-White equation

From these figures it can be seen that the data points are within the acceptable range of error. This indicates that the calibration of the instruments was done correctly.

3.3.5 Digital depth gauges

The depth of the flow in each flume shape is measured using two digital vernier type depth gauges, which are linked electronically to a personal computer (PC) with an RS232 interface. The measurement is carried out by inserting them vertically onto the flow surface. A previous study by Haldenwang (2003) showed that the flow is steady between the 5 m and 6 m positions from the entrance of the flume. The interface transmits the depth signal directly to the PC in mm, and no calibration is required.

3.3.6 The slope measurement of the flume

The flume was levelled using a contractors's automatic dumpy level. By setting up in the middle of the flume, the level can be checked to within 1mm over 10m (0.01%).

The vertical displacement distances for the slopes of 1-5 degrees were then calculated and used to set the slopes required. A ruler was placed vertically on the frame next to the flume and a marker was connected to the flume. This was done where the hydraulic ram is positioned. The various slopes can then be easily set to within 1 mm.

3.4 MEASURED VARIABLES

3.4.1 The slurry density

The slurry density (ρ) is obtained by first calculating the relative density (S_m) of the slurry using the following procedure:

- The equipment needed is a one litre volumetric flask and a scale that can measure in milligrams.

- The flask is then dried thoroughly and the mass of it is weighed as M1.

- A well-mixed sample of the slurry is taken from the mixing tank and poured partially into the flask to weigh M2

- The remaining part of the flask is filled with water up to the graduated mark to weigh M3.

- The flask must then be emptied and cleaned thoroughly with water and filled again with water to the same graduated mark to weigh M4.

- The procedure is repeated at least three times to check the accuracy of the test.

The relative density is defined as the ratio of density of fluid to the density of water as follows:

$$S_m \cong \frac{\rho_m}{\rho_w} \qquad (3.6)$$

Using the measurements taken under the procedure guide, the relative density can be defined as:

$$S_m = \frac{M_2 - M_1}{M_4 - M_3 - M_1 + M_2} \qquad (3.7)$$

From Equation 3.6:

Slurry density is given by: $\rho_m = S_m \rho_w$ $\qquad (3.8)$

3.4.2 Slurry temperature

The temperature of the slurry is measured at two positions in the pipe loop with thermocouples. The two positions are at the end of the first heat exchanger that is just before the tube viscometer and the second is at the inlet to the flume. Both thermocouples are directly linked to the data acquisition unit that reads the temperature in degrees Celsius. As the data acquisition unit reads the thermocouple directly, no signal calibration is required. The heat exchangers are linked to a central water-cooling system. The accuracy of the thermocouples according to the manufacturers specification is in the order of 1 degree Celsius. The temperature was monitored only to check the temperature of the slurry does not vary during tests.

3.5 EXPERIMENTAL PROCEDURE

This section explains the procedure used to gather the data that will be used to evaluate models mentioned in the literature. The procedure to gather the data for the rheology test using the tube viscometer rig and for the flume tests using the flume rig is presented.

3.5.1 Tube viscometer rig.

This procedure involves collecting the data for the ranges of differential pressure (Δp) and velocity (V), which will be used to calculate the wall shear stress (τ_0) and pseudo- shear rate (8V/D). These two variables are plotted against each other to establish the pseudo shear diagram. It is called a pseudo shear diagram because pseudo shear rate is not the true shear rate. The procedure is the same for all three tube diameters and is as follows:

- Approximately 2000 litres of slurry is mixed in the 2500 litres mixing tank shown in Figure 3-3 until it is well mixed.

- A sample is taken from the tank to calculate the relative density of the slurry. If the desired concentration is not achieved, more solids are added and mixed or the slurry is diluted with water depending whether the concentration is below the desired one or exceeds it.

- During the mixing process the slurry is circulated through all three tubes so that any water in the system is mixed in the slurry. The slurry relative density is again measured after the water in the system is mixed in the flowing slurry.

- Before any tests are conducted, the flow meters have to be calibrated for that slurry that will be tested using the calibration procedure explained previously.

- The pods that prevent solids from entering the DPTs (Figure 3-2) are connected to the pressure tappings. The lines linking the tappings and the DPTs are flushed with water. This sometimes has to be repeated during testing when solids start to enter the system.

- The flow rate is regulated by means of a series of valves, as the pump cannot achieve very low flow rates. The excess flow is diverted through a by-pass line back to the mixing tank. This also helps to ensure the slurry is well mixed.

- The data logger is switched on and the visual basic program on the PC is activated. The data is exported to an Excel spreadsheet.

- When the correct flow rate is set, the data-logger is triggered and the program takes flow rates and differential pressure readings over a preset time interval.

- The average flow rate and differential pressure are exported to the Excel spreadsheet to calculate the pseudo shear rate and wall shear stress respectively. These points are visually displayed on the pseudo shear diagram.

- This is repeated for a wide range of flow rates until there are sufficient points on the pseudo shear diagram.

- The process is repeated for 13mm, 28mm, and 80mm tubes.

- All the three sets of data are plotted on one graph, which enables one to see whether there are any errors during the testing of the data. If the laminar flow data of all the three tube diameters coincide, that indicates that there is no wall slip occurring in the tubes.

3.5.2 The flume rig

This procedure involves the establishment of a range of flow rates (Q) and fluid depths (h) as follows:

- The flume slope is adjusted to the correct slope with the hydraulic ram.

- The slurry is then diverted to the flume from the tube viscometer rig. This enables one to check whether the rheology of the slurry has changed during testing at regular intervals but only for laminar flow regime. If the centrifugal pump is used, the rheology of the slurry cannot be checked because this pump is used to obtain turbulent flow in this test work.

- The data logger is switched on and the visual basic program on the PC is activated. The data is exported to an Excel spreadsheet.

- The two depth verniers are fitted to the flume and connected to the data logger.

- The depth verniers are zeroed on the bottom of the flume.

- When the correct flow rate is set, the depth gauges are manually adjusted to the surface of the flowing fluid.

- The data logger is triggered and the program takes the flow rates over the set time interval.

- The average flow rate and the flow depth recorded by two depth verniers are exported to the spreadsheet.

- The procedure is repeated for a range of flow rates, as well as for different slopes.

- The spreadsheet contains a Moody diagram; therefore the Reynolds numbers are plotted against friction factors on this diagram.

- The data points taken should sufficiently cover all three flow regimes, which are laminar, transition, and turbulent.

3.6 MATERIALS TESTED

The materials selected for this study represent three non-Newtonian fluids classifications that have different rheological properties, which are power law fluid (pseudo-plastic), Bingham plastic fluid, and yield pseudo-plastic fluid. The power law fluid selected was Carboxymethyl Cellulose (CMC), which is regarded as an ideal solution for experimental work. The CMC is widely known as wallpaper glue. The Bingham plastic selected was a bentonite suspension, which is a drilling mud. The yield pseudo-plastic fluid selected was kaolin clay mostly used to make ceramic products. The kaolin suspension has been used over a long period at the Cape Technikon Flow Process Research Centre for testing purposes.

For calibration purposes, water was used as a Newtonian fluid.

3.7 TYPICAL TEST RESULTS

The following show examples of the test results from the rectangular, semi-circular, and trapezoidal channel shape as well as rheological results using CMC fluid. The rest of the results are presented in Appendix A for all the flume shapes and materials used.

Table 3-1 below shows the fluid properties of the 3% CMC.

Table 3-1. Slurry properties of 3% CMC

SLURRY PROPERTIES	3% (m/m) CMC
Solids Relative Density	2
Slurry Relative Density	1.0175
Yield Stress	0 Pa
Fluid Consistency Index	0.1272 $Pa.s^n$
Flow Behaviour Index	0.8122
Apparent Viscosity (100 s^{-1})	0.0536 Pa.s
Apparent Viscosity (500 s^{-1})	0.0396 Pa.s

Figure 3-15 shows the rheogram of the 3% CMC
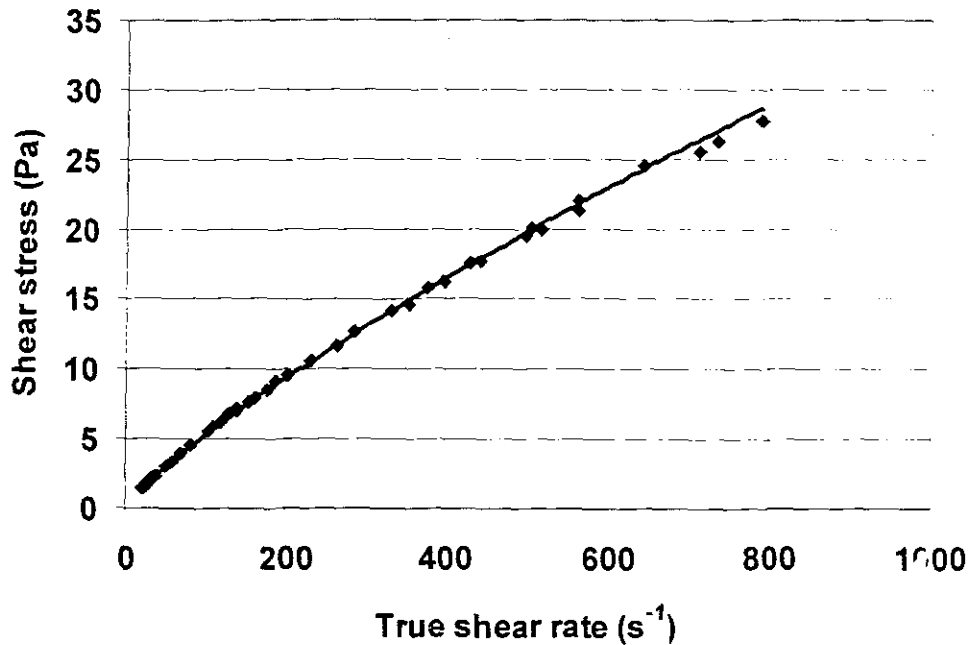
Figure 3-15. Rheogram 3% CMC

Figures 3-16 to 3-18 show examples of the Moody diagram for the rectangular, semi-circular, and trapezoidal flume shapes.
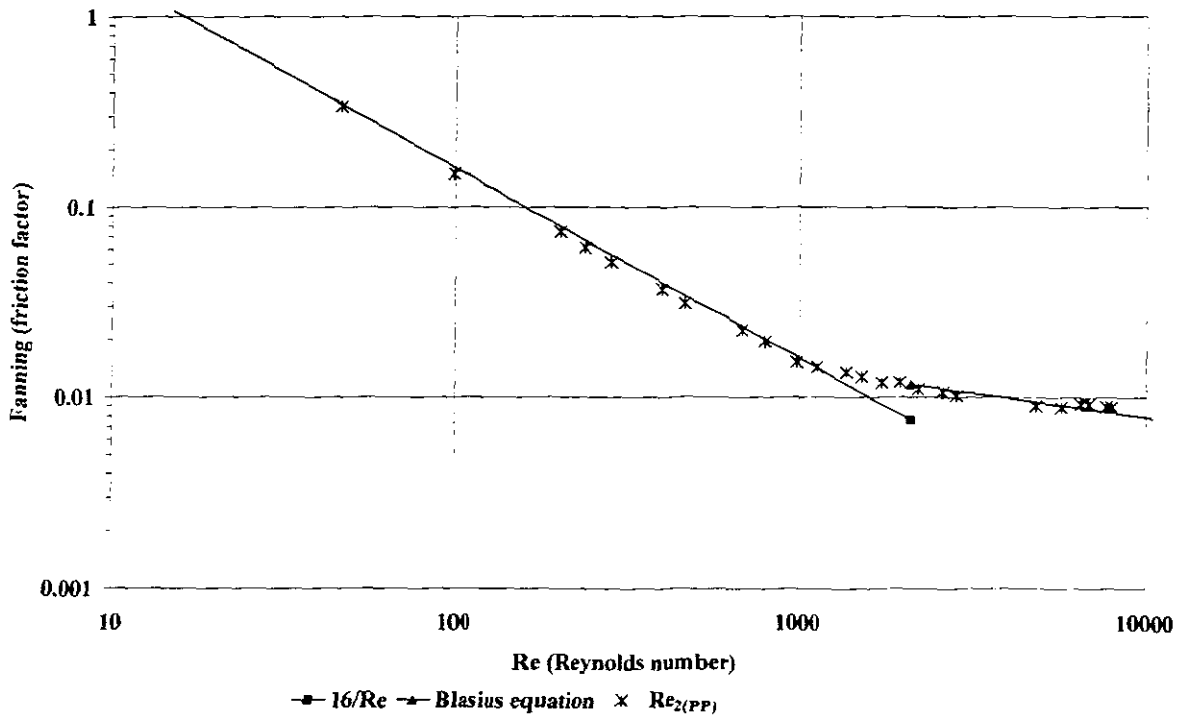
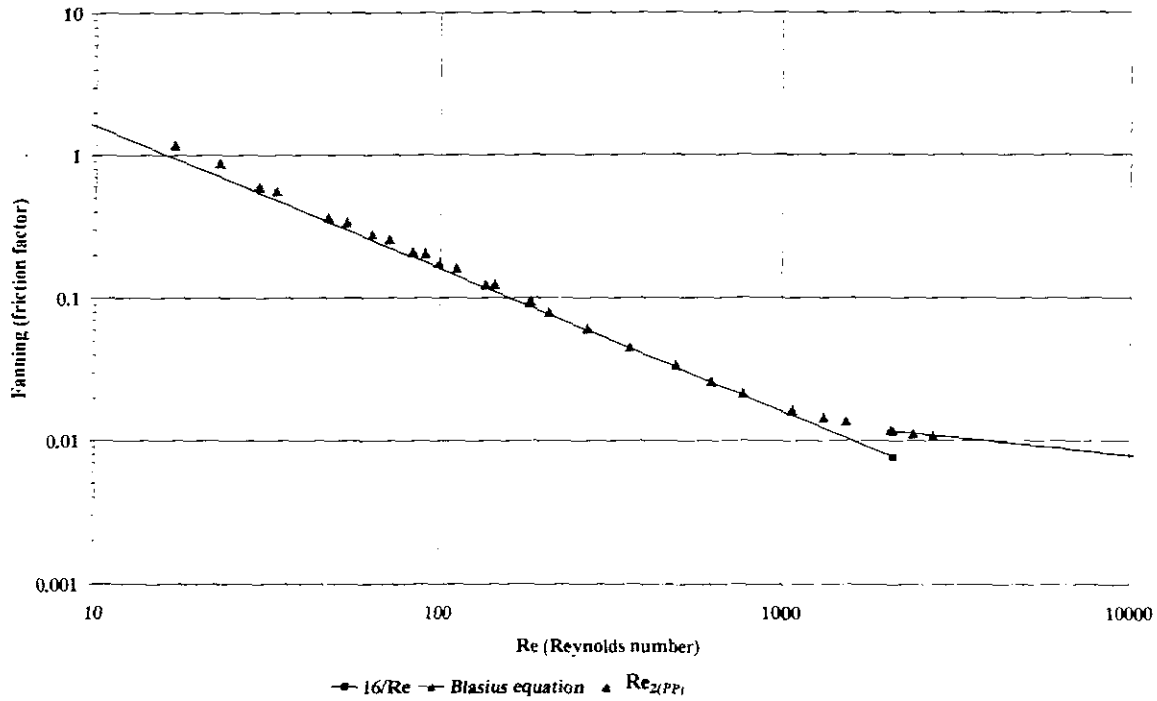**Figure 3-16. Moody diagram of the 3% CMC in a semi-circular channel**

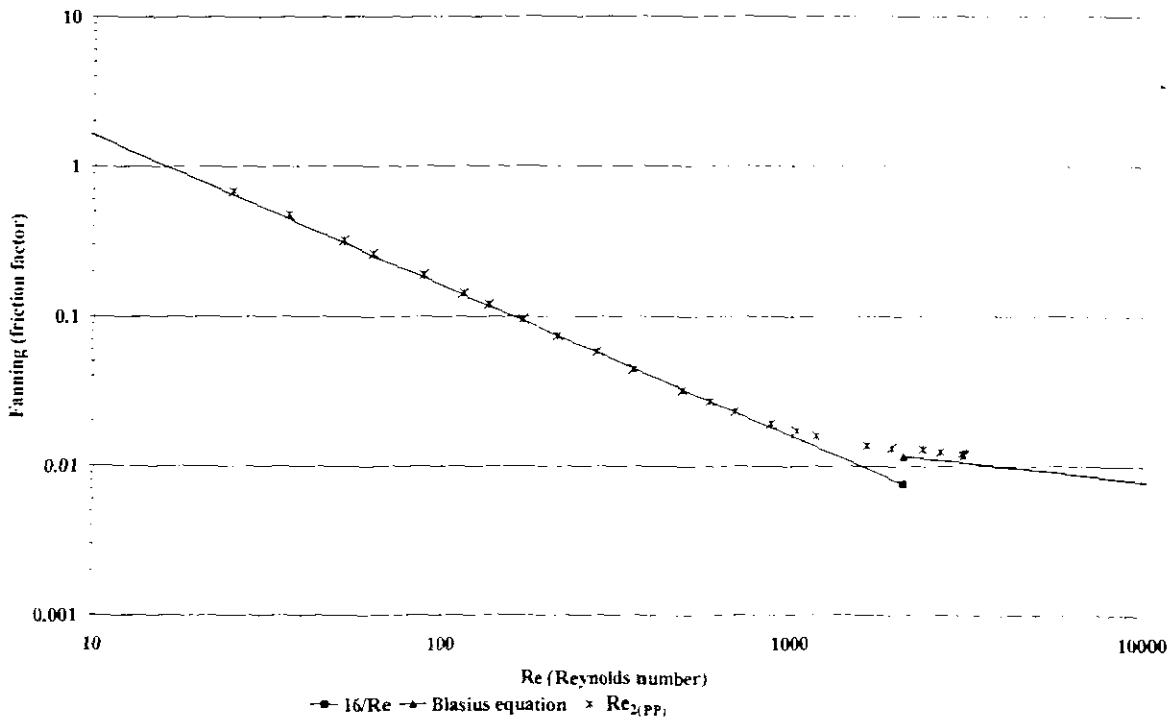Figure 3-17. Moody diagram of the 3% CMC in a rectangular channel

Figure 3-18. Moody diagram of the 3% CMC in a trapezoidal channel

3.8 GENERAL OBSERVATIONS

3.9 FLOW BEHAVIOUR

The Moody diagrams depicted in Figures 3-16 to 3-18 classify two flow regimes, namely laminar and turbulent flow.

For the laminar flow, the 16/Re line was used and for the turbulent flow the Blasius line was used. From where the data deviates from the 16/Re line to the Blasius line, shows the transition zone. For Newtonian fluids the transition occurs between 2000<Re<3000. For the non-Newtonian fluids as can be seen from Figures 3-16 to 3-18 above, the transition occurs earlier than that.

For the less viscous fluids it can be observed that there is a jump in friction factor similar to that of water from laminar to turbulent flow at Reynolds number between 2000 and 3000 (see Figures 3-19 to 3.21). For the more viscous fluid the transition becomes smooth and the more viscous the fluid, the earlier the onset transition occurs (see Figures 3-22 to 3-24).

The transition of non-Newtonian fluids is not the same as for Newtonian fluids and cannot be accurately established from the Moody diagram.
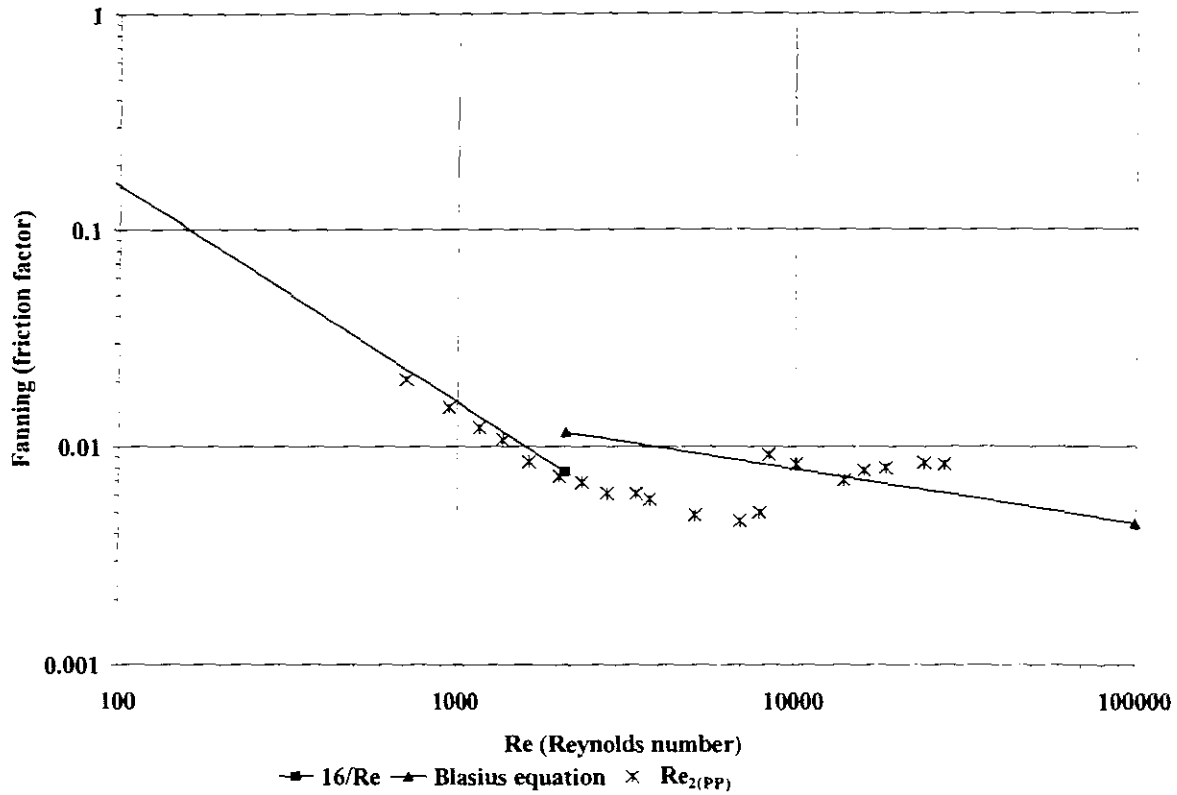
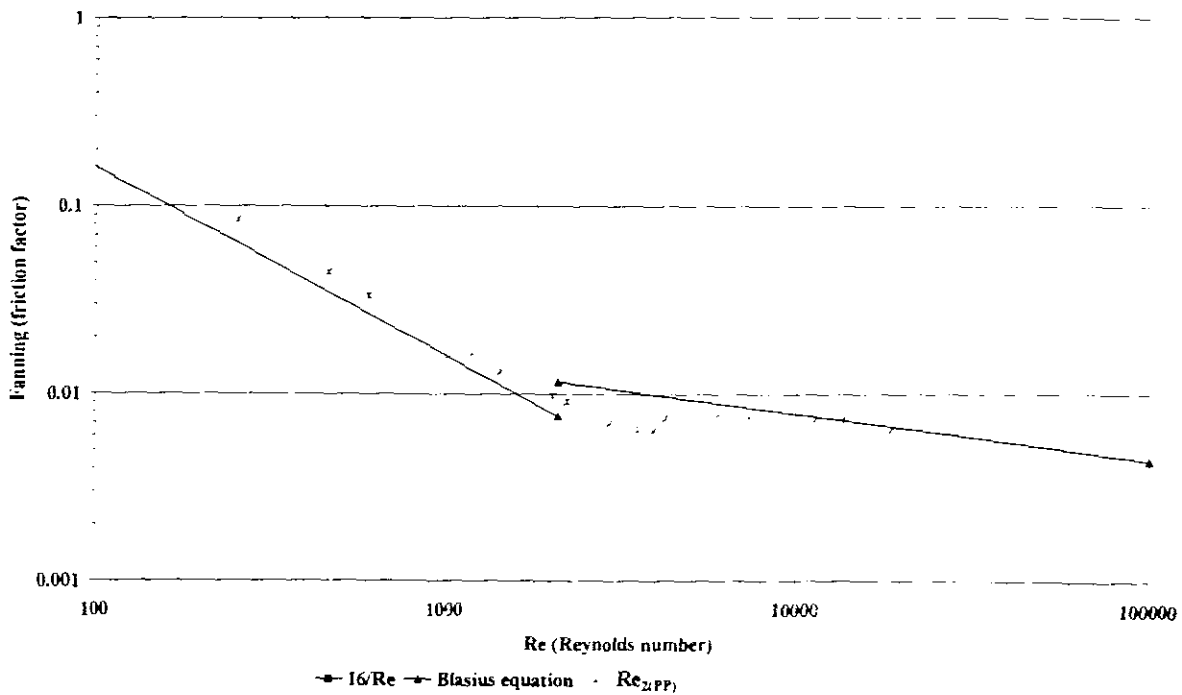**Figure 3-19. Moody diagram of 1.5% CMC in a semi circular flume shape**

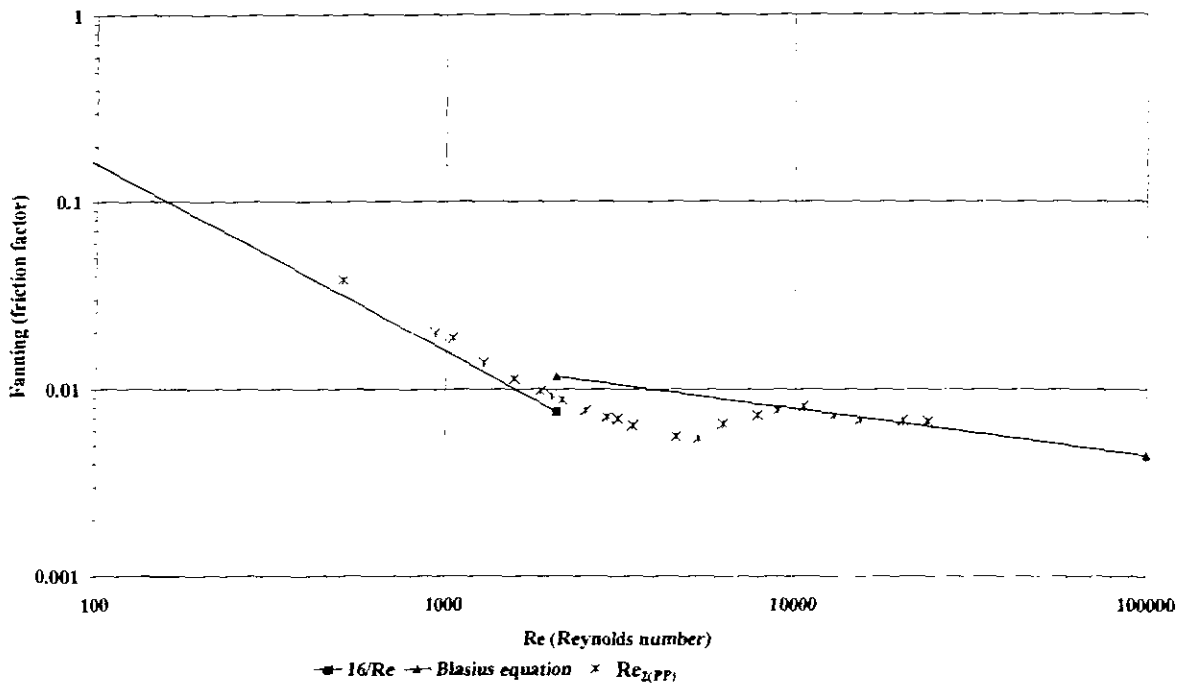**Figure 3-20. Moody diagram of 1.5% CMC in a rectangular flume shape**

Figure 3-21. Moody diagram of 1.5% CMC in a trapezoidal flume shape
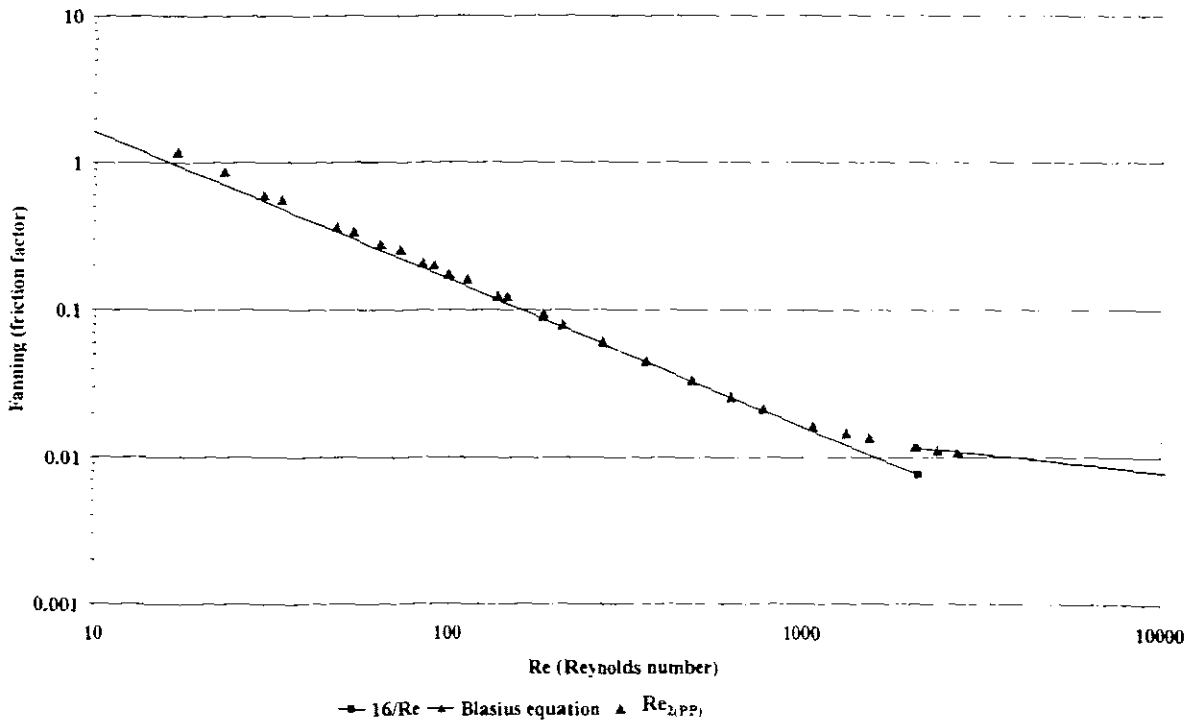

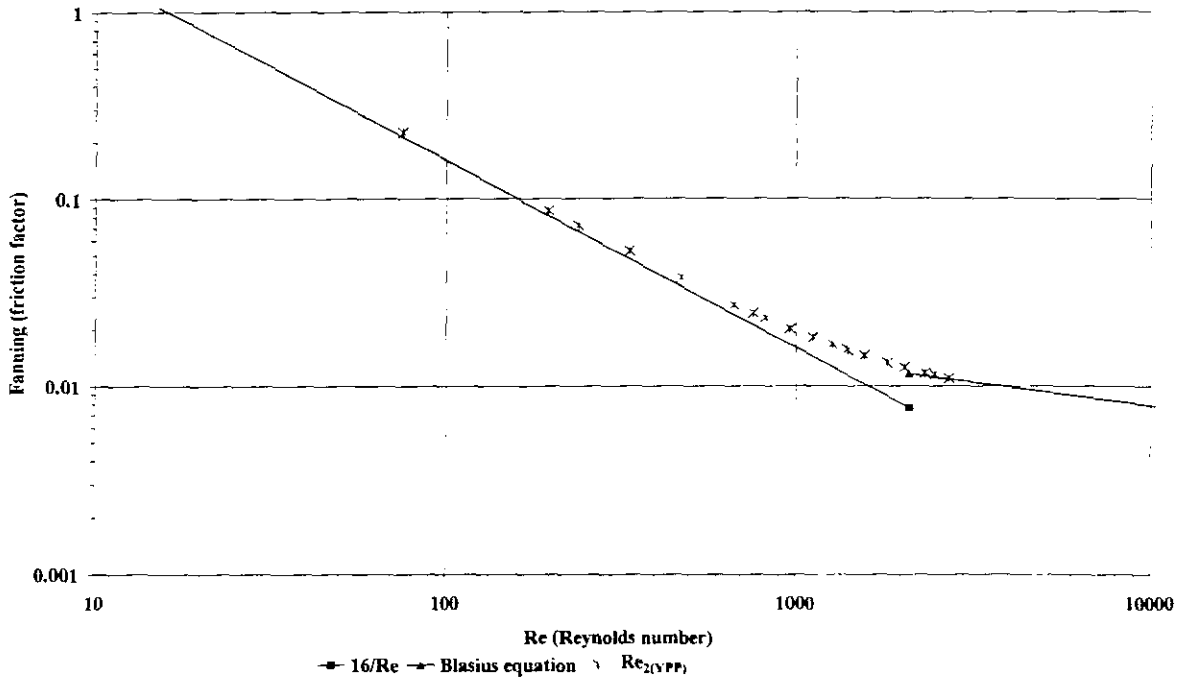**Figure 3-22. Moody diagram of 4% CMC in a rectangular flume shape**

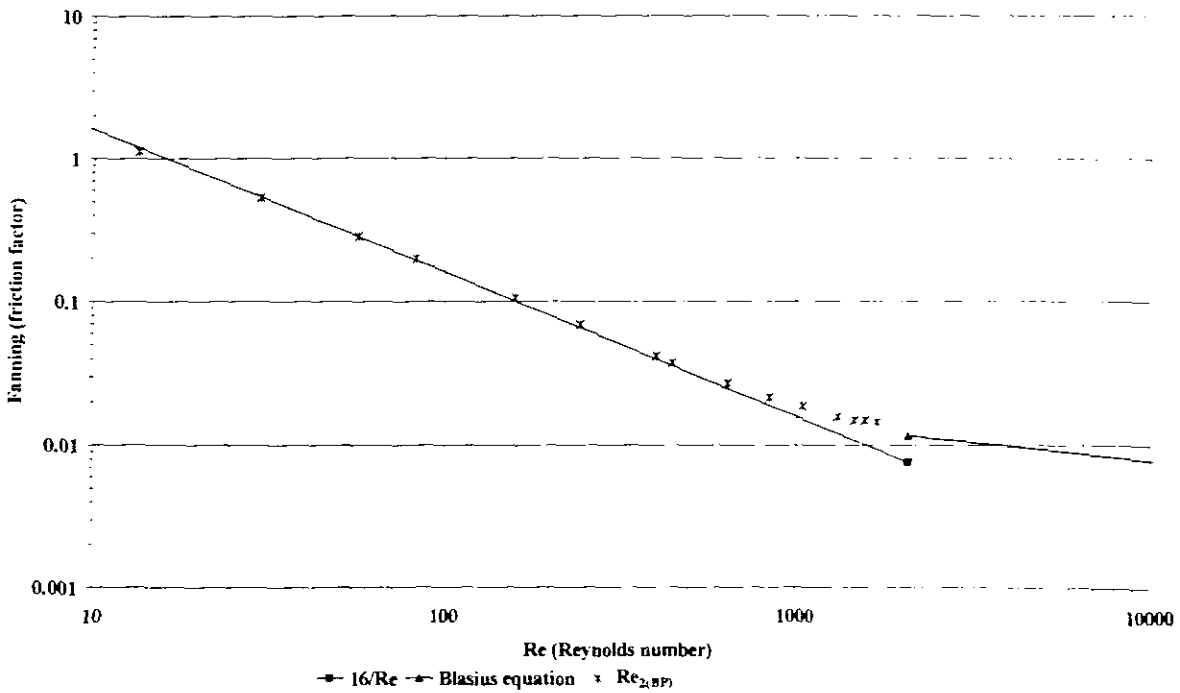Figure 3-23. Moody diagram of 7.1% kaolin in a semi circular flume shape

Figure 3-24. Moody diagram of 6.2% bentonite in a trapezoidal flume shape

3.9.1 Rheological behaviour

The fluids tested exhibited different rheological characteristics (See Figures 3-15, 3-25 and 3.26). CMC solution has the rheological characteristics of a power law fluid, bentonite suspension has the characteristics of a Bingham fluid (a yield stress fluid), and kaolin suspension has the characteristics of a Herschel-Bulkley fluid (also a yield stress fluid).
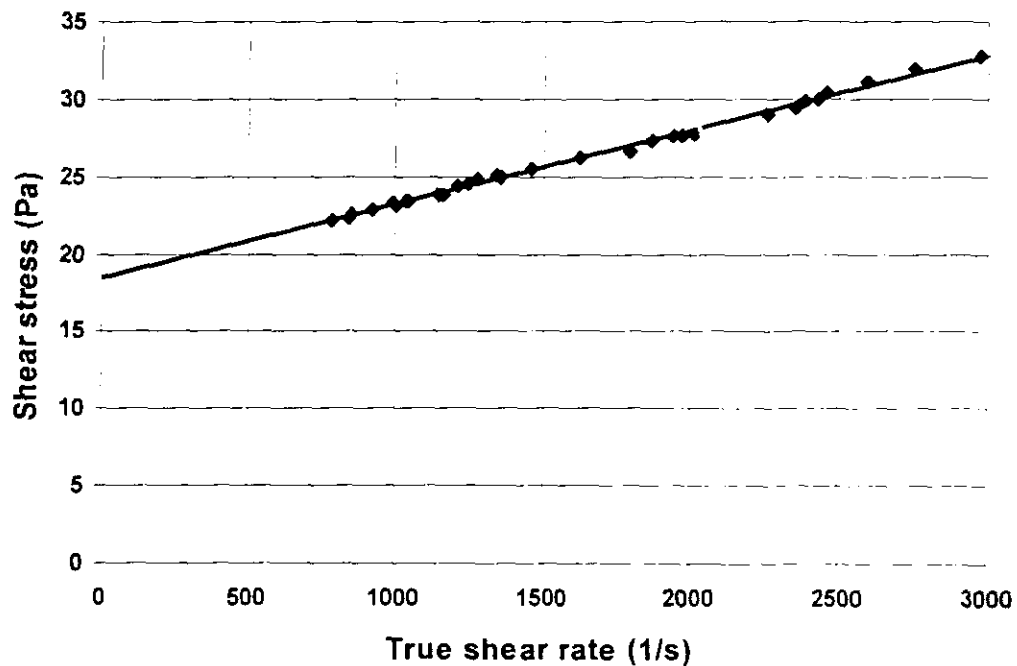

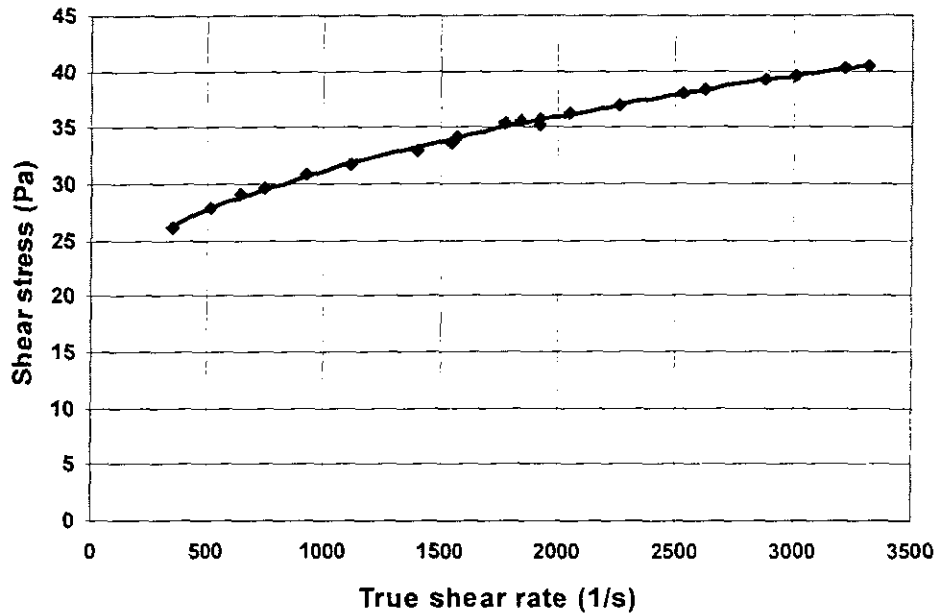Figure 3-25. Rheogram of 6.2% bentonite

Figure 3-26. Rheogram of 9% kaolin

3.10 CONCLUSION

3.10.1 Experimental equipment and procedures

All the equipment discussed in this thesis was built and commissioned at Cape Technikon Flow Process Research Centre by Haldenwang (2003), who used clear water to commission the equipment.

The equipment includes the tube viscometer with 3 diameter tubes linked to the 300mm-wide by 10m-long tilting flume that can be partitioned to form a 150mm-w'de flume. Inside this flume, three flume shapes were fitted namely, rectangular, semi-circular and trapezoidal shapes.

A unique feature of this experimental facility is that the tube viscometer connected to the progressive cavity pump is in line with the flume.

Calibration and test procedures were developed to accurately produce pipe flow data to establish relevant rheological parameters of all the fluids tested.

The flume data was gathered over a wide range of flow rates (0.1- 45 l/s) and slopes (1-5°) for all the flume shapes used.

Several concentrations of CMC (1, 2, 3, 4 % m/m) solutions, bentonite (4.6 and 6.2 % m/m) and kaolin (5.4, 7.2, 9% v/v) suspensions were tested to compile a large database.

The database compiled will be used to evaluate the models mentioned in the literature review and this will be presented in Chapter 4.

CHAPTER 4

CHAPTER 4
ANALYSIS OF RESULTS AND DISCUSSIONS

4.1 INTRODUCTION

In this chapter some models mentioned in the literature will be evaluated using the database compiled for this study. As mentioned before, some of the models found in the literature were not verified experimentally, so this chapter will test these models with the data compiled for the study in all the flume shapes chosen. The data was compiled for different materials that have different rheological characteristics over a wide range of concentrations and channel slopes. The flow rates used covered all three-flow regimes, i.e., laminar, transition, and turbulent regions.

This chapter will only concentrate on two flow regions, which will be analysed separately namely:

- The laminar flow region.

- The transitional flow region.

These flow regions are differentiated from each other visually on the well-known Moody diagram, which is a plot of friction factor versus Reynolds number on a logarithmic scale. The initial part of the plot is the laminar flow region and the other part is the turbulent flow region. The transition region can be seen when the data points start deviating from the laminar line to the turbulent region. In this region the flow regimes are mixed, indicating the ending of the laminar region and the beginning of the turbulent region.

These flow regions are analysed separately for each flume shape for the following materials at different slopes as mentioned in the previous chapter:

- CMC solutions of 1, 2, 3, and 4% (m/m) concentrations.

- Kaolin suspensions of 5.4, 7.1, and 9% (v/v) concentrations.

- Bentonite suspensions of 4.6 and 6.2% (m/m) concentrations.

4.2 LAMINAR FLOW REGION

There are few authors that have proposed Reynolds number models for the laminar flow of non-Newtonian fluids in open channels (Kozicki & Tiu, 1967; Coussot, 1994; Abulnaga, 1997; Haldenwang et al., 2002). Some of them did not verify their work experimentally (Kozicki and Tiu, 1967), where they used pipe data to present their work on open channel flow. Some of them went to the lengths of suggesting that the laws of closed pipes can be used for open channels, and for the latter one must use equivalent diameter (Chow, 1959 for Newtonian fluids, Abulnaga, 1997 and Haldenwang et al., 2002 for non-Newtonian fluids). For laminar flow there seems to be some evidence that this may be true.

The database compiled for this study is analysed using the models mentioned above to predict the nature of flow in this flow regime. These models are evaluated separately to predict the laminar flow of CMC solutions, kaolin suspensions, and bentonite suspensions in the following sections.

When analysing the laminar flow regime, it is important to choose the correct rheological model that will characterise the non-Newtonian fluid tested because the Reynolds number models mentioned in literature contain these rheological parameters.

4.2.1 Evaluation of work done by Kozicki and Tiu

Kozicki and Tiu (1967) derived Reynolds numbers for a number of cross-sectional shapes and different rheological models. Their Reynolds numbers included the geometric shape factors of the cross-sectional shape of the channel; however they did not verify their work experimentally. In this thesis the Reynolds number models they proposed are evaluated.

4.2.1.1 Effect of shape

Kozicki and Tiu (1967) contended in their proposition to predict the flow rate and the maximum velocity in the steady and uniform laminar flow that the effect of cross sectional shape of the channel is of great importance, especially in the laminar flow region. They used two geometric coefficients of the flume first proposed by Straub *et al.* (1958). They did this for rectangular, triangular, semi-circular, and semi-elliptical channels. For this thesis, the rectangular and semi-circular channel shapes will be evaluated. Their work is evaluated for all the three non-Newtonian fluids used in this study. Since they did not present their work for the Herschel-Bulkley fluids (as kaolin suspension behaves), kaolin suspensions are rheologically characterised as power law and Bingham fluids to obtain the rheological parameters so that Kozicki and Tiu's Reynolds numbers could be evaluated.

4.2.1.1.1 Effect of shape on power law fluids

Kozicki and Tiu (1967) expressed the Reynolds number for a power law fluid, which includes two geometric coefficients (a and b) that make corrections for the effect of cross-sectional shape of the channel wall as follows:

$$Re = \frac{\rho V^{2-n} R_h{}^n}{2^{n-3} K \left(\dfrac{a + bn}{n} \right)^n}$$

(2.42)

The following Figures 4-1 and 4-2 show the analysis of CMC results which have the rheological characteristics of power fluids using Kozicki and Tiu's Reynolds number for rectangular and semi-circular flume shapes. Their work is only restricted to these flume shapes in this thesis because they did not evaluate the geometric coefficients for the trapezoidal channel. This analysis is presented on the Moody diagram, which depicts the fanning friction factor and Reynolds number.
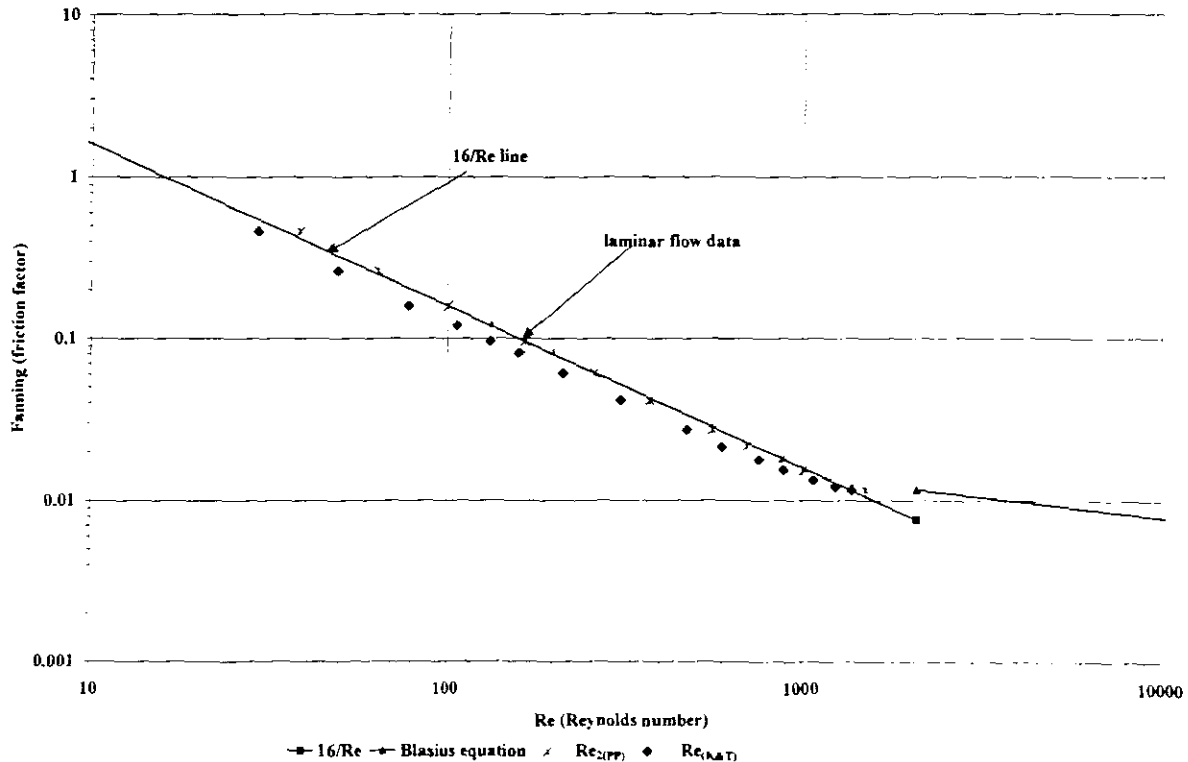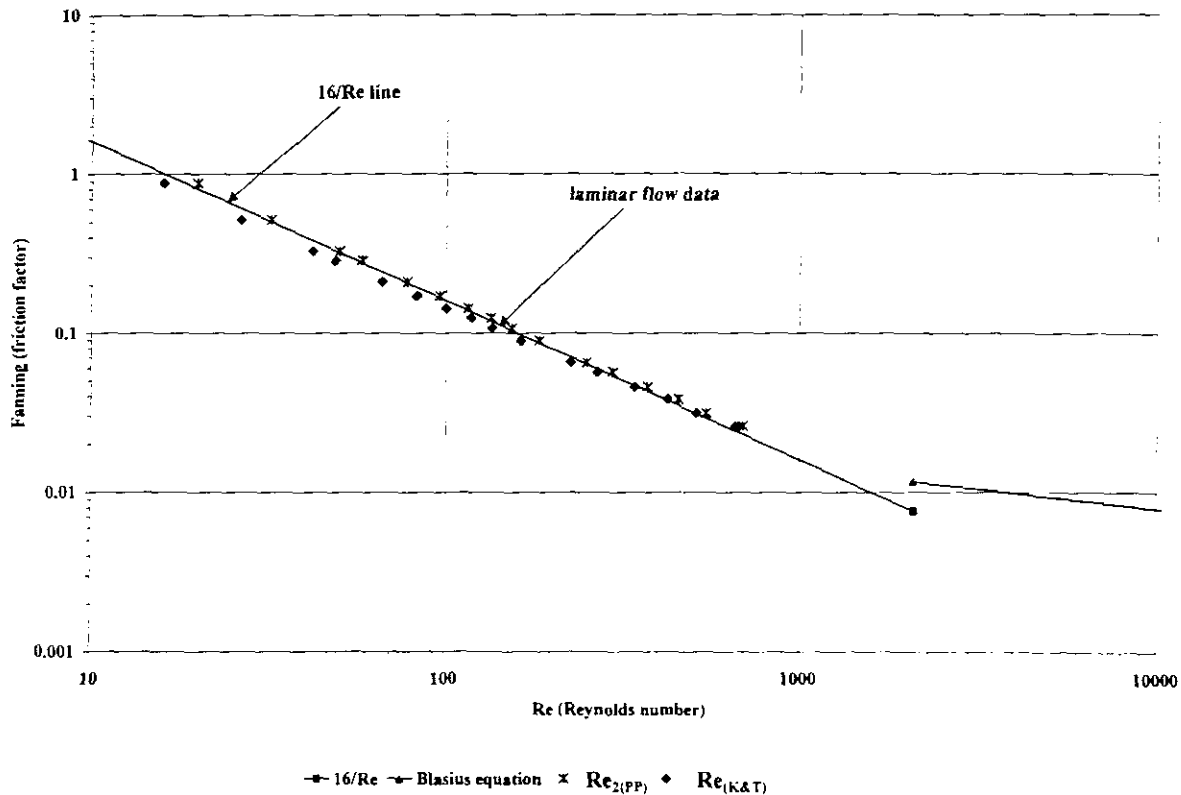

Figure 4-1. CMC 3% in a rectangular flume shape using $Re_{k\&t}$ model for 1-degree slope

Figure 4-2. CMC 3% in a semi-circular flume shape using $Re_{k\&t}$ model for 2-degree slope

Figure 4-1 and 4-2 show the evaluation of the Reynolds number model presented by Kozicki and Tiu (1967) on power law fluids. From these figures it can be seen that the model they presented under-predicts the laminar flow in both these flume shapes. This is evident by seeing the laminar flow data collapsing below the 16/Re line.

At this stage it is not clear whether the effect of the cross-sectional shape of the flume plays a major role in predicting the laminar flow of power law fluids in open channels. This will be confirmed by making a detailed comparison between their Reynolds number and Haldenwang's Reynolds number in the later stage of this chapter.

4.2.1.1.2 The effect of shape on the Bingham plastic fluids

Kozicki and Tiu (1967) also derived the Reynolds number for Bingham plastic fluid, which also incorporates the geometric shape factors (a and b) as follows:

$$Re = \frac{4R_h V \rho}{K} \left[\frac{1}{a+b} - \frac{1}{b}\left(\frac{\tau_y}{\tau_o}\right) + \frac{a}{b(a+b)}\left(\frac{\tau_y}{\tau_o}\right)^{1+\frac{b}{a}} \right]$$ (2.43)

Since Kozicki and Tiu (1967) did not present the effect of shape for trapezoidal channels, this equation is limited to rectangular and semi-circular flume shapes in this thesis. The following figures show the evaluation Kozicki and Tiu's Reynolds number for the bentonite results which has the rheological characteristics of a Bingham fluid. The results are also depicted on a Moody diagram as shown in Figures 4-3 and 4-4.
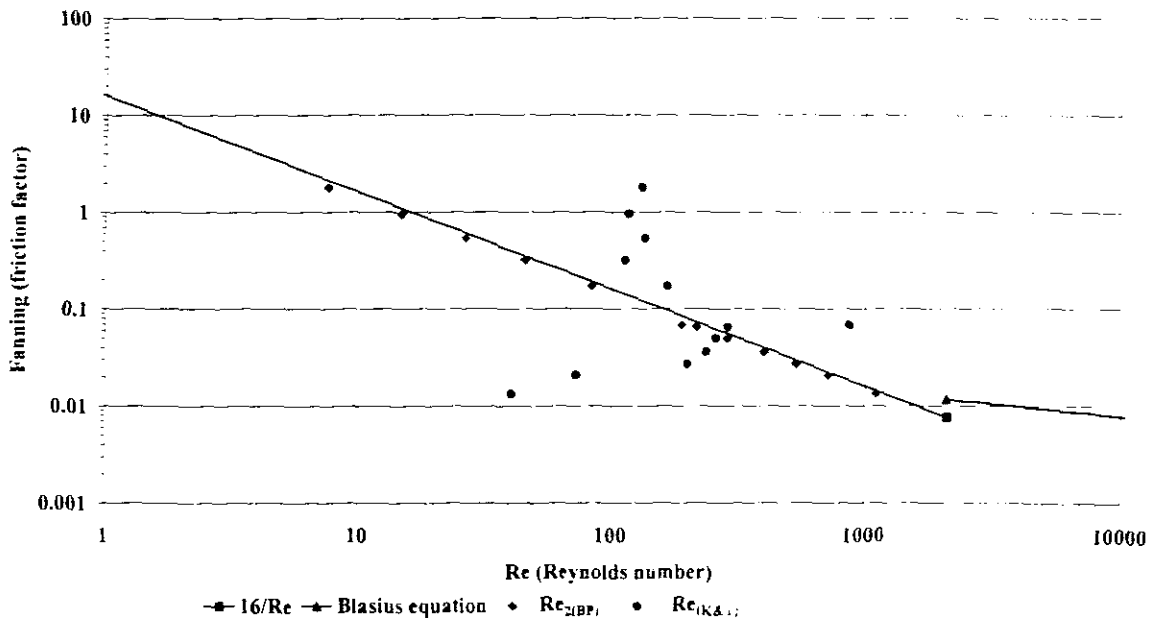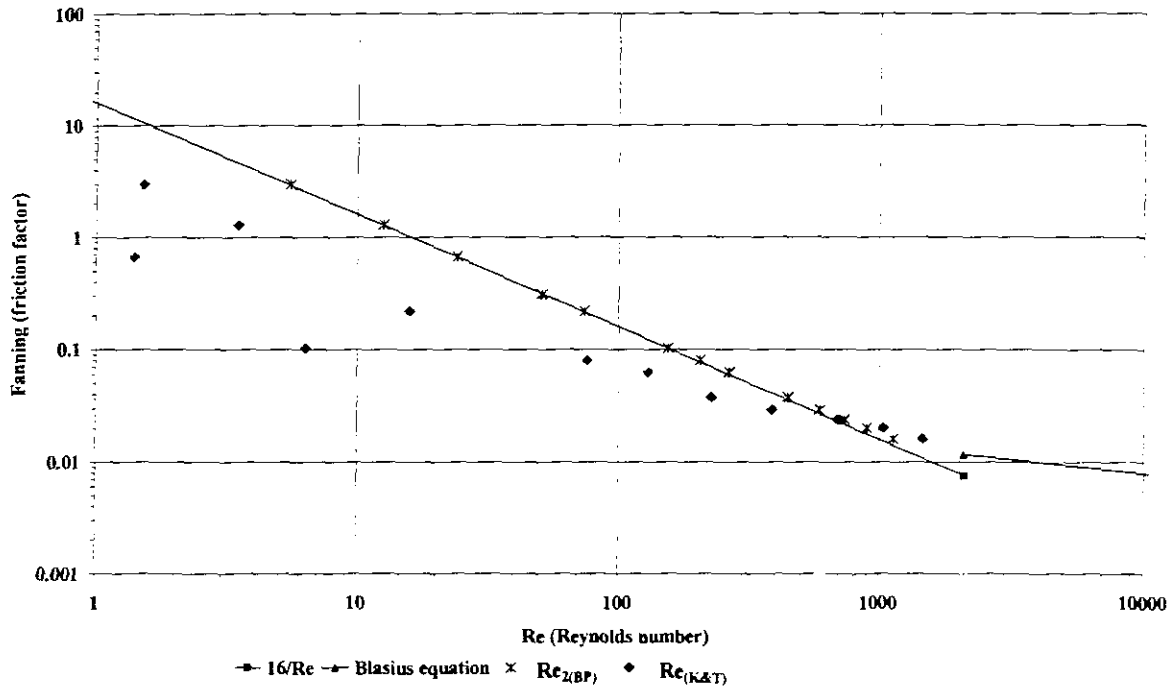

Figure 4-3. Bentonite 4.6% in a rectangular flume shape using Re$_{k&}$ model for 2-degree slope

Figure 4-4. Bentonite 4.6% in a semi circular flume shape using $Re_{k\&t}$ model for 1-degree slope

From Figure 4-3 and 4-4 it can be clearly seen that the Reynolds number model proposed by Kozicki and Tiu (1967) for Bingham plastic fluids does not predict the laminar flow for both these flume shapes at all because the laminar data points are scattered below and above the 16/Re line. The correction factors they suggested for the effect of cross-sectional shape of the channel seem not to be working in their Reynolds number for Bingham plastic fluid used in this thesis.

4.2.1.1.3 The shape effect on kaolin results

Kozicki and Tiu (1967) did not propose the Reynolds number for the Herschel-Bulkley fluids as kaolin suspension behaves. Some authors have chosen to characterise kaolin clay as a Bingham fluid (Hao and Zhenghai, 1982), therefore in this thesis the kaolin clay will also be characterise as a power law and a Bingham fluid to evaluate Kozicki and Tiu's model.

4.2.1.1.4 Characterising the kaolin suspension as a power law fluid

This is done by rheologically characterising the kaolin suspension as a power law fluid. The resulting rheological parameters are used to determine Kozicki and Tiu's Reynolds number for a power law fluid that incorporates the shape factors, which will be used in a Moody diagram to predict the laminar flow of kaolin suspension.

The following figures show the evaluation of the Kozicki and Tiu's Reynolds number model of a kaolin suspension, which has been rheologically characterised as a power law fluid.
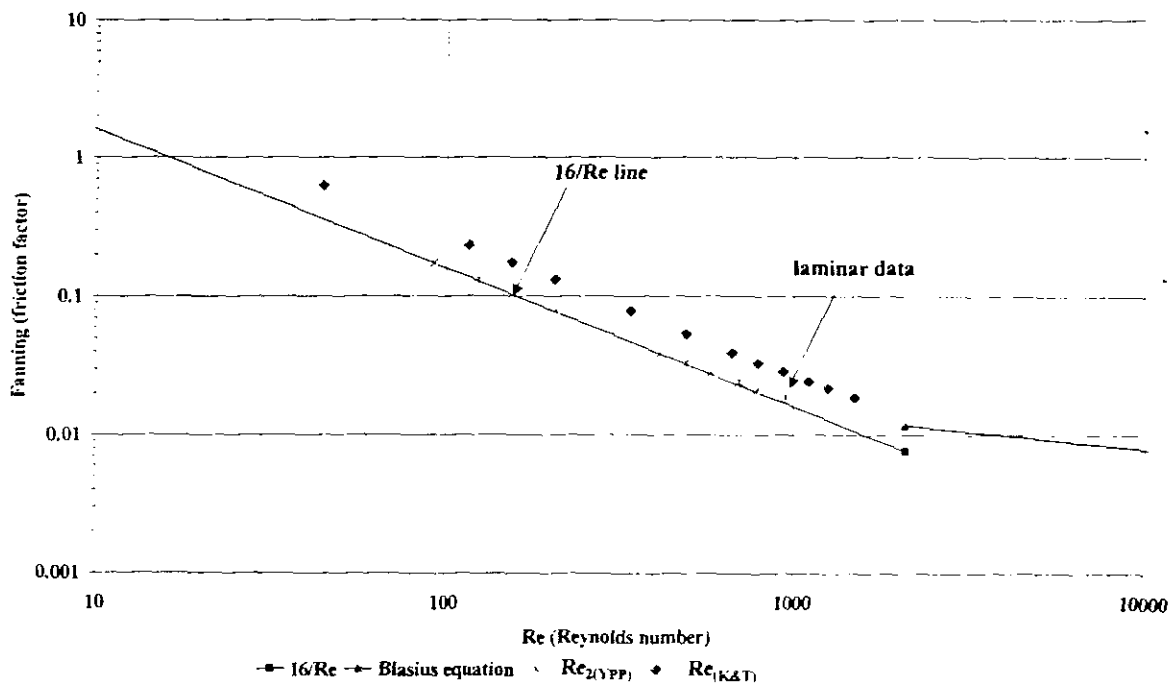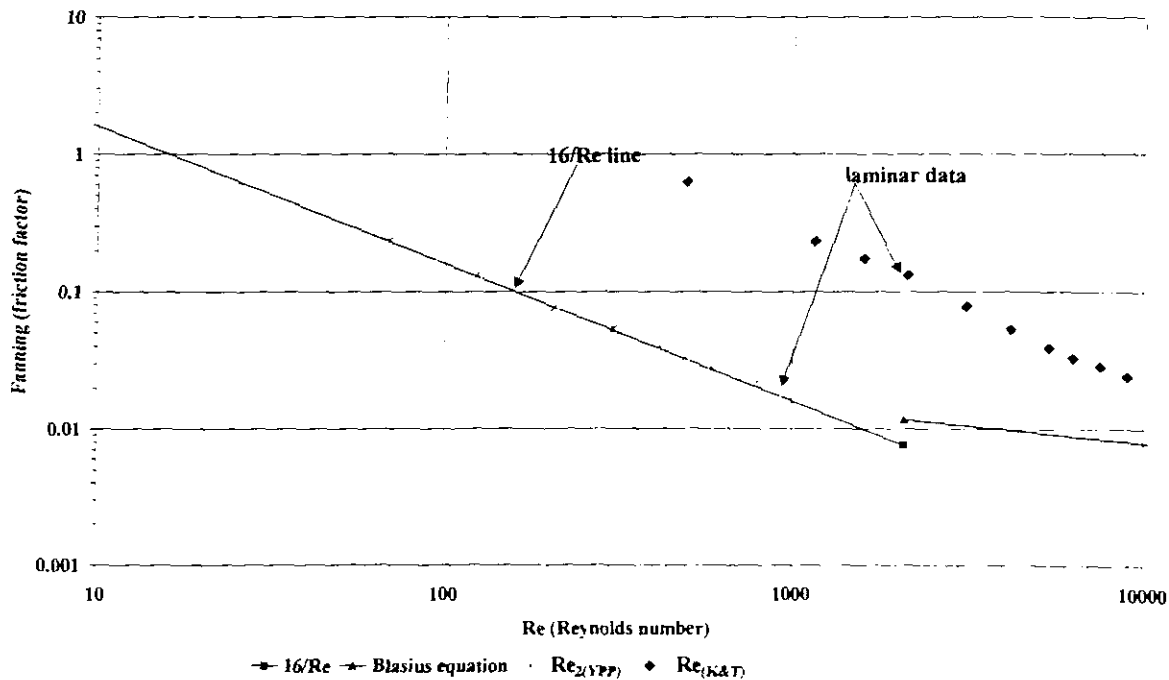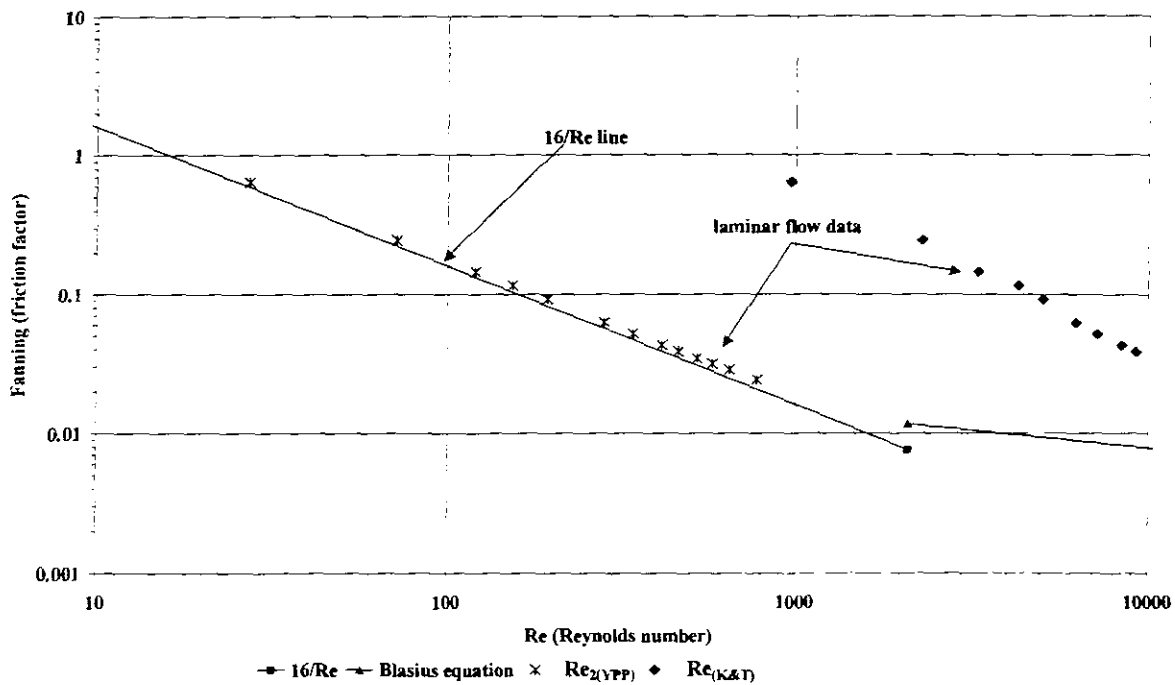

Figure 4-5. Kaolin 7.1% in a rectangular flume shape using $Re_{K\&t}$ model
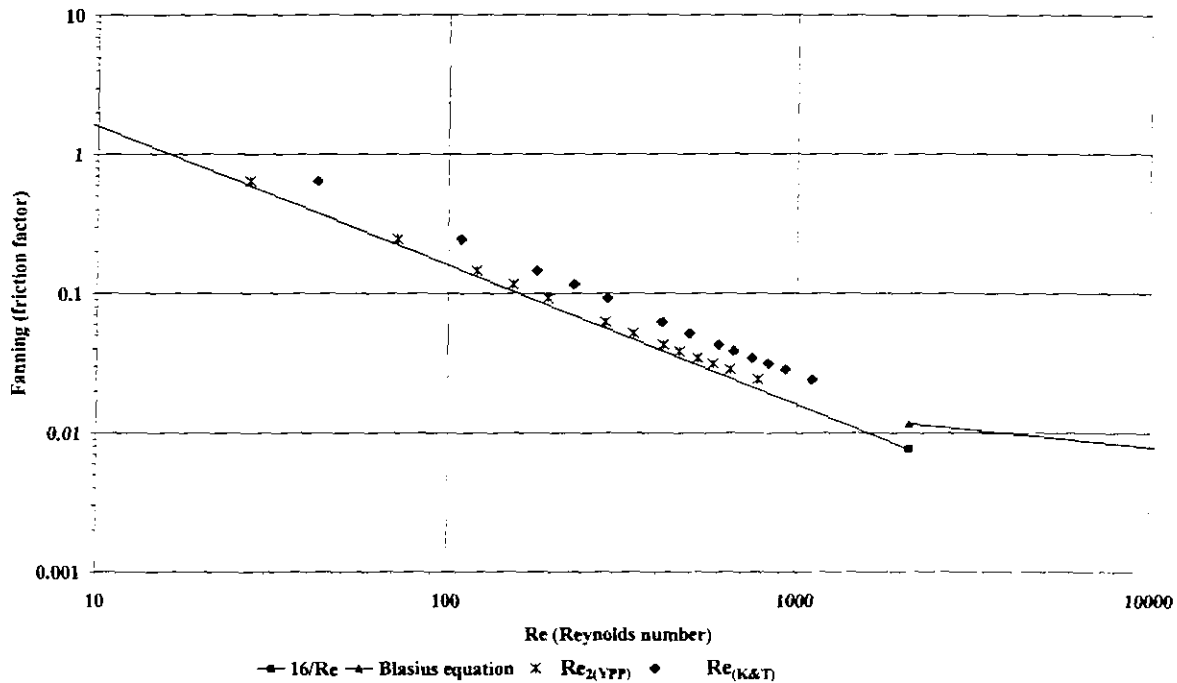
Figure 4-6. Kaolin 7.1% in a semi-circular flume shape using Re$_{k\&t}$ model

From Figure 4-5 and 4-6 it can be seen that the laminar data points do not collapse on 16/Re line, they are all above it. This shows that the Reynolds number model proposed by Kozicki and Tiu (1967) for the power law fluid does not adequately predict the laminar flow of kaolin suspension in both flume shapes.

But this gives a better prediction than the Bingham fluids results as shown in Figure 4-3 and 4-4. Possibly the problem lies with the yield stress in the evaluation of Kozicki and Tiu's Reynolds numbers.

4.2.1.1.5 Characterising kaolin suspension as a Bingham plastic fluid

Here the kaolin suspension is rheologically characterised as a Bingham plastic fluid. The resulting rheological parameters are used to determine the Kozicki and Tiu's Reynolds number for Bingham fluids that incorporates the shape factors, which will also be used in a Moody diagram to predict the laminar flow of kaolin suspension.

Such Moody diagrams are depicted in Figure 4-7 and 4-8 as follows:

Figure 4-7. Kaolin 7.1% in a rectangular flume shape using Re$_{k\&t}$ model

Figure 4-8. Kaolin 7.1% in a semi-circular flume shape using Re$_{k\&t}$ model

From Figure 4-7 and 4-8 it can be seen clearly that the laminar data points do not collapse at all on 16/Re line, they are in the region where the laminar flow cannot be expected. This shows that Kozicki and Tiu's Reynolds number for Bingham fluids cannot predict the laminar flow of kaolin suspension in both these flume shapes.

But the results of the kaolin suspension when it was characterised as a power law fluid gave a better prediction (though not good) than when it was characterised as a Bingham fluid. This shows that the Kozicki and Tiu's model cannot predict the laminar flow of the yield stress fluids used in this thesis.

4.2.2 Evaluation of the work done by Hao and Zhenghai

Hao and Zhengai developed the Reynolds number model similar to the Re_2 model for Bingham fluids proposed by Haldenwang et al. (2002). Their Reynolds number is only valid for the Bingham plastic fluids and is written as follows:

$$Re_{zhang} = \frac{4\rho R_h V}{K + \frac{\tau_y R_h}{2V}} \tag{2.45}$$

Although this equation is written in a different format than the Re_2 model for Bingham fluids, when simplified mathematically it will be the same. Therefore Hao and Zhengai's model will not be evaluated separately from the Re_2 model for Bingham fluids proposed by Haldenwang et al. (2002), which will be evaluated in the later sections of this chapter.

4.2.3 Evaluation of the work done by Coussot

The design protocol presented by Coussot (1994) for Herschel-Bulkley fluids, which is described in chapter 2, is evaluated in this chapter with the database compiled for the kaolin suspension since it has rheological characteristics of the Herschel-Bulkley fluid.

This evaluation is made by comparing the actual velocity data (experimentally found) with the velocity obtained from the Coussot prediction as depicted in Figure 4-11 and 4-12 for both rectangular and trapezoidal channel shapes respectively. This relationship is expected to be theoretically linear, if it is not linear then the Coussot predicrion is not precise.
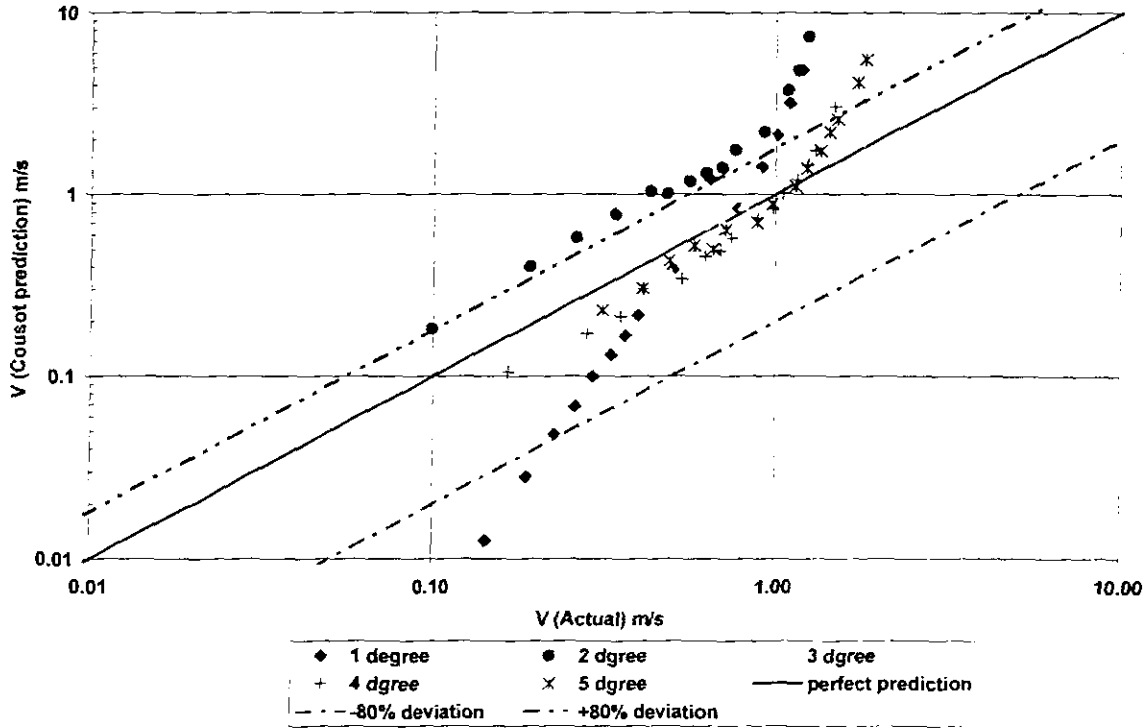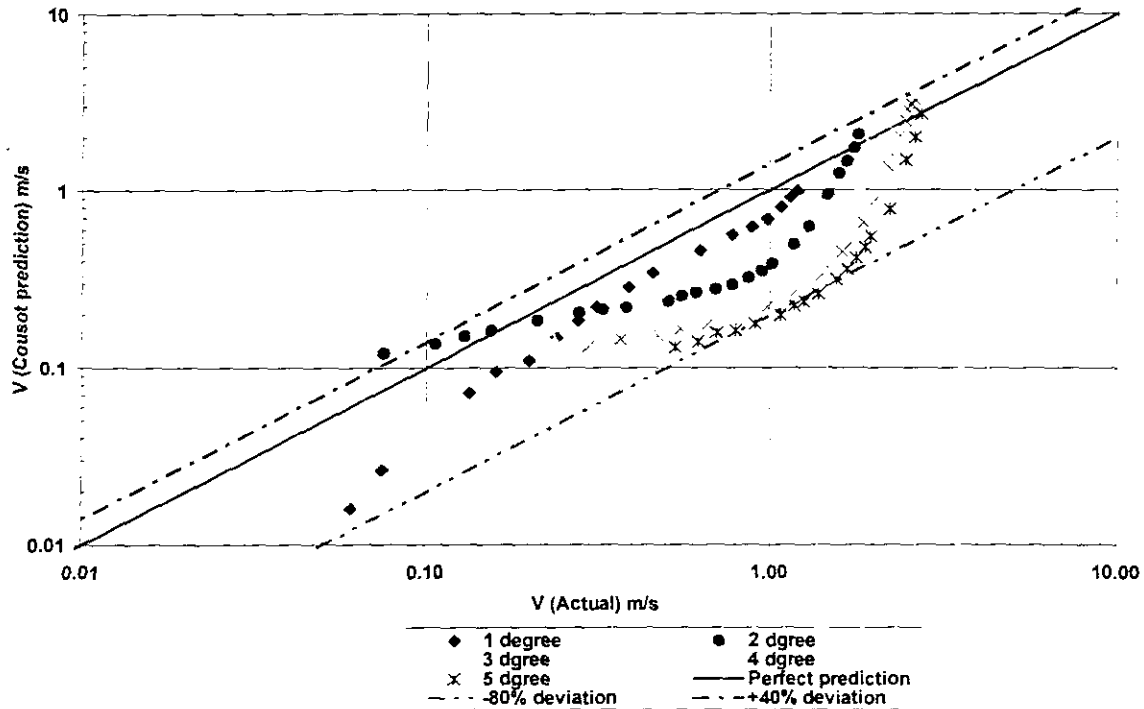
Figure 4-9. V predicted (Coussot) versus V actual. 7.1% kaolin in a rectangular flume shape

Figure 4- 10. V predicted (Coussot) versus V actual. 7.1% Kaolin in a trapezoidal flume shape

From Figure 4-9 and 4-10 it can be seen that the velocity obtained from the Coussot prediction does not have a linear relationship as expected with the actual velocity for both rectangular and trapezoidal channel shapes. It seems as if there is a slope effect, though not clear because the data points for all the slopes are collapsing on top of each other in an ascending order.

The shape factor Coussot (1994) introduced is not valid for all the range of depth/width ratios he claims it to be effective over.

It can be said that the Coussot prediction does not predict the laminar flow of Herschel-Bulkley fluid used in this study for both rectangular and trapezoidal flume shapes and does not clearly show the effect of cross-sectional shape of these channels over the ranges that were tested in this thesis. This could be caused by the effect of yield stress, which Coussot did not take into account in the formulae.

4.2.4 Evaluation of the work done by Abulnaga

The design protocol presented by Abulnaga (1997) for the Bingham plastic fluids described in Chapter 2 is evaluated with bentonite results since it has the characteristics of the Bingham plastic fluid. Although he did this for a semi circular flume shape, in this thesis his work is extended to rectangular and trapezoidal flume shapes to check if there is any role a shape effect might play when evaluating his work. This is possible by using the different hydraulic radius of each channel shape.

He modified equations for the full pipe flows by expressing the Reynolds number (Re) and Hedström number (He) in terms of hydraulic radius as follows:

$$Re = \frac{4R_h V \rho}{\mu} \qquad (2.52)$$

$$\text{and} \qquad He = \frac{16R_h^2 \rho \tau_o}{\mu^2} \qquad (2.53)$$

He also modified the friction factor from the Buckingham equation as follows:

$$f_L = \frac{16}{Re}\left(1 + \frac{He}{6Re}\right) \qquad (2.55)$$

Both the Reynolds number and friction factor, which Abulnaga (1997) modified, are evaluated with the database for the bentonite suspension and depicted or a Moody diagram as shown in Figure 4-11 to 4-13.
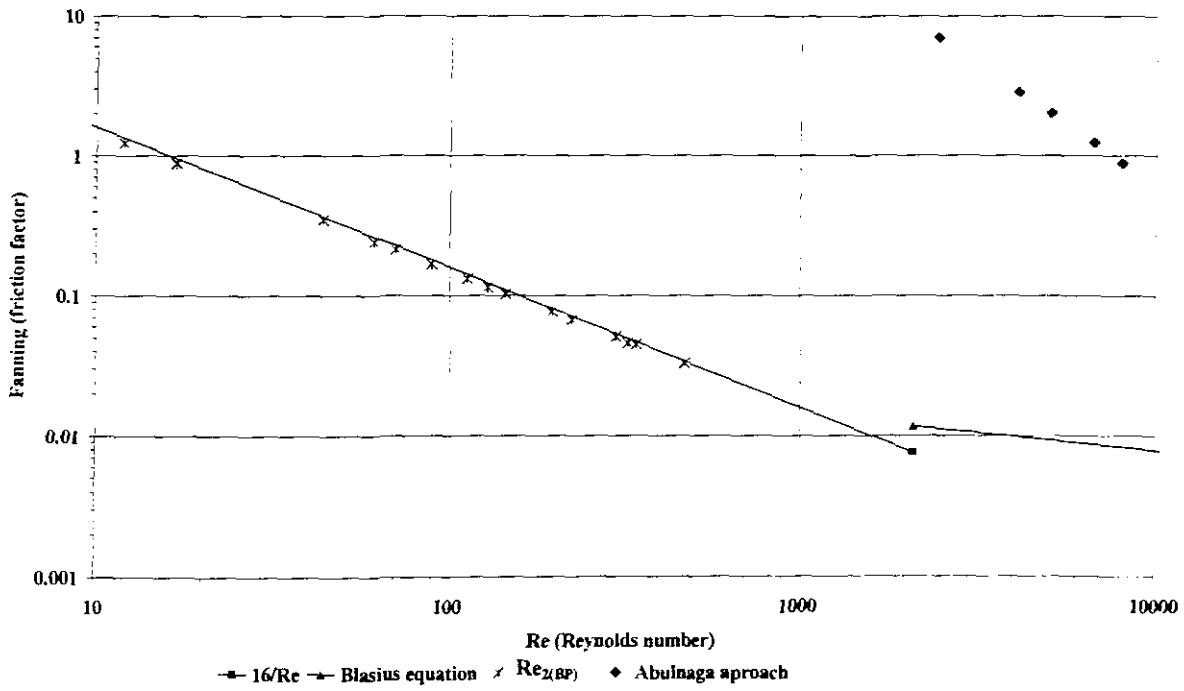
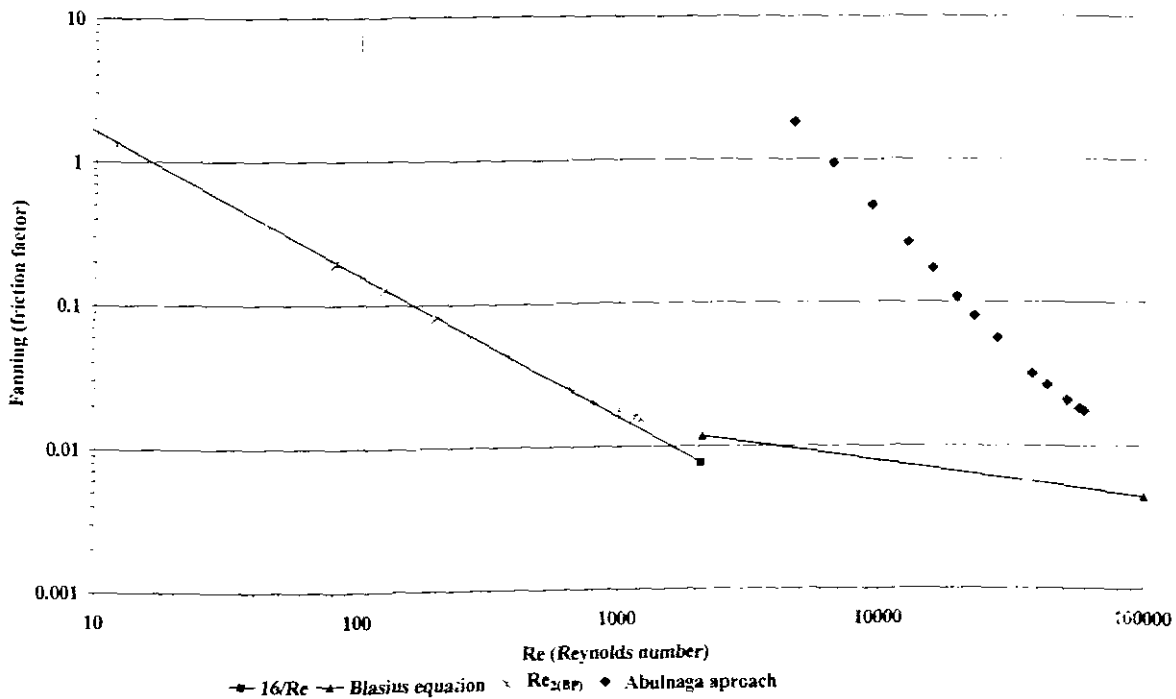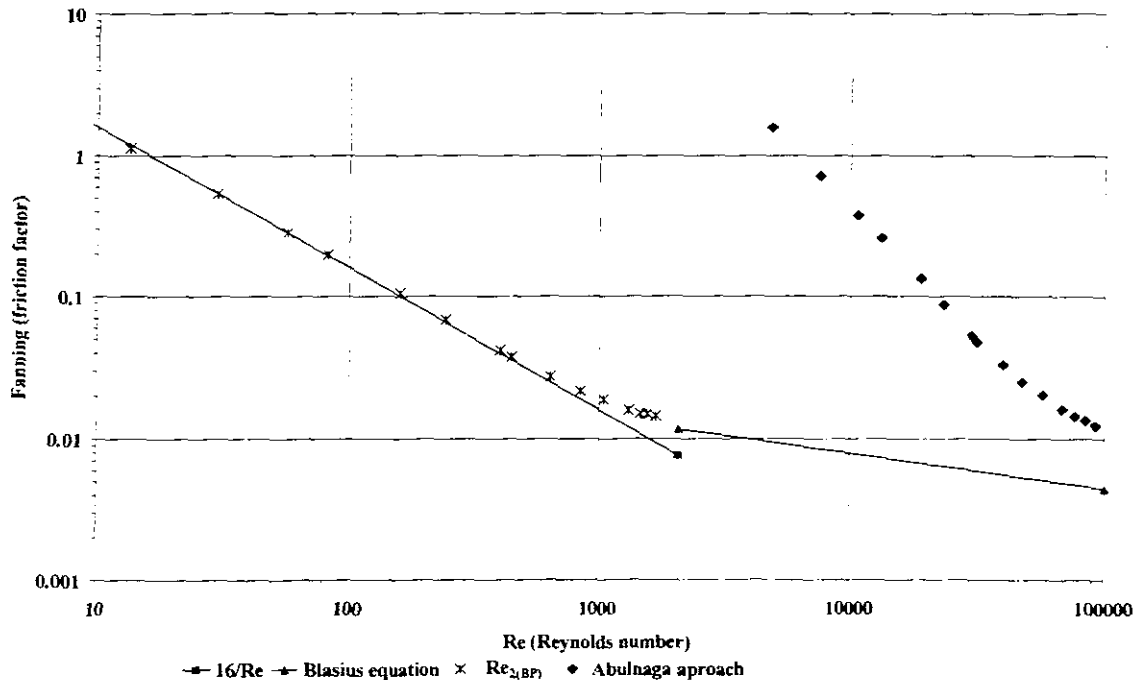**Figure 4-11. 6.2% Bentonite in a semi-circular flume shape showing Abulnaga's approach**

Figure 4-12. 6.2% Bentonite in a rectangular flume shape showing Abulnaga's approach

Figure 4-13. 6.2% Bentonite in a trapezoidal flume shape showing Abulnaga's approach

From Figure 4-11 to 4-13 it can be seen that the evaluation of Abulnaga's approach gives results that are far off the 16/Re line for all three flume shapes and those points are in the turbulent region. This is not possible considering that the fluid tested was very viscous. This shows that the design protocol Abulnaga (1997) devised is not valid for the Bingham fluid tested for this study.

From these figures it can also be said that there is no effect of shape in evaluating the design protocol presented by Abulnaga (1997) because these figures give similar results that are in the region where the laminar flow cannot be expected. This was the case when the effect of shape was evaluated previously using Kozicki and Tiu's model. Here just like in the evaluation of Kozicki and Tiu's model for Bingham fluids, the problem seems to be the yield stress.

The one simplification Abulnaga used in his design protocol is the negligence of the yield stress in the Reynolds number he proposed.

4.2.5 Evaluation of the work done by Haldenwang

Haldenwang *et al.* (2002) extended the Slatter model (1994) to non-Newtonian open channel flow by substituting pipe diameter with equivalent channel radius to predict the laminar flow region as follows:

$$Re_2 = \frac{8\rho V^2}{\tau_y + K\left(\frac{2V}{R_h}\right)^n} \qquad (2.56)$$

He tested the above formula for the rectangular flume shape only. However in this thesis it was extended to other channel shapes, namely semi-circular and trapezoidal shapes.

This model is evaluated with the laminar flow data compiled for CMC, bentonite and kaolin concentrations separately in the following section.

4.2.5.1 Evaluation of Re_2 model for CMC (power law fluid)

This evaluation is depicted on a Moody diagram to predict the laminar flow of power law fluids as shown in the following figures.
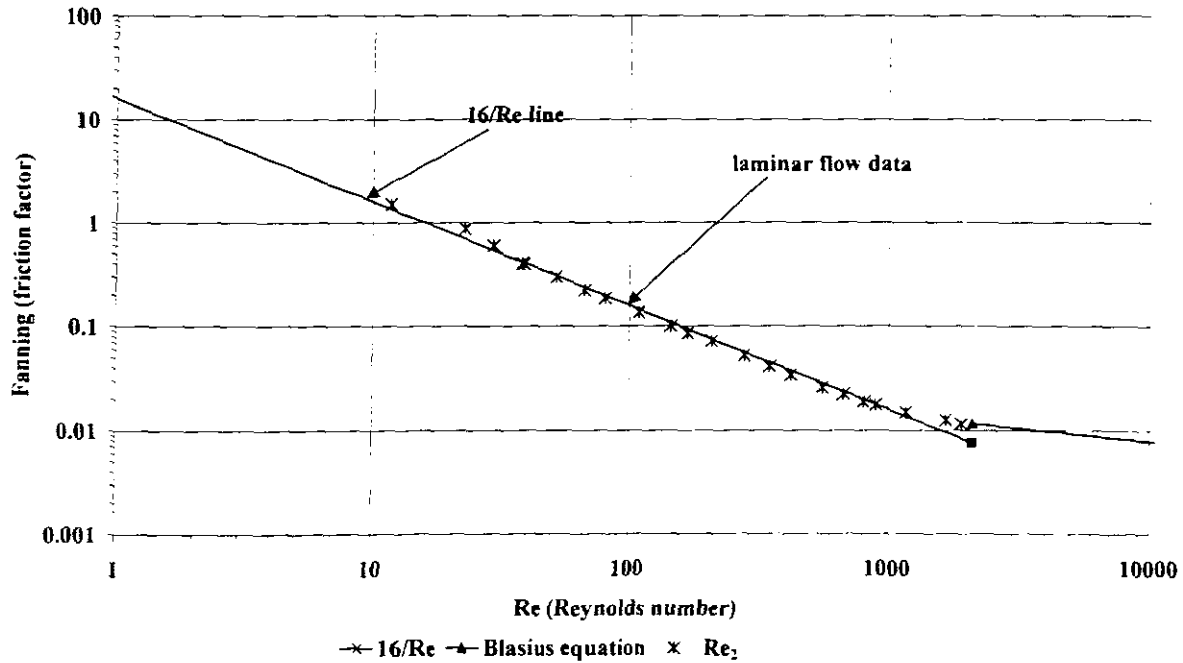
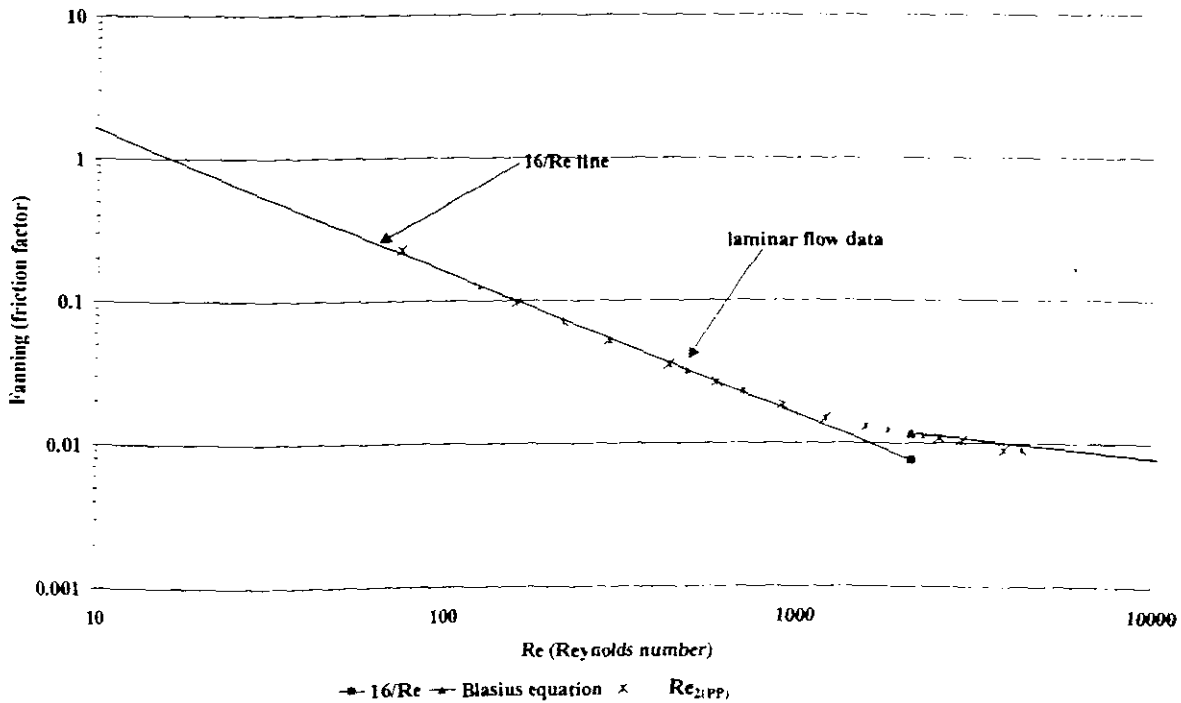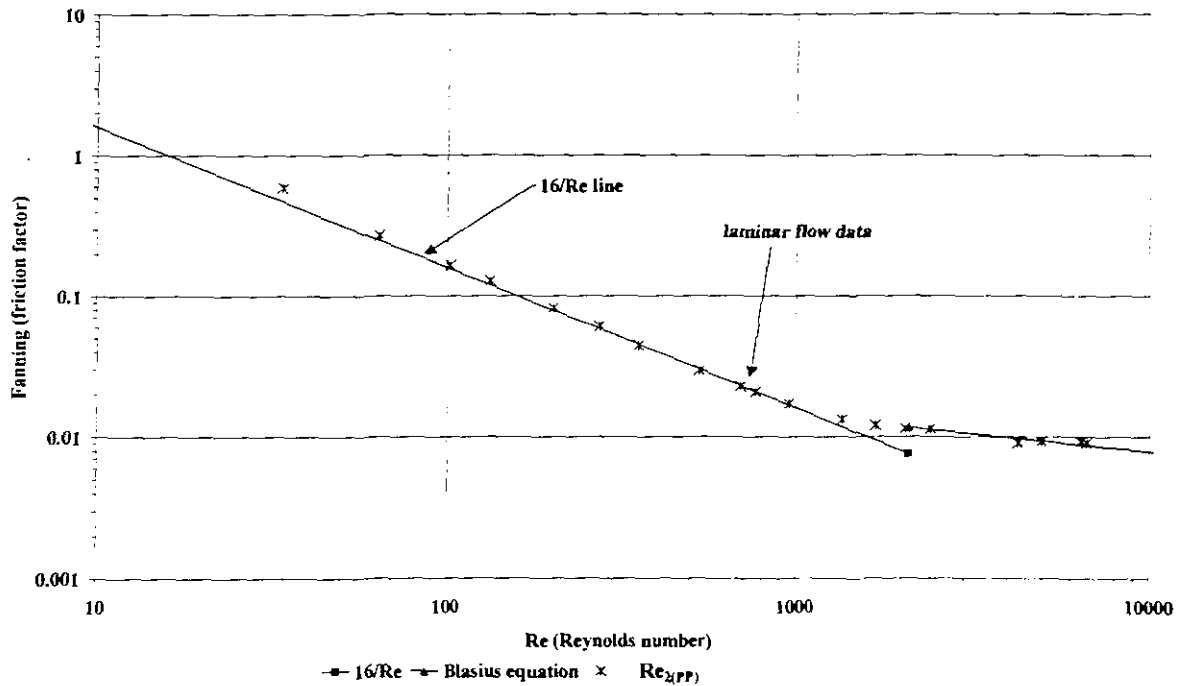**Figure 4-14. CMC 3% in a rectangular flume shape using Re₂ model**

Figure 4-15.CMC 3% in a semi-circular flume shape using Re₂ model

Figure 4-16.CMC 3% in a trapezoidal flume shape using Re₂ model

From Figure 4-14 to 4-16 it can be seen that the laminar data collapse well on the 16/Re line in all these flume shapes. This means that the Reynolds number model proposed by Haldenwang *et al.* (2002) predicts the laminar flow of power law fluids adequately.

These figures were taken for one-degree slope only. The results on other channel slopes can be found in Appendix A, and they confirm that the Reynolds number proposed by Haldenwang *et al.* (2002) predicts the laminar flow of power law fluids adequately.

4.2.5.2 The evaluation of the Re₂ model for bentonite results (Bingham plastic fluid)

The bentonite results, which have the rheological characteristics of Bingham plastic fluid, are analysed in the same way as the CMC results (power law fluid) were analysed.

The following figures show the bentonite results for all the three channel shapes used in this thesis using the Reynolds number model proposed by Haldenwang *et al* (2002) for predicting the laminar flow of non-Newtonian fluids in open channels.
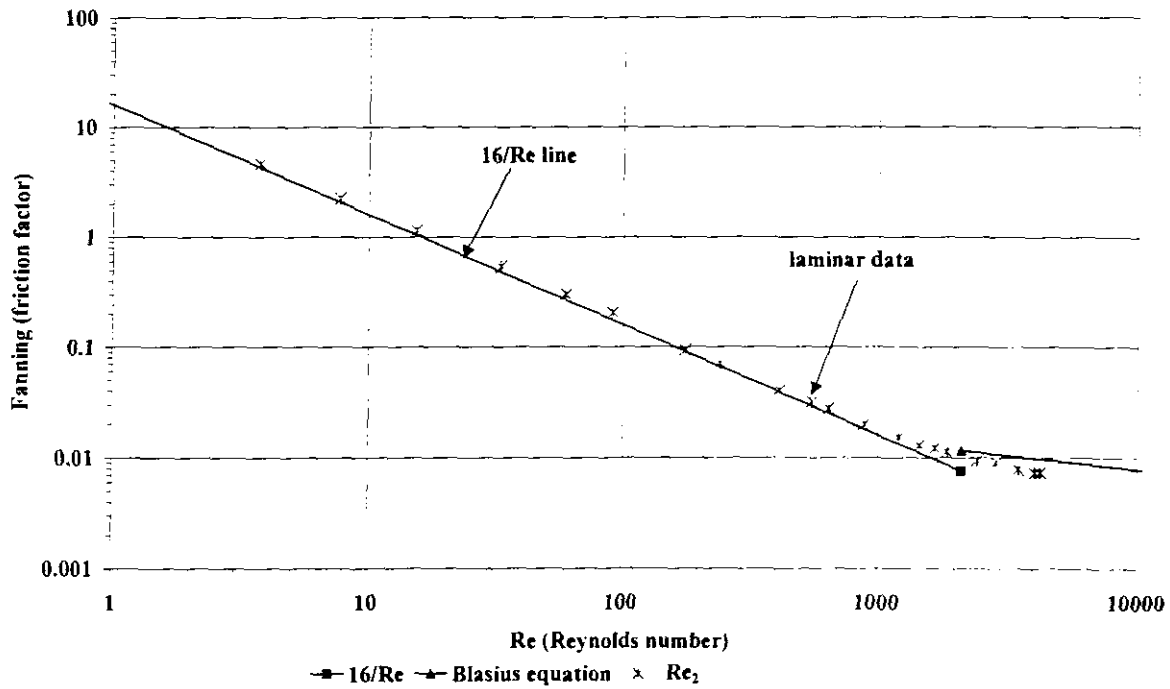
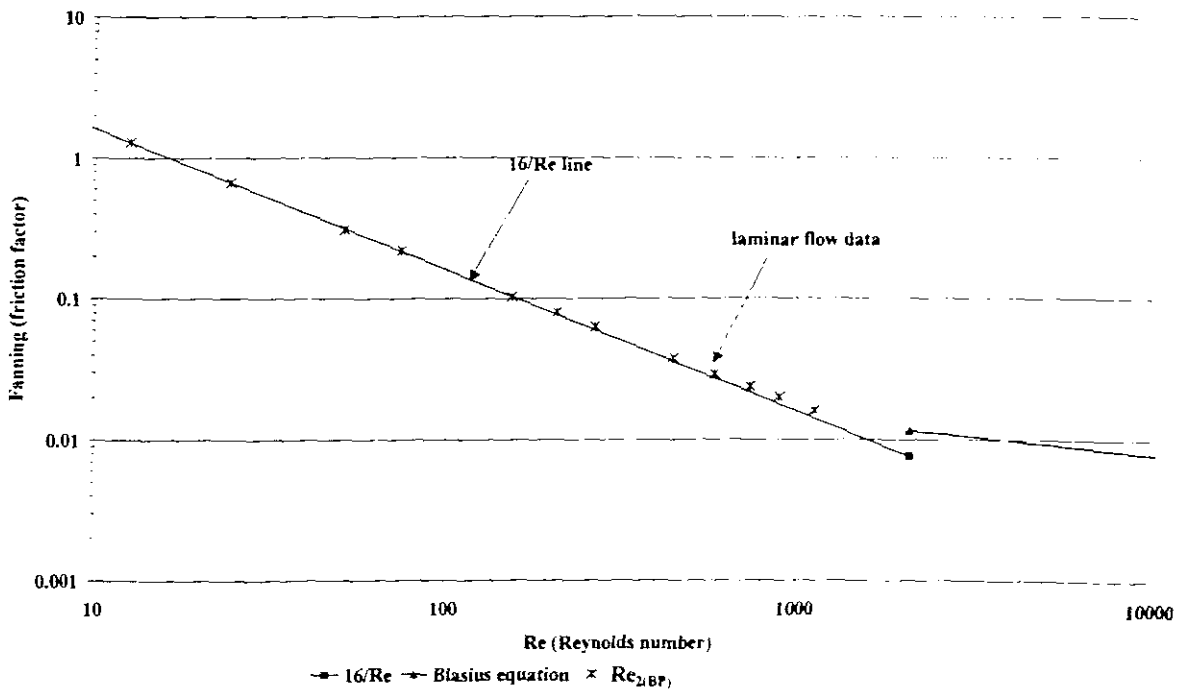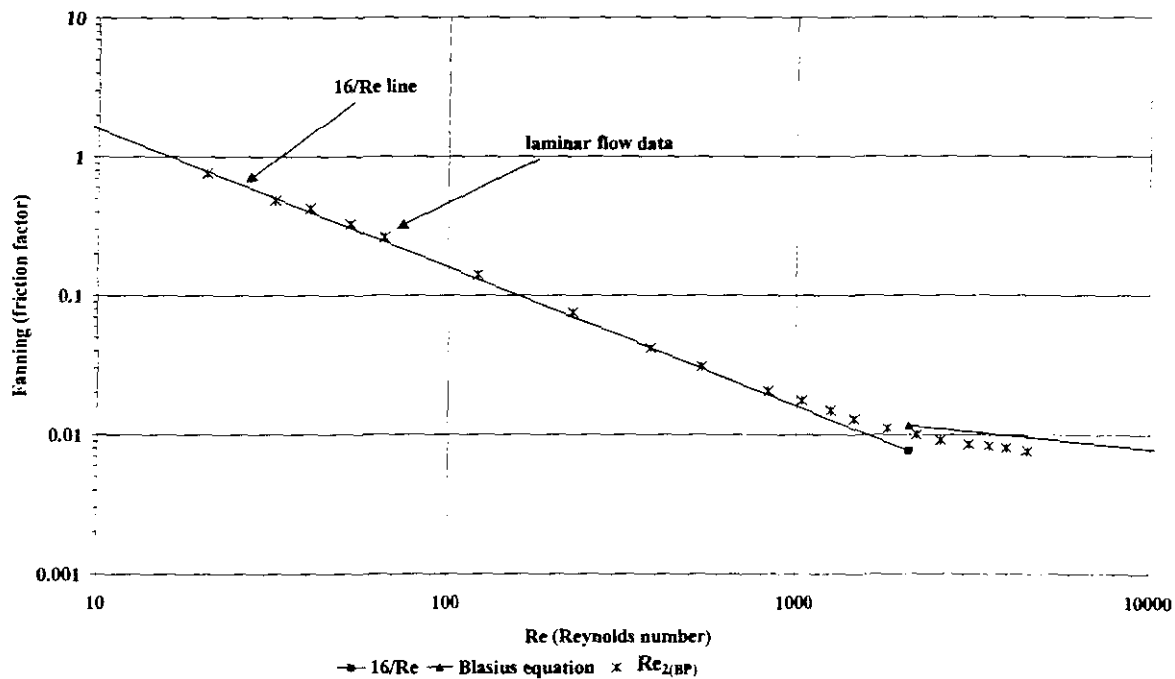**Figure 4-17. Bentonite 4.6% in a rectangular flume shape using Re₂ model in 1-degree slope**

Figure 4-18. Bentonite 4.6% in a semi-circular flume shape using Re₂ model in 1-degree slope

Figure 4-19. Bentonite 4.6% in a trapezoidal flume shape using Re₂ model in 2-degree slope

From Figure 4-17 to 4-19 it can be seen that the laminar data collapse well on the 16/Re line. This shows that the Reynolds number model proposed by Haldenwang *et al.* (2002) predicts the laminar flow of Bingham fluids adequately for all flume shapes used in this thesis.

4.2.5.3 The evaluation of the Re₂ model for kaolin results (Herschel-Bulkley fluid)

The kaolin results, which have the rheological characteristics of a Herschel-Bulkley (yield pseudoplastic) fluid are analysed the same way as the CMC and bentonite results.

The following figures show the kaolin results for all the three channel shapes used in this thesis using the Reynolds number model proposed by Haldenwang *et al.* (2002) for predicting the laminar flow of non-Newtonian fluids in open channels.
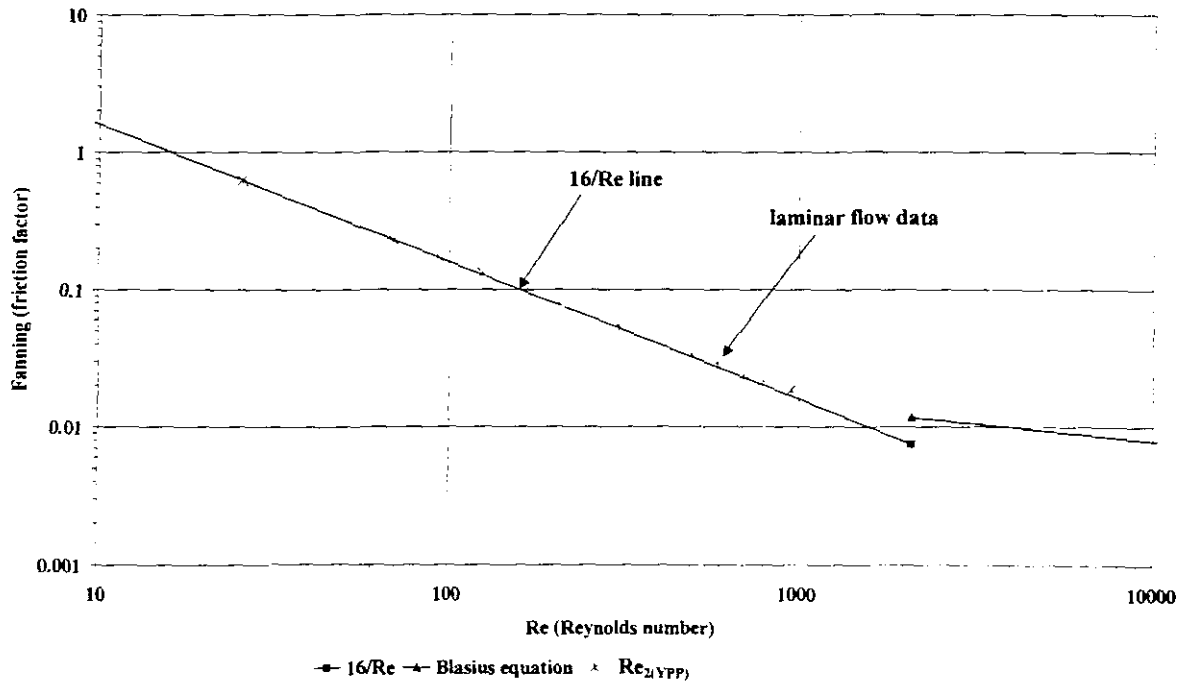
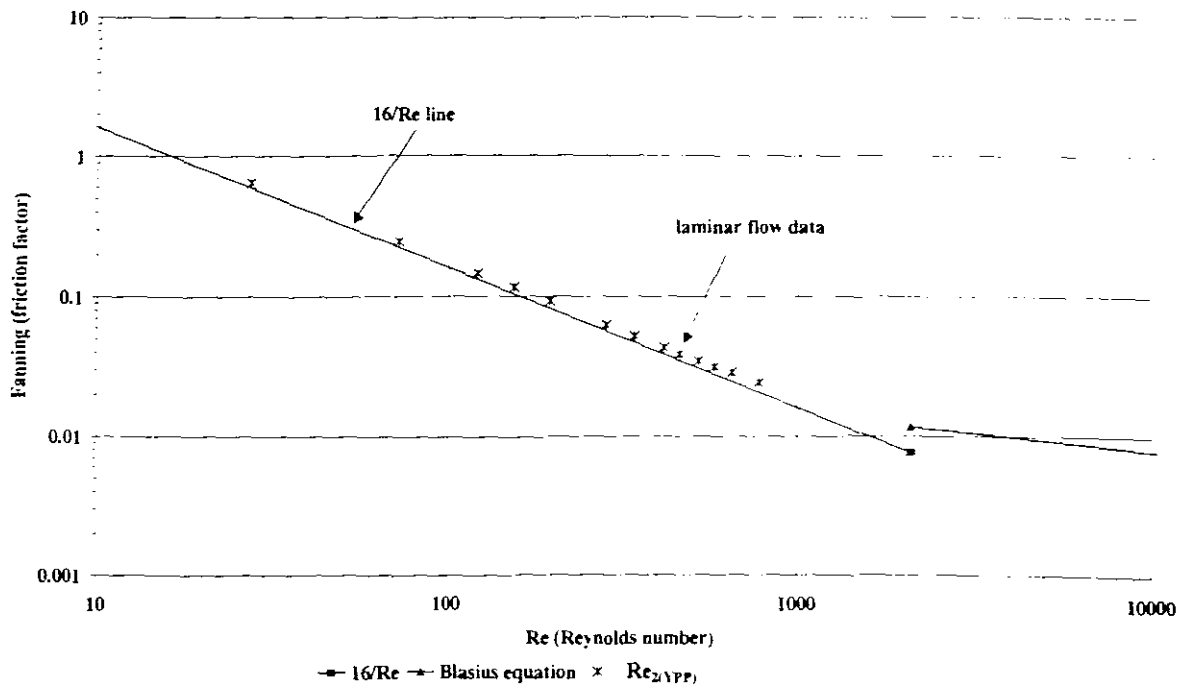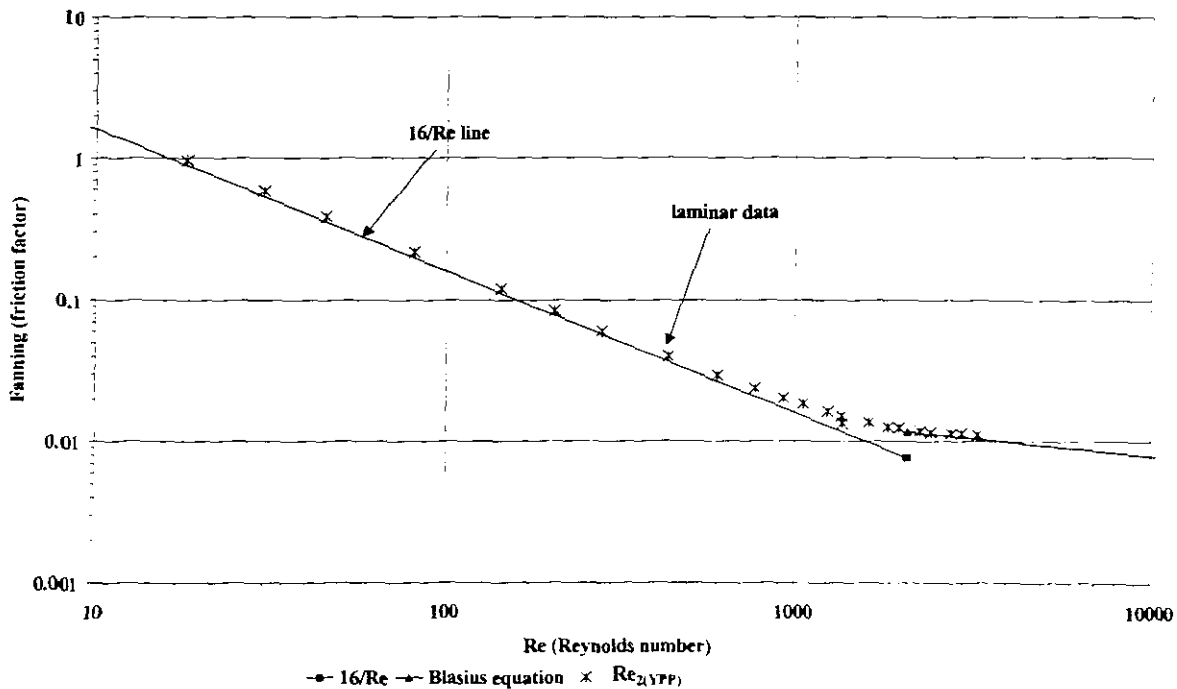Figure 4-20. Kaolin 7.1% in a rectangular flume shape using Re₂ model for 3-degree slope.

Figure 4-21. Kaolin 7.1% in a semi-circular flume shape using Re₂ model for 3-degree slope

Figure 4-22. Kaolin 7.1% in a trapezoidal flume shape using Re₂ model for 3-degree slope

From Figure 4-20 to 4-22 it can be seen that the all the laminar data points collapse well on the 16/Re line. This again shows that the Reynolds number model proposed by Haldenwang *et al.* (2002) predicts the laminar flow of the Herschel-Bulkley fluids adequately for all flume shapes.

4.2.5.4 Comments on Re₂ model

It is evident from the results in Figure 4-14 to 4-22 that the Reynolds number model proposed by Haldenwang *et al.* (2002) adequately predicts the laminar flow of all non-Newtonian fluids used in this thesis for all the flume shapes. The advantage of using this model is that it is not very complicated and that it does not include the corrections for the effect of the cross-sectional shape of the flume as has been previously proposed by Kozicki and Tiu (1967). The effect of shape in the Reynolds number proposed by Haldenwang *et al.* (2002) is adequately accounted for by the use of hydraulic radius in

the formula. The other important advantage of the Re_2 model is that it is reliable and can be used for all the channel shapes and slopes chosen in this study.

4.2.5.5 Comments on the effect of shape

It was shown in figure 4-1 and 4-2 that the model presented by Kozicki and Tiu (1967) that incorporates the effect of shape under predicts the laminar flow of power law fluids. For the Bingham fluid it was shown in figure 4-3 and 4-4 that their model does not predict the laminar flow of this fluid at all. These comments show that the effect of cross-sectional shape they suggested is not necessary to be included when predicting the laminar flow of these two fluids in both the rectangular and semi-circular flume shapes.

To quantify the above statement, a detailed comparison is made between the Reynolds number presented by Kozicki and Tiu (1967), which includes the correction factors for the effect of shape and the Reynolds number proposed by Haldenwang et $al.$ (2002).

4.2.6 COMPARISON BETWEEN Re_2 AND $Re_{(K\&T)}$ MODELS.

This comparison was made to find out more quantitatively which Reynolds number model predicts the laminar flow better for the rectangular and semi-circular channel shapes. The actual friction factors (fanning friction factors) are compared with the predicted friction factors given by the following equation:

$$f = \frac{16}{Re},$$

2.21

This comparison was made by:

- Calculating the friction factor using Equation 2.21 for each Reynolds number model.

- Calculating the percentage error between the differences of these friction factors and the actual friction factors.

- The resulting percentage errors of both Reynolds number models are compared by plotting them on a histogram. On the histogram the frequency shows the number of friction factor values and the percentage deviation shows the deviation range these values lie in.

Since Kozicki and Tiu (1967) did not present the geometric shape factors for the trapezoidal channel, this comparison is limited to the rectangular and semi-circular channels only.

This comparison is made for the power law and Bingham fluids as shown in the following histograms figures 4-23 to 4-26.
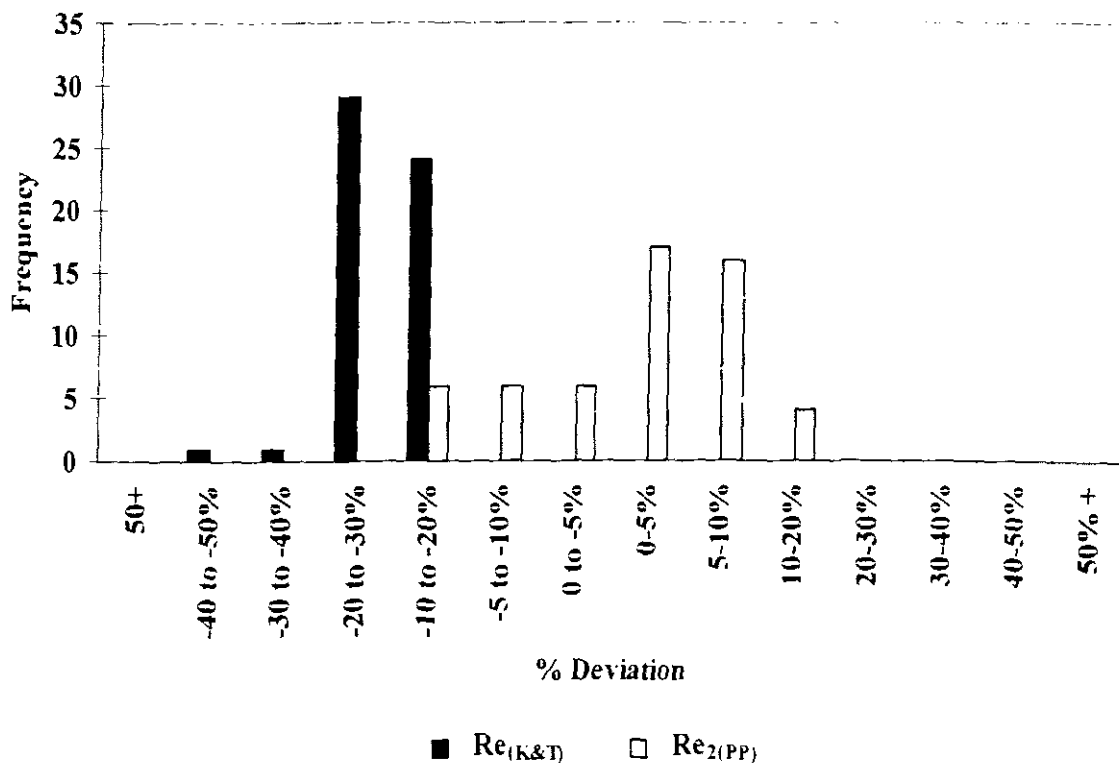

Figure 4-23. Friction factor deviation in laminar flow. 3% CMC in 300 mm rectangular flume shape
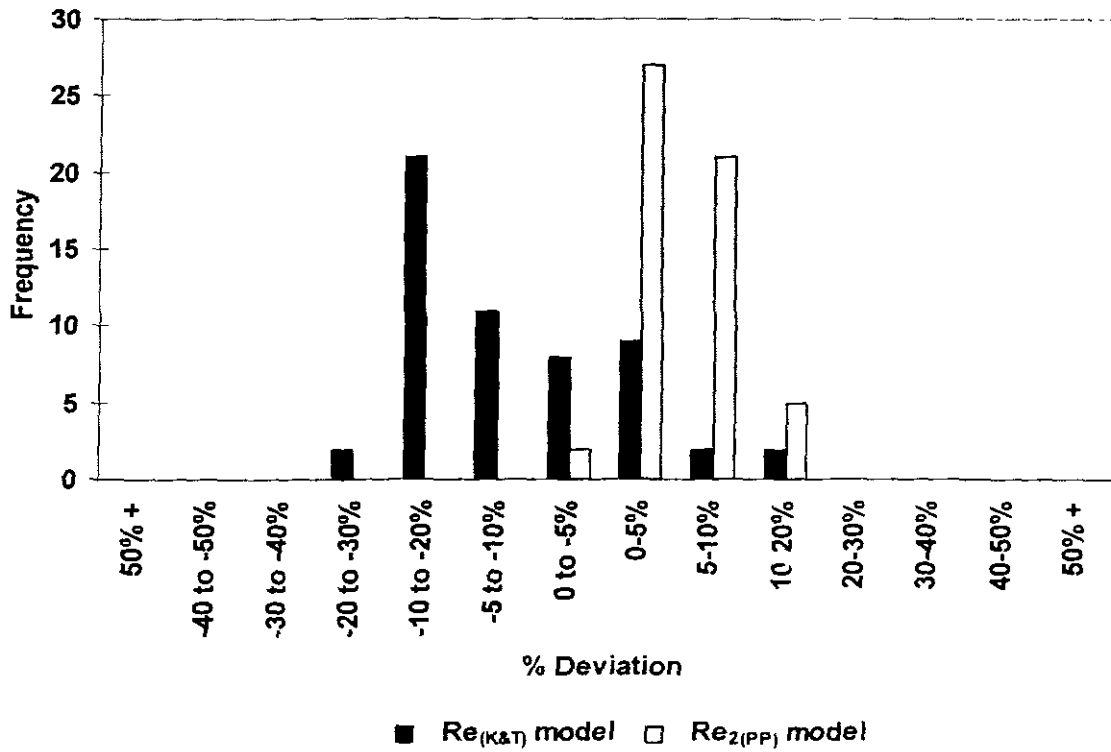
Figure 4-24. Friction factor deviation in laminar flow. 4% CMC in 300 mm semi-circular flume shape
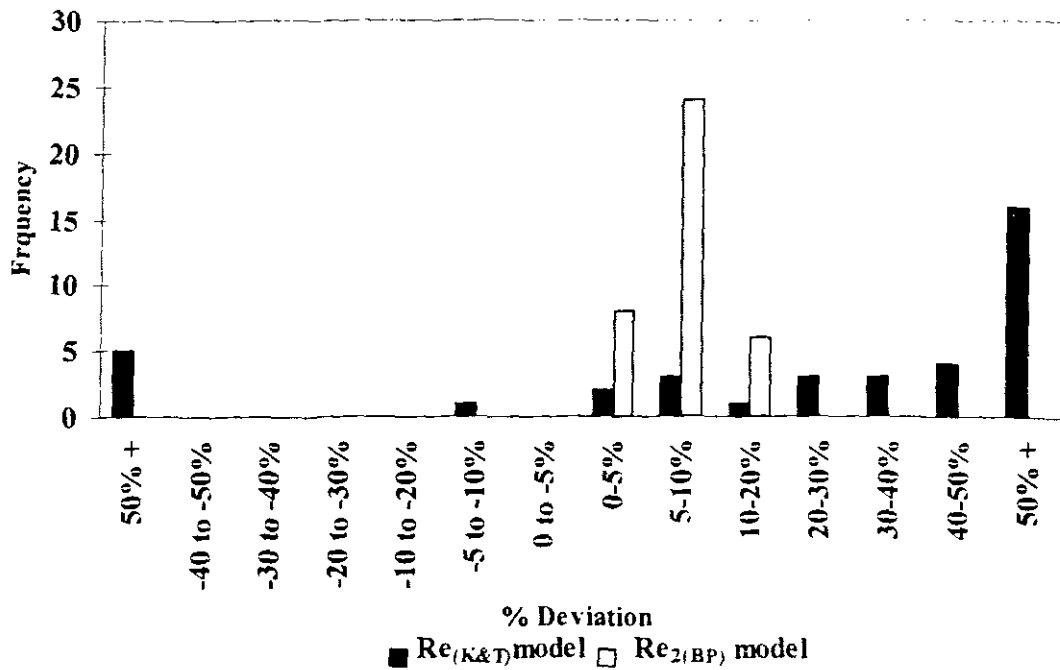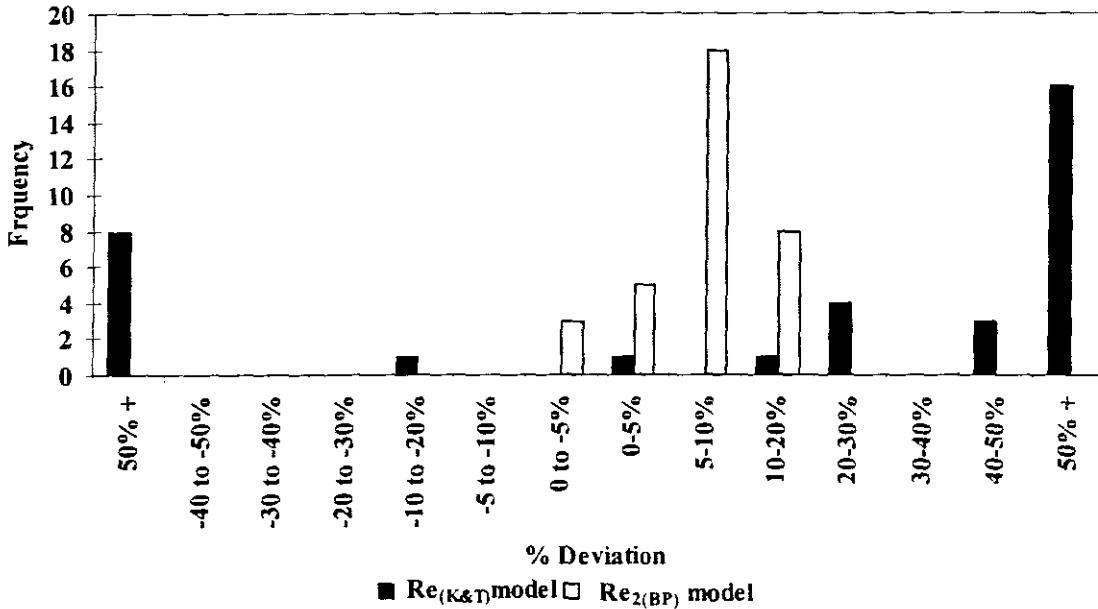

Figure 4-25. Friction factor deviations in laminar flow. 6.2% bentonite in 300 mm rectangular flume shape

Figure 4-26. Friction factor deviations in laminar flow. 6.2% bentonite in 300 mm semi-circular flume shape

From Figure 4-23 to 4-26 it can be seen that the Kozicki and Tiu Reynolds number gives deviation of friction factor value that lies at higher percentage ranges when compared with the Re_2 model proposed by Haldenwang et al. (2002). This shows that the Re_2 model predicts the laminar flow of both power law and Bingham fluids better than the Reynolds number model proposed by Kozicki and Tiu (1967). This is not that clear if one looks only at the histogram especially for the power fluids, therefore more evidence was needed to compare these Reynolds number models. This evidence was produced by calculating the log square error of the friction factor deviation.

4.2.6.1 The log square error (LSE) to compare the accuracy of Re_2 and $Re_{K\&T}$

The "log square error" (LSE) is used to check the accuracy between these two models when the percentage deviation errors on a histogram plot did not give clear evidence. This is also the difference between the measured friction factor (from Moody diagram plot) and the calculated friction factor using each Reynolds number model, but this is in a logarithmic form and it was presented as follows by Lazarus and Nielson (1978):

$$LSE = \frac{\sqrt{\sum\left[\log(f_{mes.}) - \log(f_{calc.})\right]^2}}{N-1}$$ (4.1)

Where: $f_{mes.}$ = Measured friction factor

$f_{calc.}$ = Calculated friction factor

and N = Number of observation or data points.

The smaller the LSE value, the more accurate the model and vice versa. The following table shows the LSE values for rectangular and semi circular flume shapes.

Table 4-1. Comparison of the friction factor deviation using Re $_{K\&T}$ and Re$_2$ model for the 3%CMC and 6.2% bentonite results

	Re$_2$ Model	Re $_{(K\&T)}$ Model
Flume Shape	LSE	LSE
Rectangular (CMC)	0.0049	0.0161
Semi-circular (CMC)	0.0027	0.0048
Rectangular (bentonite)	0.0062	0.0867
Semi-circular (bentonite)	0.0067	0.1744

From Table 4-1 it can be seen that the LSE values for the Re$_2$ are less than LSE values for Re $_{(K\&T)}$ for both flume shapes. This is enough confirmation that the Re$_2$ model gives friction factor values that have less error than the Re $_{(K\&T)}$ for both these flume shapes.

All the above evidence together with the histograms shows that the Reynolds number model proposed by Haldenwang *et al.* (2002) predicts the laminar flow region of the power law and Bingham fluids better than the Reynolds number model proposed by Kozicki and Tiu (1967) for all the flume shapes used in this study. Therefore there is no need to include the effect of shape in predicting the laminar flow of power law and Bingham fluids.

4.3 THE EFFECT OF THE RHEOLOGICAL MODEL USED IN LAMINAR FLOW

When characterising the non-Newtonian fluid, it is important to make sure that the correct model is fitted to the rheogram.

The Reynolds numbers used in this thesis to analyse the laminar flow regime contain rheological parameters τ_y, K, and n to characterise the fluid. After the tube viscometer data has been corrected using the Rabinowitsch-Mooney transformation the curve is fitted to the data to be either a Bingham, or a power law, or a Herschel-Bulkley fluid.

In this thesis, CMC solution was classified as a power law fluid, kaolin suspension as a Herschel-Bulkley fluid, and bentonite suspension as a Bingham fluid. In this section each material is rheologically classified as a power law, Herschel-Bulkley, and a Bingham fluid to determine if this will have an effect on the results.

The Reynolds number model used to check this effect is the one proposed by Haldenwang *et al.* (2002), since it has been shown that it predicts the laminar flow adequately for all the non-Newtonian fluids used in this thesis. This is also depicted on a Moody diagram for all the three flume shapes used in this thesis.

4.3.1 4% CMC in a rectangular channel shape

The following figure shows an example where three rheological models were applied in characterising 4% CMC. This is depicted in a Moody diagram using Reynolds number proposed by Haldenwang *et al.*, 2002.
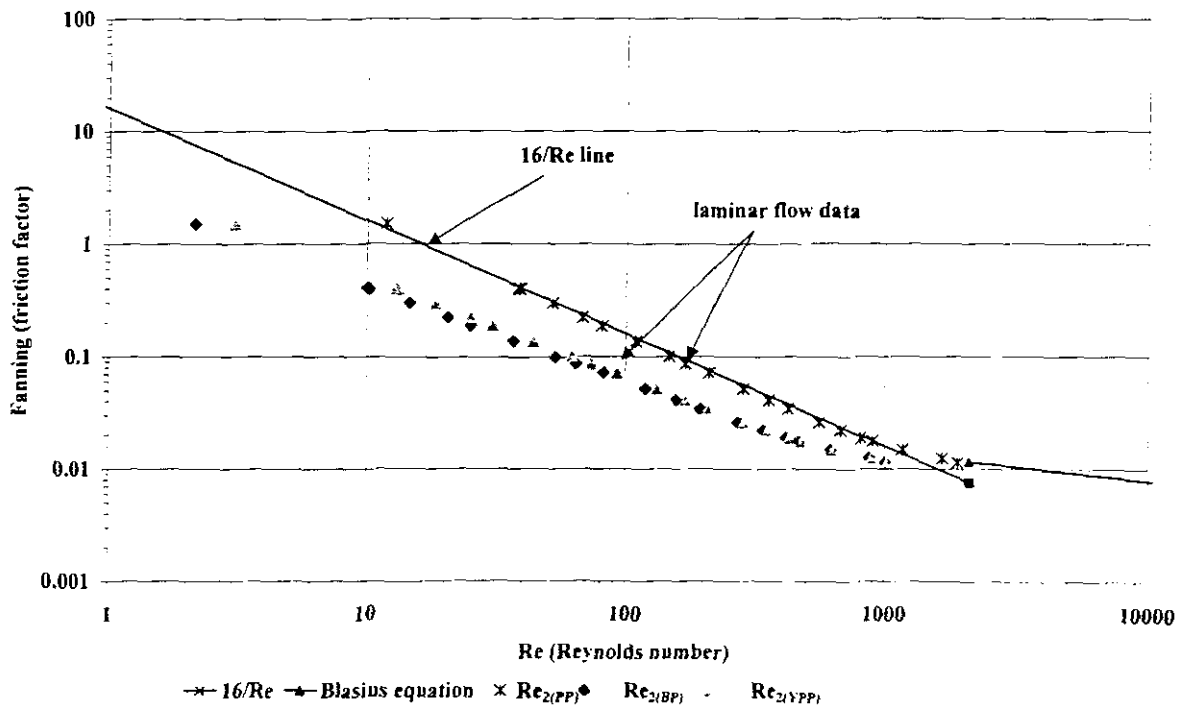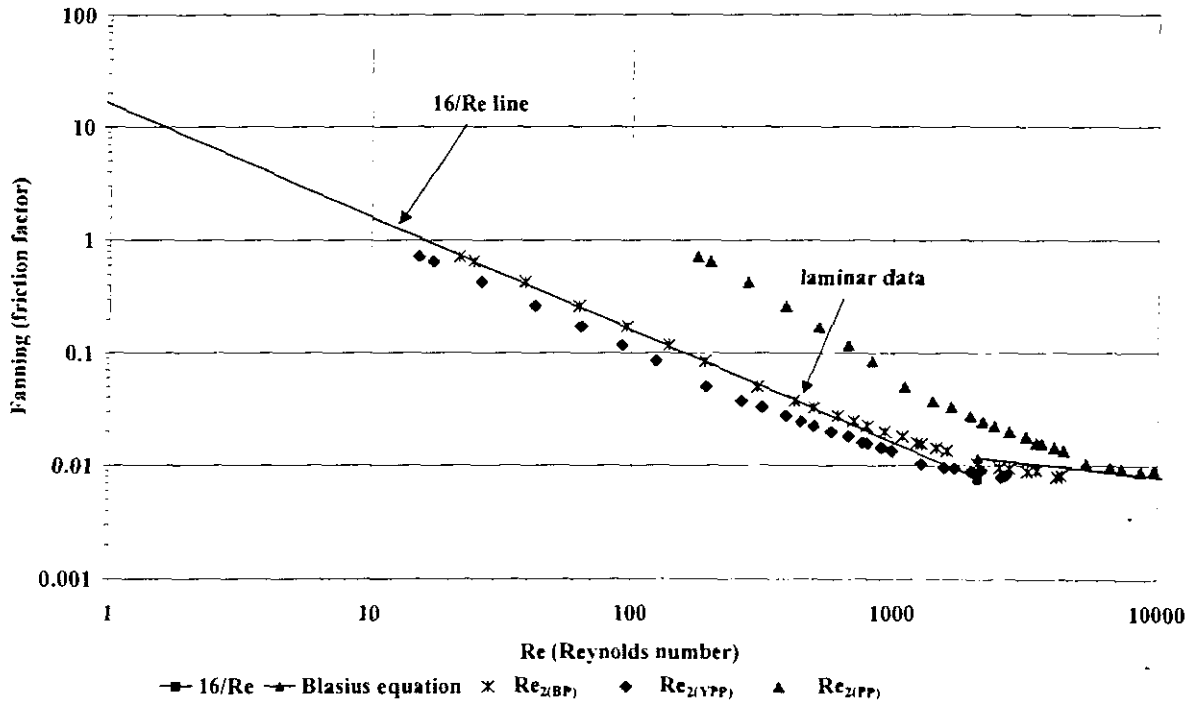

Figure 4-27. Effect of different rheological models. 4% CMC in 300 mm rectangular flume shapes

Figure 4-27 clearly shows that the Bingham model and Herschel-Bulkley model give a bad fit in characterising the CMC solution because the laminar data does not collapse on the 16/Re line. It is clear from this figure that CMC can be best characterised as a power law fluid (pseudoplastic), because this model gives a good fit with data points collapsing on the laminar line.

4.3.2 4.6% Bentonite in a semi-circular channel shape

Figure 4-28 shows an example of 4.6% bentonite, which has been characterised the same way as in Figure 4-27 with all the three rheological models.
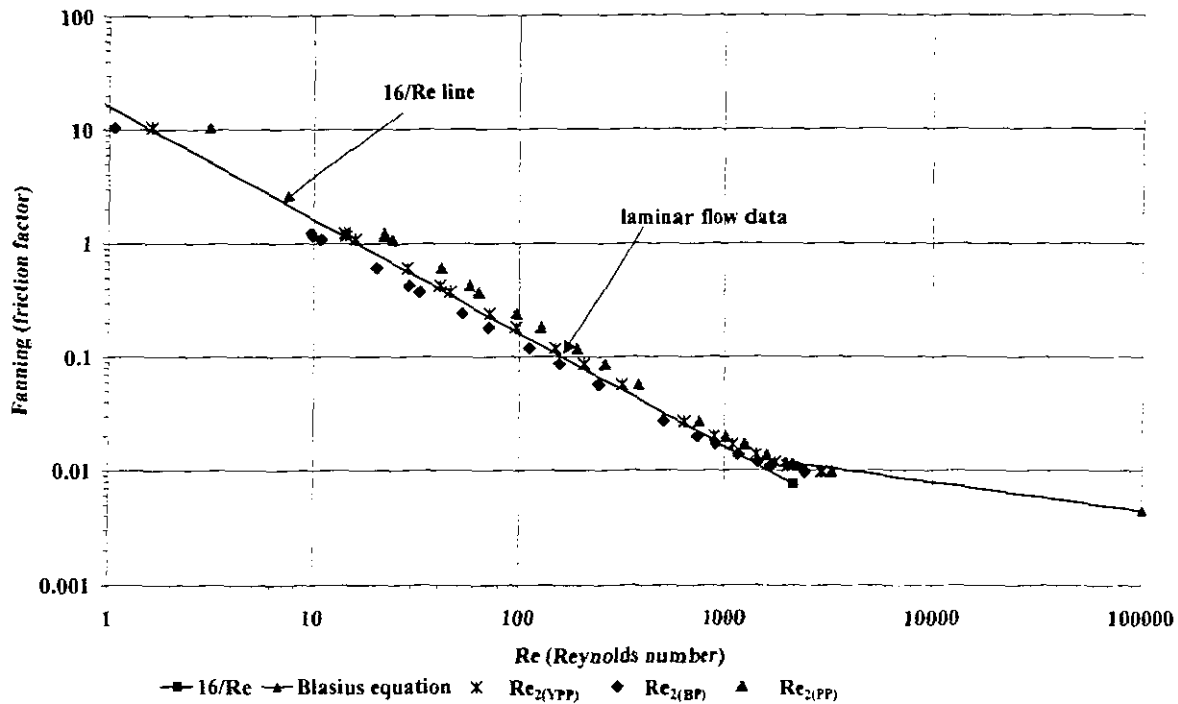

Figure 4-28. Effect of different rheological models. 4.6% bentonite in 300 mm semi circular flume shapes

Figure 4-28 clearly shows that bentonite suspension can be classified as a Bingham fluid because all the laminar flow data collapse on the 16/Re line when the Bingham model was used. It is also clear from this figure that bentonite cannot be classified as either power law or Herschel-Bulkley fluid.

4.3.3 5.4% kaolin in a trapezoidal channel

Kaolin suspension is characterised in Figure 4-29 in the same way other materials were characterised using all the three rheological models mentioned in the literature.

Figure 4-29. Effect of different rheological models. 5.4% kaolin in 150 mm trapezoidal channel shape.

Figure 4-29 shows that the kaolin suspension can be best characterised as a Herschel-Bulkley fluid because all the laminar points collapse on the 16/Re line. When kaolin was characterised as either a Bingham fluid or a power law fluid the results were not as good as when it was characterised as a Herschel-Bulkley fluid. To substantiate this, the histogram plot and the LSE values are used in the Following figure 4-30 and Table 4-2 to compare the deviation of friction factors calculated using the Reynolds numbers of these models from the measured friction factors.
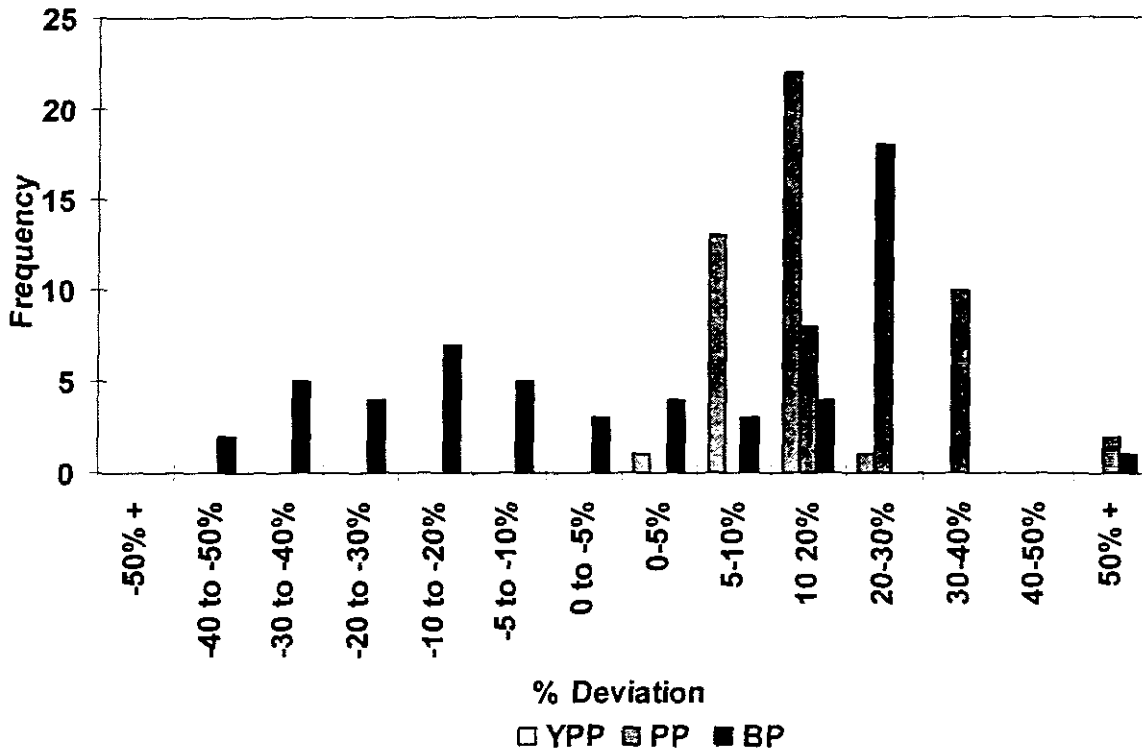
Figure 4-30. Friction factor deviations in laminar flow. 5.4% kaolin in a trapezoidal channel shape.

Table 4-2. Comparison of the friction factor deviation between the three rheological models. 5.4% kaolin in a trapezoidal channel.

	YPP model	PP model	BP model
LSE	0.0099	0.0453	0.0218

In Figure 4-30 it can be seen that the friction factor deviations for the Herschel-Bulkey model (YPP) are in the lower deviation ranges as compared to the power law (PP) and Bingham model (BP). In Table 4-2 it can be seen that the YPP model has the lowest LSE value when compared to other models. From this it is clear that the kaolin suspension can be best characterised as a Herschel-Bulkley (YPP) fluid.

4.4 CONCLUSION FOR THE LAMINAR FLOW

It is important to characterise the fluid tested with the best rheological model that describe the behaviour of that fluid. This is a fundamental part of the analysis of the results because all the Reynolds number models mentioned in literature contain the rheological parameters. CMC solution was best characterised as a power law fluid, the bentonite suspension was best characterised as a Bingham fluid, and the kaolin suspension was best characterised as a Herschel-Bulkley fluid.

Kozicki and Tiu's model for the power law fluids, which incorporates the shape effect of the channel, under-predicted the laminar flow region. In this thesis the analytical work they presented was analysed for two channel shapes, namely the rectangular and semi-circular shapes. They did not evaluate the geometric shape factors for a trapezoidal shape, which is one of the channel shapes studied in this thesis.

The evaluation of Kozicki and Tiu's Reynolds number for Bingham fluids gave a poor prediction of the laminar flow regime. This could be caused probably by the yield stress effect, which they did not take into account.

The evaluation of Coussot's prediction of a Herschel-Bulkley fluid gave a bad prediction of the laminar flow of this fluid when the actual velocities were compared with the predicted velocities using his model. Coussot's model requires the restriction of the n value to be 0.333 when obtaining the rheological parameters of a Herschel-Bulkley fluid. Even when the value of n was fixed to 0.333 in curve fitting, Coussot's prediction still did not work for both the rectangular and the trapezoidal flume shapes. This c ould be also caused by the yield stress effect, which is not taken into account in the prediction formulae.

The evaluation of Abulnaga's approach of Bingham fluids showed that his approach could not predict the laminar flow of a Bingham fluid used in this thesis. This could be caused by his negligence of a yield stress in the Reynolds number he proposed.

The Reynolds number model (Re_2) proposed by Haldenwang *et al.* (2002) predicts the laminar flow region adequately for all flume shapes and materials or fluids used in this thesis. The advantage of using it is that it is easy and can be used for all the different rheological fluid models and for all the different channel shapes. The effect of shape has been accounted for by the use of hydraulic radius in the Reynolds number formula Haldenwang *et al.* (2002) proposed.

The comparison that was made between the two Reynolds number models for the power law and Bingham fluids showed that Re_2 works better than $Re_{K\&T}$ for both rectangular and semi-circular channel shapes. The comparison was not made for trapezoidal channel shape because Kozicki and Tiu (1967) did not evaluate this flume shape.

With the above comments it can be concluded that the effect of cross-sectional shape of the channel when predicting the laminar flow of all the non-Newtonian fluids used in this thesis can be accounted for by the hydraulic radius in a much simpler Reynolds number proposed by Haldenwang *et al.* (2002). It has been also shown that Haldenwang's Reynolds number works better than Kozicki and Tiu's Reynolds numbers for all the flume shapes and fluids used in this thesis. The Re_2 model is easy to use, unlike Kozicki and Tiu's model where one has to make complicated calculations for the geometric coefficients they suggested.

4.5 TRANSITIONAL FLOW REGION

There has been very little work done on establishing the transition point of non-Newtonian open channel flow. Straub *et al.* (1958) measured various Reynolds numbers for different cross-sectional shapes of the channel for Newtonian fluids. He found that the transition point for water ranges between 2000 and 3100 for rectangular and triangular channel shape. From the literature available it seems that no one developed the model that predicts the point of transition for open-channel flow. All that authors note in the literature is that the laws of pipe flow should also work for open-channel flow (Wilson, 1991, Coussot, 1997). Transition is a complex flow region.

Haldenwang *et al.* (2002) commented that transition occurs when the data deviates from the standard 16/Re line visually. At the time he could not comprehend how the transition point could be predicted. In 2003 he was able to develop a model to predict the onset of transition and of turbulence as described in Chapter 2.

4.5.1 Evaluation of the work done by Coussot

Coussot (1997) used the Hanks criteria to predict the laminar turbulent transition for the mudflow he characterised as a Herschel-Bulkley fluid. He suggested that the flow becomes turbulent when the flow depth becomes larger than:

$$h = \frac{1}{\rho g \sin \alpha}\left[\tau_y + K\left(\frac{404(m+1)\rho(g\sin\alpha)^2}{Kv}\right)^{\frac{1}{(2m+1)}}\right] \qquad (2.59)$$

$$\text{with:} \quad m = \frac{1}{n} \qquad (2.60)$$

and $\quad v = \left[\left(\dfrac{m}{2m+1} \right)^{\left(\frac{m}{m+1} \right)} - \left(\dfrac{m}{2m+1} \right)^{\left(\frac{2m+1}{m+1} \right)} \right]$ \hfill (2.61)

.

He claimed that this is valid for infinitely wide channels; however in this thesis it was tested for the three flume shapes that were chosen. His prediction is evaluated with 7.1% kaolin since it has the characteristics of a Herschel-Bulkley fluid.

Tables 4-3 to 4-5 show the evaluation of Coussot's prediction of transition by comparing the transition velocity calculated using the Coussot prediction and the experimental critical velocity. The critical velocity was found by calculating the **"normalised adherence function"** (NAF) and the Froude number, which are then plotted against each other.

The NAF is the ratio of the Reynolds number determined experimentally to the theoretically established Reynolds number for laminar flow; this ratio should be equal to one (Slatter and Wasp, 2000). If the value of NAF is equal to one, the flow is still laminar and if it is greater than one the flow is turbulent. When the value starts to shift from one or becomes greater than one, then that is a critical value meaning the flow is in the transition state. The corresponding velocity is called the critical velocity.

Figure 4-31 shows an example of how the critical velocity is established by plotting the NAF against the Froude number. This value is also checked on a Moody diagram in Figure 4-32 to see if this point starts to deviate from the 16/Re line.
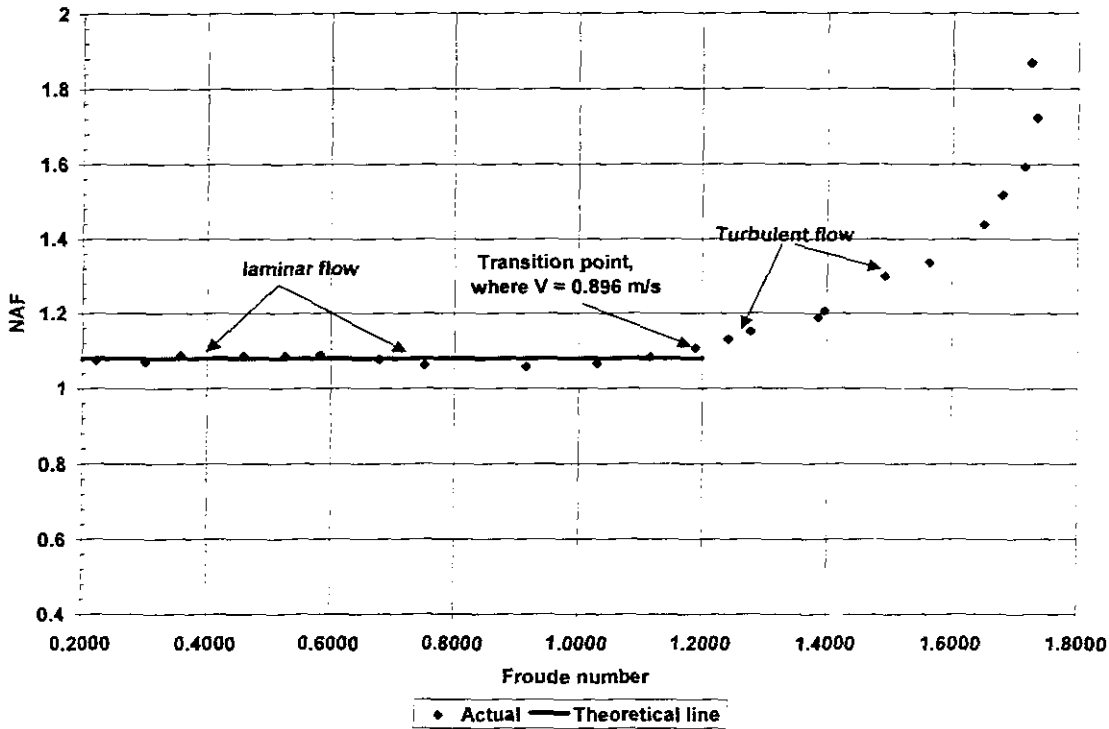
Figure 4-31. Prediction of the actual transition point using 7.1 % kaolin in 300 mm semi circular channel shape
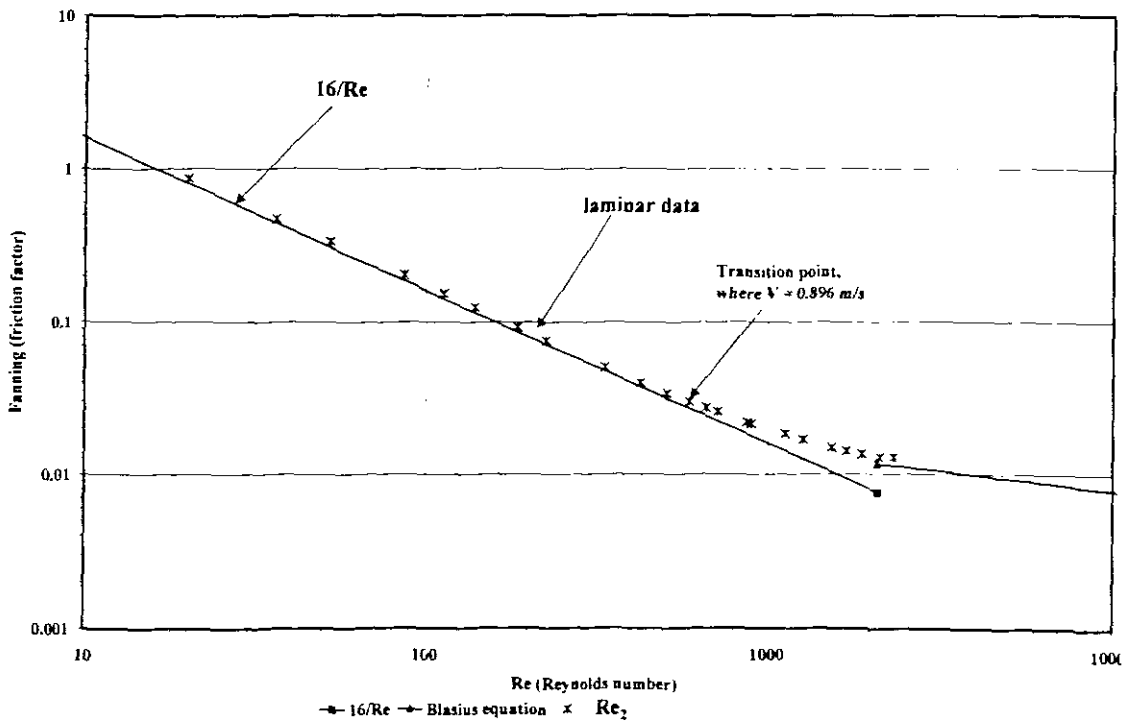
Figure 4-32. 7.1% kaolin in 300 mm semi-circular channel shape

From Figures 4-31 and 4-32 it can be seen that the deviation from the laminar flow is the same from both graphs; therefore this means the onset of transition can be seen from both graphs.

This experimentally found transition velocity is compared with the transition velocity found using Coussot's prediction to check the accuracy of his approach in predicting the transition for all flume shapes used in this thesis and some values are showed in the following Tables 4-3 to 4-5.

Table 4-3. Comparison of the actual critical velocity with Coussot's transition velocity. 7.1% kaolin in a rectangular channel shape

Slope	Critical Velocity	Coussot's Velocity	Error
2	0.894	1.315	47.13%
3	1.093	1.382	26.44%
4	1.325	1.432	8.11%
5	1.466	1.472	0.38%

Table 4-4. Comparison of the actual critical velocity with Coussot's transition velocity. 7.1% kaolin in a semi-circular channel shape

Slope	Critical Velocity	Coussot's Velocity	Error
2	0.894	1.316	48.88%
3	1.038	1.383	38.22%
4	1.217	1.433	17.71%
5	1.279	1.473	15.15%

Table 4-5. Comparison of the actual critical velocity with Coussot's transition velocity. 7.1% kaolin in a trapezoidal channel shape

Slope	Critical Velocity	Coussot's Velocity	Error
2	0.892	1.315	47.51%
3	0.962	1.382	43.65%
4	1.102	1.432	29.94%
5	1.255	1.472	17.23%

From table 4-3 to 4-5 it can be seen that the Coussot prediction of transition gets better with an increase in flume slope. It can also be noticed from these tables that Coussot prediction works better for the rectangular channel shape, but only at higher slopes. For the other channel shapes his prediction did not work well.

For all the flume shapes it can be seen that the Coussot prediction is the same at each channel slope; this shows that the cross-sectional shape of the channel does not have an effect on Coussot prediction of transition.

4.5.2 Evaluation of the work done by Haldenwang

Haldenwang (2003) developed the Reynolds number models for predicting the onset of transition and of turbulence of non-Newtonian open channel flow. These Reynolds number models include the use of the Froude number and an apparent viscosity at the shear rate of $100s^{-1}$ for onset of transition and $500s^{-1}$ for onset of turbulence:

$$Re_c = \frac{200}{\left(\mu_{app(100s^{-1})}\right)^{0.21}}Fr + \frac{71}{\left(\mu_{app(100s^{-1})}\right)^{0.75}} \qquad (2.62)$$

$$Re_c = \frac{105}{\left(\mu_{app(500s^{-1})}\right)^{0.52}}Fr + \frac{108}{\left(\mu_{app(500s^{-1})}\right)^{0.65}} \qquad (2.63)$$

These Reynolds numbers were developed for a rectangular channel shape only, but in this thesis they are also evaluated for semi-circular and trapezoidal channel shapes to ascertain if there is any significant effect that the channel shape might have in predicting the transition region.

Haldenwang's Reynolds numbers to predict the transition are evaluated for a power law fluid (CMC solution), Herschel-Bulkley fluid (kaolin suspension), and Bingham fluid (bentonite suspension).

The accuracy of his model was first checked by comparing the actual critical velocity at transition with the critical velocity calculated using his model to predict the onset of transition as shown in the following tables for all flume shapes.

Table 4-6. Comparison of the actual critical velocity with Haldenwang's velocity to predict onset of transition. 7.1% kaolin in a rectangular flume

Slope	Critical velocity	Haldenwang velocity	Error
2	0.893	1.014	13.43%
3	1.093	1.194	9.2%
4	1.325	1.351	1.99%
5	1.466	1.494	1.92%

Table 4-7. Comparison of the actual critical velocity with Haldenwang's velocity to predict onset of transition. 6.2% bentonite in a semi circular flume

Slope	Critical velocity	Haldenwang's velocity	Error
3	1.102	1.24	12.89%
4	1.282	1.41	10.39%
5	1.453	1.56	7.68%

Table 4-8. Comparison of the actual critical velocity with Haldenwang's velocity to predict the onset of transition. 4% CMC in a trapezoidal flume

Slope	Critical velocity	Haldenwang's velocity	Error
1	0.833	0.68	18.55%
2	1.055	0.96	9.32%
3	1.241	1.21	2.90%
4	1.373	1.44	4.66%
5	1.605	1.66	3.42%

Table 4-6 to 4-8 show that Haldenwang's model predicts the onset of transition reasonably well for all the flume shapes and materials used because the percentage error difference between the critical velocities is not that much especially at higher slopes.

If this can be compared with the evaluation of Coussot's approach in Tables 4-3 to 4-5, it can be seen that the velocity calculated using Haldenwang's model is better than the one calculated using Coussot's prediction. To quantify this Haldenwang's transition model is compared with Coussot's model to check which model predicts the transition reasonably well as shown in Figure 4-33.
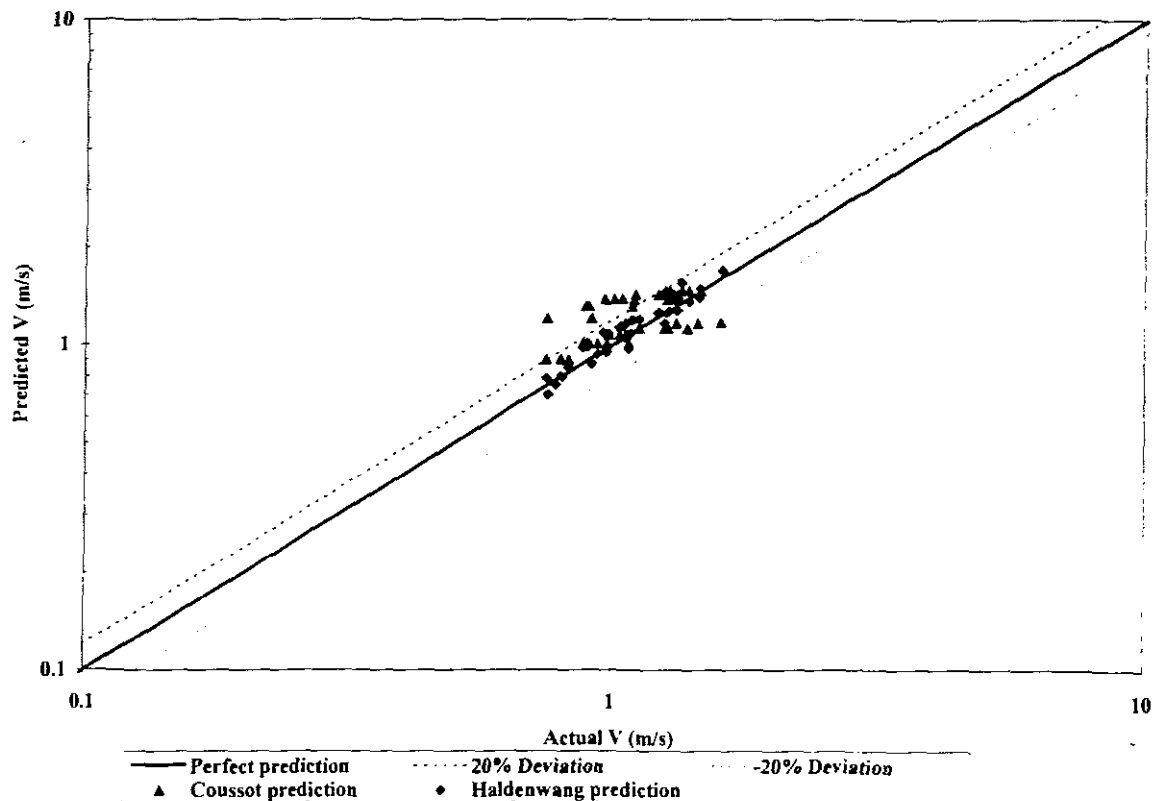
Figure 4-33. Comparison between Coussot's and Haldenwang's transition model

From Figure 4-33 it can be seen that the transition points fall within 20% deviation as compared to Coussot's prediction which has some transition points that are more than 20% out. Therefore this means the model developed by Haldenwang predicts the laminar-turbulence transition better than Coussot's model.

The following sections show the evaluation of Haldenwang's model, this time using the Moody diagrams for all flume shapes and fluids chosen in this thesis.

4.5.2.1 Evaluation with power law fluid

This evaluation was made with CMC results for rectangular, semi-circular and trapezoidal flume shapes and depicted on a Moody diagram as shown in the following Figures 4-34 to 4-36.
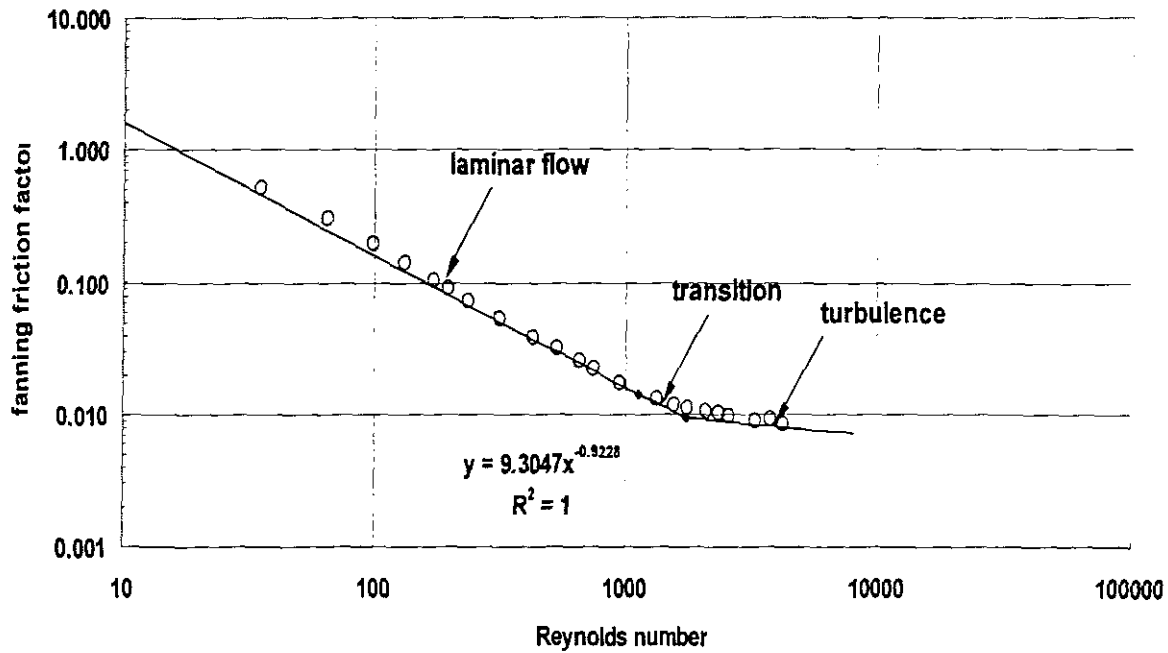
**Figure 4-34. Prediction of the transition. 3% CMC in a rectangular flume shape at 1-degree slope**
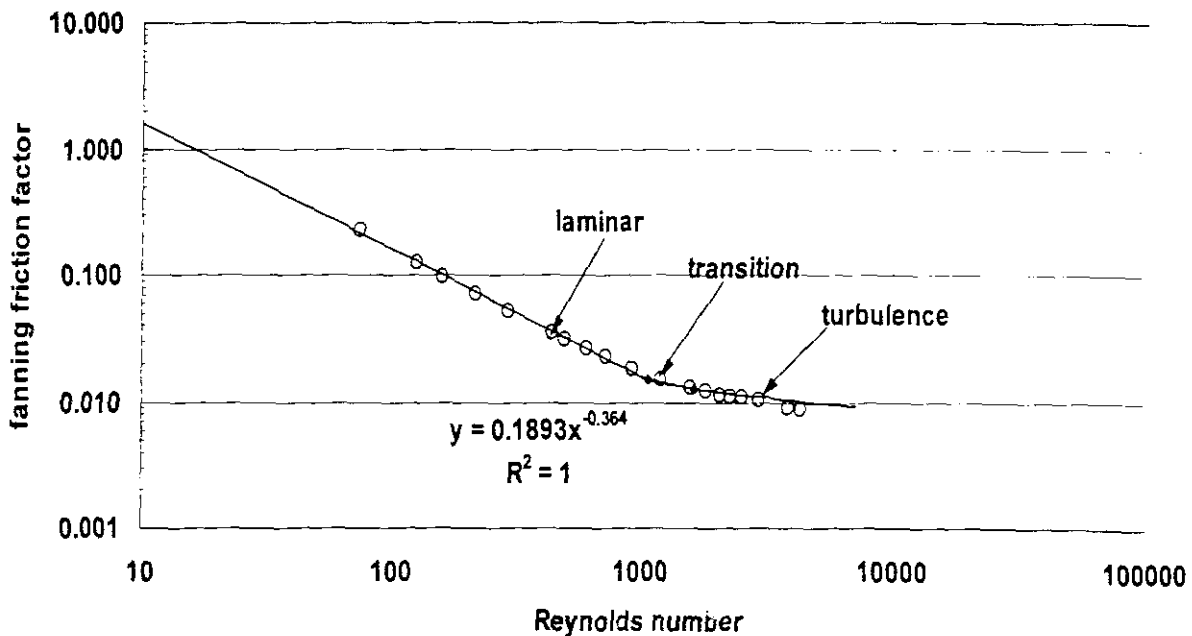
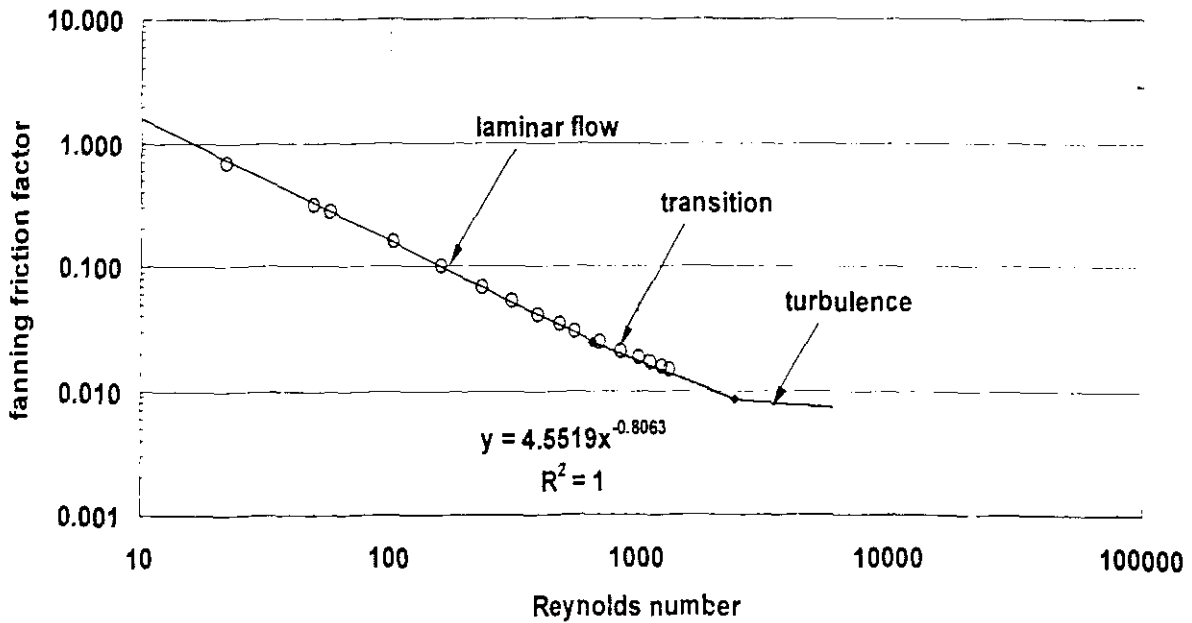**Figure 4-35. Prediction of the transition. 3% CMC in a semi circular flume shape at 1 degree slope**
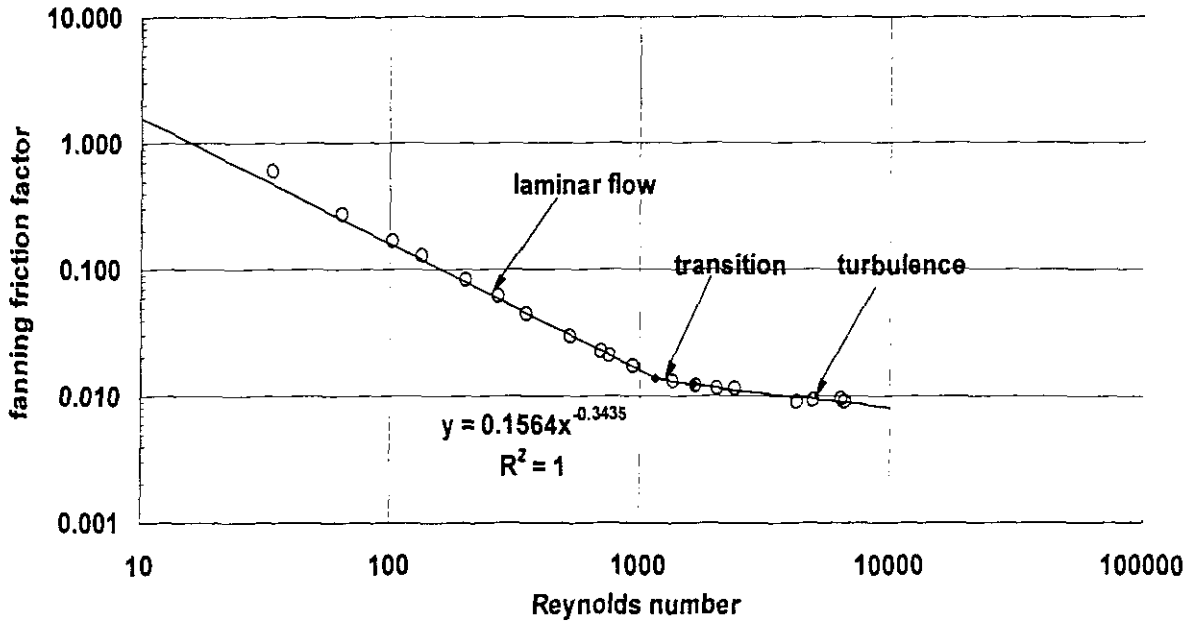
Figure 4-36. Prediction of transition. 3% CMC in a trapezoidal flume shape at 1-degree slope

Figures 4-34 to 4-36 show that the Reynolds number models developed by Haldenwang (2003) predict the transition of flume shapes other than rectangular shape adequately. As can be seen, the transition points collapse well on the theoretical line of transition developed by Haldenwang (2003), which he developed by fitting the power-law curve between his prediction for onset of transition and of turbulence for all channel shapes used. This was done for the 1-degree slope for all these flume shapes.

This model does not incorporate the shape factors of the channel, yet it works well in predicting the transition for all flume shapes chosen in this study. This means there is no need to make corrections for the shape effect of the flume in predicting the transition of power law fluids (CMC).

4.5.2.2 Evaluation with Herschel-Bulkley fluids

The following Figures 4-37 to 4-39 depict the prediction of transition of the Herschel-Bulkley fluids in a rectangular, semi circular and trapezoidal channel shapes using the critical Reynolds number model developed by Haldenwang (2003).
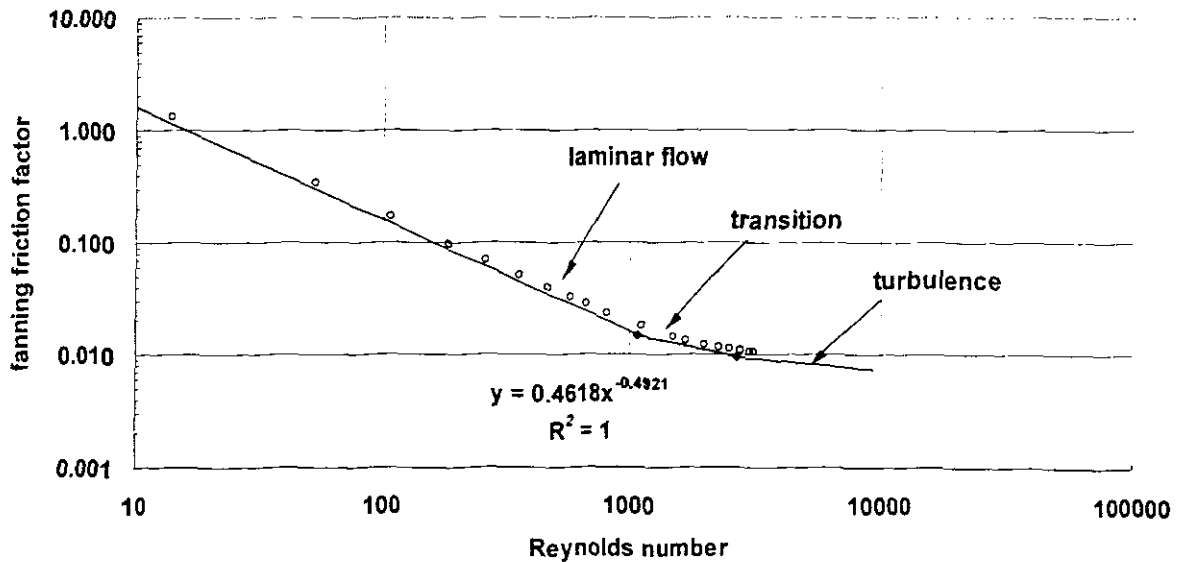
Figure 4- 37. Prediction of transition. 7.1% kaolin in a rectangular flume shape at 3-degree slope
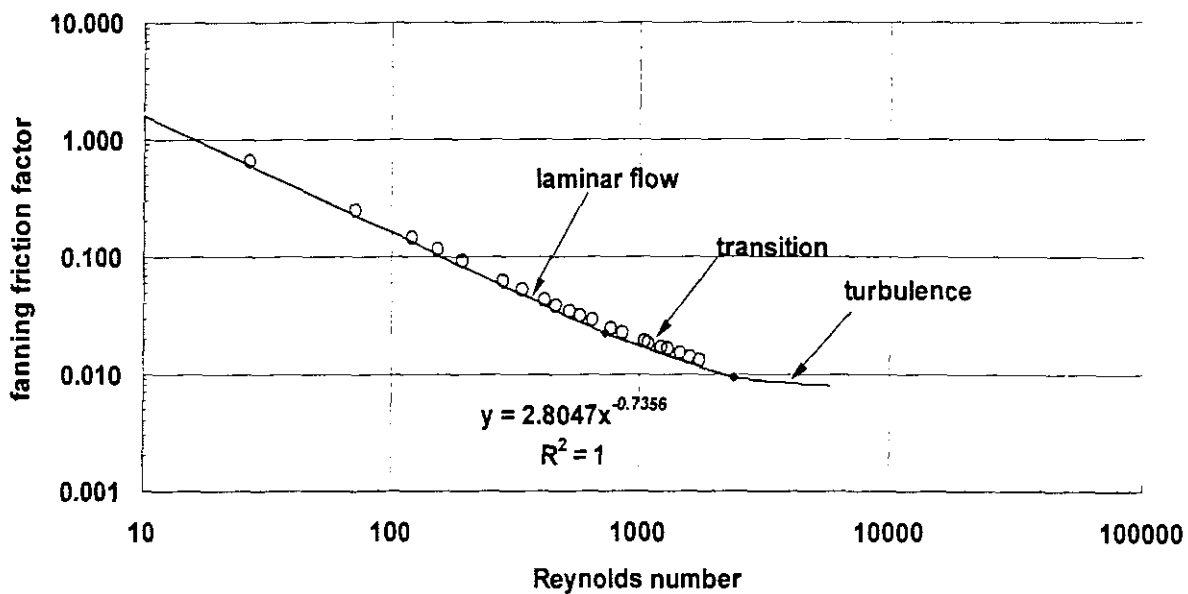
Figure 4-38. Prediction of transition. 7.1% kaolin in a semi circular flume shape at 2-degree slope
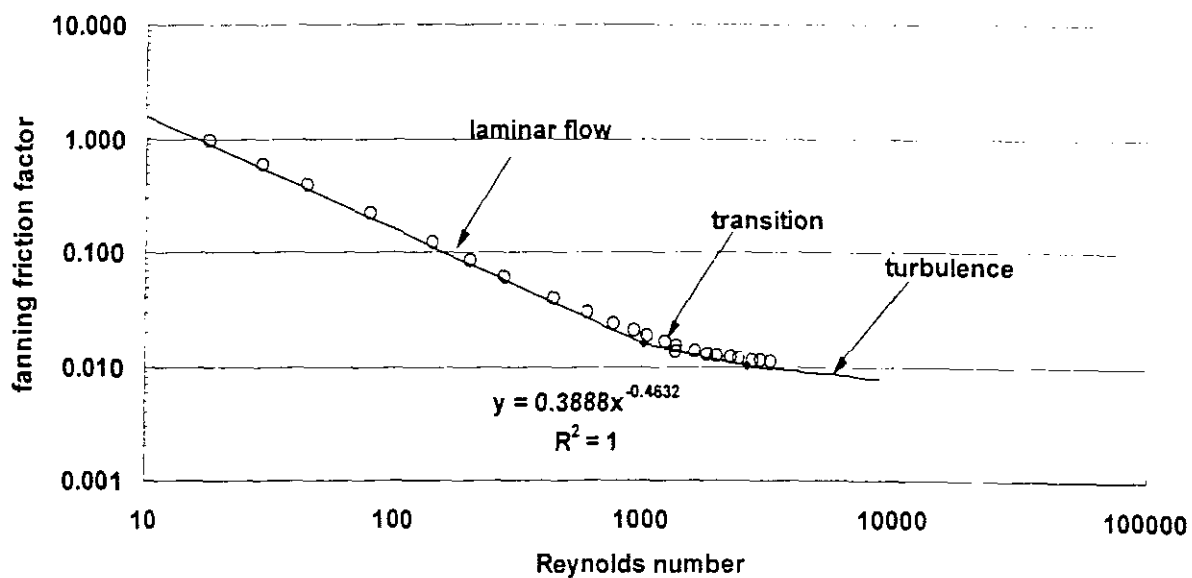
Figure 4-39. Prediction of transition. 7.1% kaolin in a trapezoidal flume shape at 3-degree slope

Figures 4-37 to 4-39 also show that the model developed by Haldenwang (2003) adequately predicts the transition of Herschel-Bulkley fluids for all the flume shapes used in this study. This is evident by seeing all the transition points collapsing on the theoretical transition line developed by Haldenwang (2003) by fitting the power-law curve between his predictions for the onset of transition and onset of turbulence.

The above results show there is no need to include the effect of the channel shape in predicting the transition of Herschel-Bulkley fluids because the new model by Haldenwang (2003) predicts it well.

4.5.2.3 Evaluation with Bingham plastic fluid

The model developed by Haldenwang (2003) is evaluated with Bingham plastic fluid in the same way it was evaluated with power law and Herschel-Bulkley fluids as follows in Figure 4-40 to 4-42:
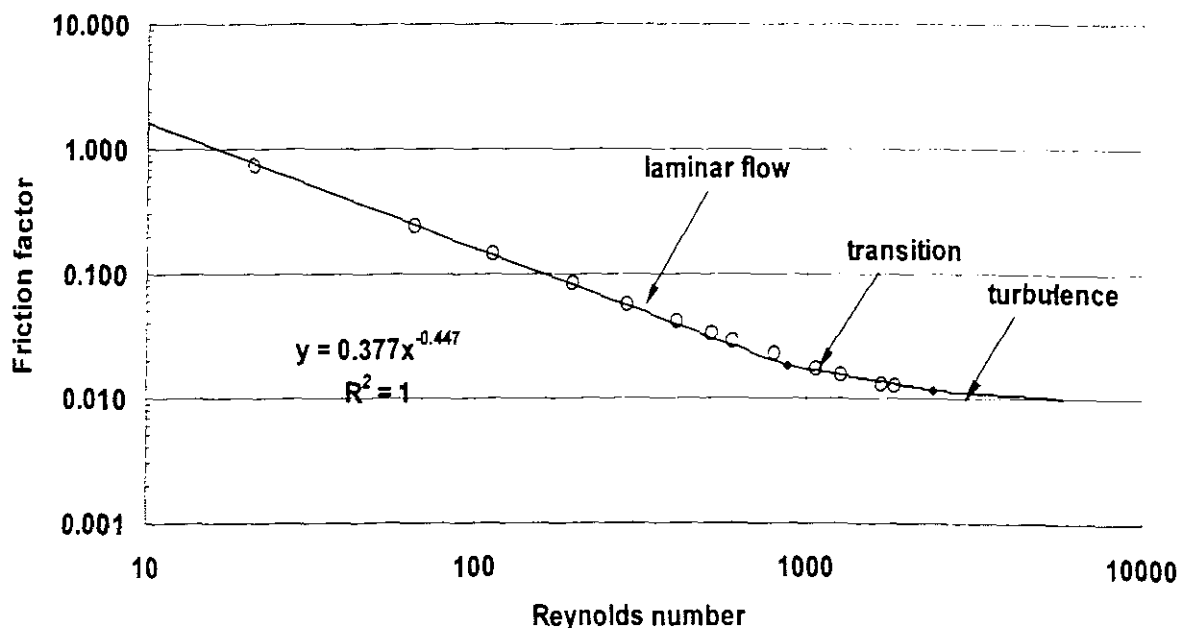
Figure 4-40. Prediction of transition. 6.2% bentonite in a rectangular flume shape at 4-degree slope
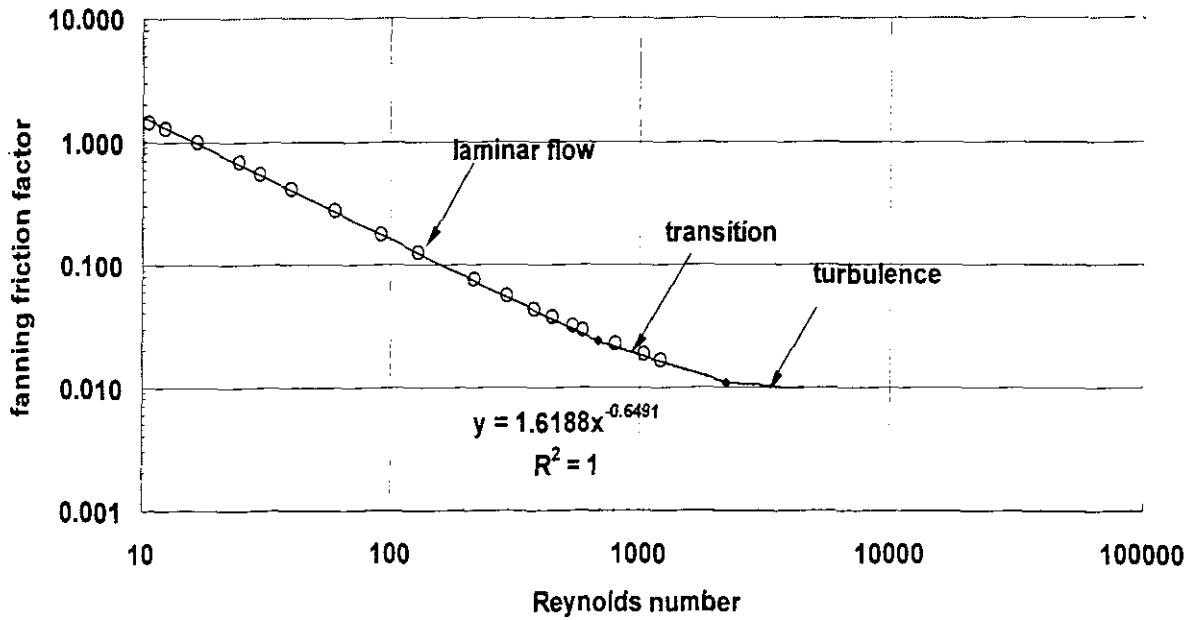
Figure 4-41. Prediction of transition. 6.2% bentonite in a semi circular flume shape at 3-degree slope

Figure 4-42. Prediction of transition. 6.2% bentonite in a trapezoidal flume shape at 4-degree slope

Figures 4-40 to 4-42 also show that Haldenwang's Reynolds numbers predict the transition of Bingham plastic fluids adequately for all the three channel shapes used in this study. This is evident by seeing all the transition points collapsing on the theoretical transition line developed by Haldenwang (2003).

This means there is no need to include the effect of the cross-sectional shape of the channel in predicting the transition of Bingham plastic fluid as well.

Now it is evident that the effect of the cross-sectional shape of the channel is not necessary to be included when predicting the transition of non-Newtonian open channel flow as this has been confirmed with three different non-Newtonian fluids models and three flume shapes. The design protocol Haldenwang (2003) developed for predicting the transitional flow does this adequately.

The following tables show the examples of the predicted transition points of the non-Newtonian fluids used in this thesis for the entire flume shapes used using the model developed by Haldenwang (2003). This prediction was done for highly viscous concentrations of CMC, kaolin, and bentonite suspensions.

Table 4-9. Prediction of transition using Haldenwang's model. 3% CMC

SLOPE (degrees)	FLUME SHAPE	TRANSITION RANGE (Re)
1	Rectangular	1125-1762
2	Rectangular	1451-2095
3	Rectangular	1750-2346
4	Rectangular	2037-2555
5	Rectangular	2317-2739
1	Semi circular	1071-1636
2	Semi circular	1332-1912
3	Semi circular	1565-2119
4	Semi circular	1786-2291
5	Semi circular	1999-2441
1	Trapezoidal	1152-1652
2	Trapezoidal	1485-1936
3	Trapezoidal	1791-2150
4	Trapezoidal	2084-2328
5	Trapezoidal	2370-2483

The transition of the 3% CMC solution was predicted to be between the Reynolds numbers of 1125 and 2739 over the flume slope ranges of 1-5 degrees as can be seen in Table 4-9. This prediction is not the same for all these slopes as can be seen, it changes with flume slope.

Table 4-10. Prediction of transition using Haldenwang's model. 7.1% kaolin

SLOPE (degrees)	FLUME SHAPE	TRANSITION RANGE (Re)
1	Rectangular	
2	Rectangular	743-2515
3	Rectangular	970-2811
4	Rectangular	1186-3055
5	Rectangular	1396-3264
1	Semi circular	
2	Semi circular	725-2382
3	Semi circular	892-2640
4	Semi circular	1046-2849
5	Semi circular	1194-3028
1	Trapezoidal	
2	Trapezoidal	708-2327
3	Trapezoidal	900-2574
4	Trapezoidal	1095-2778
5	Trapezoidal	1292-2954

Table 4-10 shows that the prediction of transition for 7.1% kaolin is between the Reynolds numbers of 708 and 3264 at the flume slope ranges of 2-5 degrees. At 1-degree slope the transition could not be predicted because the flow was still laminar. Also for this material the prediction of transition changes with flume slope.

Table 4-11. Prediction of transition using Haldenwang's model. 6.2% bentonite

SLOPE (degrees)	FLUME SHAPE	TRANSITION RANGE (Re)
1	Rectangular	
2	Rectangular	
3	Rectangular	686-2214
4	Rectangular	879-2395
5	Rectangular	1063-2549
1	Semi circular	
2	Semi circular	
3	Semi circular	685-2236
4	Semi circular	878-2420
5	Semi circular	1062-2578
1	Trapezoidal	
2	Trapezoidal	
3	Trapezoidal	657-2208
4	Trapezoidal	807-2380
5	Trapezoidal	966-2526

Table 4-11 shows that the transition of 6.2% bentonite was predicted to be at the Reynolds numbers of between 657 and 2578 over the flume slope ranges of 3 –5 degrees. The transition could not be reached at 1- and 2-degree slopes as the flow was still laminar. Also here it can be seen that the prediction of transition changes with flume slope.

4.5.3 The slope effect on transitional flow

Although the model developed by Haldenwang (2003) works well in predicting the transition of all fluids tested in different channel shapes. there is a slope effect in predicting the transition using this model especially for the less viscous fluids. On very

steep slopes the model does not predict the transition adequately, especially on less viscous fluids because the points are not collapsing on the theoretical line of transition; there is a jump in transition friction factor similar to that of Newtonian fluids, which is difficult to model.

Some examples to show this are given in Figures 4-43 to 4-45.
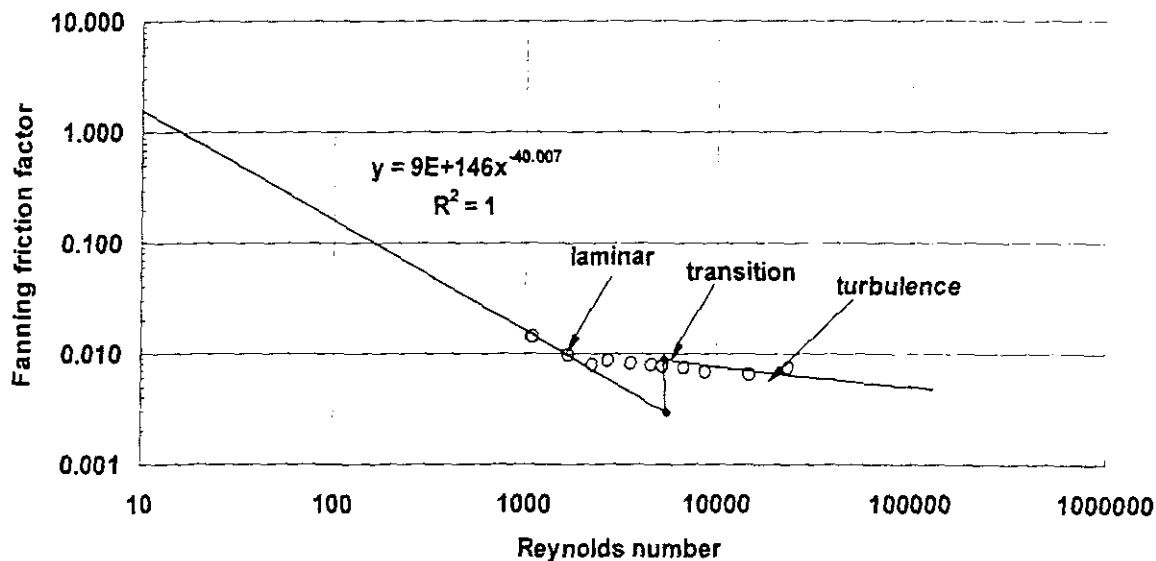
Figure 4-43. Prediction of transition. 1.5% CMC in a rectangular shape at 5-degree slope
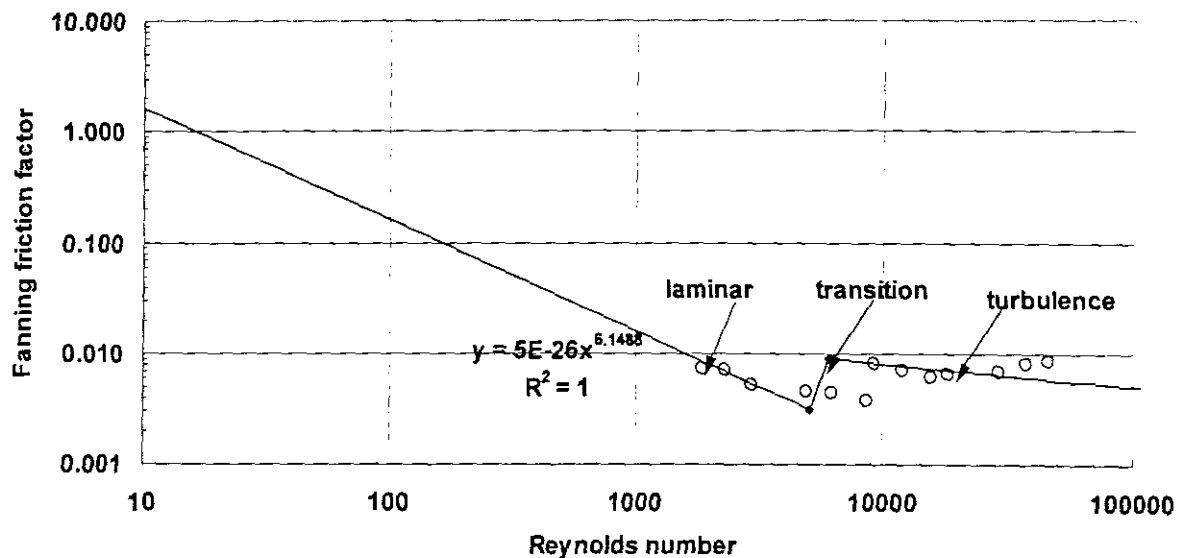
Figure 4-44. Prediction of transition. 1.5% CMC in a semi circular shape at 5-degree slope
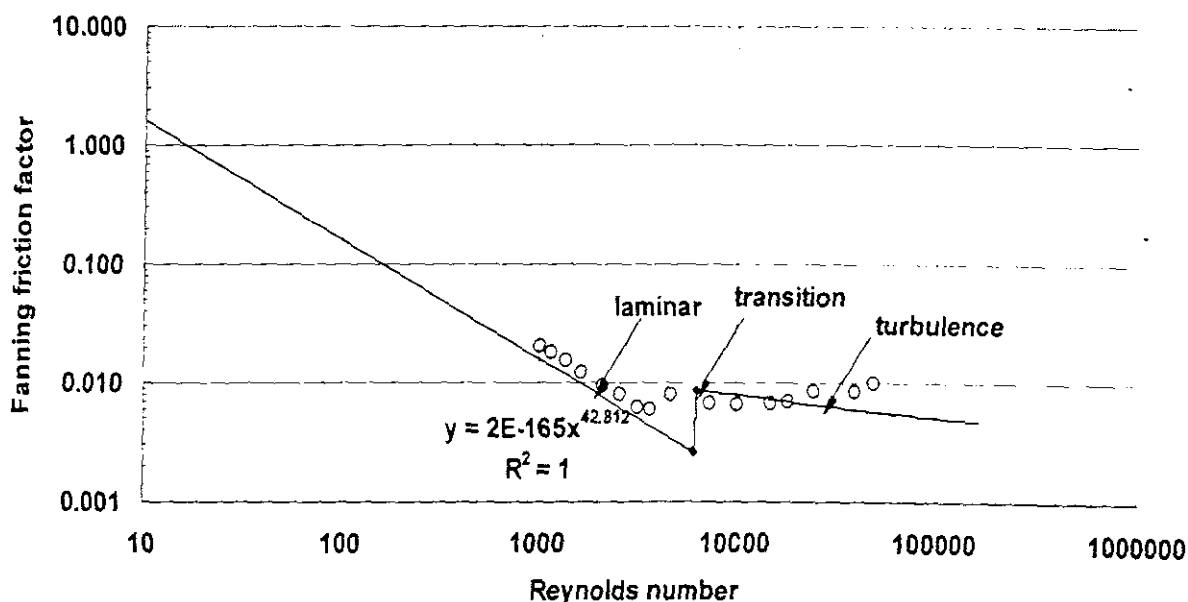
Figure 4-45. Prediction of transition. 1.5% CMC in a trapezoidal shape at 5-degree slope

These three figures show the effect the steeper slope causes in predicting the transition of the more Newtonian-like fluids using Haldenwang's Reynolds number models. These were taken for the steepest slope of the channels, which is 5°. These figures show that Haldenwang's model does not predict the transition adequately at higher channel slopes,

especially for low concentrations of the fluid, which are more Newtonian fluid in behaviour.

This shows there is a slope effect in predicting the onset of transition that is difficult to model.

4.5.4 CONCLUSION FOR TRANSITIONAL FLOW

The Coussot's prediction of transition could not predict the transition in all the flume shapes used in this thesis.

The model developed by Haldenwang (2003) predicts the transition adequately for all non-Newtonian fluids used and the flume shapes chosen in this study. There is no need to make corrections for the effect of cross-sectional shape of the channel in predicting the transition because Haldenwang's model works well for all the channel shapes that are chosen for this thesis.

The prediction of transition using Haldenwang's model changes with channel slopes and concentration of the material tested.

The only problem with this new model is that it is very sensitive to the slope of the flume for less viscous fluids (more Newtonian fluids). At steeper slopes it has been shown that it does not predict the transition very accurately for these nearly Newtonian fluids.

Figures 4-31 and 4-32 show that the onset of transition can be seen in both NAF and Moody diagrams. It would be interesting to investigate this by using a pressure cell in the flume attached to a Pitot tube. In laminar flow the pressure should be constant and when the turbulence starts the pressure should start fluctuating.

CHAPTER 5

CHAPTER 5

CONCLUSIONS AND RECOMMENDATIONS

5.1 INTRODUCTION

This study reported on the effect of the cross-sectional shape of the channel on the flow behaviour in the laminar and transitional flow regimes.

This effect was checked by evaluating the models that were presented by previous researchers in the field of non-Newtonian open-channel flow for both laminar and transitional flow.

In evaluating the models that predict the laminar flow, further elaboration was done on the work of Kozicki and Tiu (1967), because they are the only researchers of the non-Newtonian open-channel flow who emphasised the importance of including the effect of cross-sectional shape of the channel in this flow regime. Coussot (1994) referred to their work, but did not comprehensively verify it experimentally. The evaluation of these models in predicting the laminar flow regime did not give good prediction especially for fluids having a yield stress. A possible explanation could be that the presence of a yield stress has a significance effect in the derivation of their models, which these researchers did not take into consideration.

Also in transitional flow, the models that were used to predict this flow regime did not show the need to include the effect of shape.

5.2 SUMMARY

The effect of shape in non-Newtonian open channel flow is not well understood. This thesis envisaged the study of this effect in laminar and transitional flow. The relevance of this work is in the mining industries where high concentrated slurries have to be

transported to the tailings dams using the launders (as they are called in the mines). The mines in South Africa are restricted to operate at high concentrations by the new water law in order to save water.

This thesis aids to a better understanding of the effect of the cross-sectional shape of the channel when designing the open channels that transport highly viscous non-Newtonian slurries in laminar and transitional flow regimes.

Some research has been conducted in laminar flow of non-Newtonian fluids in open channels by Kozicki and Tiu (1967), Hao and Zhenghai (1982), Coussot (1994), Abulnaga (1997), and Haldenwang *et al.* (2002). With the exception of Kozicki and Tiu (1967), none of these researchers emphasised the importance of the cross-sectional shape effect.

In predicting the transition zone, some work has been presented by Coussot (1997) to predict the onset of turbulence, but he did this for infinitely wide channels without considering the effect of the channel shape. Haldenwang (2003) developed the model that predicts the onset of transition and of turbulence, but it also does not include the effect of the channel shape.

To be able to evaluate the models mentioned in literature, a large database was compiled from the test facility that was built and commissioned at the Cape Technikon Flow Process Research Centre. It includes a 10 m long by 300 m wide tilting flume linked to an on-line tube viscometer with three diameter tubes, namely 13 mm. 28 mm, and 80 mm. The flume can be fitted with three flume shapes, namely rectangular, semi-circular, and trapezoidal. The flume can also be partitioned into two sizes to make half the size of each flume shape. The test procedures were developed to determine the rheological parameters of the fluids tested, which were 1-4% CMC solutions. 4.6 and 6.2% bentonite suspensions, 5, 7, and 9% kaolin suspensions. The test work also included collecting a wide range of flow data starting from laminar to turbulent flow.

The database compiled was used to evaluate the models mentioned in literature in both the laminar and the transitional flow, which was then used to evaluate if the effect of shape should be included when designing the open channels. After the literature models were evaluated, the following conclusions were drawn.

5.3 CONCLUSION

5.3.1 Laminar flow

In predicting the laminar flow of non-Newtonian fluids, it has been shown that choosing the correct rheological model for each fluid tested is of great importance since the Reynolds numbers used contain the rheological parameters. Therefore the most accurate prediction of this flow region has been shown to occur when the correct rheological model was chosen. CMC solution was found to have rheological characteristics of a power law fluid, bentonite suspension to have those of Bingham fluid, and kaolin suspension to have those of Herschel-Bulkley fluids.

From all the models that were evaluated in Chapter 4, the Reynolds number proposed by Haldenwang *et al.* (2002) predicted the laminar flow better than the other models. This was evident on the Moody diagram where the laminar flow data collapse well on 16/Re line for all the flume shapes and fluids that were chosen for this thesis. This model only requires that the rheological model be chosen carefully. This model also takes into account the effect of cross-sectional shape by the use of the hydraulic radius.

The Kozicki and Tiu Reynolds model, which emphasised the importance of the shape effect, could not adequately predict the laminar flow of the non-Newtonian fluids used in this thesis. Their model only seemed to work to a certain extent for the power law fluids. This led to the comparison that was made between their model and Haldenwang's model.

When compared, the Re_2 model proposed by Haldenwang *et al.* (2002) worked better than Kozicki and Tiu's Reynolds number for both rectangular and semi-circular channel

shapes. This comparison was also made for Bingham fluids and the same trend was found.

The Kozicki and Tiu model could not predict the laminar flow of the Bingham fluids at all. This could be caused by the yield stress effect, which Kozicki and Tiu (1967) did not take into account for in their derivations.

Kozicki and Tiu (1967) did not present work for a Herschel-Bulkley fluid (which is one of the fluids that were tested for this thesis), therefore the effect of shape for this fluid could not be evaluated.

The model presented by Coussot (1994), which includes the shape factor for rectangular and trapezoidal channel shapes could not predict the laminar flow for the concentrations of Herschel-Bulkley fluid used in this thesis for both these flume shapes. This could be again possible caused by the yield stress effect, which Coussot (1994) did not account for it in his prediction formulae.

The evaluation of the design protocol presented by Abulnaga (1997) could not predict the laminar flow of a Bingham fluid at all for all the flume shapes used in this thesis. This was caused by his ignorance of yield stress in the Reynolds number he proposed.

Based on the evaluation of the models mentioned in literature, it can be said for all the fluids tested in the different flume shapes in this thesis that the effect of shape is sufficiently accounted for by the use of the hydraulic radius as shown in the Reynolds number proposed by Haldenwang et al. (2002).

5.3.2 Transitional flow

It has been shown that the onset of transition can be seen in both the "NAF" and Moody diagrams. Therefore it will be interesting to investigate this by using a pressure

transducer in the flume attached to a Pitot tube. In laminar flow the pressure should be constant, and when turbulence starts the pressure should show fluctuations.

The evaluation of Coussot's approach (1997) to predict the transition point of a Herschel-Bulkley fluid did not give good results for all the flume shapes used because it was intended for infinitely wide channels. Therefore the effect of shape on transitional flow could not be shown by his prediction.

The model presented by Haldenwang (2003) to predict the transition of non-Newtonian fluids has been shown to predict this zone adequately for all the flume shapes and non-Newtonian fluids used in thesis without showing any need to correct for the effect of the cross-sectional shape of the channel.

The transition of the more viscous fluids occurs earlier than the transition of the less viscous fluids. At low concentrations Haldenwang's model did not predict the transition as well because the fluids had a more Newtonian behaviour with a sudden increase in friction factor, which makes it difficult to model.

Haldenwang's model is very sensitive to the rheology of the material and the slope of the flume.

5.3.3 Final conclusions

For all the three non-Newtonian fluids tested in three different flume sha es that have slopes varying from 1-5 degrees, the effect of shape on laminar flow is sufficiently accounted for in the hydraulic radius of the channel and the shape factors suggested by Kozicki and Tiu (1967) are not necessary have to be included. For the transitional flow, the effect of shape is not necessary if the model developed by Haldenwang, (2003) is used.

When designing the open channels that transport the non-Newtonian slurries this study showed that the effect of the cross-sectional shape of the channel is sufficiently accounted for by the use of the hydraulic radius when predicting the laminar flow, when predicting the transitional flow this study showed that the model developed by Haldenwang (2003) can be used without including the effect of shape in this flow regime. However this is not for all the existing open channel shapes that the non-Newtonian slurries can be transported in, this is only for those studied here.

5.4 RECOMMENDATIONS

The effect of shape was evaluated only for rectangular, se.ni-circular, and trapezoidal channel shapes, further channel shapes evaluated by Kozicki and Tiu (1967) like semi-elliptical and triangular shapes should also be investigated.

The following aspects, which are not covered in this thesis, should also be investigated:

- The Normalised Adherence Function (NAF approach) which shows experimentally the transition point (refer to section 4.5) can be used to more accurately determine the onset of transition. This could be used and broaden the empirical base and improve the model proposed by Haldenwang (2003).

- A link needs to be established between the empirical evidence of transition and more physical evidence such as measuring turbulence intensities. This will help to establish the onset of transition and validate the transition model.

- The transition model used in this thesis is an empirical model. To be able to more fundamentally analyse the non-Newtonian flow behaviour, it is important to measure the shear stress distribution. As there does not seem to be any possibility to do this at this moment, accurate velocity profiling may be an option to investigate.

- The effect of slope on transition also needs to be studied further as the model presented by Haldenwang (2003) is only valid for a maximum slope of 5 degrees.

- A large database is now available to be used to calibrate computational fluid dynamics software (CFD) to extend the scope of the work done in this thesis.

- All the tests have been conducted in flume sizes of maximum width of 300mm. It would be very valuable to obtain data from larger flume sizes in industry to validate the models described in this thesis.

REFERENCES

ABULNAGA, B. 1997. *Slurry systems handbook.* New York: McGraw-Hill

BRAGG, R. & HOLLAND, F.A. 1995. *Fluid flow for chemical engineers.* London: Edward Arnold.

CHANSON, H. 1999. *The hydraulics of open channel flow.* London: Edward Arnold.

CHHABRA, R.P. & RICHARDSON, J.F. 1999. *Non-Newtonian flow in the process industries.* Oxford: Butterworth Heineman..

CHHABRA, R.P. & SLATTER P.T. 2001. The flow of non-Newtonian slurries and sludges. Unpublished course notes.

CHOW, V.T. 1959. *Open channel hydraulics.* New York: McGraw-Hill.

COUSSOT, P. 1994. Steady laminar flow of concentrated mud suspensions in open channels. *Journal of Hydraulic Research.* 32 (4): 535-558.

COUSSOT, P. 1997. *Mudflow rheology and dynamics.* Rotterdam: A.A. Balkema.

FEATHERSTONE, R. E. & NALLURI, C. 1995. *Civil engineering hydraulics.* Oxford: Blackwell Science.

HALDENWANG, R. 2003. Flow of non-Newtonian fluids in open channels. Unpublished D.Tech. Dissertation. Cape Technikon. Cape Town. South Africa.

HALDENWANG, R., SLATTER, P.T. & CHHABRA, R.P. 2002. Laminar and transitional flow in open channels for non-Newtonian fluids. *15th International Conference on Hydrotransport, Incorporating the 11th International Symposium of Freight Pipelines*, Banff, Canada, 3-5June 2002: 755-768

HAO, Z. & ZHENGHAI, R. 1982. Discussion on law resistance of hyperconcentrated flow in open channel. *Scientia Sinica (Series A)*, 25 (12): 1332-1342

HEYWOOD, N.I., & RICHARDSON, J.F. 1978. Head loss reduction by gas injection for highly shear-thinning suspensions in horizontal pipe flow. *Proceedings of the Hydrotransport 5th International Conference*, Cranfield, UK, May 1978: 1-22. [Paper C1].

KOZICKI, W. & TIU, C. 1967. Non-Newtonian flow through open channels. *The Canadian Journal of Chemical Engineering*, 45: 127-134.

LAU, H.H. 1979. A literature study on slurry transport by flumes. BHRA project no. 13195: 1-11.

LAZARUS, J.H. & NIELSON, I.D. 1978. A generalised correlation for friction head losses of settling mixtures in horizontal smooth pipelines. *Proceedings of the Hydrotransport 5th International Conference*, Cranfield, UK, May 1978: 1-22. [Paper B1].

LAZARUS, J.H. & SLATTER P.T. 1988. A method for the rheological characterisation of tube viscometer data, *Journal of Pipelines*, 7: 165-176

SANDERS, R.S., SCHAAN, J., GILLIES, R.G., MCKIBBEN, M.J., SUN, R. & SHOOK, C.A. 2002. Solids transport in laminar, open-channel flow of non-Newtonian slurries. *15th International Conference on Hydrotransport, Incorporating the 11th International Symposium of Freight Pipelines*, Banff, Canada, 3-5June 2002: 597-611.

SESTAK, J. 1974. Flow of non-Newtonian fluids in open circular channels. *The Canadian Journal of Chemical Engineering*, 52: 670-672

SLATTER, P.T. 1994. Transitional and turbulent flow of non-Newtonian slurries in pipes. Unpublished PhD thesis. University of Cape Town, South Africa.

SLATTER, P.T. & WASP, E.J. 2000. The laminar/turbulent transition in large pipes. *10th International Conference on Transport and Sedimentation of Solid Particles*, Wroclaw, Poland, 4-7 September 2000: 389-399

STRAUB, L.G., SILBERMAN, E. & NELSON, H.C. 1958. Open-channel flow at small Reynolds numbers. *Transactions of the American Society of Civil Engineers*, 123: 685-713

WILSON, K.C. 1991. Slurry transport in flumes. *Slurry Handling Design of Solid-Liquid Systems*. Eds. Brown, N.P. & Heywood, N.I., London: Chapter 8: 167-180

APPENDICES

EXPERIMENTAL RESULTS

A.1 RHEOGRAMS OF THE MATERIALS TESTED

CMC 1-4 %

Bentonite 4.6 – 6.2 %

Kaolin 4.6- 7.2 %

A.2 FLUME DATA

CMC 1-4 % in 150 and 300 mm rectangular and semi circular flume shapes and also in 75 mm and 150 mm trapezoidal flume shapes.

Bentonite 4.6 – 6.2 % in 150 and 300 mm rectangular and semi circular flume shapes and also in 75 mm and 150 mm trapezoidal flume shapes.

Kaolin 5.4 – 7.2% in 150 and 300 mm rectangular and semi circular flume shapes and also in 75 mm and 150 mm trapezoidal flume shapes.

A.1   RHEOGRAMS

1% CMC

SLURRY PROPERTIES	
Slurry Relative Density	1.006
Mass Concentration	1%
Fluid Consistency Index	0.009 Pa.s^n
Flow Behaviour Index	0.945
Apparent viscosity (100 s^{-1})	0.007 Pa.s
Apparent viscosity (500 s^{-1})	0.0064 Pa.s
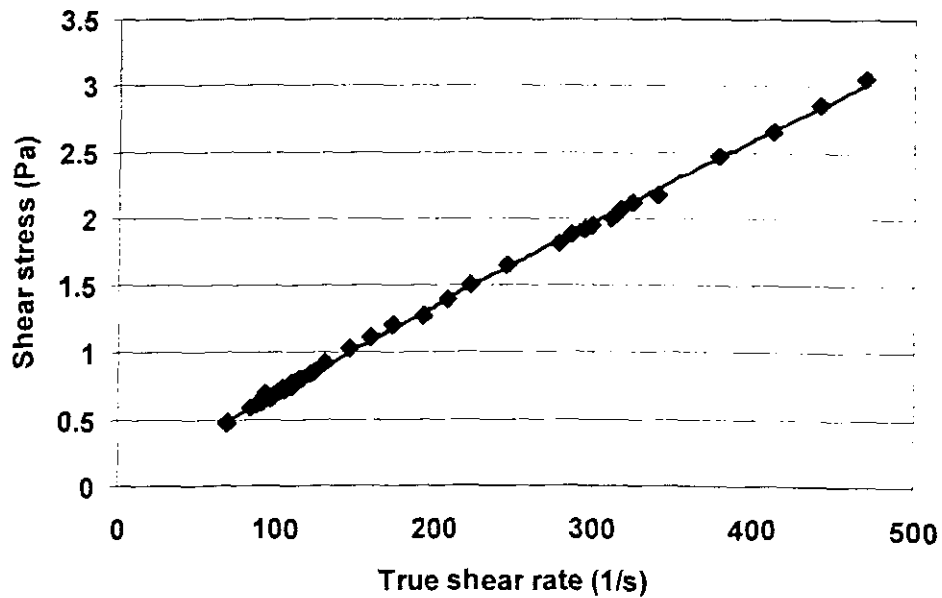
Rheogram 1% CMC

1.5% CMC

SLURRY PROPERTIES	
Slurry Relative Density	1.009
Mass Concentration	1%
Fluid Consistency Index	0.0142 Pa.s^n
Flow Behaviour Index	0.944
Apparent viscosity (100 s^{-1})	0.01097 Pa.s
Apparent viscosity (500 s^{-1})	0.01002 Pa.s
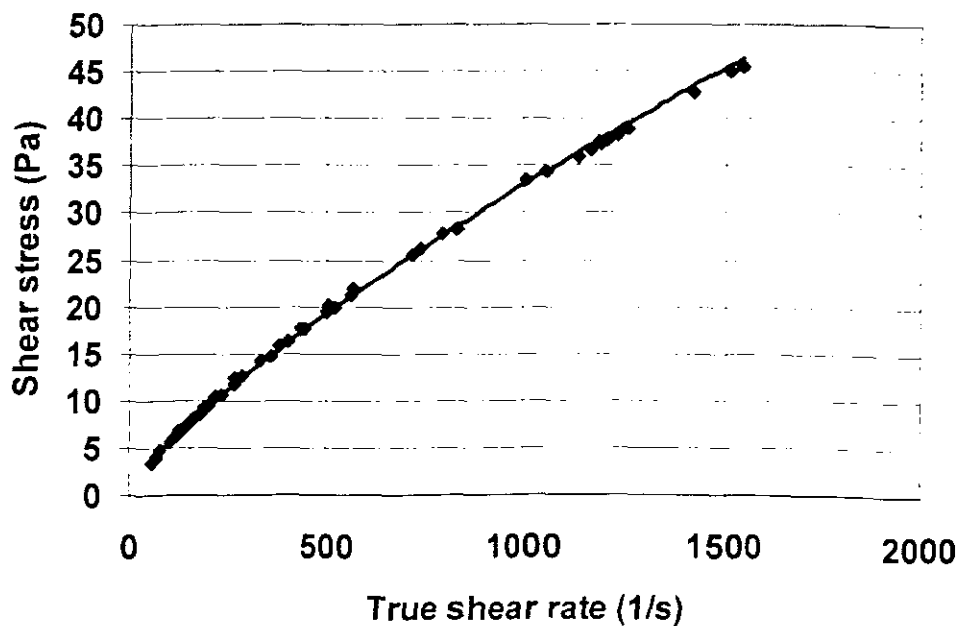
Rheogram 1.5% CMC

3% CMC

SLURRY PROPERTIES	
Slurry Relative Density	1.0169
Mass Concentration	3%
Fluid Consistency Index	0.1263 $Pa.s^n$
Flow Behaviour Index	0.7799
Apparent viscosity ($100\ s^{-1}$)	0.0458 Pa.s
Apparent viscosity ($500\ s^{-1}$)	0.0322 Pa.s
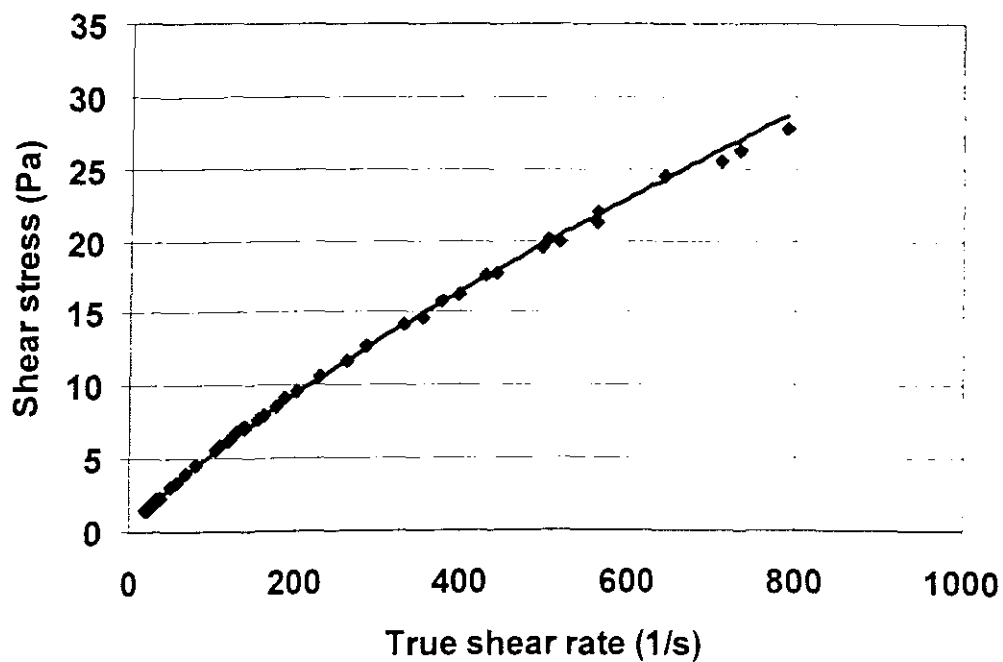
Rheogram 3% CMC

4 % CMC

SLURRY PROPERTIES	
Slurry Relative Density	1.023
Mass Concentration	4%
Fluid Consistency Index	0.3709 Pa.s^n
Flow Behaviour Index	0.7093
Apparent viscosity (100 s^{-1})	0.0972 Pa.s
Apparent viscosity (500 s^{-1})	0.0609 Pa.s
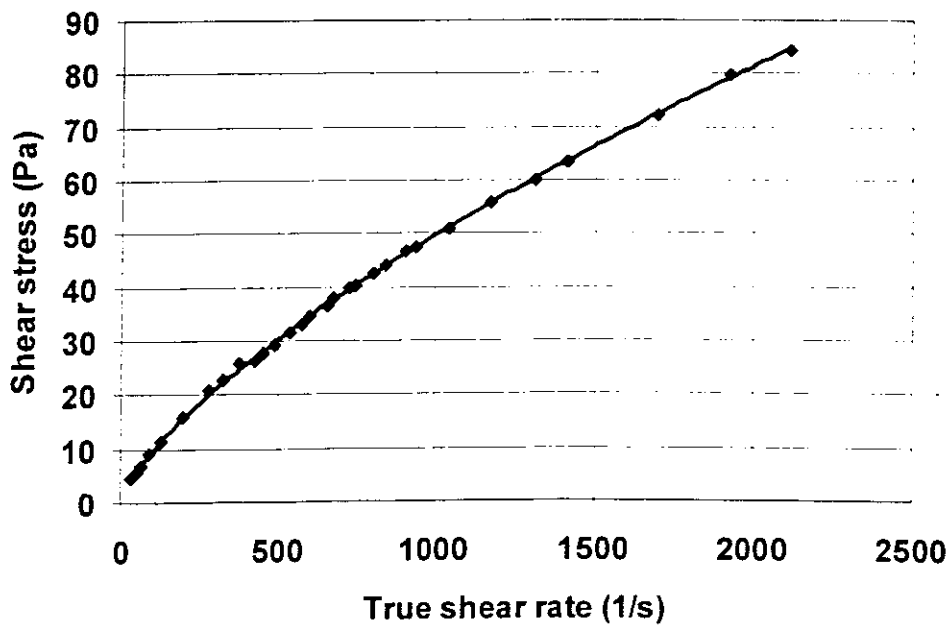
Rheogram 4 % CMC

4.6 % Bentonite

SLURRY PROPERTIES	
Slurry Relative Density	1.028
Mass Concentration	4.62%
Yield Stress	5.833 Pa
Fluid Consistency Index	0.0045 Pa.s^n
Flow Behaviour Index	1
Apparent viscosity (100 s^{-1})	0.0628 Pa.s
Apparent viscosity (500 s^{-1})	0.0162 Pa.s
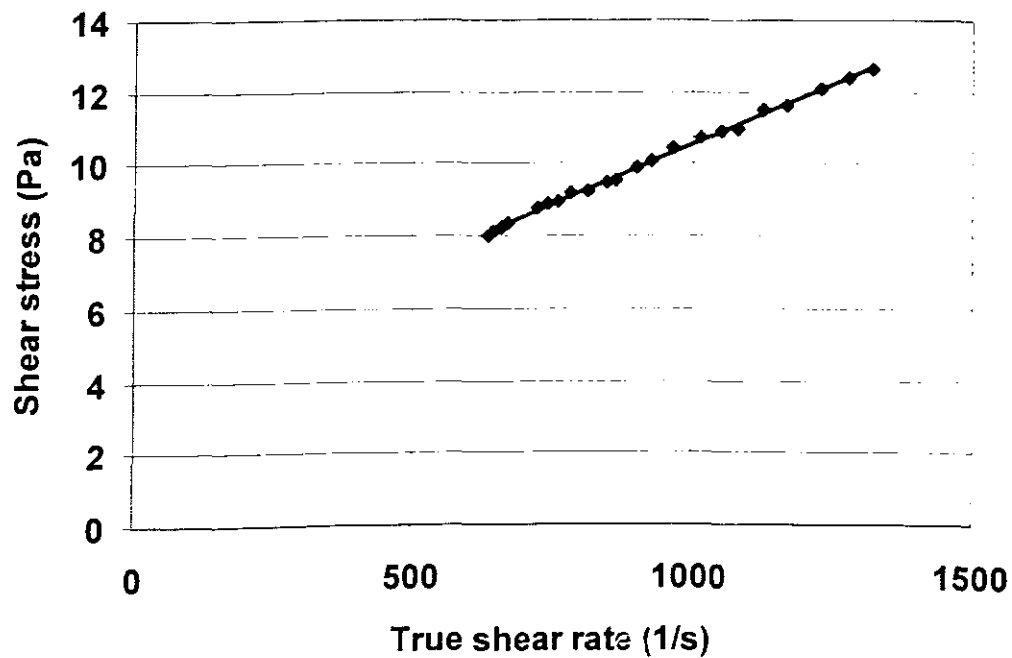
Rheogram 4.6% Bentonite

6.2% Bentonite

SLURRY PROPERTIES	
Slurry Relative Density	1.039
Mass Concentration	6.2%
Yield Stress	18.431 Pa
Fluid Consistency Index	0.0048 Pa.s^n
Flow Behaviour Index	1
Apparent viscosity (100 s^{-1})	0.1891 Pa.s
Apparent viscosity (500 s^{-1})	0.0417 Pa.s
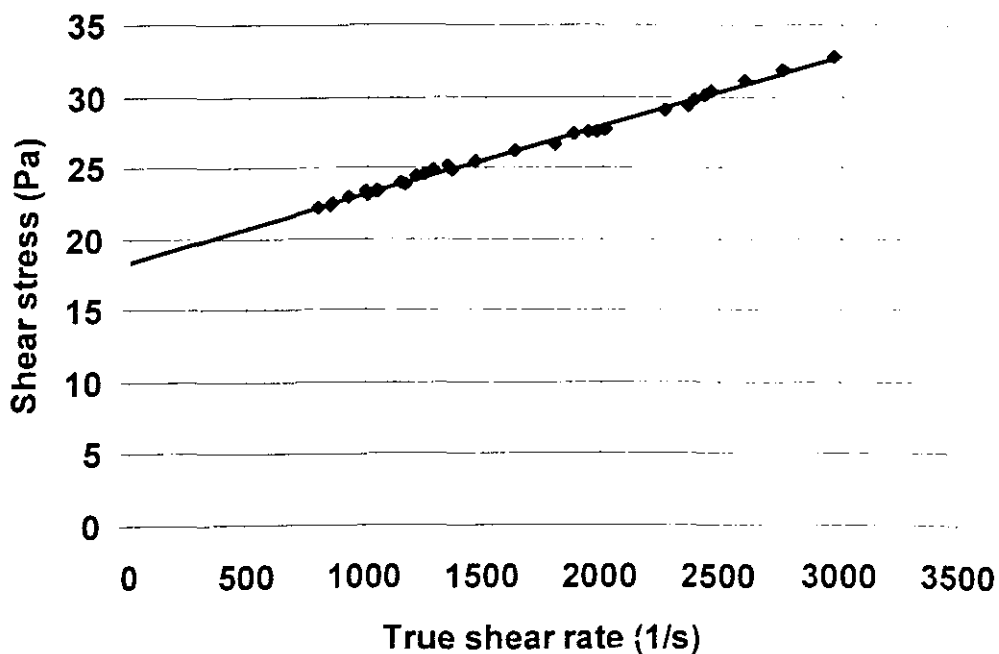
Rheogram 6.2 % Bentonite

5.4 % Kaolin

SLURRY PROPERTIES	
Solids Relative Density	2.65
Slurry Relative Density	1.088
Mass Concentration	5.4%
Yield Stress	3.43 Pa
Fluid Consistency Index	0.2484 Pa.s^n
Flow Behaviour Index	0.4527
Apparent viscosity (100 s^{-1})	0.0542 Pa.s
Apparent viscosity (500 s^{-1})	0.0151 Pa.s
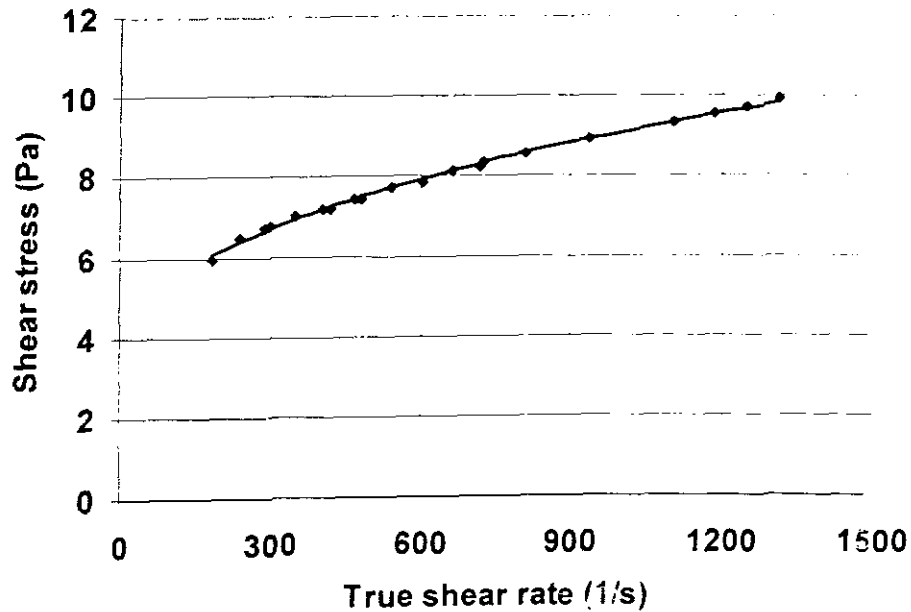
Rheogram 5.4% Kaolin

7.1% Kaolin

SLURRY PROPERTIES	
Solids Relative Density	2.65
Slurry Relative Density	1.118
Mass Concentration	7.1%
Yield Stress	8.1 Pa
Fluid Consistency Index	1.1409 Pa.s^n
Flow Behaviour Index	0.32
Apparent viscosity (100 s^{-1})	0.1308
Apparent viscosity (500 s^{-1})	0.0329
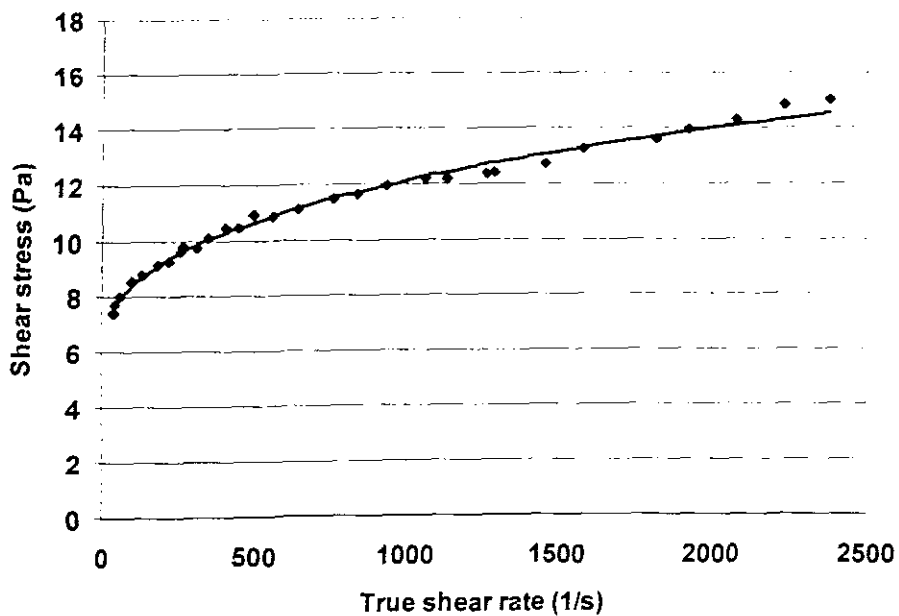
Rheogram 7.1% Kaolin

9 % Kaolin

SLURRY PROPERTIES	
Solids Relative Density	2.65
Slurry Relative Density	1.149
Mass Concentration	9%
Yield Stress	18.2 Pa
Fluid Consistency Index	0.4965 Pa.s^n
Flow Behaviour Index	0.4716
Apparent viscosity (100 s^{-1})	0.2256 Pa.s
Apparent viscosity (500 s^{-1})	0.055 Pa.s
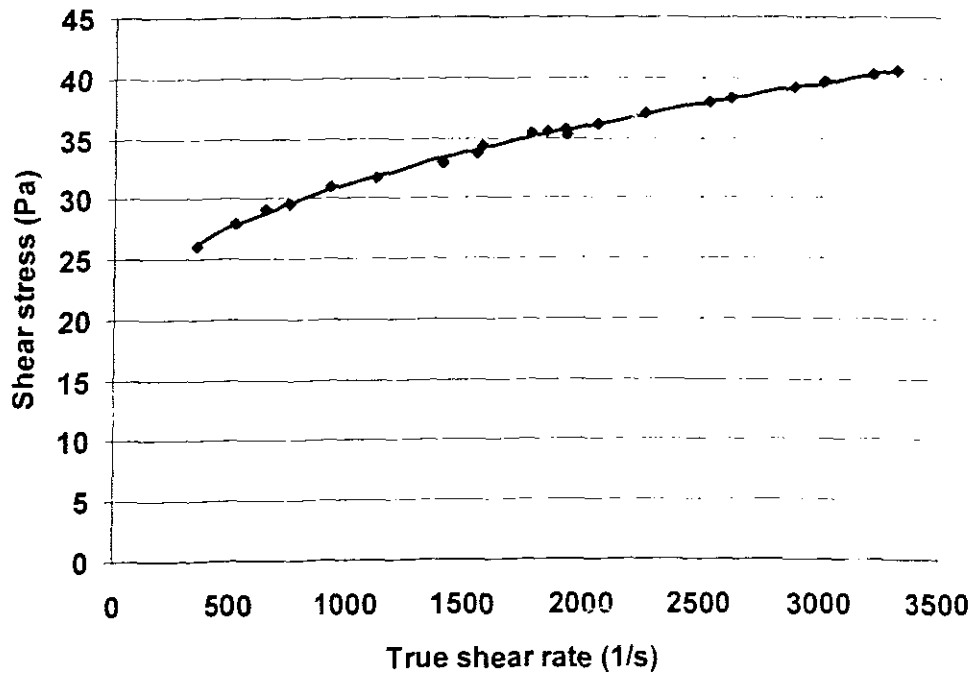
Rheogram 9 % Kaolin

A.2 FLUME DATA
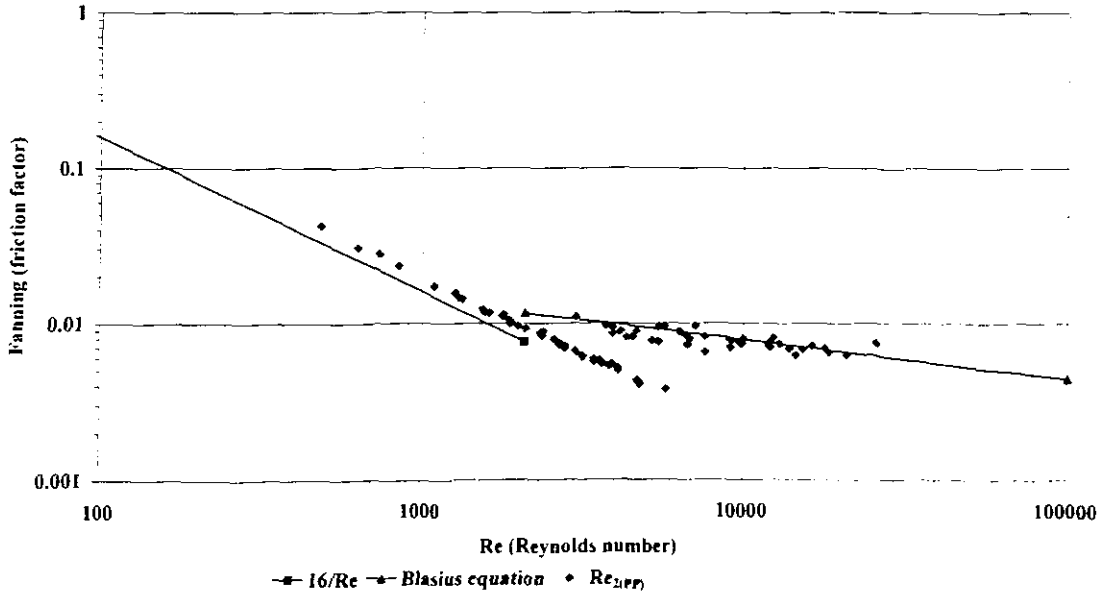
1% CMC in 150mm rectangular flume shape.
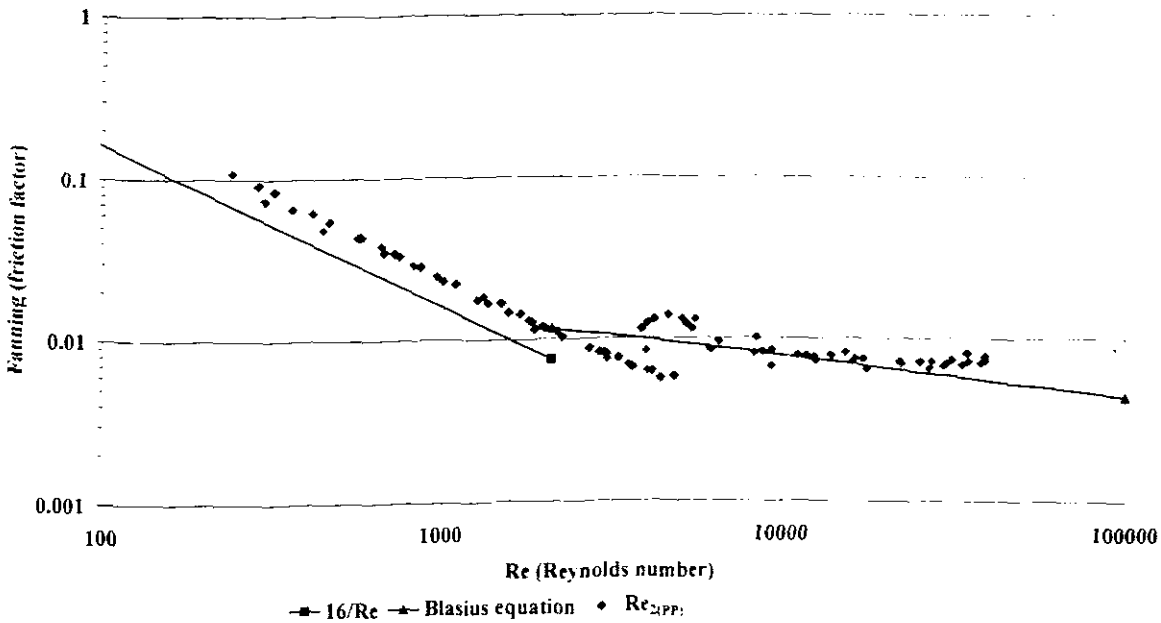
1% CMC in 300mm rectangular flume shape.
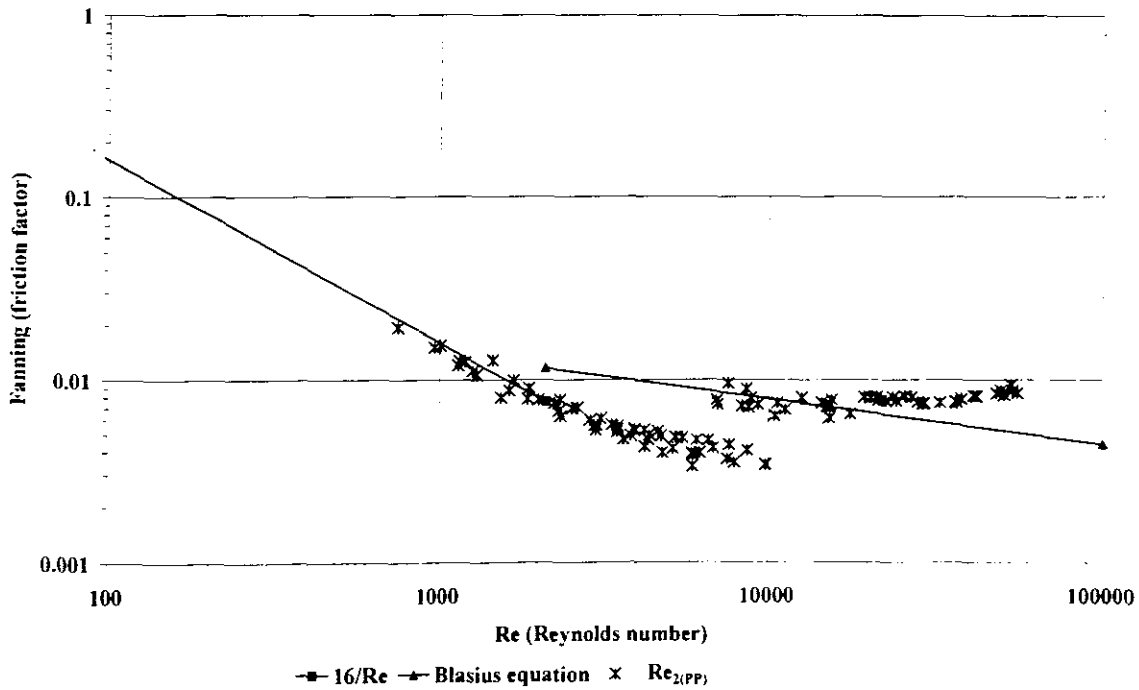
1% CMC in a 300mm semi circular flume shape
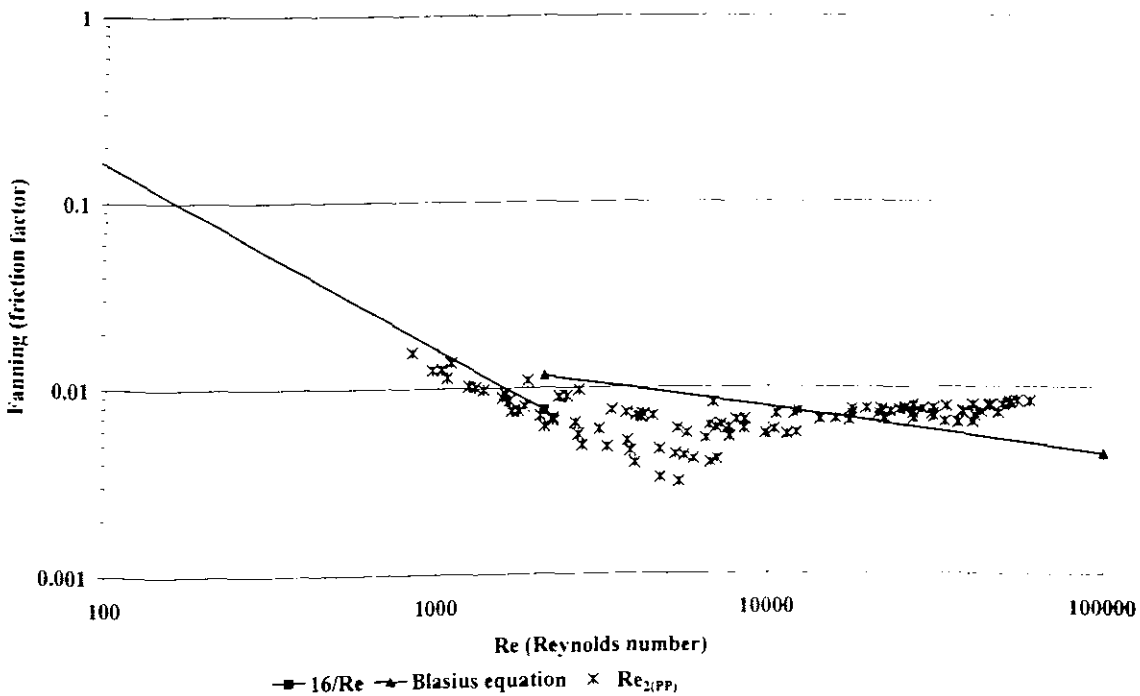
1% CMC in a 150mm semi circular flume shape
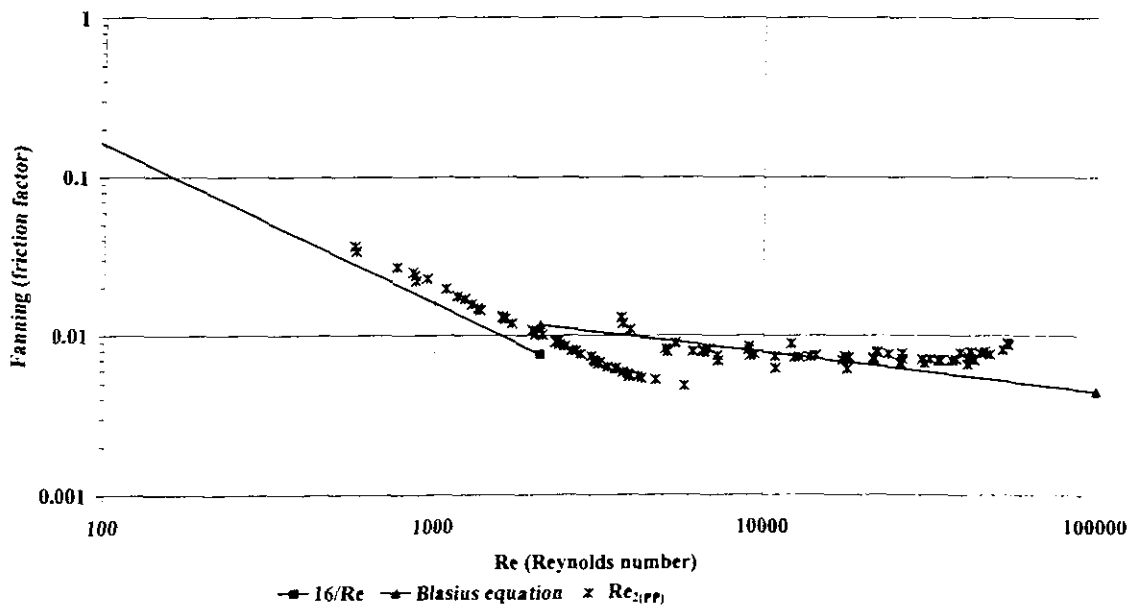
1% CMC in a 150mm trapezoidal flume shape
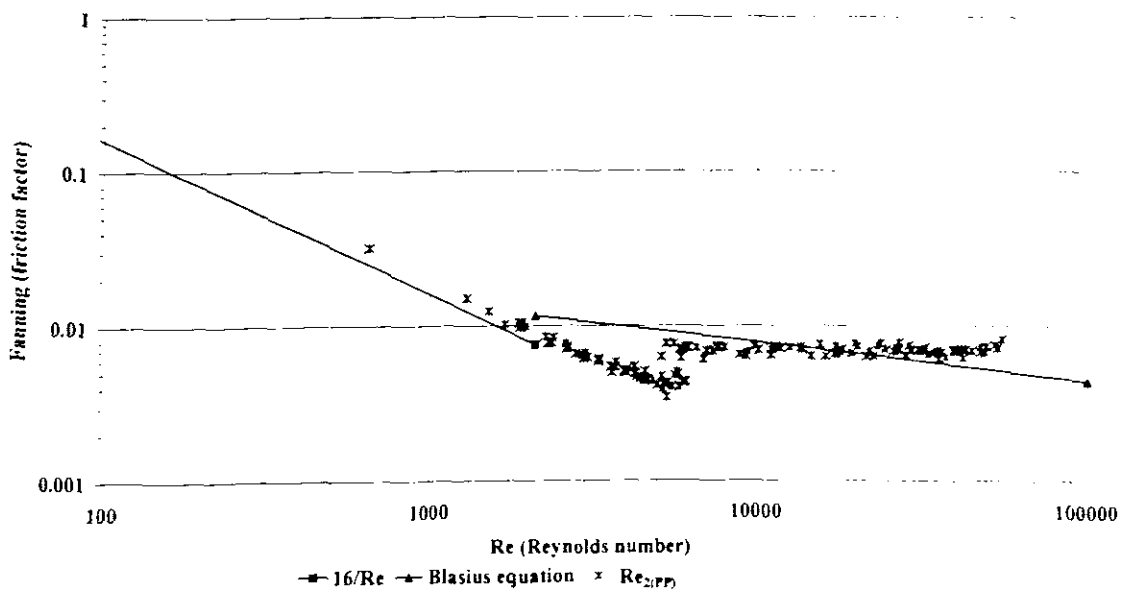
1% CMC in a 75mm trapezoidal flume shape
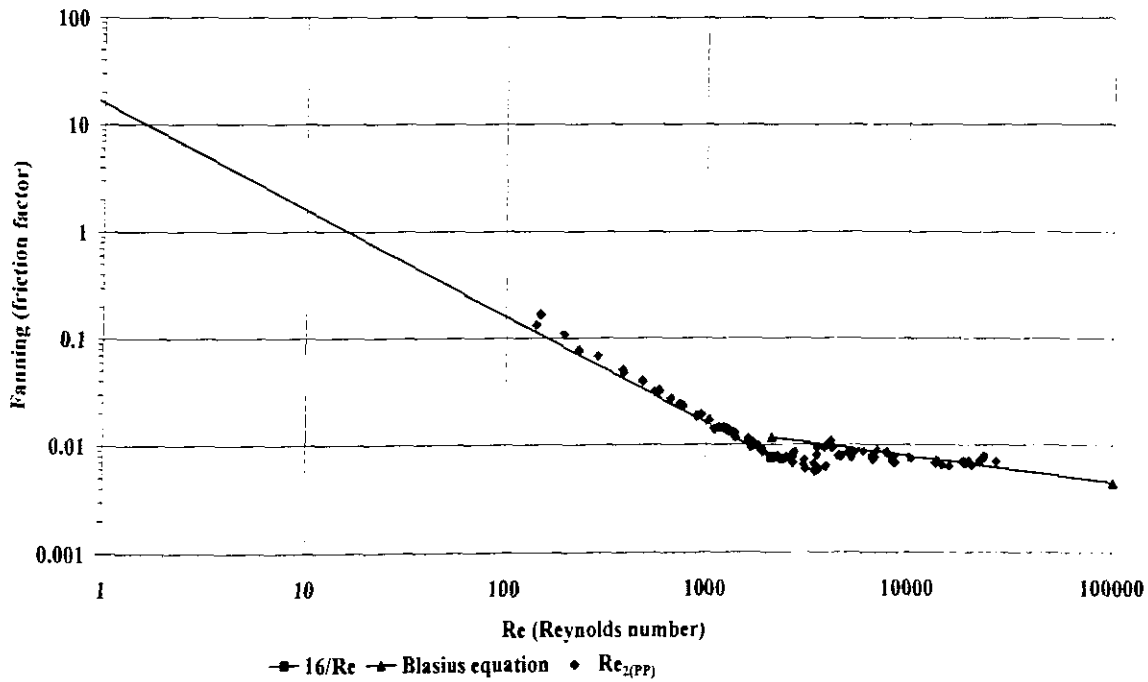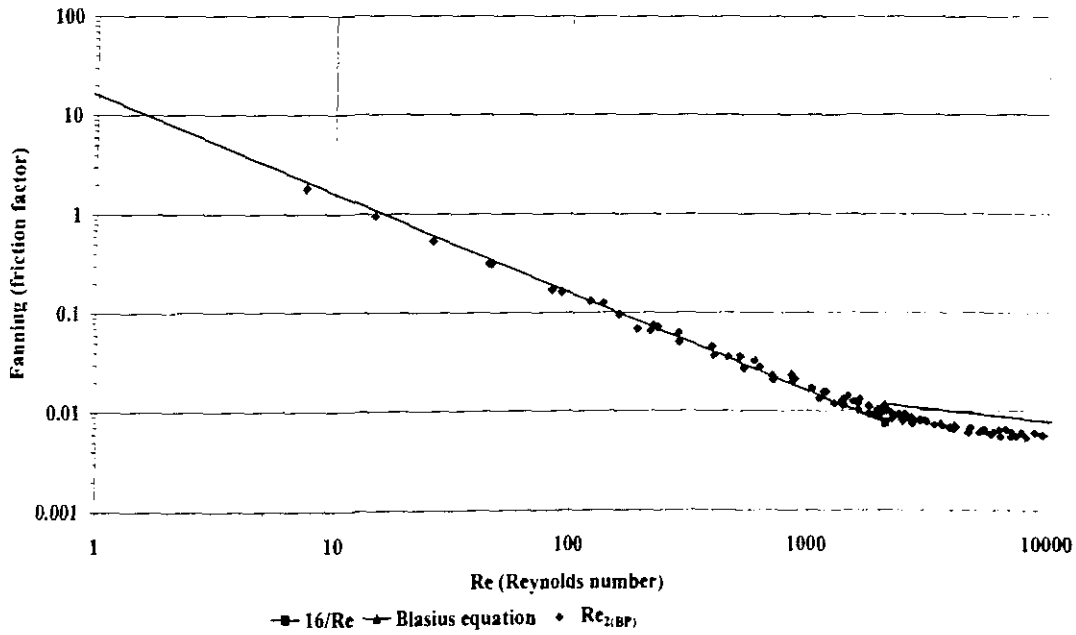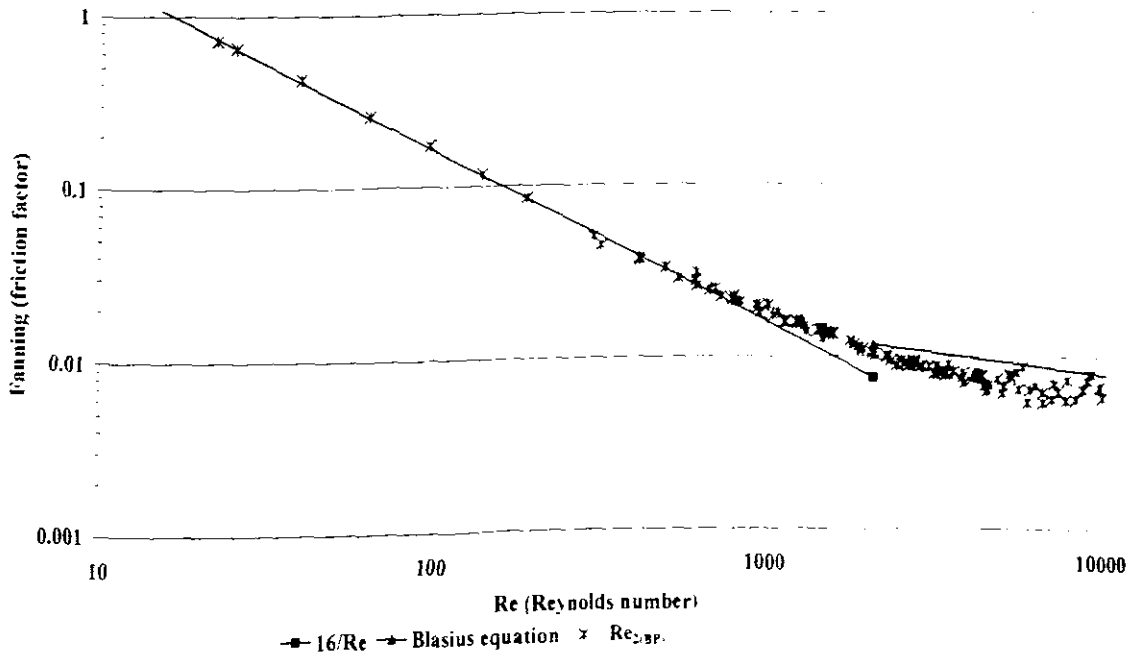
1.5% CMC in 300mm rectangular flume shape
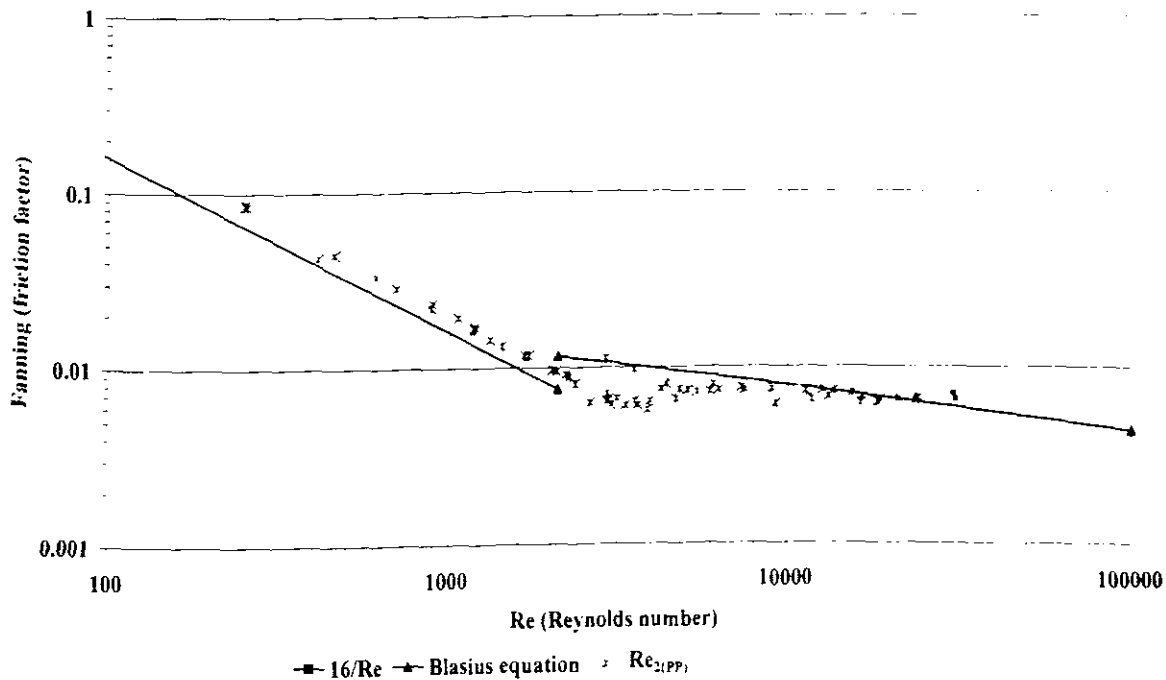
1.5% CMC in 150mm rectangular flume shape
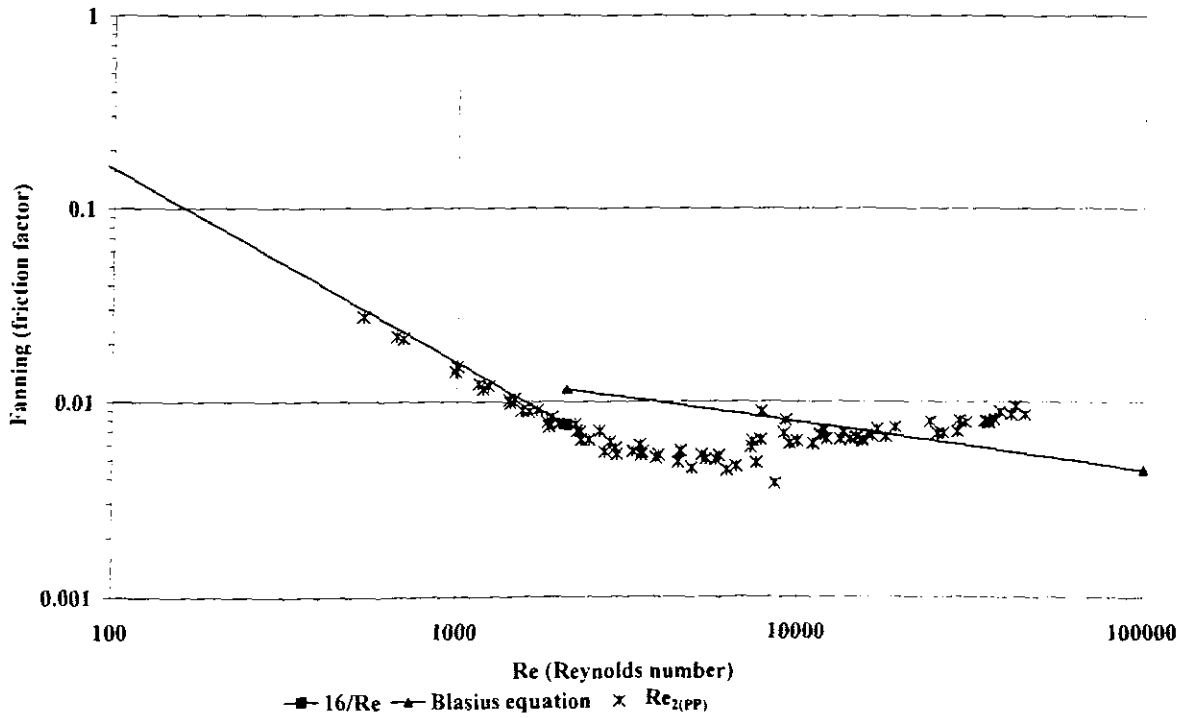
1.5% CMC in 300mm semi circular flume shape
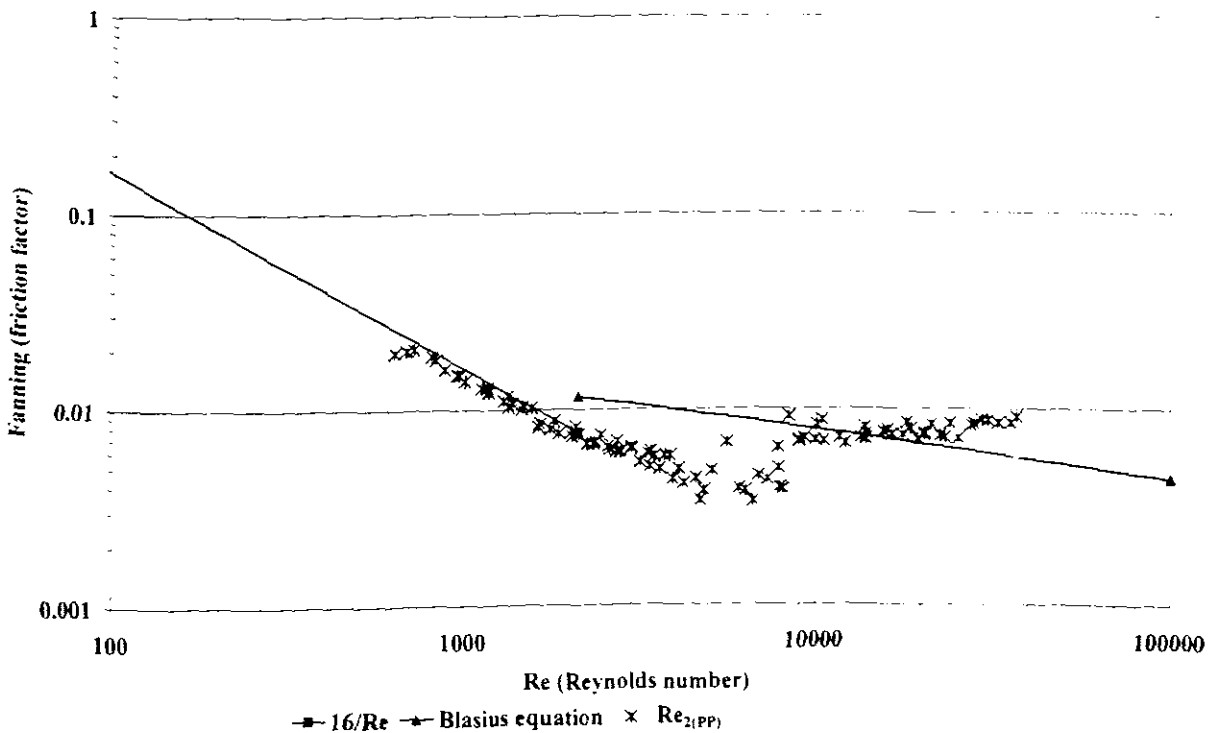
1.5% CMC in 150mm semi circular flume shape
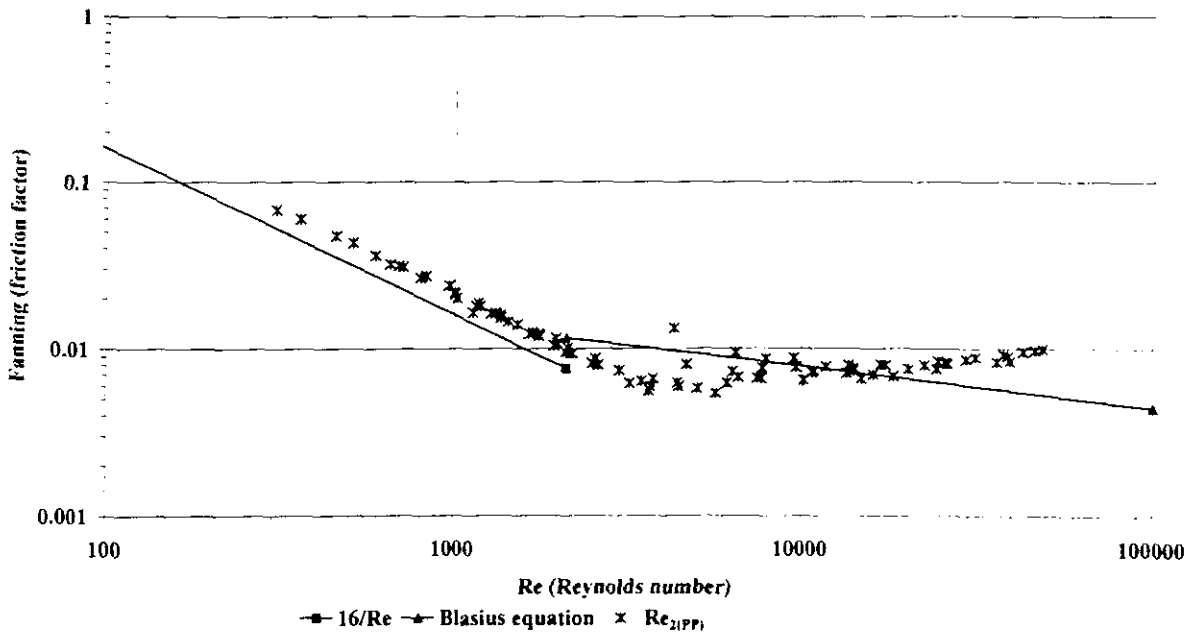
1.5% CMC in 150mm trapezoidal flume shape

1.5% CMC in 75mm trapezoidal flume shape

3% CMC in 300mm rectangular flume shape
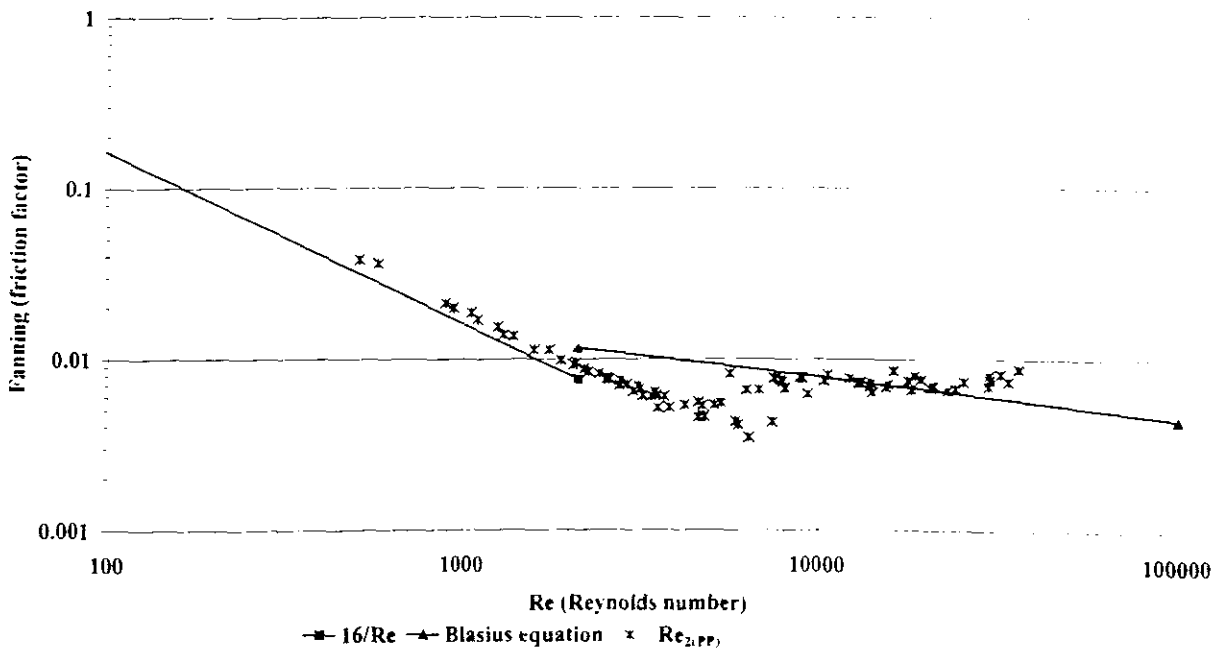
3% CMC in 150mm rectangular flume shape
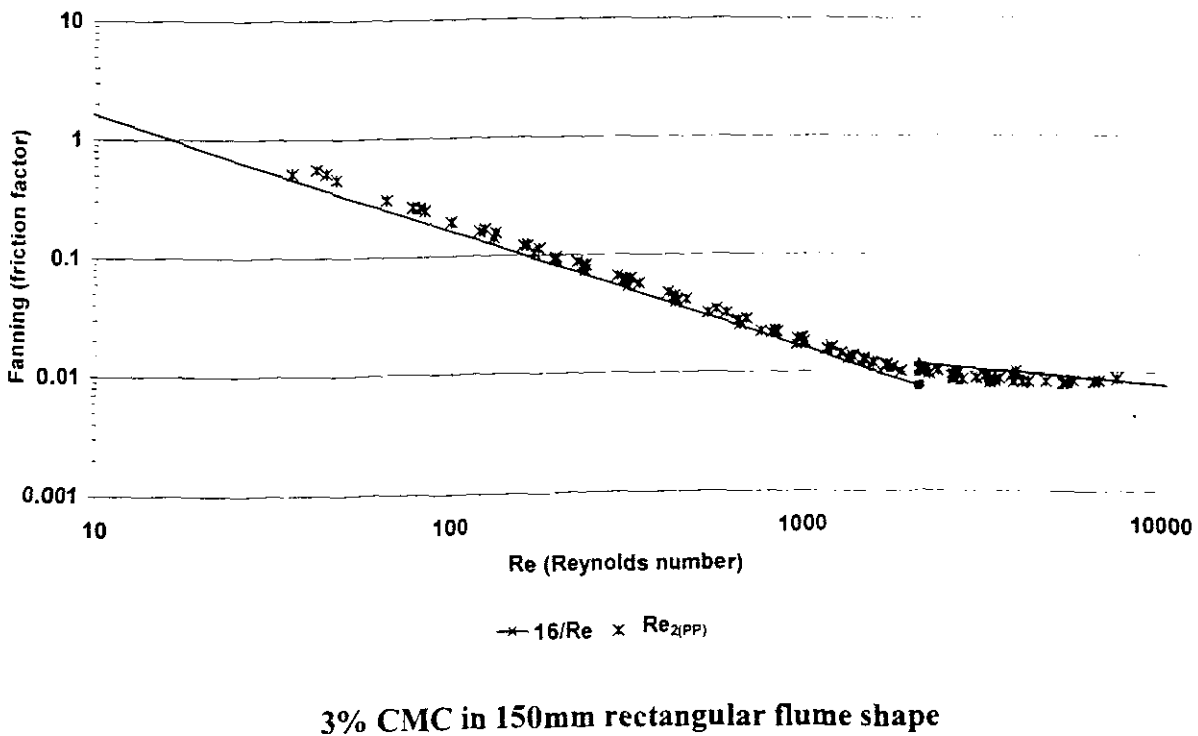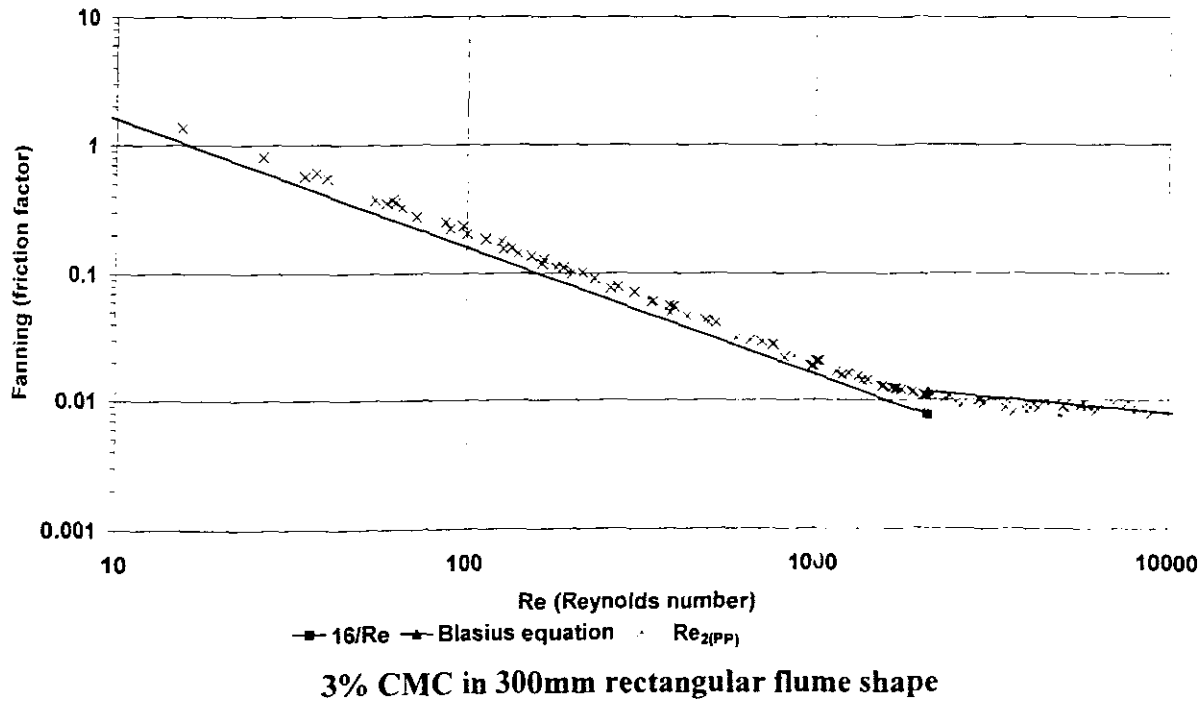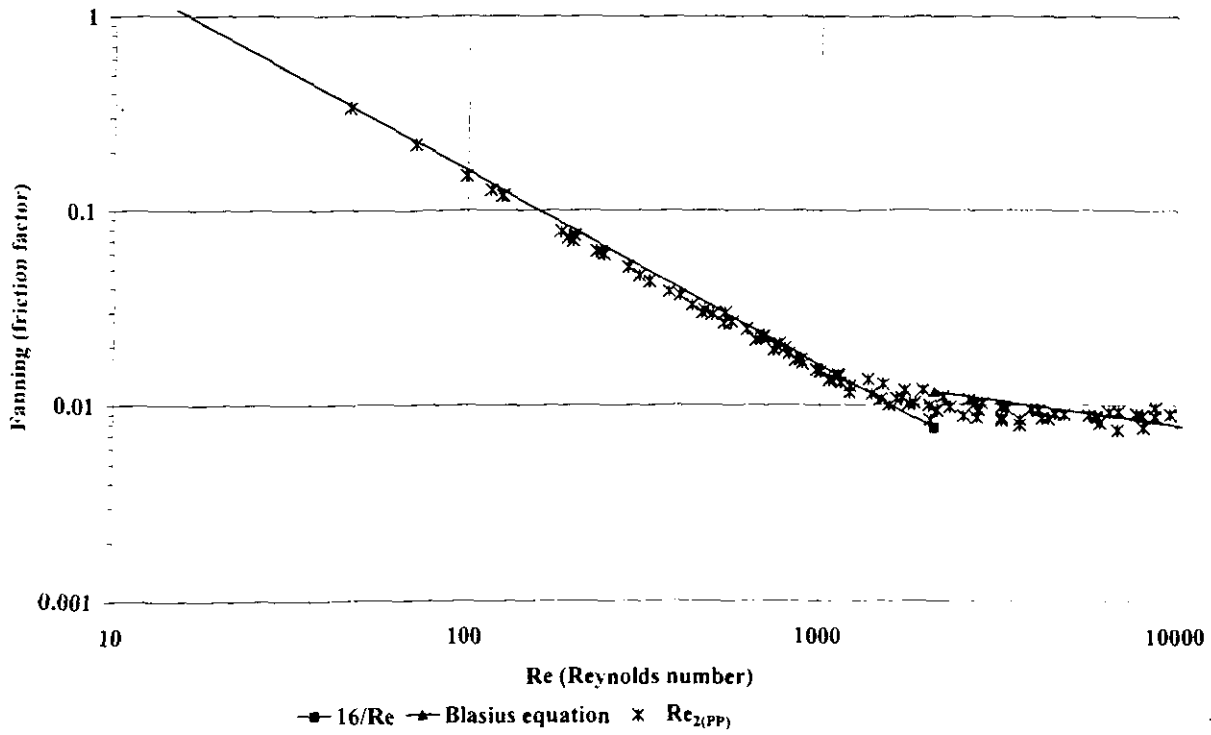
3% CMC in 300mm semi circular flume shape
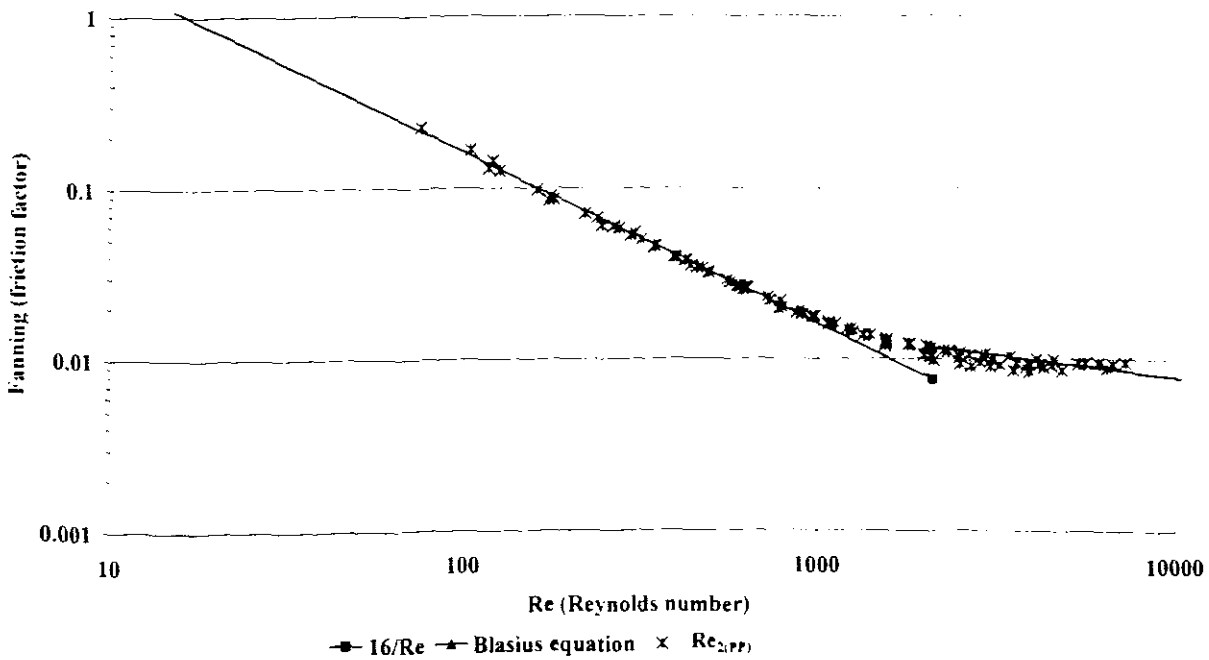
3% CMC in 150mm semi circular flume shape
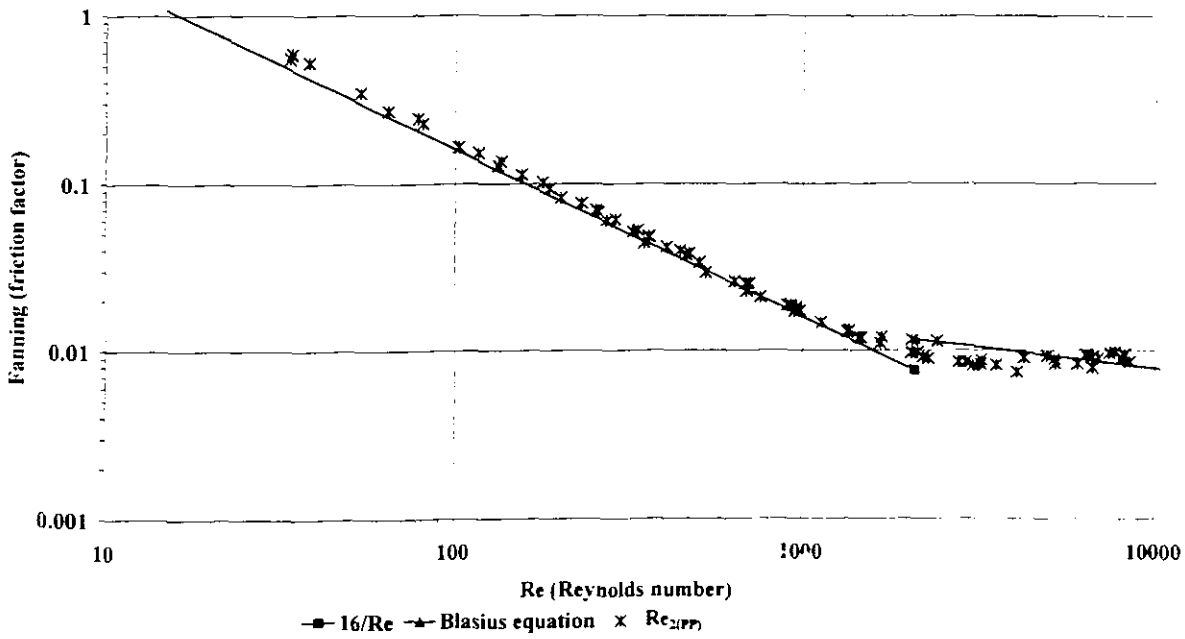
3% CMC in 150mm trapezoidal flume shape
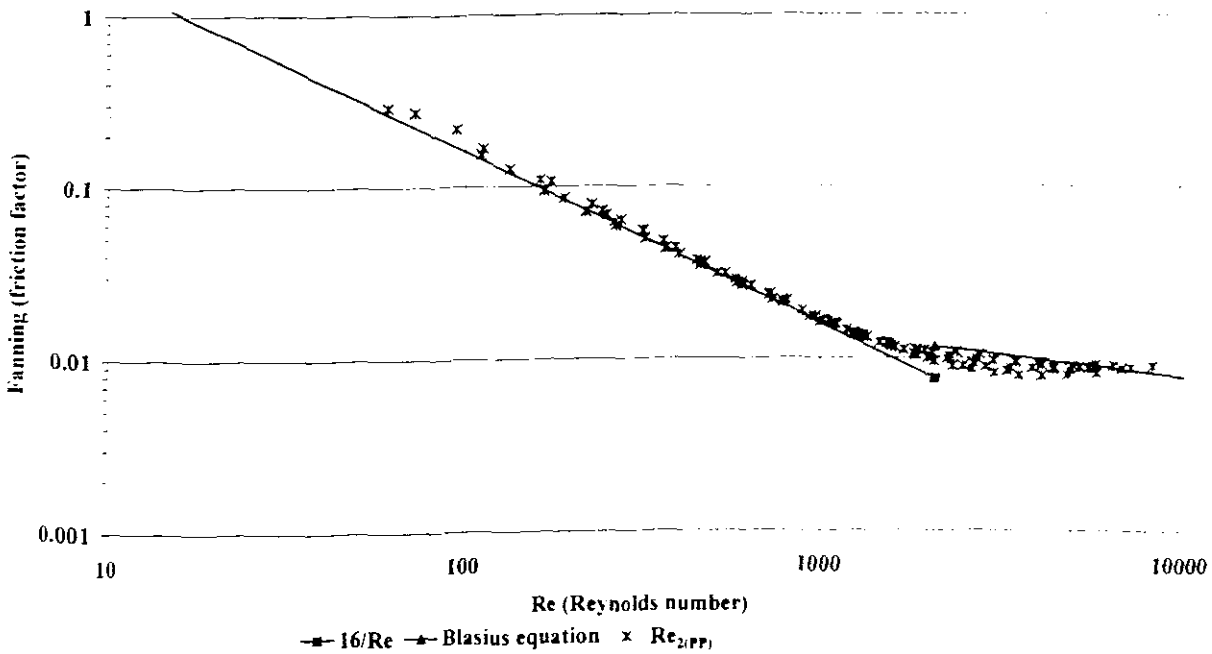
3% CMC in 75mm trapezoidal flume shape
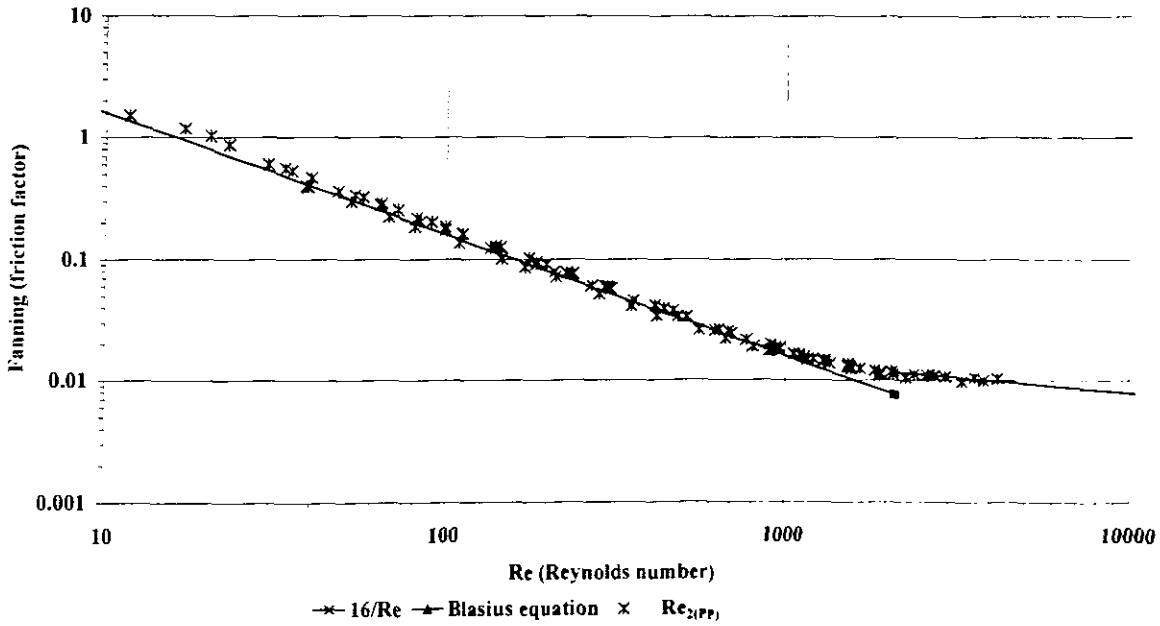
4% CMC in 150mm rectangular flume shape
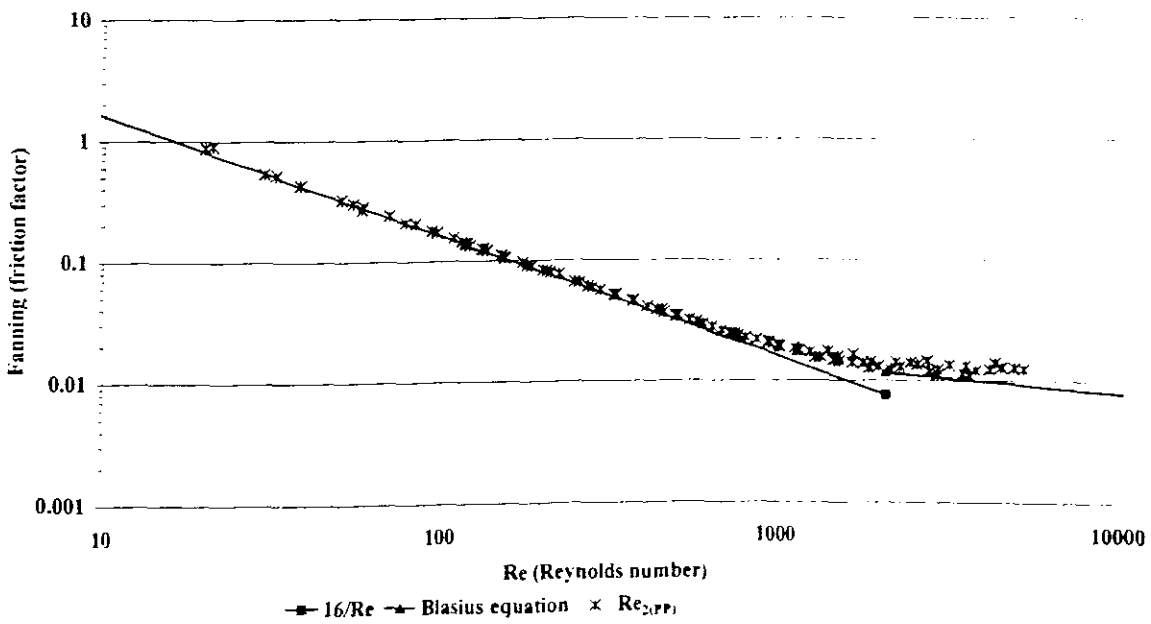
4% CMC in 300mm semi circular flume shape
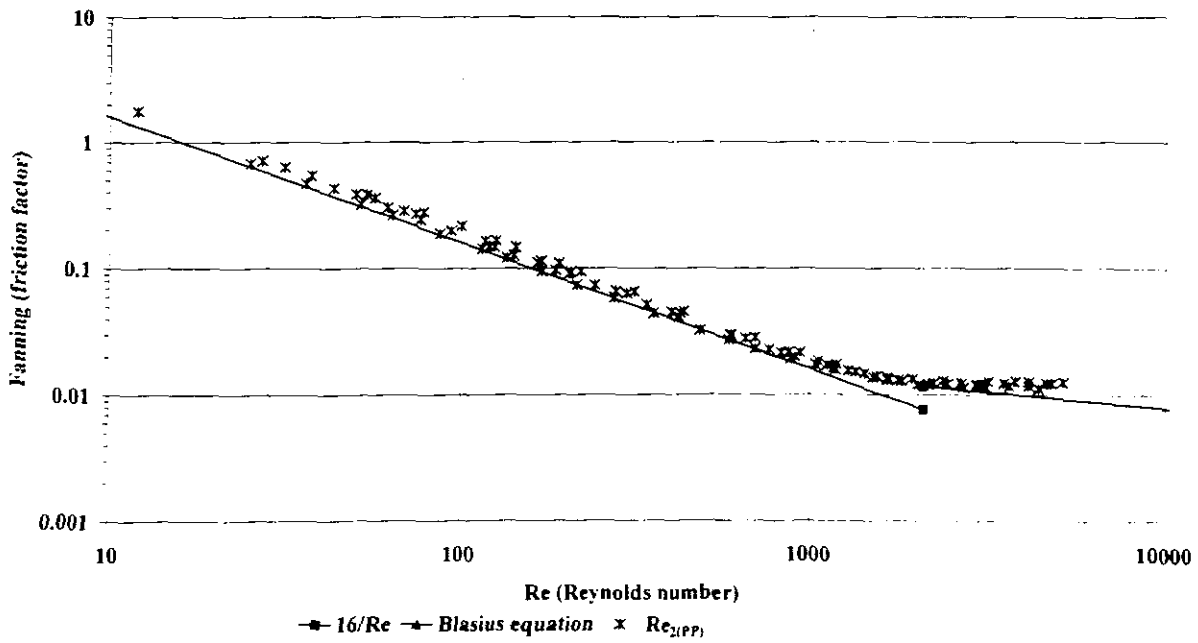
4% CMC in 150 mm trapezoidal flume shape
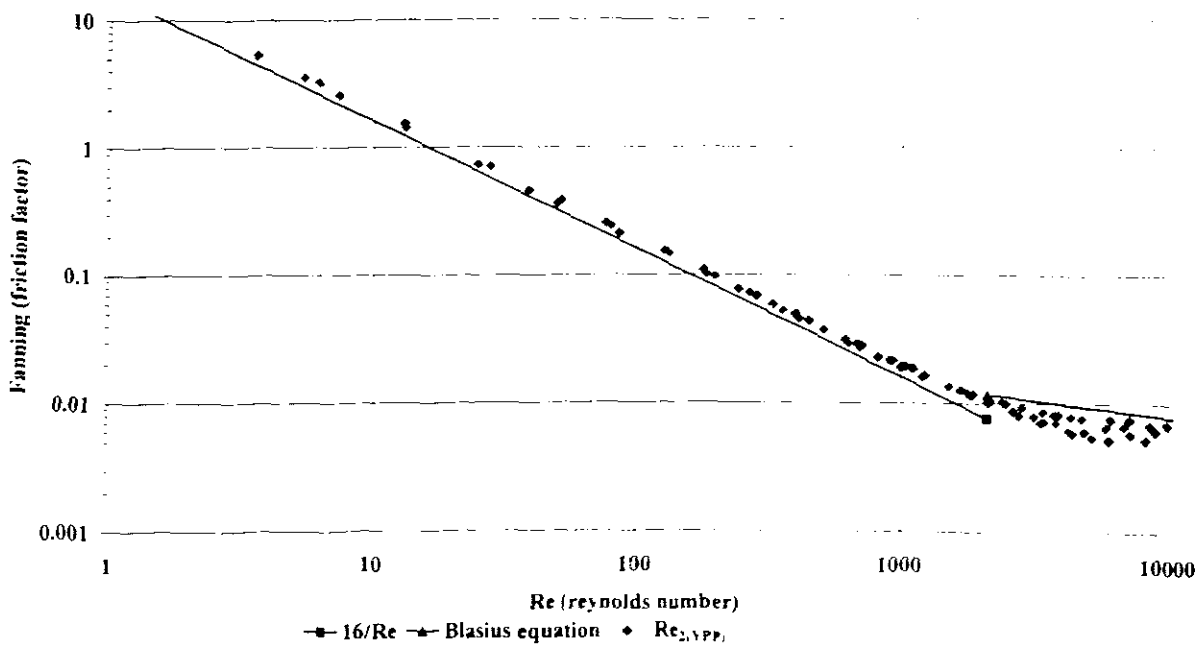
5.4% kaolin in 300 mm rectangular flume shape
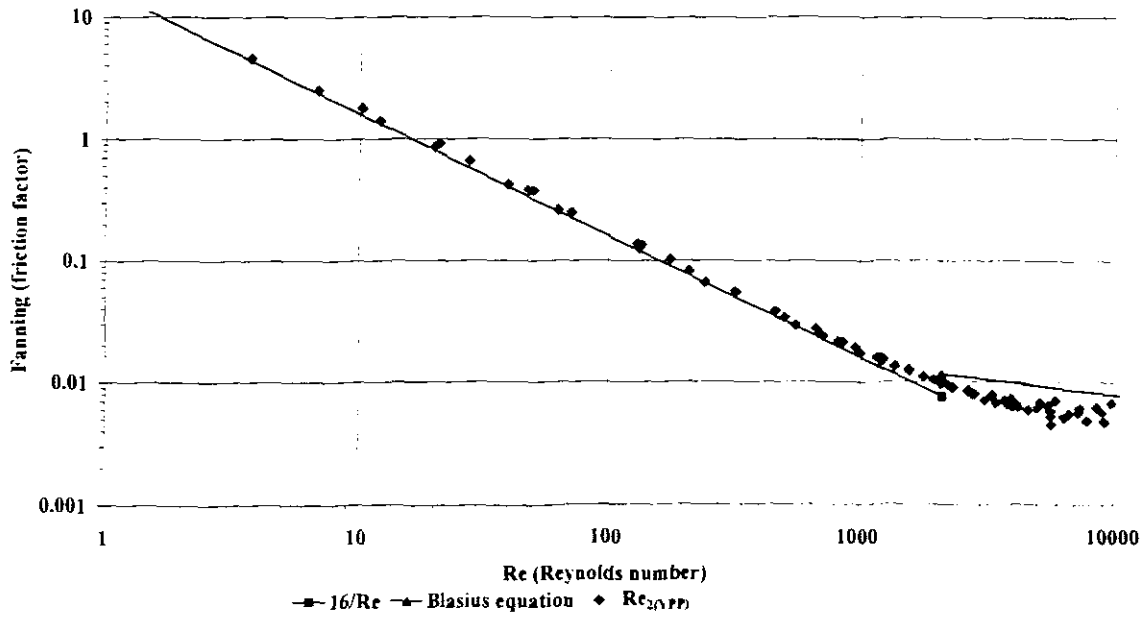
5.4% kaolin in 150 mm rectangular flume shape
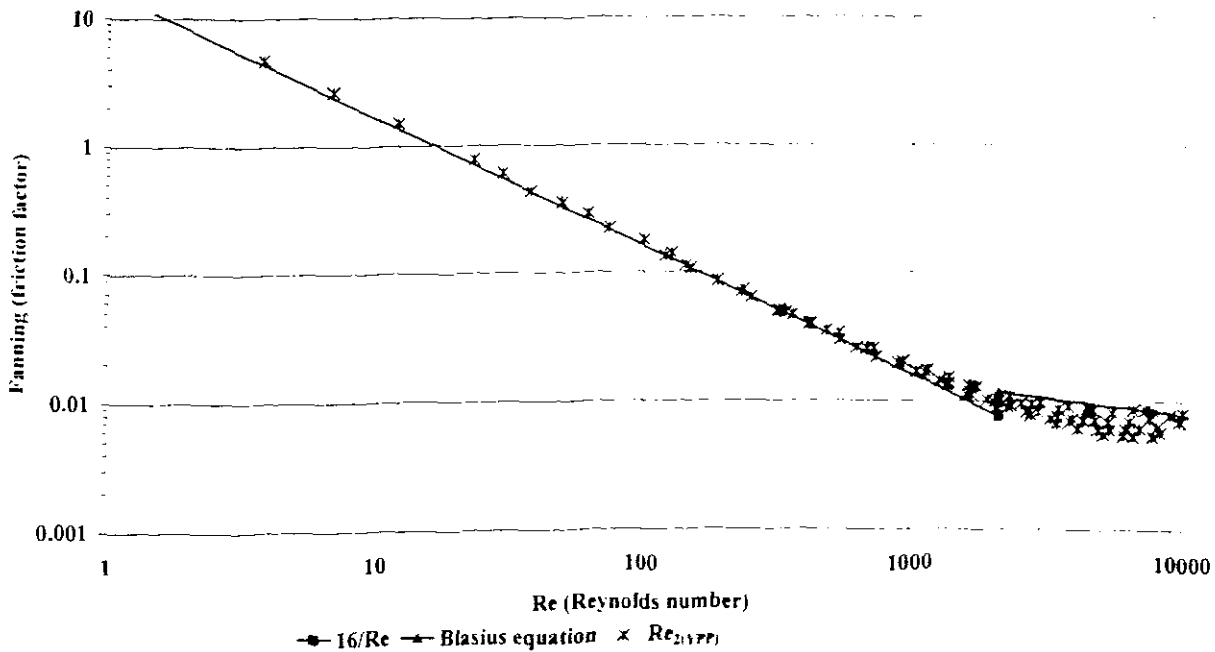
5.4% kaolin in 300 mm semi circular flume shape
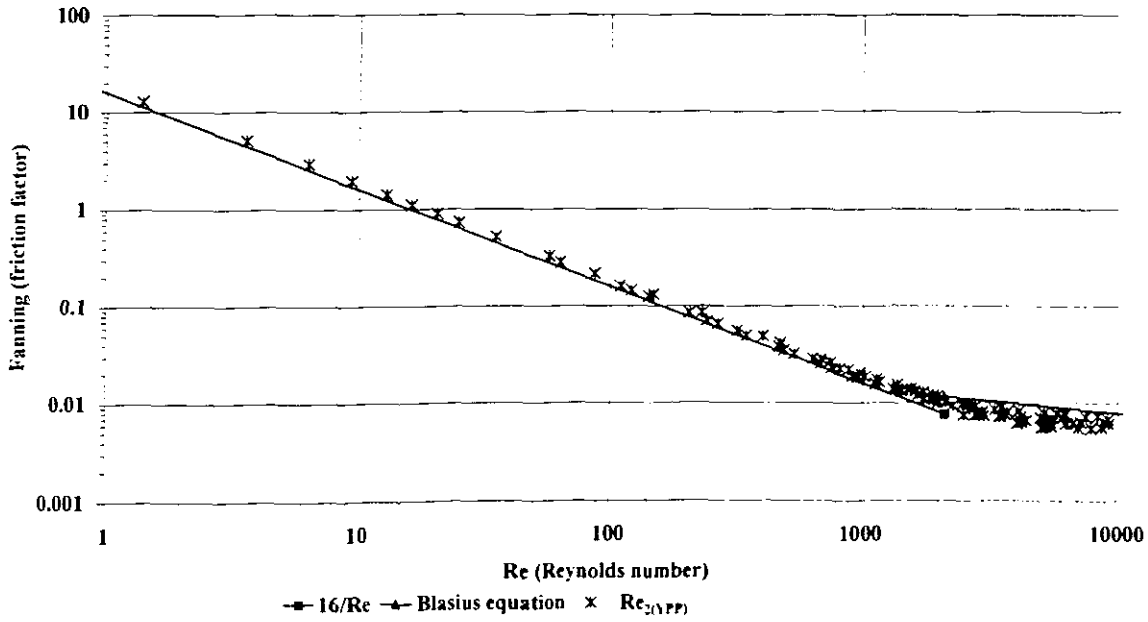
5.4% kaolin in 150 mm semi circular flume shape
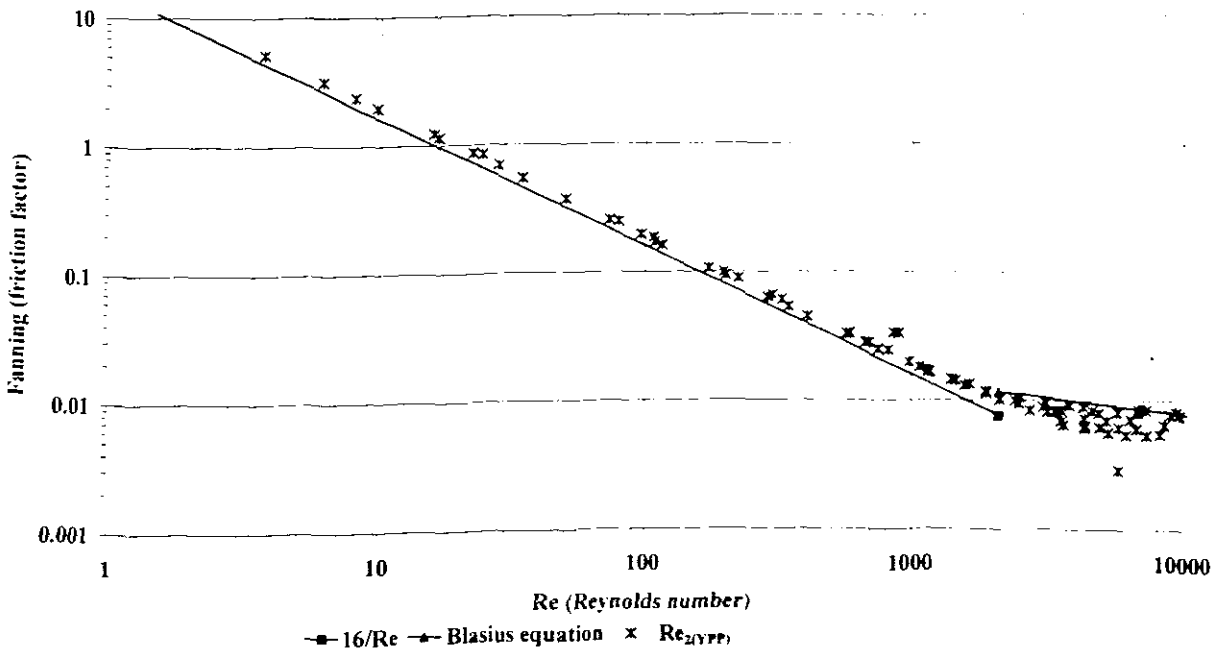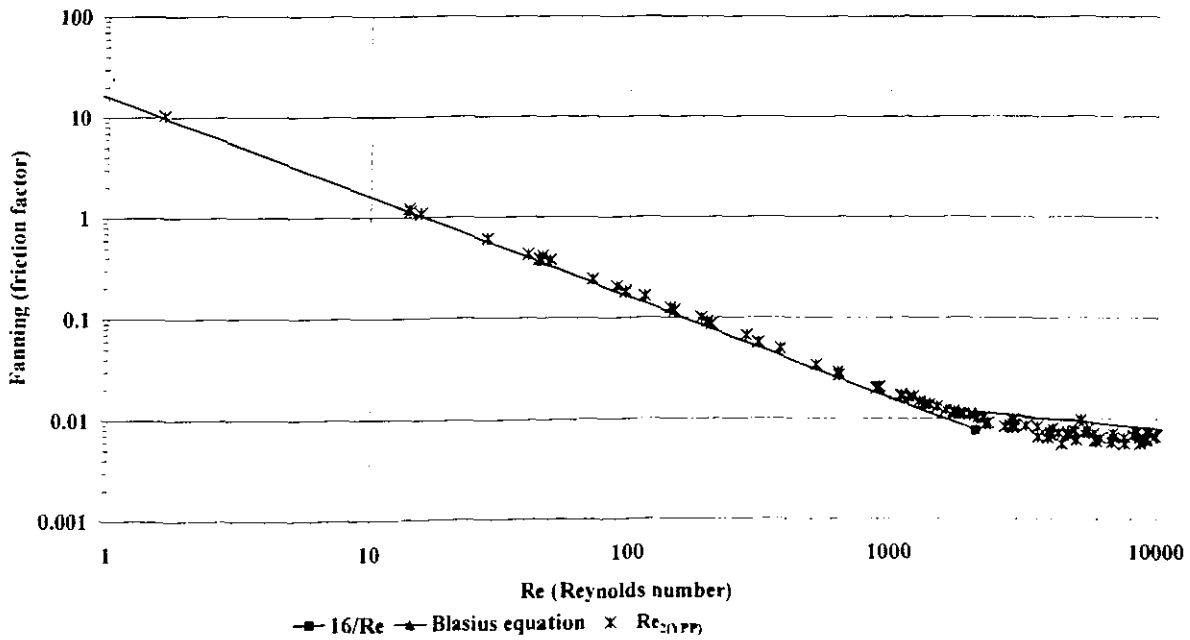
5.4% kaolin in 150 mm trapezoidal flume shape

5.4% kaolin in 75 mm trapezoidal flume shape
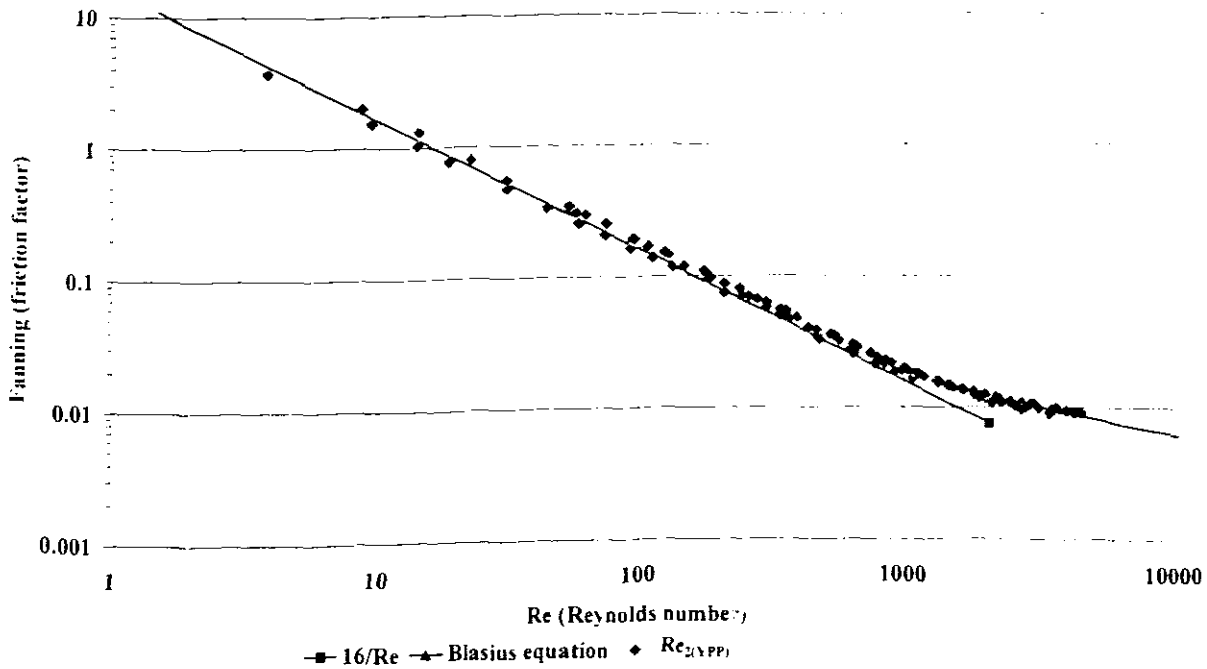
7.1% kaolin in 300 mm rectangular flume shape

7.1% kaolin in 150 mm rectangular flume shape

7.1% kaolin in 300 mm semi circular flume shape

7.1% kaolin in 150 mm semi circular flume shape
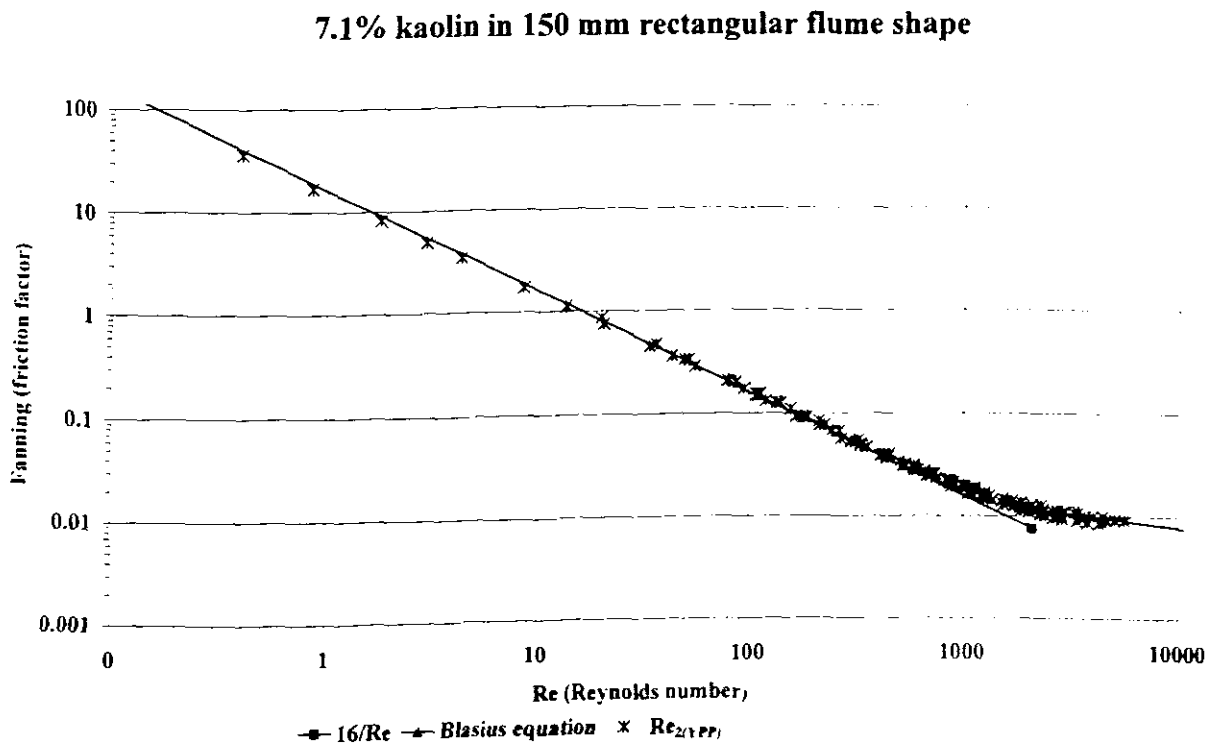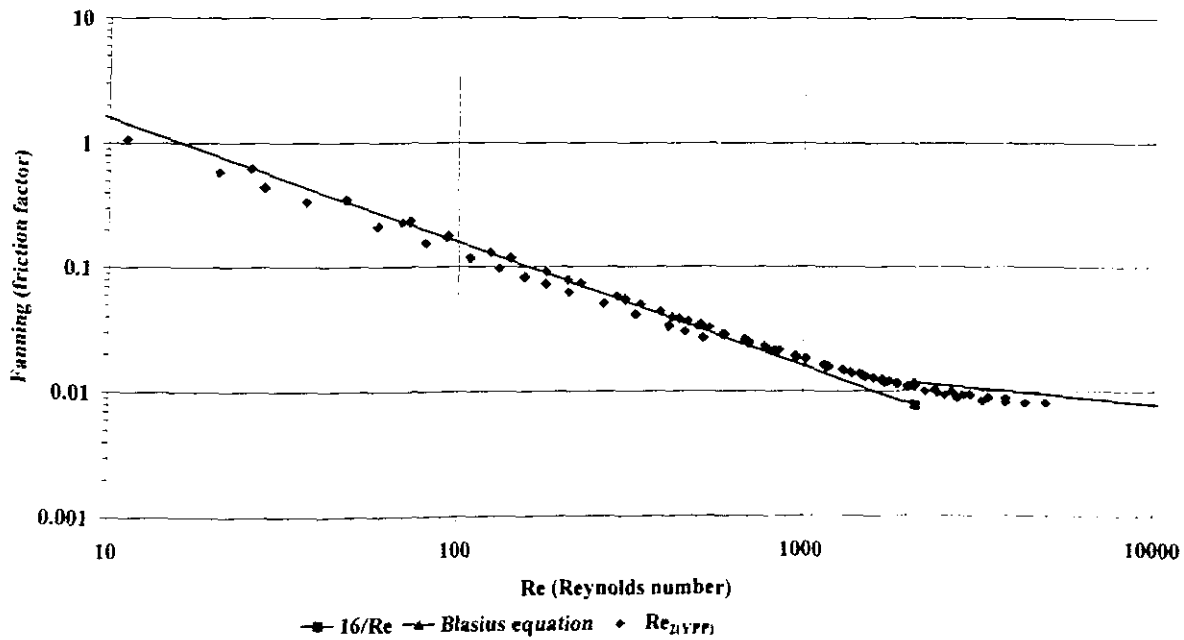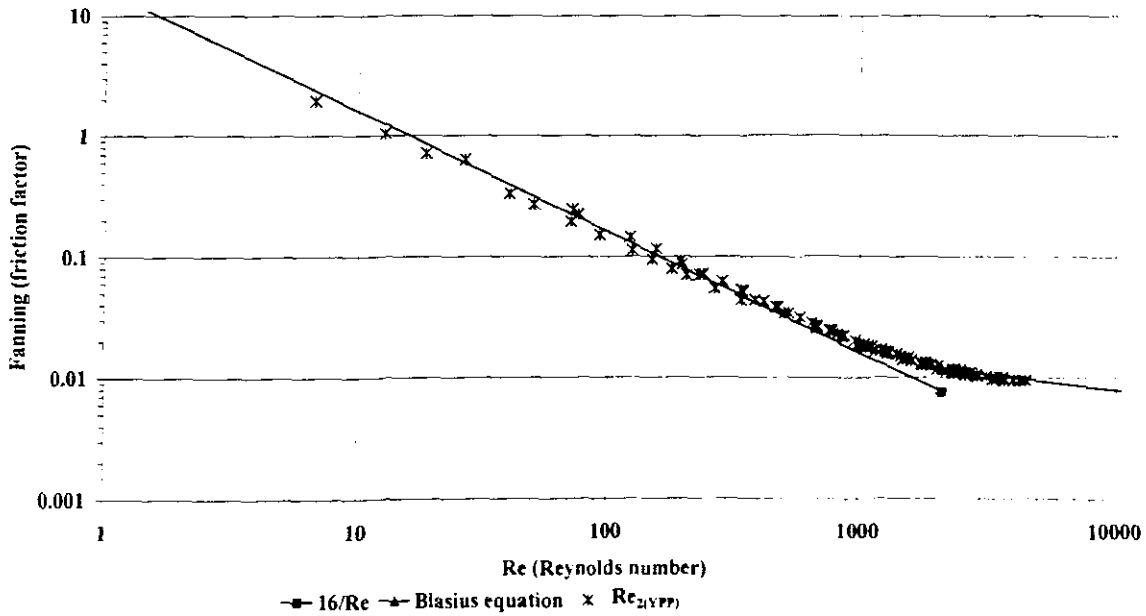
7.1% kaolin in 150 mm trapezoidal flume shape
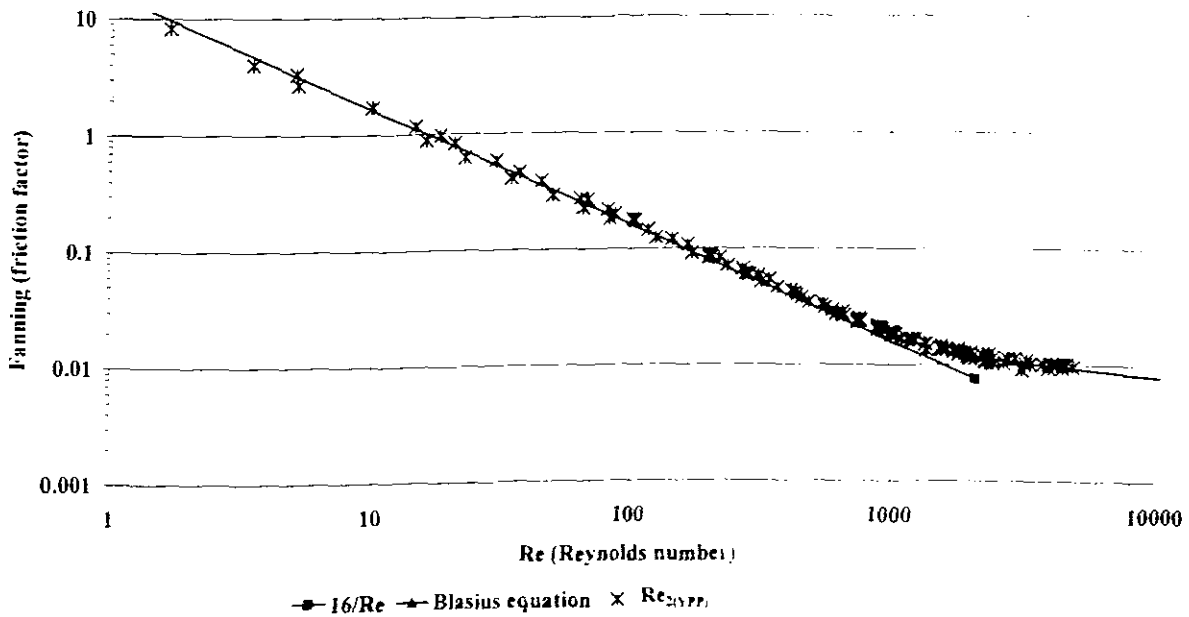
7.1% kaolin in 75 mm trapezoidal flume shape


4.6% Bentonite in 300mm rectangular channel
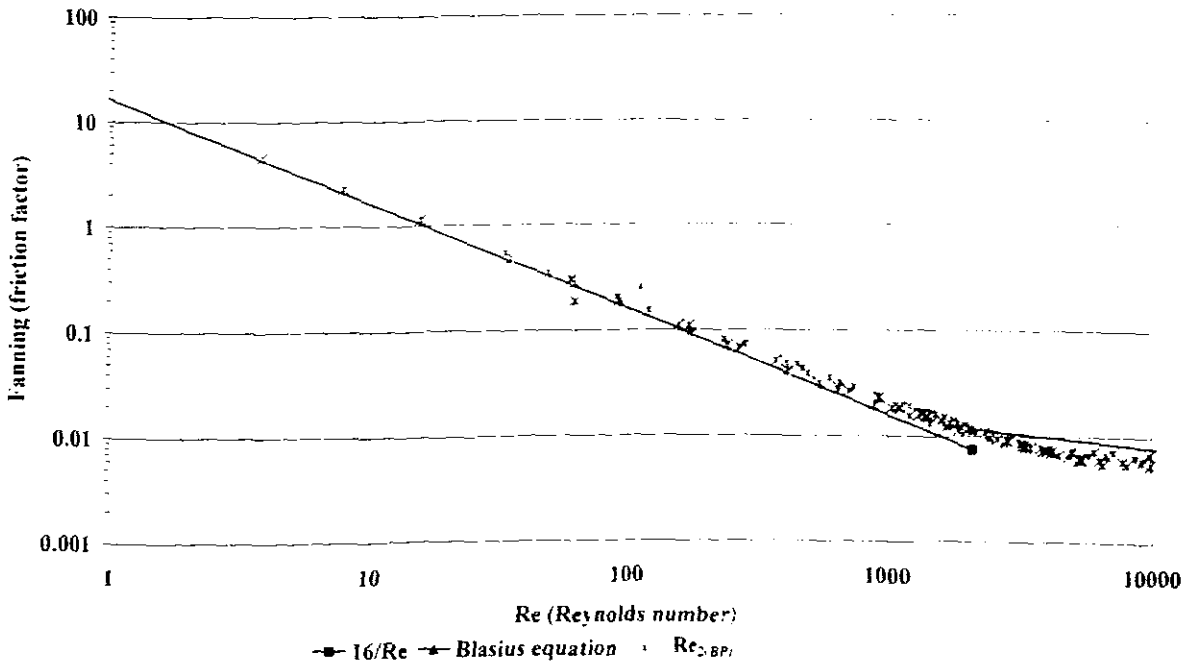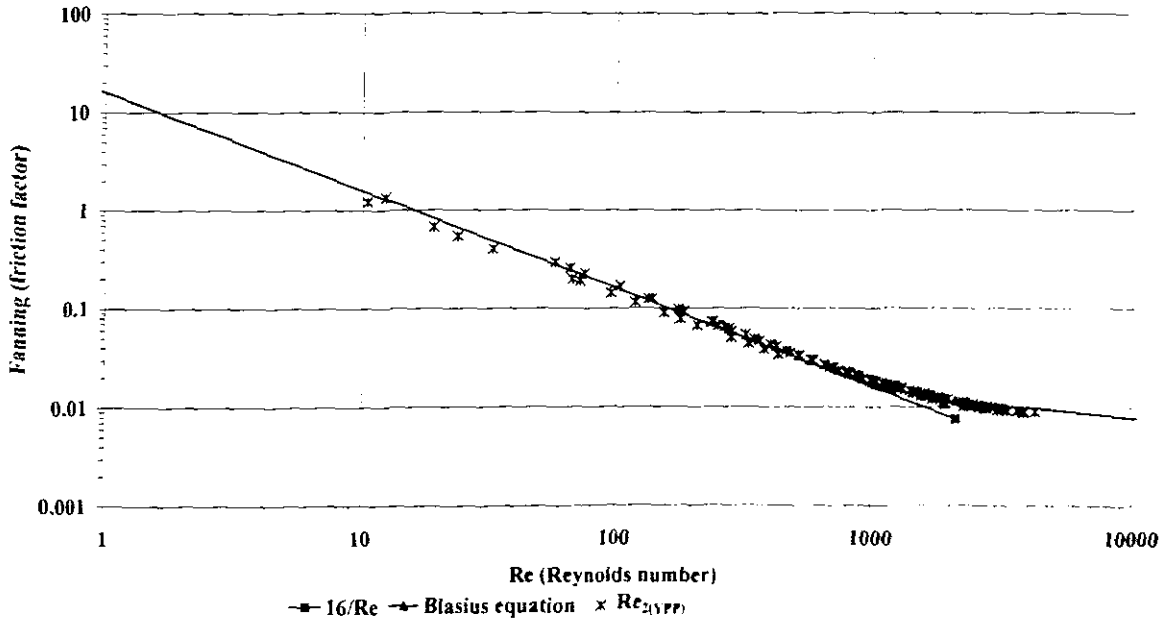
**4.6% Bentonite in 150 mm rectangular channel**

4.6% Bentonite in 300 mm semi circular flume channel
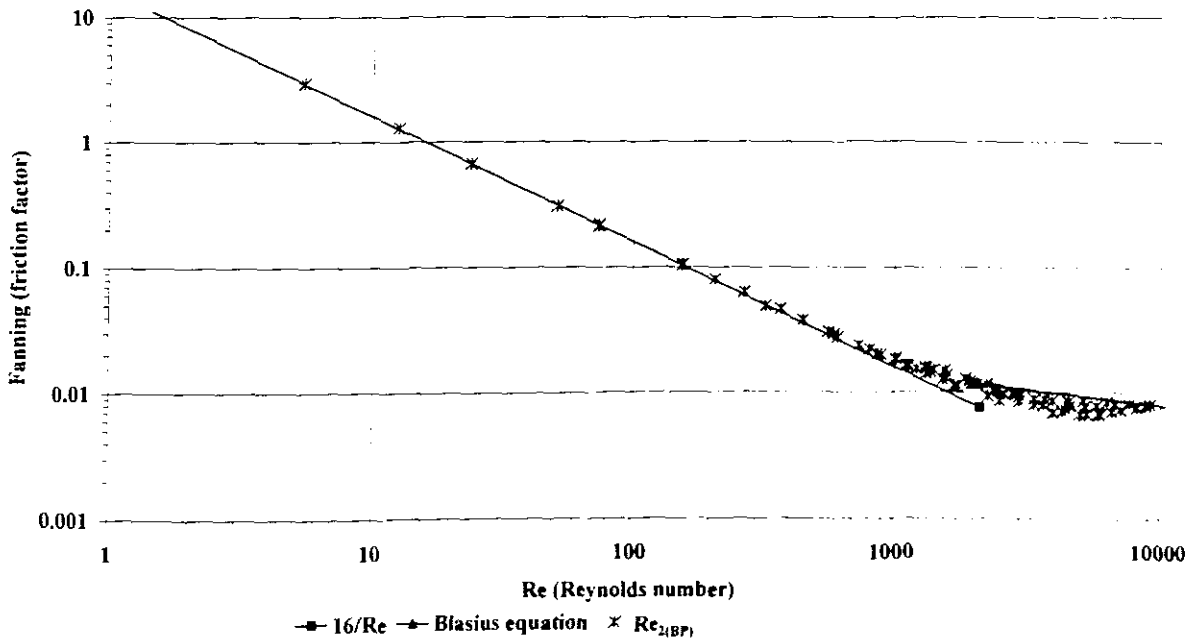
4.6% Bentonite in 150 mm semi circular flume channel
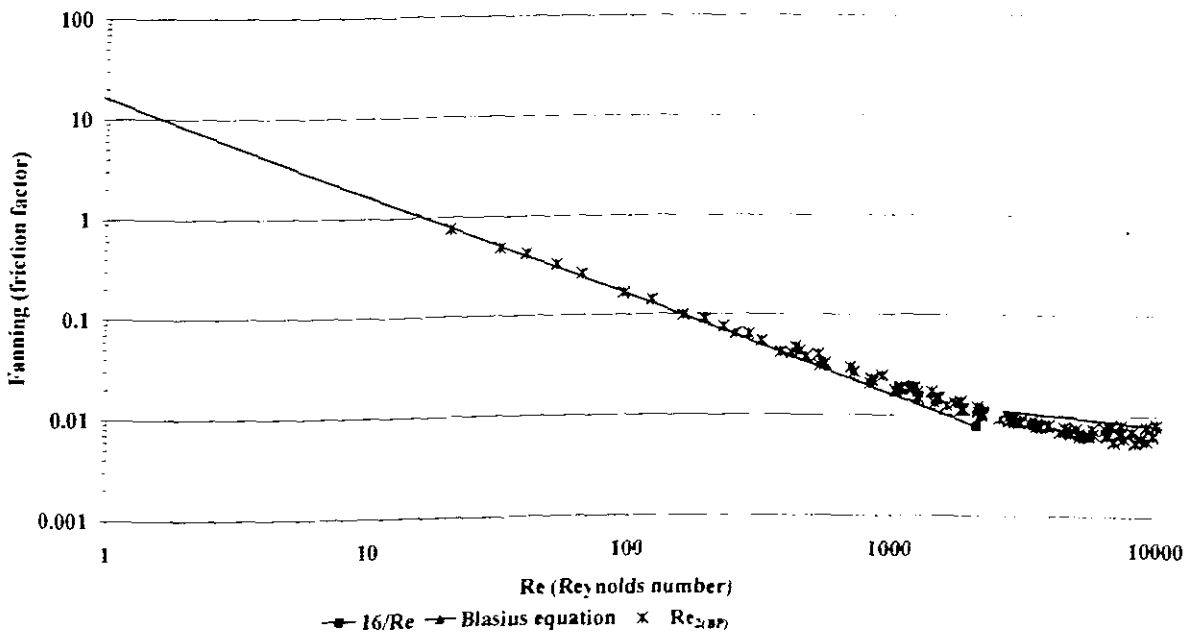
4.6% Bentonite in 150 mm trapezoidal flume channel
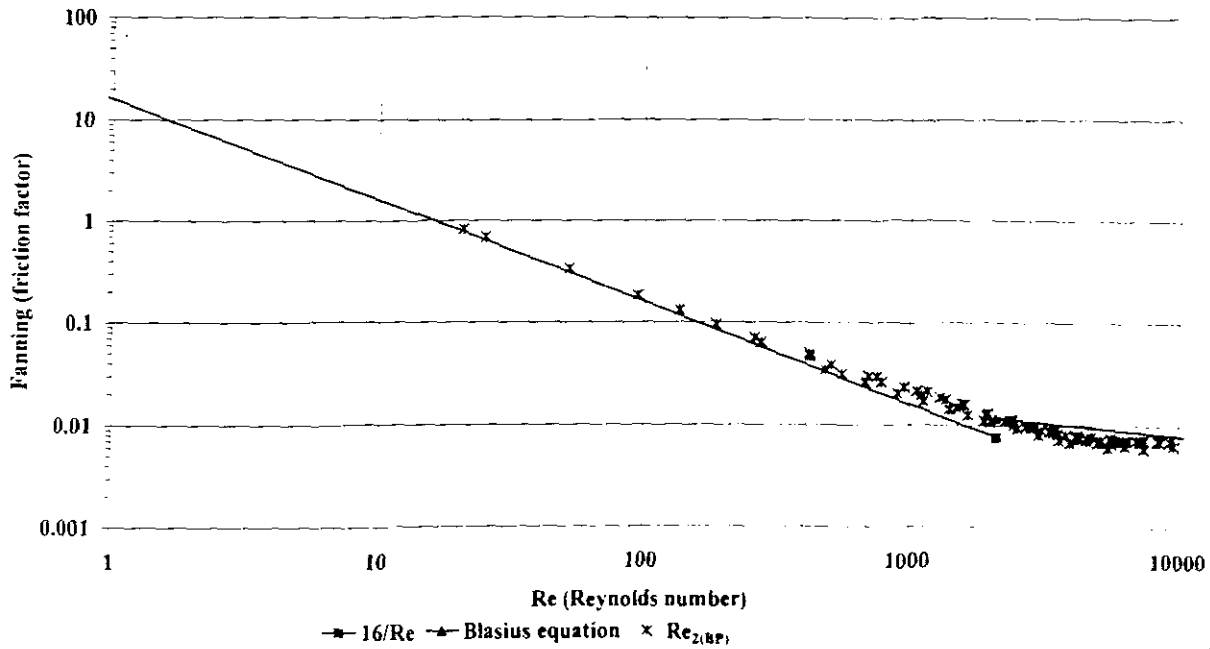
4.6% Bentonite in 75 mm trapezoidal flume channel
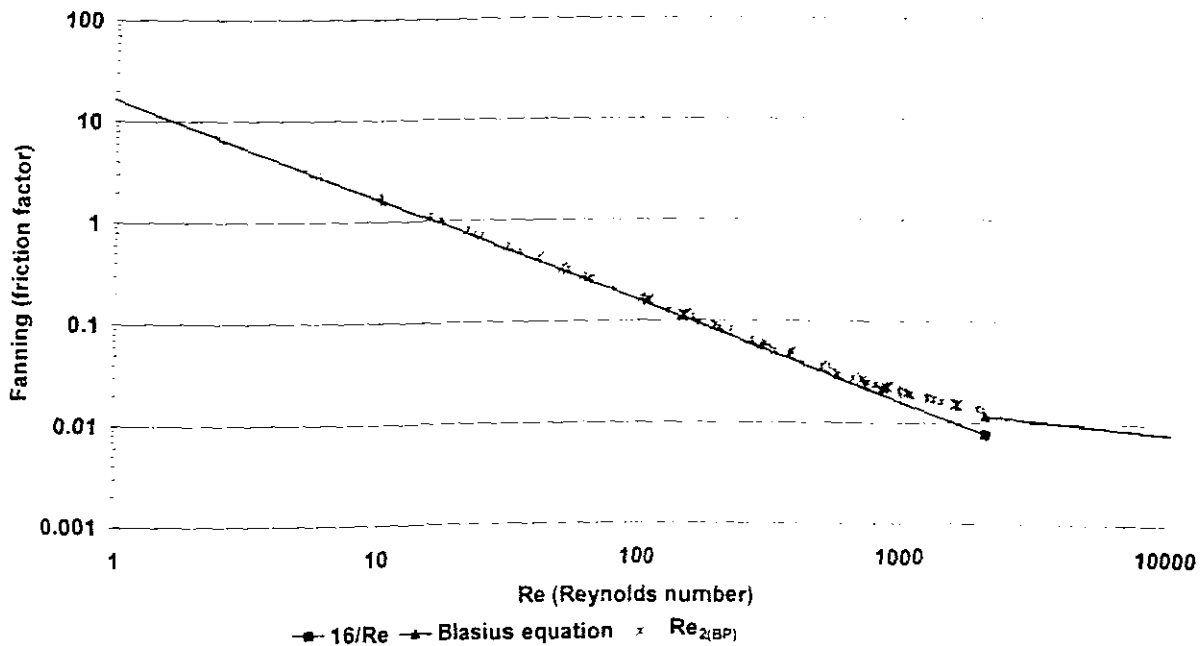
6.2% Bentonite in 300mm rectangular flume shape
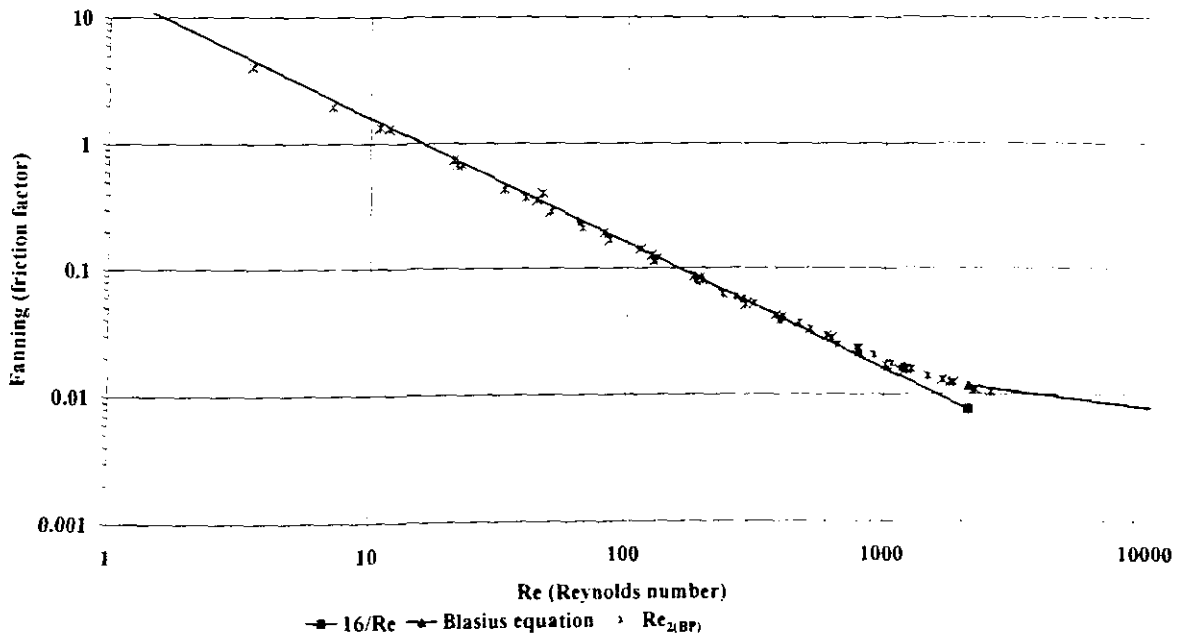
6.2% Bentonite in 150 mm rectangular flume shape
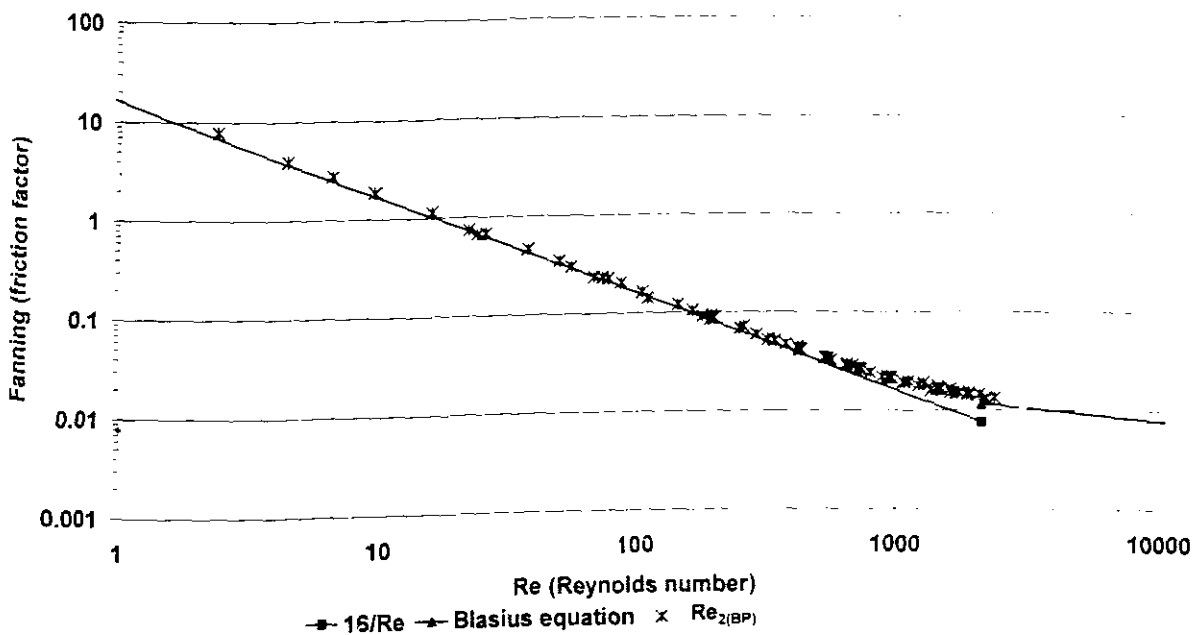
6.2% Bentonite in 300 mm semi circular flume shape
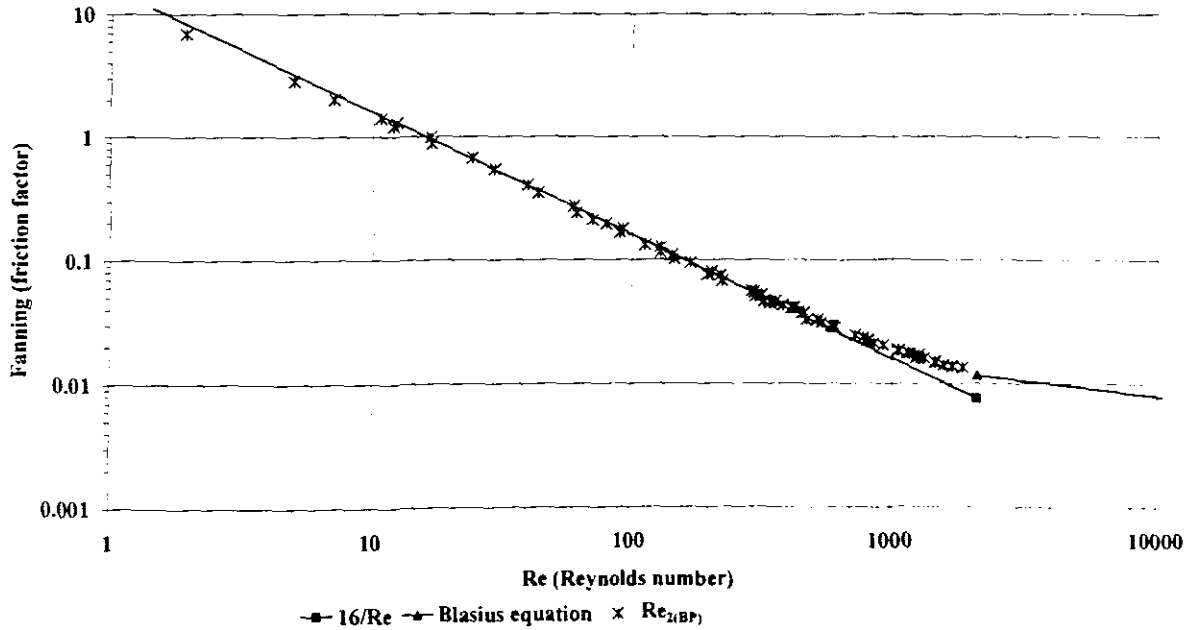
6.2% Bentonite in 150 mm semi circular flume shape
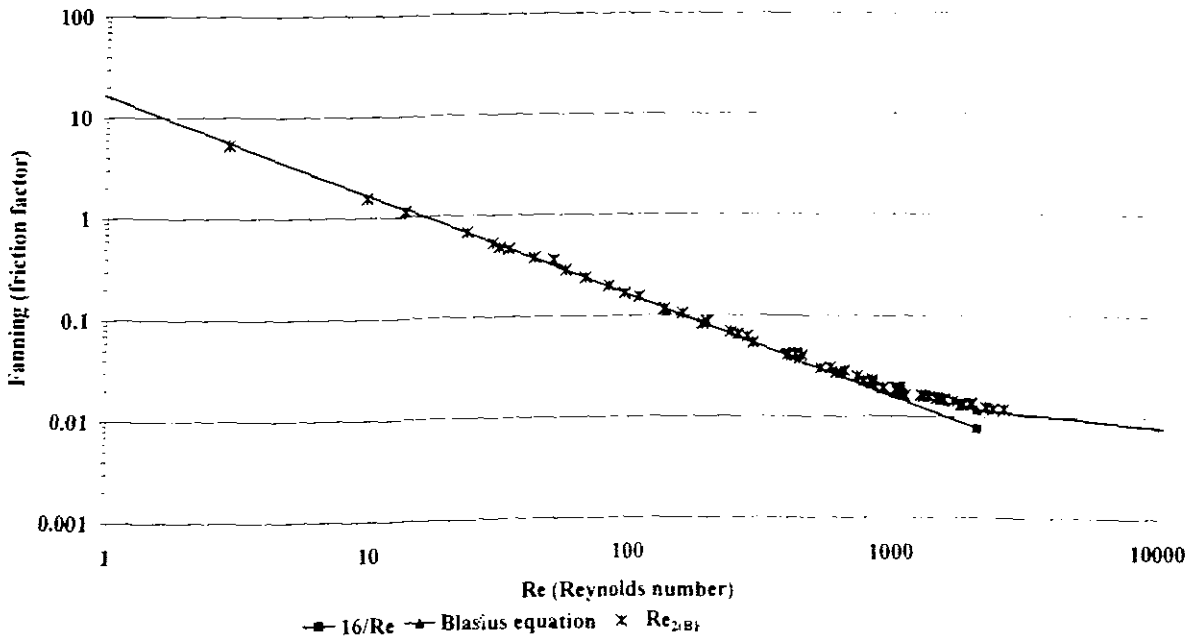
6.2% Bentonite in 150 mm trapezoidal flume shape
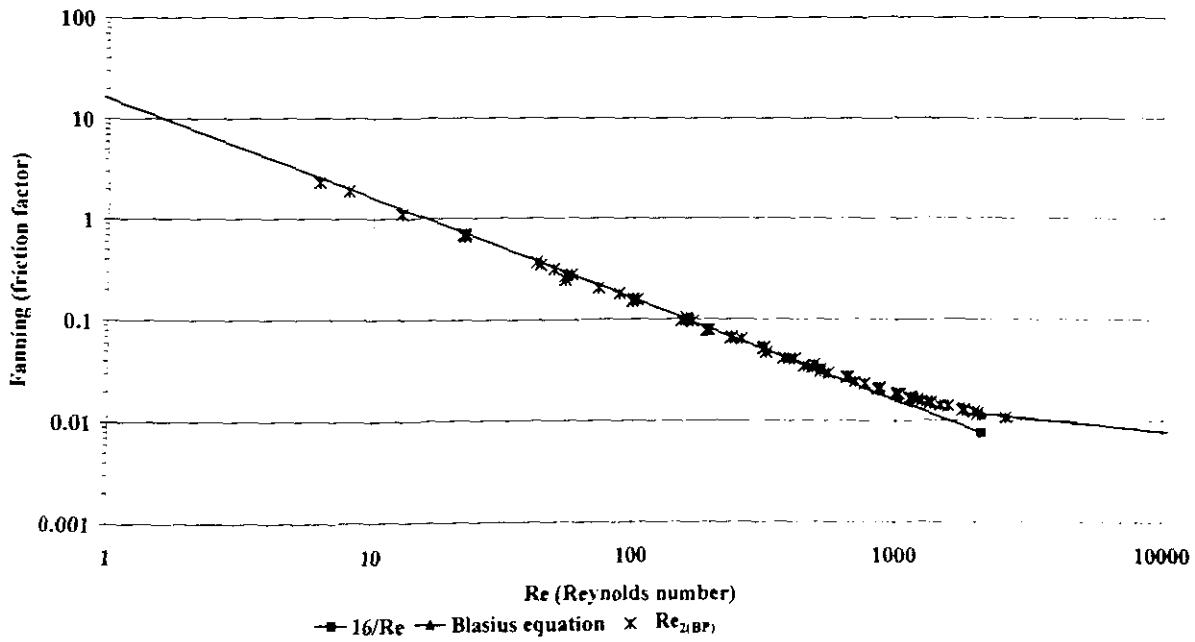
6.2% Bentonite in 75 mm trapezoidal flume shape
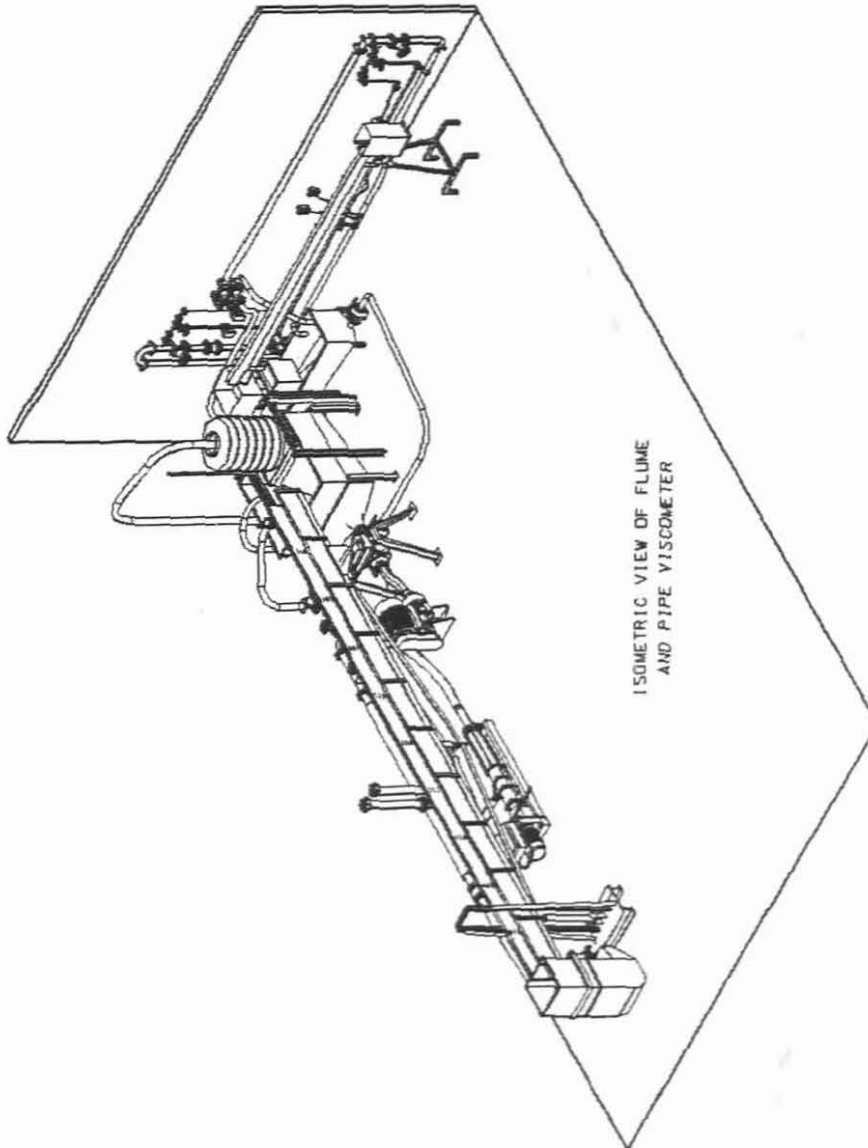
DRAWINGS OF THE FLUME AND PIPE VISCOMETER RIGS

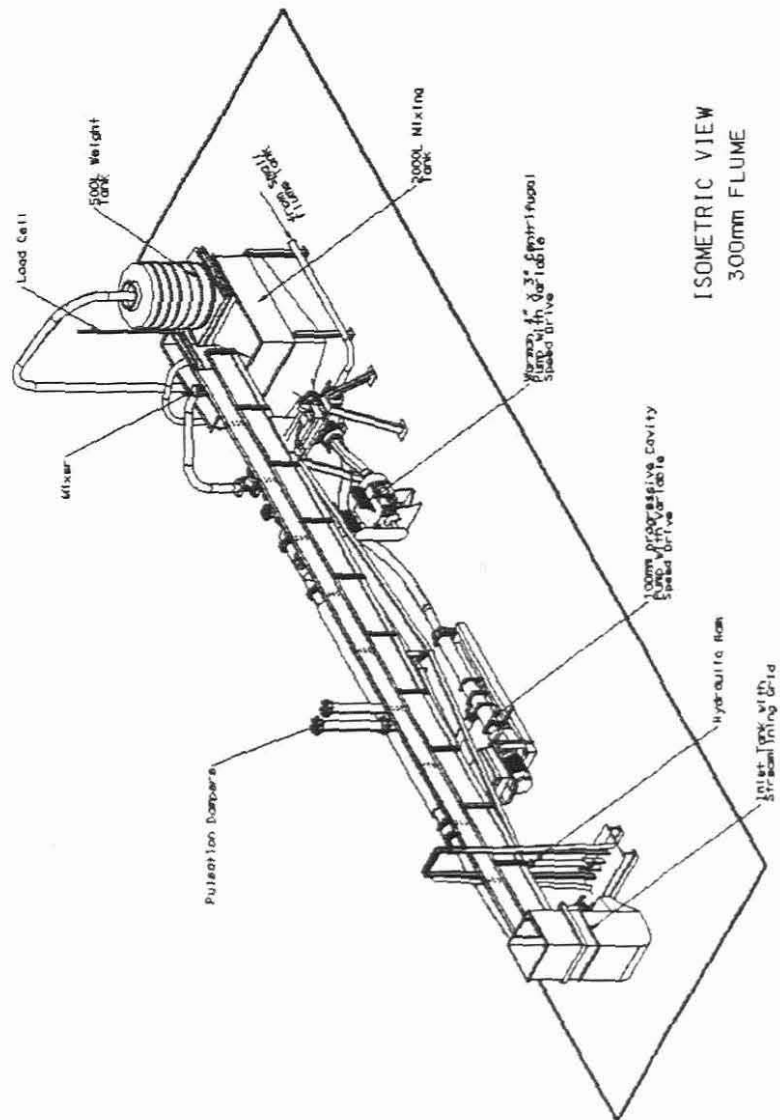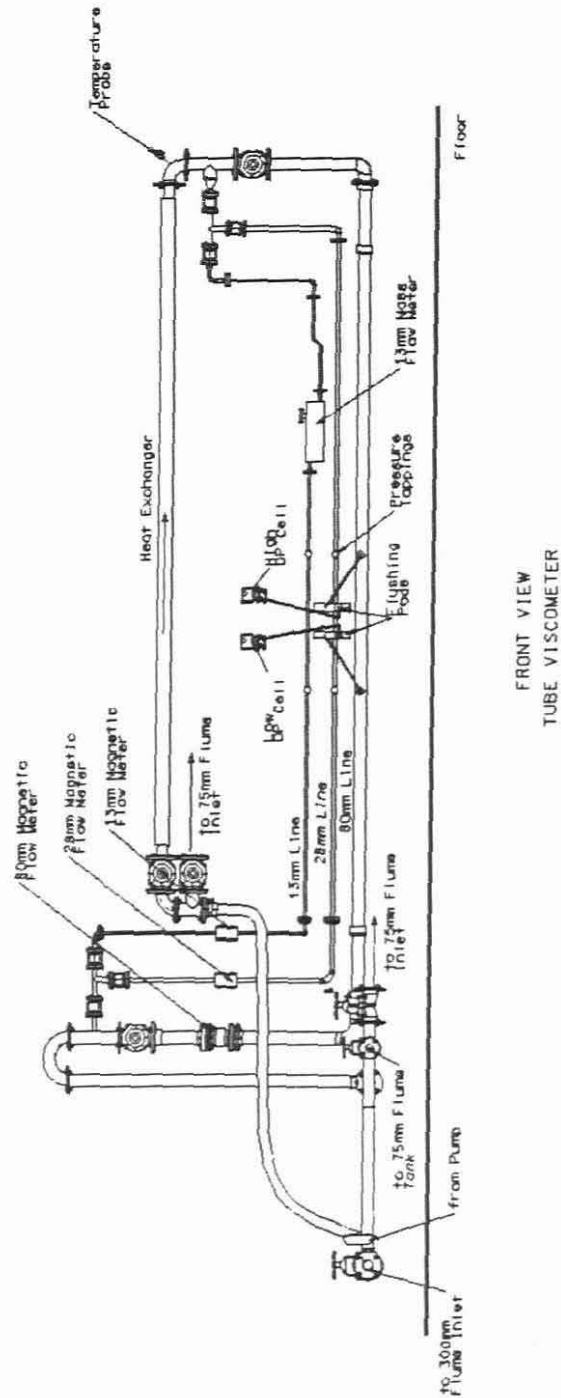Figure (i) Complete rig with flume and tube viscometer rig.

Figure (ii) Isometric view of the 10 m long by 300 mm wide tilting flume

Figure (iii) Tube viscometer rig